



Interaction between synaptic conductances and actionpotential initiation in cortical neurons: computationalmodels and analysis of intracellular recordings

Martin Pospischil

► To cite this version:

Martin Pospischil. Interaction between synaptic conductances and actionpotential initiation in cortical neurons: computationalmodels and analysis of intracellular recordings. Neurons and Cognition [q-bio.NC]. Université Pierre et Marie Curie - Paris VI, 2007. English. NNT : . tel-00180968

HAL Id: tel-00180968

<https://theses.hal.science/tel-00180968>

Submitted on 22 Oct 2007

HAL is a multi-disciplinary open access archive for the deposit and dissemination of scientific research documents, whether they are published or not. The documents may come from teaching and research institutions in France or abroad, or from public or private research centers.

L'archive ouverte pluridisciplinaire **HAL**, est destinée au dépôt et à la diffusion de documents scientifiques de niveau recherche, publiés ou non, émanant des établissements d'enseignement et de recherche français ou étrangers, des laboratoires publics ou privés.



THÈSE DE DOCTORAT DE L'UNIVERSITÉ PARIS VI
ÉCOLE DOCTORALE: Cerveau, Cognition, Comportement
SPÉCIALITÉ: Neurosciences Computationnelles

**Interaction between synaptic conductances and action
potential initiation in cortical neurons: computational
models and analysis of intracellular recordings**

présentée par:
Martin POSPISCHIL

pour obtenir le grade de DOCTEUR de l'UNIVERSITÉ PARIS VI
soutenue le 10 Septembre 2007

Devant le jury composé de:

Dr. Alain DESTEXHE
Dr. Wulfram Gerstner
Dr. Anders Lansner
Dr. Stephane Charpier

Directeur de thèse
Rapporteur
Rapporteur
Examineur

Interaction entre conductances synaptiques et l'initiation du potentiel d'action dans les neurones corticaux: modèles computationnels et analyse d'enregistrements intracellulaires

Résumé de la thèse

Pendant les états naturels d'activité *in vivo*, les neurones neocorticaux sont sujets à une conductance membranaire forte et fluctuante. Cependant, les propriétés intégratives des neurones ne sont pas connues pendant ces états de "haute conductance" (HC). Nous avons (1) caractérisé le lien entre la dynamique des conductances et l'initiation du potentiel d'action (PA) dans les neurones corticaux dans les états HC; (2) comparé différents modèles de réponse de PA (PSTH) pendant ces états. Nous distinguons deux modes de décharge, selon que le PA est évoqué par une augmentation d'excitation ou par une diminution d'inhibition. Nous avons proposé une nouvelle méthode pour calculer les "spike-triggered average" (STA) des conductances à partir du V_m , testé cette méthode numériquement et *in vitro*, ainsi que appliqué cette méthode aux enregistrements *in vivo*. Nous démontrons que les PAs inhibiteurs sont majoritaires chez le chat éveillé, ce qui révèle un rôle majeur de l'inhibition.

Mots clés: corrélation inverse, clamp dynamique, états de haute conductance, modèles computationnels, *in vitro*, *in vivo*.

Summary of the thesis

During natural network states *in vivo*, neocortical neurons are subject to a high and fluctuating membrane conductance. However, the integrative properties of neurons during such "high-conductance" (HC) states are still unknown. We have (1) characterized the link between conductance dynamics and action potential (AP) initiation in HC states; (2) compared different models of AP response (PSTH) during such states. We distinguish two discharge modes, according to whether the AP is evoked by an increase of excitation or by a decrease of inhibition. We have proposed a new method to calculate the "spike-triggered average" (STA) of conductances solely from the V_m , tested this method numerically and *in vitro*, as well as applied this method to *in vivo* recordings. We demonstrate that inhibitory APs are predominant in the awake cat, which reveals a major role for inhibition.

Keywords: spike-triggered average, dynamic clamp, high-conductance state, computational models, *in vitro*, *in vivo*.

Contents

1	Introduction	1
1.1	Preface	1
1.2	Computational neuroscience	3
1.2.1	Models with a single state variable	3
1.2.2	Models with multiple state variables	4
1.3	The point-conductance model	6
1.4	The dynamic-clamp technique	8
1.4.1	Overview	8
1.4.2	The AEC-method	9
1.5	Spike-triggered averages	11
1.6	Outline of the thesis	12
2	Inhibitory conductance dynamics in cortical neurons during activated states	17
2.1	Abstract	19
2.2	Introduction	19
2.3	Spike-triggered averages during activated states	21
2.4	Discussion	21
2.5	References	22
3	Calculating event-triggered average synaptic conductances from the membrane potential	23
3.1	Abstract	25
3.2	Introduction	25
3.3	Material and Methods	26
3.3.1	Models	26
3.3.2	In vitro experiments	27
3.4	Results	28
3.4.1	Method to extract conductance STA	29
3.4.2	Test of the accuracy of the method using numerical simulations	30
3.4.3	Test of the method in real neurons	35

CONTENTS

3.5	Discussion	39
3.6	Acknowledgments	42
3.7	References	42
4	Inhibition determines membrane potential dynamics and controls action potential generation in awake and sleeping cat cortex	45
4.1	Abstract	47
4.2	Introduction	47
4.3	Materials and Methods	48
4.3.1	Intracellular recordings in awake and naturally sleeping animals	48
4.3.2	Analysis and computational models	49
4.4	Results	52
4.4.1	Intracellular recordings in awake and naturally sleeping animals	52
4.4.2	Synaptic conductances in wakefulness and natural sleep	56
4.4.3	Conductance time course during up and down state transitions	61
4.4.4	Dynamics of spike initiation during activated states	63
4.5	Discussion	67
4.5.1	Supplementary Information	71
4.6	References	78
5	Characterizing synaptic conductance fluctuations in cortical neurons and their influence on spike generation	81
5.1	Abstract	83
5.2	Introduction	83
5.3	Methods	85
5.3.1	Computational methods	85
5.3.2	Biological preparation	86
5.3.3	Electrophysiology	86
5.3.4	Data analysis	87
5.4	Results	88
5.4.1	The VmD method for extracting synaptic conductance parameters	89
5.4.2	Estimating time constants from V_m power spectral density	95
5.4.3	Estimating spike-triggering conductance configurations	98
5.4.4	Estimating spike-triggered averages of synaptic conductances from the V_m	104
5.5	Discussion	110
5.6	References	116

6	Which model best captures the spiking response of cortical neurons to excitatory inputs?	121
6.1	Abstract	123
6.2	Introduction	123
6.3	Materials and Methods	125
6.3.1	<i>In vitro</i> experiments	125
6.3.2	Models	126
6.3.3	Integrate-and-fire models	127
6.3.4	The 2-state-variable models	128
6.3.5	The Hodgkin-Huxley model	129
6.3.6	The protocol	130
6.3.7	The optimisation	131
6.4	Results	132
6.5	Discussion	138
6.6	References	140
7	General Conclusions	143
7.1	Summary	143
7.2	Outlook	146
A	Estimating conductance parameters from the membrane potential time course	149
A.1	Synopsis	150
A.2	The Method	150
A.3	Application to model data	151
A.4	Application to <i>in vitro</i> data	154
A.5	Discussion	156
	Bibliography	159

CONTENTS

Chapter 1

Introduction

1.1 Preface

The brain of vertebrates is a highly complex organ. It consists of up to 100 billion processing units, the neurons, each being connected to up to 60,000 others. The connections are realized by synapses, directed couplings that transmit signals emitted by a presynaptic neuron to a postsynaptic one. The signal itself consists in a brief voltage pulse termed “action potential” or simply “spike”. There is a plurality of neuron types. While all neurons consist of a dendritic tree (responsible for signal reception), an axon (forwarding signals to other neurons) and a cell body (the soma, connecting input and output signals), they differ greatly in shape, their pattern of sending action potentials and the type of synapse they establish with postsynaptic neurons. Functional neurons display a voltage difference across their membrane, the so-called membrane potential. It is maintained by permanently active ion pumps that maintain concentration gradients of certain ion types between the interior and exterior of the neuron. The concentration of sodium ions (Na^+) e.g. is reduced inside the cell, while that of potassium ions (K^+) is increased. As a result, in the absence of input signals, the membrane potential saturates at a “leak-” or “resting-” potential. Besides the ion pumps, ion channels are located in the membrane. They control the flux of a specific ion type from one side of the membrane to the other, depending on parameters like the actual membrane voltage or the presence of transmitter molecules. If, due to flux of ions or stimulation with an electrode, the membrane potential depolarizes (rises) sufficiently, an action potential will be emitted. It is subsequently conducted along the axon and eventually reaches a synapse.

The principle of a chemical synapse is depicted in Fig. 1.1. The axon terminal, containing vesicles filled with some neurotransmitter, is located very close to the dendrite of the postsynaptic neuron. The space between pre- and postsynaptic neuron is called the synaptic cleft. The arrival of an action potential triggers the fusion of vesicles with the terminal membrane, thus releasing their contents into

1.1. PREFACE

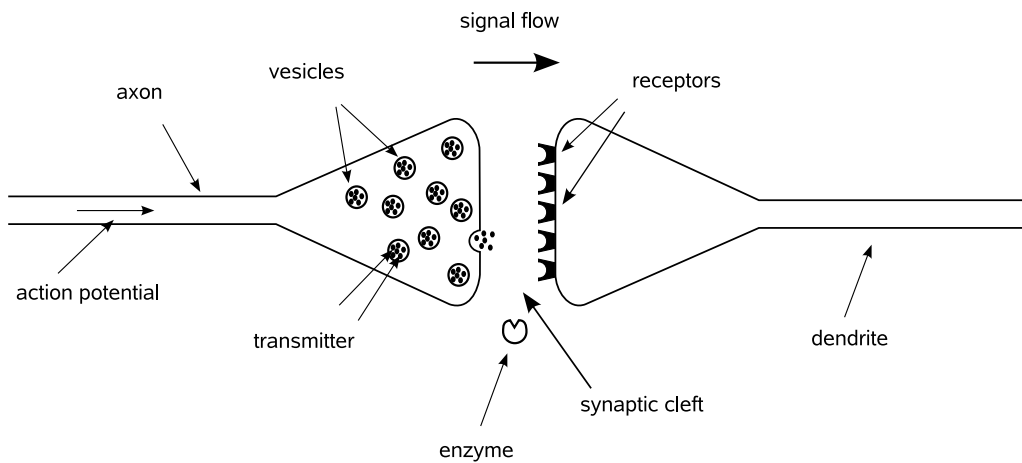


Figure 1.1: Scheme of a chemical synapse. Upon arrival of an action potential, a vesicle fuses with the membrane and releases transmitter into the synaptic cleft. In some synapses, enzymes keep the effect of transmitter local. The transmitter docks to the receptors on the postsynaptic side.

the synaptic cleft. The transmitter diffuses to the opposite side, where receptors are located in the membrane. Once transmitter reaches the receptors, ion channels in the membrane will open either directly or involving a second messenger, allowing ions to cross the membrane thus evoking an electrical signal (post-synaptic potential, PSP) in the postsynaptic neuron.

Synapses either have a depolarizing or a hyperpolarising (decreasing) effect on the membrane potential of the postsynaptic neuron. According to their impact, they are termed excitatory and inhibitory, respectively. One and the same neuron establishes only one type of synapse with its postsynaptic partners. For most excitatory synapses, glutamate takes the role of the transmitter. It binds to two different types of receptors, AMPA (α -amino-3-hydroxy-5-methyl-4-isoxazolepropionic acid) and NMDA (N-methyl-D-aspartate) receptors. In principle, both receptor types are activated by the same synaptic events. However, the number of AMPA receptors is much higher than that of NMDA receptors. Furthermore, the activation of NMDA receptors depends on the membrane potential and is completely inactivated at low (~ -70 mV) voltage levels. It is thus a good approximation to assume only AMPA receptors to be active at voltage levels usually reported in neurons during active states. The most common inhibitory synapse type uses GABA (γ -aminobutyric acid) as its neurotransmitter. The binding to the respective receptors opens channels that allow the influx of chloride ions (Cl^-), whose reversal potential is about -80 mV.

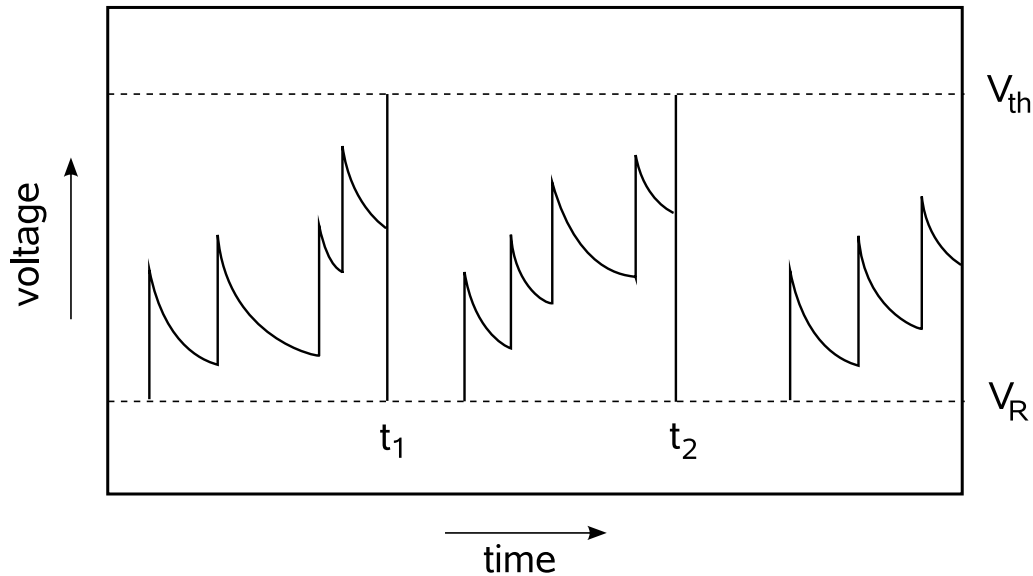


Figure 1.2: The integrate-and-fire model. Synaptic input causes a jump in the membrane potential, in between synaptic events the voltage decays exponentially. Upon hitting the threshold V_{th} the model is said to emit a spike (i.e. at times t_1, t_2), and the membrane potential is set to the reset voltage V_R .

1.2 Computational neuroscience

Since the beginning of the last century, neuroscientists have made attempts to find a formal description of the units involved in brain functioning. Predominantly, they looked for mathematical representations of spiking neurons and synapses, that capture the way neurons collect (“integrate”) input from presynaptic cells and pass on signals depending on the input history. A very complete review of the field is e.g. given in Dayan & Abbott (2001) or Gerstner & Kistler (2002).

1.2.1 Models with a single state variable

There exists a class of models whose state is completely described by the membrane potential. The simplest and most-used of such models is the linear integrate-and-fire (IF) model (Lapicque 1907). It assumes that the membrane acts as a leaky capacitance, whose potential saturates to a resting value, the leak reversal potential, in absence of inputs. Synaptic inputs induce jumps in the voltage, which relaxes exponentially to its resting value. If the potential difference exceeds a certain threshold, the model is said to fire a spike, whereupon the integration starts again from a reset voltage. Sometimes, a “refractory period” after spikes is included in the model, during which synaptic input is disregarded. Several extensions to this model have been suggested, e.g. the time constant (i.e. the leak conductance) can

1.2. COMPUTATIONAL NEUROSCIENCE

be time or input dependent. Other suggestions include a threshold, that depends on the input history and/or the time of the last spike. Here, we briefly describe variants, so-called non-linear IF models, where the leak current is no longer proportional to the difference between voltage and the leak reversal, but depends on it in a non-linear way.

Two of such models are the quadratic and the exponential IF models. In the quadratic IF model (Ermentrout 1996, Latham et al. 2000), the current-voltage relation (also called I-V curve) is described by a parabola. Here, spiking is defined in a different way. Due to the parabolic shape, if the neuron is depolarized sufficiently, it receives a positive feedback and can diverge to infinity in a finite time. This event is called a spike. Subsequently, the voltage is reset to negative infinity, from where it will depolarize to the leak potential in finite time. Using an appropriate transformation, the voltage can be mapped to a phase. Spiking then corresponds to crossing the point where the phase equals π . Instead of a quadratic nonlinearity, a popular model, termed exponential IF model (Fourcaud et al. 2003), uses an exponential supplement to the I-V curve. This provides an important step towards a physiological model, since the exponential term imitates the behavior of biological neurons close to threshold, but leaves the properties at rest unaltered. As for the quadratic IF model, spiking is defined as the divergence of the membrane potential to infinity, the reset, however, has to be finite. In this thesis, we suggest a hybrid model. It behaves as the leaky IF model for voltages below a voltage V_C , and rises quadratically above (cf. Chapter 6). It has properties similar to the exponential IF model, but might prove to be better manageable in a mathematical analysis.

1.2.2 Models with multiple state variables

All the models described in the previous subsection have in common that they are very limited in the type of firing pattern they can display. Recently, models have been suggested that are much richer in this respect, while maintaining a relatively low demand in computational effort for their simulation. Two examples of such models are the Izhikevich model (Izhikevich 2003) and the adaptive exponential IF model (Brette & Gerstner 2005). Besides the membrane voltage, these models comprise a second state variable which is not subject to a stereotypical reset after spikes, thus providing a memory of the cell's state beyond spike time. They are able to reproduce most, if not all types of firing patterns seen in biological neurons.

An even more faithful model of biological neurons is the Hodgkin-Huxley (HH) model (Hodgkin & Huxley 1952). The two authors conducted experiments on the giant axon of the squid and identified three different ion channels. In addition to a leak current (which is mainly driven by chloride ions), their model describes the activation and inactivation of voltage-dependent sodium and potassium channels, that are responsible for spike initiation. The respective state variables

controlling the activation of the sodium and potassium channels are usually named m and n , in addition the sodium channel inactivates according to a state variable h . m , h and n decay in time towards a voltage-dependent equilibrium state, each with a specific time constant. The maximal channel conductances are multiplied by powers of the state variables. At relatively low voltages, neither the sodium nor the potassium channel are considerably activated, thus only small currents flow through these channels. Only above a certain voltage, m activates quickly and the influx of sodium further depolarizes the membrane. Through this positive feedback the membrane potential rises very sharply and forms the onset of the spike. With a certain delay given by the respective time constants, the sodium channel inactivates, i.e. no more positive ions enter the cell and the voltage stops to rise. On a similar time scale the potassium channels open and K^+ ions flow in the opposite direction. This way, the membrane potential is brought back to hyperpolarized values, for which the ion channels take on their default states. During several milliseconds after a spike, the high potassium conductance acts as a “shunt”, meaning that presynaptic input has less effect on the membrane potential. Furthermore, the sodium channels are still inactivated. As a consequence the responsiveness of the neuron is markedly reduced, it is in a refractory state. While the IF mechanism is usually inserted into a single compartment model (i.e. voltage changes take immediate effect in the whole cell), the spike initiation according to Hodgkin and Huxley is also used in detailed models of biological neurons that take into account the complex morphology of the axon and the dendrites, and the effect of synapses situated on the latter.

For synapses as well, there exist different models. They fall into two main categories: current-based and conductance-based models. An example of a current-based synapse is the instantaneous increase of the membrane voltage by a fixed amount upon arrival of a presynaptic input, as it was described in the context of the IF model. In this case the current wave form is a delta pulse. Another widely used waveform is a current that jumps to a finite value and subsequently decays exponentially. A similar shape can be obtained by modeling the current as an alpha-function or as the difference of two exponentials. The same waveforms can be used to model a transient increase in membrane conductance rather than a current. In addition, there exist synapse models that take into account the physiological functioning of synapses in a detailed manner, assuming forward and backward rates for the transition between open and closed states of the respective ion channels in the presence or absence of transmitter molecules (two-state kinetic model, see e.g. Destexhe et al. 1994). Such models can describe a saturation of the synapse, i.e. the amount of conductance per presynaptic spike added to the membrane becomes smaller when the synapse is activated at high rates.

All current based models have in common that the impact of a synaptic input on the membrane potential does not depend on its present state. This is different for conductance-based synapses. There, the current that flows across the mem-

1.3. THE POINT-CONDUCTANCE MODEL

brane is proportional to the conductance, but also to the difference between the membrane potential at the time and the reversal potential of the ion type used by the synapse. The impact of an input to an excitatory synapse (with a reversal potential E_{rev} of ~ 0 mV) e.g. is less during elevated voltage levels compared to hyperpolarized states, while the opposite is true for an inhibitory synapse ($E_{rev} \sim -80$ mV). For the latter, an inhibitory input can even have an excitatory effect on the membrane, if the voltage is below the respective reversal potential. Kuhn et al. (2004) describe another effect that comes with conductance-based synapses. They stimulate a model neuron with increasing excitatory and inhibitory conductance inputs in a manner that the mean membrane potential stays constant. Up to a certain input rate they observe an increase in output firing rate, because the voltage fluctuations increase. However, with even increasing stimulation the output rate reaches a maximum and eventually drops. Due to the large amount of membrane conductance the effect of synaptic input is shunted, effectively reducing the voltage fluctuations and thus decreasing the firing rate. Current-based synapses cannot capture this effect.

1.3 The point-conductance model

Cortical neurons form connections with many thousand presynaptic neurons. Thus, during activated network states where neurons discharge at rates of several Hz, postsynaptic neurons receive tens of thousands of synaptic inputs per second. The effect is a dramatic decrease in input resistance (5–40 M Ω) and a membrane voltage that is depolarized compared to the resting state (around -60 mV). Furthermore, the voltage is characterized by large fluctuations ($\sigma_V = 2$ –6 mV) causing the neuron to spike irregularly at rates of about 5–40 Hz (cf. Destexhe et al. 2003). The integrative properties of neurons in these so-called “high-conductance states” (Destexhe & Paré 1999; Shelley et al. 2002) are likely to be different compared to neurons recorded from in *in vitro* preparations. In a study using tetrodotoxin (TTX, a Na⁺-channel blocker) in order to suppress the effect of network activity (Paré et al. 1998), it was possible to investigate the influence of synaptic conductances on the membrane potential. After the application of TTX, the membrane hyperpolarized, large fluctuations disappeared and the input resistance increased by roughly a factor of five. From the same measurements it was possible to estimate the relative fraction of excitatory and inhibitory synaptic conductances. During high-conductance states, the excitatory contribution was ~ 0.7 times the leak conductance, whereas the inhibitory conductance was ~ 3.7 times higher than the leak conductance. These states are thus dominated by the inhibitory contribution.

However, despite the electrophysiological necessity to include synaptic background conductance in model simulations, the computational burden is huge. Given the computational power to date, it is impossible to simulate a detailed

1.3. THE POINT-CONDUCTANCE MODEL

neuron model in real-time. To simplify the model, the idea is to replace the spatial structure of the dendrites as well as the synapses located on them by their effect on the membrane conductance at the soma, i.e. close to the site of action potential initiation in the axon. Destexhe et al. (2001) proposed such a model, where the distributed synaptic activity is represented by two channels of fluctuating conductances situated in a single compartment. The channels take the role of excitatory (AMPA) and inhibitory (GABA_A) synapses, respectively, and are modelled as Ornstein-Uhlenbeck stochastic processes. This process was defined for the description of a particle undergoing Brownian motion (Uhlenbeck & Ornstein 1930). The time evolution of the velocity of that particle is given by a stochastic first-order differential equation. A change in velocity is due to two components: a deterministic deceleration due to friction and a stochastic acceleration through collisions with other particles. Similarly, in the point-conductance model, the change in synaptic conductance is decomposed into a deterministic deactivation of postsynaptic channels and the stochastic arrival of presynaptic spikes.

A comparison of a detailed biophysical model to a single compartment equipped with the point-conductance model (Destexhe et al. 2001) shows that the simple model captures very well a variety of characteristics: Looking at the conductances at the level of the soma, the power spectra of excitation and inhibition in the detailed model show a dependency proportional to the inverse of the squared frequency, which is exactly what has been derived for the Ornstein-Uhlenbeck process (e.g. Gillespie 1996). Also, the shape of the conductance distributions in the detailed model was very close to Gaussian, which is the analytic solution for the point-conductance model. A fit of the simple to the detailed model thus provided very good results. In a subsequent simulation, the mean voltage level as well as the amount of voltage fluctuations were very similar in both models. Although there was a discrepancy in the average firing rate, its variation as a function of the conductance parameters was well captured by the point-conductance model. The model was also applied to cortical pyramidal cells *in vitro* using dynamic clamp. Adjusting its free parameters according to earlier observations (Paré et al. 1998; Destexhe & Paré 1999) it was possible to recreate intracellular conditions similar to *in vivo* recordings. Even the irregularity of discharges was high (quantified using the coefficient of variation, C_V , defined as the ratio between the standard deviation and the mean of the interspike intervals (ISIs)) and comparable to what is observed in awake animals. Another study (Badoual et al. 2005) showed that a fluctuating current can only account for this observation, when the time constant of the synaptic input is chosen to be similar to that of the membrane. However, in this situation the neurons tend to fire more than one spike at a time (burst-like behavior), and the distribution of the ISIs departs from that observed *in vivo*.

1.4 The dynamic-clamp technique

Many of the results presented in this thesis have also been tested on recordings, that were obtained from *in vitro* preparations using dynamic clamp. Therefore we briefly review the technique and highlight its advantages and mention some achievements obtained by its use (cf. Prinz et al. 2004).

1.4.1 Overview

The dynamic-clamp technique has been introduced almost fifteen years ago (Robinson & Kawai 1993; Sharp et al. 1993a). The key idea is to create artificial conductance in the membrane of a neuron by injecting a current that depends on its membrane potential. The current is computed as the product of the conductance that is to be injected, and the difference of the actual membrane potential and the reversal potential of the ions that are to be conducted. It thus requires recording of the voltage at the same time. The conductance can depend on time and/or voltage, it can be determined as a purely mathematical process, from a model neuron, or it can be derived from the behavior of another neuron in the preparation. The only requirement is that the resulting current can be computed sufficiently fast in order to insure it can be injected in real-time. To date, there is a multitude of implementations of such systems that run under different operating systems, use embedded processors or DSP boards, or analog circuits specifically designed for the conversion of conductances into currents.

Prinz et al. (2004) give examples for different applications of dynamic clamp. One of them is the injection of voltage-independent conductances. It can be used to inject constant conductances to explore e.g. the consequences of a different leak conductance, or to inject a conductance waveform emulating synaptic input. In Sharp et al. (1993b), the effect of a GABA bath application has been simulated. The voltage time course is reliably reproduced, and short current pulses of fixed amplitude, that are injected in addition, demonstrate that the input resistance of the membrane changes. Rather than adding conductances, with some restrictions it is also possible to subtract them using dynamic clamp. This fact has been used e.g. to annihilate the effect of a leakage conductance introduced by entering a sharp electrode into the cell (Cymbalyuk et al. 2002).

Furthermore, conductances that depend on the membrane potential can be simulated as well. This opens the possibility to add intrinsic membrane conductances to the neuron or alter already existing ones, in order to probe the impact on the neurons behavior. This kind of manipulation can be a, presumably more precise, alternative to the use of pharmacological substances. In Ma & Koester (1996), e.g., the effect of A-type and delayed-rectifier K^+ on spike broadening in *Aplysia* R20 neurons has been successfully removed and restored after pharmacological blocking, respectively.

The technique can also be used to create or alter networks of neurons, where a “neuron” can just as well be a software model or an analog circuit. If the presynaptic unit is a real neuron, it is necessary to record its membrane potential in order to control current injection. Then, it is possible to study the impact of either changing the strength of an existing synapse or of introducing a new connection between the neurons. In a different kind of study (Le Masson et al. 2002), a real thalamocortical neuron was connected via dynamic clamp to a software model neuron (representing a reticular interneuron) on the one hand and to an analog circuit neuron (retinal ganglion cell) on the other hand. The circuit reproduced the type of spindle activity which is seen in the thalamus during states of sleep.

Finally, the dynamic-clamp technique can be used to combine the advantages of *in vitro* and *in vivo* experiments. Preparations *in vitro* are far easier to maintain and better accessible. It is e.g. possible to record with visually guided patch electrodes. Also, the application of pharmacological substances can be precisely controlled. However, as mentioned before, during active states *in vivo*, the huge amount of synaptic input drastically decreases the input resistance and depolarizes the membrane potential. Since the network *in vitro* is rather silent, this synaptic background is missing thus putting the neuron in a different state. Using dynamic clamp, *in vivo* conditions can be recreated by injecting computer-generated conductances (Destexhe et al. 2001). This is the application that was used throughout this thesis. In particular, we used the hybrid RT-NEURON environment developed by G. Le Masson, (Université de Bordeaux), which is a modified version of NEURON (Hines & Carnevale 1997), augmented by the capacity to conduct simulations in real-time. The injected current corresponded to the point-conductance model described in the previous chapter, where the conductance time courses for excitation and inhibition are defined as stochastic processes described by their means and standard deviations.

1.4.2 The AEC-method

Like every technique, the dynamic clamp also has its limitations. First of all, since the injection with an electrode is local, only the effect of localized conductances can be simulated. This is not a problem in our case, since the point-conductance model is designed in exactly this fashion – to create an effective conductance time course at the site of action potential generation, that is a filtered version of synaptic conductances arriving at the dendrites. Nevertheless, with dendritic patch recordings it is possible to inject conductances into dendrites, opening the possibility to explore dendritic filtering in detail. However, while it is possible to inject the appropriate amount of current that flows across the membrane according to some conductance model, the intracellular concentration of the ion type in question does not change. Again, this is not a constraining factor for our purposes, since the concentration of ions involved in synaptic transmission is assumed to

1.4. THE DYNAMIC-CLAMP TECHNIQUE

vary little. Finally, the dynamic clamp has to cope with technical difficulties that come with the recording process, namely artefacts introduced by the resistance and capacitance of the recording electrode. This is particularly important due to the feedback introduced by injecting a voltage-dependent current. Different approaches have been pursued to tackle this problem. One can use low-resistance electrodes, or employ different electrodes for current injection and voltage recording. The latter option requires impaling the same cell with two electrodes at the same time. Another possibility is to separate the injection/recording process in time (discontinuous current-clamp, DCC): the voltage is recorded only after the membrane potential has reached its equilibrium value after current injection. But with this approach, the achievable sampling frequency is low (in the order of 2–3 kHz).

A different approach, termed “Active Electrode Compensation (AEC)”, has been suggested recently (Brette et al. 2005, 2007). When recording with a single high-resistance electrode in continuous mode, it is possible to partially account for electrode artefacts. To this end, the electrode is assumed to behave as a resistor–capacitor (RC) circuit. Two adjustments are possible. First, the capacitance can be neutralized by injecting an appropriate, time–dependent current. Second, in modern amplifiers it is possible to subtract the part of the voltage from the recording that is due to the electrode resistance (“bridge mode”) according to Ohm’s law. However, in reality the electrode does not behave as an ideal RC–circuit, so that the compensation is only approximate. This prevents the application during dynamic-clamp, since, as mentioned above, due to the feedback the system can become oscillatory unstable. Brette et al. (2005, 2007) suggest a different electrode model: instead of presuming a fixed number and wiring of elements in the equivalent circuit, the only assumption is that it be linear. The voltage across the electrode can then be computed as the convolution of the injected current with a kernel representing the electrode. The kernel representing the RC–circuit e.g. would just be an exponential function. Once the contribution of the electrode is known, the membrane voltage can be reliably determined allowing the application during dynamic clamp. It remains to fix the electrode kernel.

This can be done injecting a known current into the cell. Since the recording is done in discrete time, extracting the kernel amounts to solving a matrix equation, which corresponds to a least-squares fit of the kernel to the response. The recorded response represents, however, the combined kernel of the electrode and the cell. The two contributions subsequently have to be separated. Fortunately this is possible, because the response of the electrode is much faster than that of the membrane, its kernel thus very short. For currents that are small enough (such that the membrane responds linearly), a decaying exponential can therefore be fitted to the tail of the combined kernel in order to approximate the contribution of the membrane, allowing to subsequently determine the electrode kernel. In principle, any current wave form can be used, but the particular choice made in Brette

et al. (2007) (uniformly distributed white noise) is optimized to separate the two kernels.

The method has been tested in a number of protocols. First, the subthreshold voltage time course during white current noise injection was compared to the theoretical prediction for a passive cell. The voltage distributions and power spectra obtained in both cases closely resembled each other. Second, the application to dynamic clamp was tested. There the response to square conductance pulses, which can be calculated analytically, was compared between AEC, DCC and the theoretical prediction. While the recording using AEC faithfully reproduced the expectations, the DCC showed significant discrepancies. During injection of colored conductances according to the point-conductance model, the voltage distributions obtained both with AEC and DCC were compared to the expressions derived in Rudolph & Destexhe (2003a) and Rudolph et al. (2004). Both methods showed good agreement. The frequency aspects, however, were reproduced satisfactorily only by the AEC method. The DCC failed to capture the scaling properties at high frequencies in the power spectral density. Finally it was shown, that dynamic clamp recordings using AEC could resolve the shape of spikes to an extent as to recover the correlation between spiking threshold and the preceding rate of depolarization (e.g. Azouz & Gray 2000; de Polavieja et al. 2005; Wilent & Contreras 2005b).

1.5 Spike-triggered averages

Determining the optimal features of stimuli which are needed to obtain a given response is of considerable interest, for example in sensory physiology. Reverse-correlation is one of the most-used methods to obtain such estimates and, in particular, the spike-triggered average (STA) is often used to determine optimal features linked to the genesis of action potentials (de Boer & Kuypers 1968). An extensive study is given in Bryant & Segundo (1976). The authors consider Gaussian white-noise stimuli in *Aplysia* neurons and, among other questions, extract the stimulus features correlated with spikes.

Recent contributions (Badel et al. 2006; Paninski 2006a, 2006b) gave analytical expressions for the most likely voltage path, which in the low-noise limit approximates the STA of the leaky integrate-and-fire (IF) neuron. Here again, Gaussian white noise current was considered as input. In Badel et al. (2006), a second state variable was added in order to obtain biophysically more realistic behavior. In Paninski (2006a, 2006b), in addition the exact voltage STA for the non-leaky IF neuron was computed, as well as the STA input current in discrete time. Here, a strong dependence of the STA shape on the time resolution dt was found without a stable limit as $dt \rightarrow 0$.

In contrast to previous works, we use STAs in a different context. In Chapter 3,

1.6. OUTLINE OF THE THESIS

we assume that we do not have knowledge about the time course of the input injected into a cell. Also, rather than predicting the voltage STA for a given model subject to a certain stochastic stimulus, we want to go the opposite way: Given the voltage STA, what can one say about the underlying, spike-evoking stimulus?

In order to address this question, we consider IF-neurons subject to conductance based excitatory and inhibitory synaptic noise. Using intracellular recordings, it is straightforward to calculate the STA of the membrane potential, which yields the mean voltage trajectory preceding spikes. In contrast, it is much harder to determine the underlying synaptic conductance. One of my attempts consisted in using voltage recordings obtained during injection of different DC levels. The idea was to calculate the voltage STA for two DC amplitudes and subsequently solve the passive membrane equation including the point-conductance model for excitatory and inhibitory conductances. Basically, this is the inverse procedure of running a numerical simulation. This approach failed for at least two reasons, we will expose the first for the case of the estimation of the total conductance using Ohm's law. It determines the conductance as the quotient of a constant current and the change in voltage due to it. This works well as long as the two voltage STAs are clearly separated. But since in the IF model spiking is defined by crossing a fixed voltage, at the time of the spike both STAs take on the same value, namely the threshold voltage. Since the difference in DC levels is constant, the estimated conductance diverges to infinity, which is clearly unphysiological. Inverting the membrane equation rather than using Ohm's law generates an equivalent denominator. The second reason for failure is slightly more subtle. During injection of a constant current, the distance of the membrane potential to threshold changes. For a reduced distance compared to a reference state, conductance patterns consisting of slightly less excitation and slightly more inhibition will be able to trigger spikes thus impacting on the average pattern. As a consequence, the conductance STAs are not the same for different DC input. This disturbs the estimation with the inverted membrane equation considerably, since independence of the DC level is assumed. Thus, determining the conductance STAs from membrane potential activity is bound to major difficulties. One of the main contributions of this thesis is to provide a way to resolve these complications.

1.6 Outline of the thesis

The topic of my thesis is the investigation of neuronal behavior during different states of synaptic input. An emphasis is put on the question of spike initiation, in particular what pattern of synaptic conductances triggers spikes, and how this pattern depends on the synaptic background. To this end we combine model simulations, theoretical investigations as well as *in vitro* and *in vivo* experiments. We also explore to what extent different types of computational models are able to

capture the response properties of cortical neurons during *in vitro* recordings.

Chapter 2 gives a brief introduction into the kind of work presented in the thesis. The simulations I did are supposed to shed light on the difference in spike-evoking conductance patterns depending on the synaptic background. The protocol consisted in injecting conductances created by the point-conductance model into a single compartment Hodgkin-Huxley model, where we contrast two extreme cases of synaptic input. The one corresponds to the high-conductance (HC) state of cortical neurons *in vivo* during activated states. It is characterized by an inhibitory conductance that exceeds excitation severalfold, and the sum of synaptic conductances is higher than the leak conductance. The other case is a “low-conductance” (LC) state. Excitation and inhibition, as well as the leak conductance, are of approximately equal magnitude. The respective parameters are chosen such that the voltage distribution as well as the amount of spontaneous activity were about the same. However, a difference between the two states in the STA of the synaptic conductances is apparent. Spiking is controlled by an increase of excitation during LC states on the one hand, but by a decrease of inhibition during HC states. The same protocol was repeated by a group in our lab during *in vitro* experiments in ferret cortical neurons using dynamic clamp. My analysis of the data revealed the same pre-spike patterns as seen in the model study. This observation provides direct evidence for an influence of the amount and composition of synaptic background on the integrative properties of neurons.

The next logical step was to try to extract conductance STAs from cortical neurons *in vivo*, preferably during activated states. While in models, as well as in dynamic clamp, one has direct access to the amount of conductance in the cell at all times, the observable quantity during intracellular experiments *in vivo* is the membrane potential. Thus, a method is needed that can determine the amount of synaptic conductances, separated into excitation and inhibition, from the membrane potential. The derivation and subsequent testing of such a method in model neurons and during dynamic clamp recordings is exposed in Chapter 3. It revealed very good agreement between the conductances during the simulation or experiment, respectively, and their estimation from the membrane potential. However, as mentioned before in the context of the point-conductance model and the dynamic clamp technique, conductances have to be understood as effective conductances at the level of the soma. By means of this method it is not possible to assess the amount of synaptic input distributed across the dendritic tree. Nevertheless, we show in a simple model of dendritic filtering that the method faithfully reproduces the conductance STAs as measured using a simulated voltage clamp at the soma. Supposedly, this is owed to the fact that the conductance distributions at the soma still have a near Gaussian shape, for which the method is developed. Destexhe et al. (2001) show that this observation also holds in a detailed model neuron with synapses distributed across active dendrites. We have thus confidence that the method can be readily applied to recordings from cortical neurons *in vivo*.

1.6. OUTLINE OF THE THESIS

This has been done recently and is part of Chapter 4.

The data used therein was obtained by one of the authors (Igor Timofeev) using a novel recording technique, which enables the experimenter to conduct recordings in awake or naturally sleeping animals. After briefly showing the behavior of representative regular spiking and fast spiking cells, the chapter continues with an analyses of the conductance state of all recorded cells. The VmD-method, that was employed for this analysis, is described in Rudolph & Destexhe (2003a, 2005) and Rudolph et al. (2004). It provides a tool that extracts the means and standard deviations of the distributions of synaptic conductances from the voltage distributions obtained at two different DC levels. In summary, cells in the awake state as well as during slow-wave sleep (SWS) up-states show the typical signs of cells in high-conductance states: a depolarized membrane potential, sustained, irregular firing and an inhibitory synaptic conductance, that is larger than excitation by roughly a factor of two. At the same time, inhibitory fluctuations dominate over excitatory ones by about the same factor. Again applying the VmD-method to short pieces of the voltage trace, the conductance time course during transitions from up- to down-states or vice versa could be determined. In the cell analyzed, the transition down-up was initiated by a rise in excitation, followed by a rise in inhibition about 20 ms later. The opposite transition was induced by a drop in inhibition, followed by a drop in excitatory conductance. My contribution to the publication consists in an estimation of the conductance STAs using the results of Chapter 3. In model studies, a drop in total conductance (due to a pronounced drop in inhibition) a few tens of milliseconds before spikes was identified as an indication of inhibition dominated states. In accordance with this, the STA analysis of several regular spiking cells revealed such a drop in the majority (7/10 during awake states, 6/6 during SWS up-states and 2/2 during REM sleep) of cells. A quantification of the pre-spike patterns showed, that most of the cells display an excess in inhibitory conductance and a net drop in total conductance at the same time. In addition, there was a clear quantitative correlation between the relative conductance change and the difference in conductance fluctuations.

Chapter 5 provides a summary of analysis tools along with some extensions, based on the point-conductance model. It consists of three parts. In the first part, the VmD-method (Rudolph & Destexhe 2003a, 2005; Rudolph et al. 2004) is reviewed. Its principle idea of relating voltage and conductance distributions as well as the testing described in Rudolph et al. (2004) and Piwkowska et al. (2005) is exposed. In addition, its application to intracellular recordings in anesthetized (Rudolph et al. 2005b) and naturally sleeping and awake cat (Rudolph et al. 2007, cf. Chapter 4) is summarized. The second part presents an approach to estimate the correlation time constants of synaptic conductances, that makes use of a theoretical expression for the power spectral density of the membrane potential. Its matching to dynamic-clamp recordings (injecting fluctuating conductances), up-

states *in vitro* and active states *in vivo* is shown. For the latter two, the matching is difficult due to a different scaling behavior for high frequencies, the dynamic-clamp data, however, is matched very well. In the third part, I sketch an extension of the STA-method. Since there is evidence, that excitatory and inhibitory conductances are co-activated during responses to sensory stimuli, I reformulate a part of the model in order to allow for a cross-correlation as well as a relative shift between synaptic conductances. Subsequently, the method as it is described in Chapter 3 is further tested on a pool of ~ 50 dynamic-clamp recordings. I fitted the recorded and estimated conductance STAs with an exponential function and compared the parameters. The accordance was surprisingly good across the whole ensemble. Finally, an earlier STA analysis of *in vivo* recordings is reviewed (cf. Chapter 4).

In Chapter 6 we take a look at spike initiation from a different point of view. We wanted to test the capacity of different computational models to reproduce the response of real neurons to excitatory input in a situation that resembles active network states. To this end, *in vitro* dynamic clamp experiments were conducted in our lab, where on top of an either LC or HC conductance background an AMPA-stimulus of varying strength was injected. I computed the post-stimulus time histogram (PSTH) of several cells and fitted a couple of computational models of different degrees of complexity to it. The objective function consisted in the RMS (root mean square) of the difference between the data and model PSTHs corresponding to different amplitudes of the stimulus and to either one or both background states. Among the various existing optimization strategies, we chose the simulated annealing algorithm. In a comparative study (Vanier & Bower 1999) it has been found to be superior to three other strategies for an intermediate number of parameters. I found that the most complex model (Hodgkin-Huxley) best reproduced the experimental PSTH, but not by far. The exponential IF model, for example, came very close. This is surprising given the difference in complexity between these models. I also tested the predictive power of a fit to either LC or HC state to produce a PSTH adapted to the respective other state. No clear dependence on a specific model was apparent, but in general the prediction was considerably worse than the respective fit. This is another hint for different integrative properties depending on the synaptic background.

After the general conclusions, I complete the thesis with Appendix A. I introduce a novel method that, under certain weak constraints, has the property to estimate the mean synaptic conductances and, even more important, their respective fluctuations, from the voltage time course at a single (zero) DC level. According to a scan of the plane of mean excitatory and inhibitory conductances, the method is particularly well suited for neurons in high-conductance states, but interestingly estimates the amount of excitatory fluctuations with high precision, independent of the mean synaptic conductances.

1.6. OUTLINE OF THE THESIS

Chapter 2

Inhibitory conductance dynamics in cortical neurons during activated states

Martin Pospischil, Zuzanna Piwkowska, Michelle Rudolph, Thierry Bal and Alain Destexhe. Inhibitory conductance dynamics in cortical neurons during activated states. *Neurocomputing* **70** (10-12):1602-1604, 2007.

Résumé

Introduction

Pendant les états naturels d'activité *in vivo*, les neurones neocorticaux reçoivent des entrées synaptiques provenant de milliers de neurones, ce qui impose une conductance membranaire forte et fluctuante. Ces états de "haute conductance" (HC) sont aussi caractérisés par d'importantes fluctuations du potentiel membranaire (V_m). Cependant, la connaissance unique du V_m n'est pas suffisante pour conclure sur les conductances sous-jacentes, car différents états de conductance peuvent correspondre à une même dynamique apparente du V_m . De plus, les propriétés intégratives des neurones, en particulier la dynamique des conductances associée aux potentiels d'action (PA), peut être très différente selon l'état de conductance de la membrane. Dans cet article court, nous étudions les différences entre ces deux états en utilisant les modèles computationnels et les expériences de type dynamic-clamp.

Résultats obtenus

Nous considérons deux types d'états, basse conductance (LC) et haute conductance (HC), qui correspondent au même type d'activité du potentiel de membrane, mais les conductances sous-jacentes sont très différentes. Nous utilisons la technique de "spike-triggered average" pour calculer le déroulement temporel des conductances relié aux PAs. Les modèles computationnels prédisent que dans les états LC, le PA est en général précédé par une forte augmentation d'excitation, qui se traduit par une augmentation de la conductance membranaire juste avant le PA. Par contre, dans les états HC, la dynamique est différente: les PAs sont précédés en général d'une forte *diminution* de la conductance inhibitrice, qui se traduit par une diminution de la conductance membranaire. Ces prédictions sont confirmées dans des neurones réels du cortex visuel *in vitro* par la technique de dynamic-clamp.

Conclusions

Cette étude révèle deux types opposés de genèse du PA dans les neurones corticaux. Soit le PA est généré par une augmentation de conductance excitatrice, ce qui constitue un mode classique. Soit le PA est généré par une diminution d'inhibition (dis-inhibition), ce qui est moins classique. Ces deux modes sont également observés dans des neurones du cortex visuel *in vitro*.

2.1 Abstract

During activated states *in vivo*, neocortical neurons are subject to intense synaptic activity and high-amplitude membrane potential (V_m) fluctuations. These "high-conductance" states may strongly affect the integrative properties of cortical neurons. We investigated the responsiveness of cortical neurons during different states using a combination of computational models and *in vitro* experiments (dynamic-clamp) in the visual cortex of adult guinea-pigs. Spike responses were monitored following stochastic conductance injection in both experiments and models. We found that cortical neurons can operate in a continuum between two different modes: during states with equal excitatory and inhibitory conductances, the firing is mostly correlated with an increase in excitatory conductance, which is a rather classic scenario. In contrast, during states dominated by inhibition, the firing is mostly related to a decrease in inhibitory conductances (dis-inhibition). This model prediction was tested experimentally using dynamic-clamp, and the same modes of firing were identified. We also found that the signature of spikes evoked by dis-inhibition is a transient drop of the total membrane conductance prior to the spike, which is typical of states with dominant inhibitory conductances. Such a drop should be identifiable from intracellular recordings *in vivo*, which would provide an important test for the presence of inhibition-dominated states. In conclusion, we show that in artificial activated states, not only inhibition can determine the conductance state of the membrane, but inhibitory inputs may also have a determinant influence on spiking. Future analyses and models should focus on verifying if such a determinant influence of inhibitory conductance dynamics is also present *in vivo*.

Supported by: CNRS, HFSP and the EU

2.2 Introduction

During activated states *in vivo*, neocortical neurons are subject to intense synaptic activity and high-amplitude membrane potential (V_m) fluctuations (Paré et al. 1998, Steriade et al. 2001). These "high-conductance" states may strongly affect the integrative properties of cortical neurons (Destexhe et al. 2003). Models show that there is an infinite number of combinations of excitatory and inhibitory conductances that can yield V_m dynamics similar to *in vivo* recordings. Two extreme regimes in this continuum are low-conductance (LC) states, where excitatory and inhibitory conductances are approximately equal, or high-conductance (HC) states, in which inhibitory conductances are several-fold larger than excitatory conductances (cf. Fig.2.1 A). In this contribution, our goal is to compare these two states with respect to the conductance dynamics underlying spike initiation.

2.2. INTRODUCTION

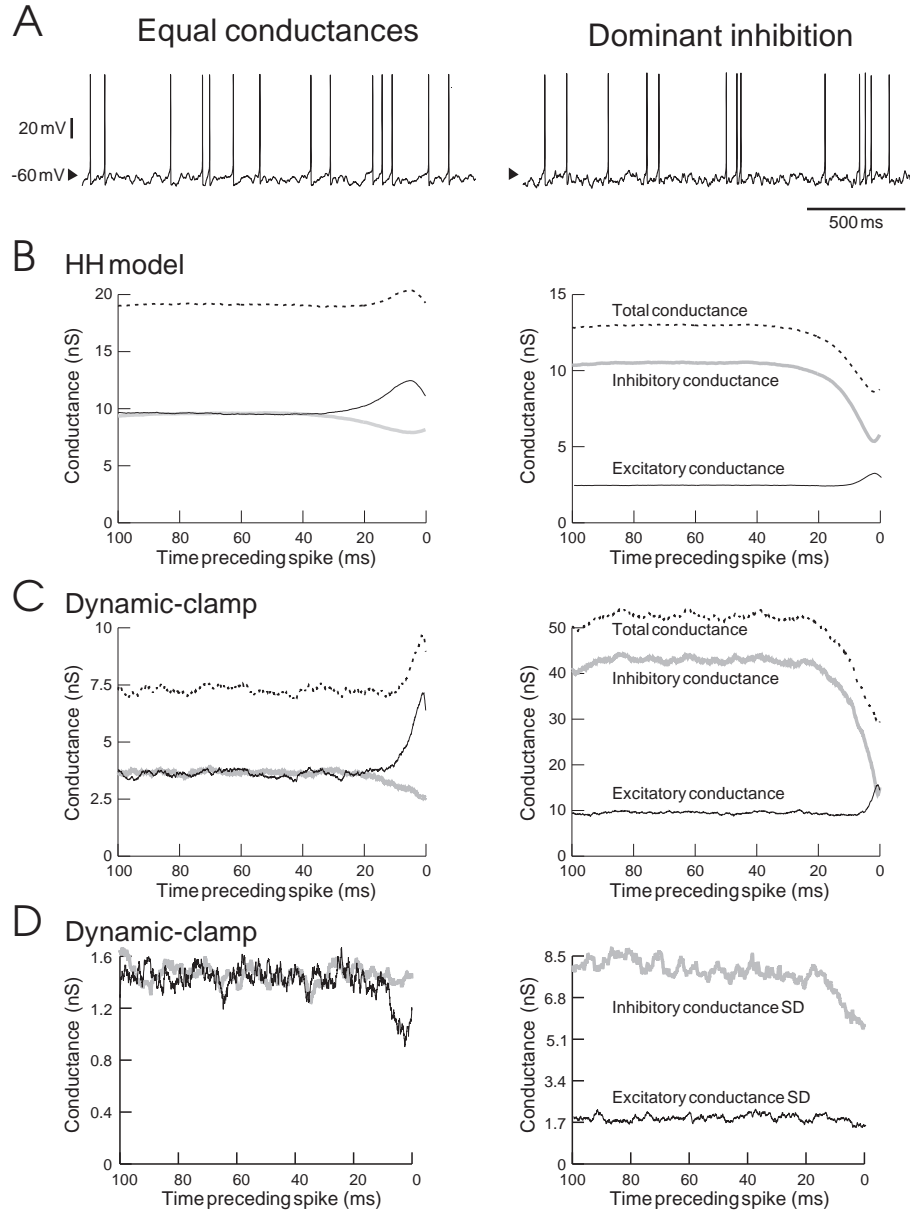


Figure 2.1: Optimal patterns of conductance related to spikes in cortical neurons. Comparison of low-conductance (left) and high-conductance states (right). **A** A spike is evoked at $t = 0$ ms. **A**. The voltage traces in the two states obtained in models are similar in terms of V_m mean and variance (model). **B**. Spike-triggered average of inhibitory, excitatory and total conductance in the model. In the LC state, the spike is preceded by a peak in excitatory and total conductance, whereas in the HC state there is a marked drop of inhibitory and total conductance just before the spike. **C**. Same as **B** for guinea-pig cortical neurons under dynamic-clamp. **D**. Conductance standard deviations (SD) from the same experiment as in **C**: in the LC state, only excitatory SD drops before the spike, whereas in the HC state only inhibitory SD shows a significant decrease.

2.3 Spike-triggered averages during activated states

In order to determine the optimal pattern of conductance that triggers spikes, we first compared LC and HC states using a Hodgkin-Huxley type model. The predictions of this model were then tested using dynamic-clamp experiments in guinea-pig cortical slices.

Using a single-compartment model, we have calculated spike-triggered averages (STA) of the excitatory and inhibitory conductances. As shown in Fig.2.1 **B**, in LC states, excitatory conductances always increase before the spike, while inhibitory conductances decrease. This is paralleled by an increase in total membrane conductance just before the spike, suggesting that spikes are preferentially evoked by an increase of excitatory conductance. In HC states, however, the total conductance decreases before the spike, which is necessarily caused by a decrease in inhibitory conductance. Thus, in this case, spikes are preferentially evoked by a drop of inhibition. Examination of single-trial conductance traces confirmed this analysis (not shown).

This prediction was tested in real cortical neurons using dynamic-clamp. LC and HC states were recreated by injecting fluctuating conductances similar to the model. The STAs showed the same behavior as in the model, also suggesting that spikes are evoked by a drop of inhibitory conductance in HC states (cf. Fig.2.1 **C**). The spike-triggered variances showed that in LC states, spikes were correlated with a decrease of variance of excitatory conductance, but not of inhibitory conductance (Fig.2.1 **D**, left panel). In contrast, in HC states only the variance of inhibitory conductance decreased shortly before spikes (cf. Fig.2.1 **D**, right panel), suggesting that the dynamics of inhibition has a determinant influence on spiking in HC states.

2.4 Discussion

We have examined two extreme cases taken from a continuum of noisy states, which evoke similar *in vivo*-like V_m dynamics. With respect to the optimal conductance pattern triggering spikes, we found that these patterns are very different in these two states. In LC states, spikes are preferentially evoked by an increase of excitation, associated with an increase of the total membrane conductance, which is a rather classic mode of firing. In HC states, however, spikes are preferentially evoked by a decrease of inhibitory conductance, which is associated to a decrease of the total membrane conductance. We predict that this mode of firing should be found *in vivo*, in high-conductance states where conductance measurements show dominant inhibitory conductances (Destexhe et al. 2003). Note that the present study was limited to conductance standard deviations (SDs) that are proportional to the respective mean conductances. Further investigations are needed to explore

2.5. REFERENCES

the effect of independently varying conductance SDs on the firing mode.

In order to identify this mode of firing from intracellular recordings *in vivo*, we need to design specific methods to extract spike-triggered patterns of conductances from V_m activity. This task is not trivial, because of the presence of dominant intrinsic voltage-dependent currents in proximity to spikes, and also because conductances are related to the V_m through the cable equation, which is in general not solvable analytically. So, in order to extract the conductance traces prior to the spike from V_m activity, one needs to use a series of approximations. We are presently considering different approximations to yield this information with the goal to characterize the role of inhibitory conductance dynamics in modulating firing activity during active states *in vivo*. Preliminary results from analyzing intracellular data from cat parietal cortex *in vivo* indeed suggest a drop of conductance prior to the spike (Pospischil et al. 2005).

2.5 References

- Paré D., Shink E., Gaudreau H., Destexhe A. and Lang E.J. Impact of spontaneous synaptic activity on the resting properties of cat neocortical neurons *in vivo*. *J. Neurophysiol.* **79**: 1450-1460, 1998.
- Steriade M., Timofeev I. and Grenier F. Natural waking and sleep states: a view from inside neocortical neurons. *J. Neurophysiol.* **85**: 1969-1985, 2001.
- Destexhe A., Rudolph M. and Paré D. The high-conductance state of neocortical neurons *in vivo*. *Nature Reviews Neurosci.* **4**: 739-751, 2003.
- Pospischil M., Rudolph M., Shulz D., Timofeev I. and Destexhe A. Are we inhibited when we are awake ? A combined intracellular and computational analysis of membrane potential dynamics in cortical neurons of awake and naturally sleeping animals. *Society for Neuroscience Abstracts* **31**: 276.15, 2005.

Chapter 3

Calculating event-triggered average synaptic conductances from the membrane potential

Martin Pospischil, Zuzanna Piwkowska, Michelle Rudolph, Thierry Bal and Alain Destexhe. Calculating event-triggered average synaptic conductances from the membrane potential. *J Neurophysiol* **97**: 2544–2552, 2007.

Résumé

Introduction

Les résultats du chapitre précédent montrent deux modes de genèse du PA dans les neurones, soit par augmentation d'excitation, soit par diminution d'inhibition. Afin de distinguer de tels modes dans les neurones *in vivo*, il est nécessaire d'estimer les "spike-triggered averages" (STA) à partir de l'activité du potentiel membranaire (V_m). Aucune méthode ne permet actuellement de faire une telle estimation. Dans cet article, nous proposons une telle méthode pour estimer les STAs des conductances à partir du V_m .

Résultats obtenus

Dans un premier temps, nous exposons la méthode d'estimation des STAs, qui est basée sur une discrétisation de l'axe du temps. On obtient un système d'équations algébriques dont la solution donne les conductances "les plus probables".

Cette méthode est ensuite testée à l'aide de modèles computationnels (modèle intègre-et-tire avec conductances stochastiques). Les tests montrent que la méthode procure une estimation en excellent accord avec les conductances réellement injectées dans le modèle.

Finalement, la méthode est testée sur des neurones du cortex visuel *in vitro* par la technique de dynamic-clamp. Parce que les conductances sont injectées par l'expérimentateur, il est également possible de comparer la méthode avec le STA obtenu avec les conductances injectées, et un excellent accord est également obtenu.

Conclusions

En conclusion, nous proposons ici une méthode qui, pour la première fois, permettra l'estimation de STA de conductances excitatrices et inhibitrices à partir du potentiel de membrane seulement. L'application de ce type de méthode *in vivo* est désormais possible.

3.1 Abstract

The optimal patterns of synaptic conductances for spike generation in central neurons is a subject of considerable interest. Ideally, such conductance time courses should be extracted from membrane potential (V_m) activity, but this is difficult because the nonlinear contribution of conductances to the V_m renders their estimation from the membrane equation extremely sensitive. We outline here a solution to this problem based on a discretization of the time axis. This procedure can extract the time course of excitatory and inhibitory conductances solely from the analysis of V_m activity. We test this method by calculating spike-triggered averages of synaptic conductances using numerical simulations of the integrate-and-fire model subject to colored conductance noise. The procedure was also tested successfully in biological cortical neurons using conductance noise injected with dynamic-clamp. This method should allow the extraction of synaptic conductances from V_m recordings in vivo.

3.2 Introduction

Determining the optimal features of stimuli which are needed to obtain a given response is of considerable interest, for example in sensory physiology. Reverse-correlation is one of the most-used methods to obtain such estimates (Agüera y Arcas and Fairhall 2003; Badel et al. 2006) and, in particular, the spike-triggered average (STA) is often used to determine optimal features linked to the genesis of action potentials (de Boer and Kuypers 1968). The STA can be used to explore which feature of stimulus space the neuron is sensitive to, or to identify modes that contribute either to spiking or to the period of silence before the spike (Agüera y Arcas and Fairhall 2003). Using intracellular recordings, it is straightforward to calculate the STA of the membrane potential (V_m), which yields the mean voltage trajectory preceding spikes. In contrast, it is much harder to determine the underlying synaptic conductance. Straightforward methods like recording at several different DC levels and estimating the total conductance from the ratio $\Delta I / \Delta V$ fail, since the presence of a voltage threshold necessitates $\Delta V \rightarrow 0$ at the time of the spike, which, in turn, artificially suggests a divergence of the total conductance to infinity. Similarly, solving the membrane equation for excitatory and inhibitory conductances separately suffers from an additional complication: because the distance to threshold changes, the time courses of the average synaptic conductances depend on the injected current.

Recent contributions (Badel et al. 2006; Paninski 2006a, 2006b) gave analytical expressions for the most likely voltage path, which in the low-noise limit approximates the STA of the leaky integrate-and-fire (IF) neuron. In those cases, Gaussian white noise current was considered as input. In Badel et al. (2006), a

3.3. MATERIAL AND METHODS

second state variable was added in order to obtain biophysically more realistic behavior. In Paninski (2006a, 2006b), in addition the exact voltage STA for the non-leaky IF neuron was computed, as well as the STA input current in discrete time. Here, a strong dependence of the STA shape on the time resolution dt was found without a stable limit as $dt \rightarrow 0$. It was argued heuristically that this behavior results from the fact that increasing the bandwidth of the input current, a point which was supported by numerical simulations (Paninski et al. 2004; Pillow and Simoncelli 2003), in which a pre-filtering of the white noise input results in a stable limit STA.

In this article, we focus on the problem of estimating the optimal conductance patterns required for spike initiation, based solely on the analysis of V_m activity. We consider neurons subject to conductance-based synaptic noise at both excitatory and inhibitory synapses. By discretizing the time axis, it is possible to obtain the probability distribution of conductance time courses that are compatible with the observed voltage STA. Due to the symmetry properties of the probability distribution, the STA time course of excitatory and inhibitory conductances can then be extracted by choosing the one with maximum likelihood. We test this method in numerical simulations of the IF model, as well as in real cortical neurons using the dynamic-clamp technique, by comparing the estimated STA with the real STA deduced from the injected conductances.

3.3 Material and Methods

3.3.1 Models

We considered neurons driven by synaptic noise described by two independent sources of colored conductance noise (point-conductance model (Destexhe et al. 2001)). The membrane equation of this system is given by:

$$C \frac{dV(t)}{dt} = -g_L(V(t) - V_L) - g_e(t)(V(t) - V_e) - g_i(t)(V(t) - V_i) + I_{DC}, \quad (3.1)$$

$$\frac{dg_s(t)}{dt} = -\frac{1}{\tau_s}(g_s(t) - g_{s0}) + \sqrt{\frac{2\sigma_s^2}{\tau_s}}\xi_s(t), \quad (3.2)$$

Here, g_L , $g_e(t)$ and $g_i(t)$ are the conductances of leak, excitatory and inhibitory currents, V_L , V_e , V_i are their respective reversal potentials, C is the capacitance and I_{DC} a constant current. The subscript s in Eq. (3.2) can take the values e, i , which in turn indicate the respective excitatory or inhibitory channel. We use g_{s0} and σ_s to indicate the mean and standard deviation (SD) of the conductance distributions, $\xi_s(t)$ are Gaussian white noise processes with zero mean and unit

standard deviation. Throughout this article we use the correlation times $\tau_e = 2.728$ ms and $\tau_i = 10.49$ ms.

This system was solved using numerical simulations of the leaky IF model, which was adjusted to match recordings of cortical neurons in slices (threshold -55 mV, refractory period 3 ms, reset -75 mV). Simulations were done using the NEURON simulation environment (Hines and Carnevale 1997). To calculate STAs, approximately 1000 spikes occurring during spontaneous activity were used, each being preceded by a period of at least 100 ms of silence to avoid “contamination” of the V_m STA by preceding spikes. The same analysis protocols (see Results) were applied to the model and to experimental data.

In order to address the influence of a dendritic filter on the reliability of our method, we used a two-compartment model based on that by Pinsky and Rinzel (1994). We removed all active channels and replaced them by an integrate-and-fire mechanism at the soma. The geometry ($L = 3.18$ μm , $\text{diam} = 10$ μm) as well as the parameters not related to the spiking mechanism ($g_L = 10^{-4}$ S/cm², $V_L = -60$ mV, capacitance $c_m = 3$ $\mu\text{F}/\text{cm}^2$, axial resistance $R_a = 5.87 \times 10^5$ Ωcm) are identical for the two compartments. In addition, we chose a threshold for spiking $V_t = -55$ mV at the soma. The parameters for leak conductance and capacitance needed for the estimation of the STAs of synaptic conductances from the V_m , g_L^{so} and C^{so} , were obtained by current pulse injection into the soma at the resting state. The superscript *so* indicates that these are effective values at the level of the soma. The values used were $g_L^{so} = 0.198$ nS and $C^{so} = 5.86$ pF. The parameters describing the distributions of synaptic conductances were chosen in a way such that the mean inhibitory conductance was four times that of excitation, and the latter was comparable to the leak conductance ($g_{e0} = 0.15$ nS, $g_{i0} = 0.6$ nS). Standard deviations were assumed to be one third of the respective means ($\sigma_e = 0.05$ nS, $\sigma_i = 0.2$ nS).

3.3.2 In vitro experiments

In vitro experiments were performed on 0.4 mm thick coronal or sagittal slices from the lateral portions of guinea-pig occipital cortex. Guinea-pigs, 4-12 weeks old (CPA, Olivet, France), were anesthetized with sodium pentobarbital (30 mg/kg). The slices were maintained in an interface style recording chamber at 33-35°C. Slices were prepared on a DSK microslicer (Ted Pella Inc., Redding, CA) in a slice solution in which the NaCl was replaced with sucrose while maintaining an osmolarity of 307 mOsm. During recording, the slices were incubated in slice solution containing (in mM): NaCl, 124; KCl, 2.5; MgSO₄, 1.2; NaHPO₄, 1.25; CaCl₂, 2; NaHCO₃, 26; dextrose, 10, and aerated with 95% O₂, 5% CO₂ to a final pH of 7.4. Intracellular recordings following two hours of recovery were performed in deep layers (layer IV, V and VI) in electrophysiologically identified regular spiking and intrinsically bursting cells. Electrodes for intracellular recordings were made on

3.4. RESULTS

a Sutter Instruments P-87 micropipette puller from medium-walled glass (WPI, 1BF100) and beveled on a Sutter Instruments beveler (BV-10M). Micropipettes were filled with 1.2 to 2 M potassium acetate and had resistances of 80-100 M Ω after beveling.

The dynamic-clamp technique (Robinson et al. 1993; Sharp et al. 1993) was used to inject computer-generated conductances in real neurons. Dynamic-clamp experiments were run using the hybrid RT-NEURON environment (developed by G. Le Masson, Université de Bordeaux), which is a modified version of NEURON (Hines and Carnevale 1997) running under the Windows 2000 operating system (Microsoft Corp.). NEURON was augmented with the capacity of simulating neuronal models in real time, synchronized with the intracellular recording. To achieve real-time simulations as well as data transfer to the PC for further analysis, we used a PCI DSP board (Innovative Integration, Simi Valley, USA) with 4 analog/digital (inputs) and 4 digital/analog (outputs) 16 bits converters. The DSP board constrains calculations of the models and data transfers to be made with a high priority level by the PC processor. The DSP board allows input (for instance the membrane potential of the real cell incorporated in the equations of the models) and output signals (the synaptic current to be injected into the cell) to be processed at regular intervals (time resolution = 0.1 ms). A custom interface was used to connect the digital and analog inputs/outputs signals of the DSP board with the intracellular amplifier (Axoclamp 2B, Axon Instruments) and the data acquisition systems (PC-based acquisition software ELPHY, developed by G. Sadoc, CNRS Gif-sur-Yvette, ANVAR and Biologic). The dynamic-clamp protocol was used to insert the fluctuating conductances underlying synaptic noise in cortical neurons using the point-conductance model, similar to a previous study (Destexhe et al. 2001). According to Eq. (3.1) above, the injected current is determined from the fluctuating conductances $g_e(t)$ and $g_i(t)$ as well as from the difference of the membrane voltage from the respective reversal potentials, $I_{DynClamp} = -g_e(V - V_e) - g_i(V - V_i)$.

All research procedures concerning the experimental animals and their care adhered to the American Physiological Society's Guiding Principles in the Care and Use of Animals, to the European Council Directive 86/609/EEC and to European Treaties series no. 123, and was also approved by the local ethics committee "Ile-de-France Sud" (certificate no. 05-003).

3.4 Results

We first explain the method for extracting STAs from V_m activity, then we present tests of this method using numerical simulations and intracellular recordings in dynamic-clamp.

3.4.1 Method to extract conductance STA

The procedure we follow here to estimate STA of conductances from V_m activity is based on a discretization of the time axis. With this approach, a probability distribution can be constructed whose maximum gives the most likely conductance path compatible with the STA of the V_m . This maximum is determined by a system of linear equations which is solvable if the means and variances of conductances are known (for a method to estimate conductance mean and variance, see Rudolph et al. 2004).

We start from the voltage STA, which is an average over an ensemble of event-triggered voltage traces. Its relation to the conductance STAs is determined by the ensemble average of Eqs. (3.1) and (3.2). In general, there is a strong correlation (or anti-correlation) between $V(t)$ and $g_s(t)$ in time. However, it is safe to assume that there is no such correlation across the ensemble, since the noise processes $\xi_s(t)$ corresponding to each realization are uncorrelated. Also, the ensemble average is commutative with the time derivative. Thus, we can rewrite Eqs. (3.1) and (3.2) to obtain

$$\begin{aligned} \frac{d\langle V(t) \rangle_x}{dt} = & -\frac{1}{\tau_L} (\langle V(t) \rangle_x - V_L) \\ & - \frac{\langle g_e(t) \rangle_x}{C} (\langle V(t) \rangle_x - V_e) - \frac{\langle g_i(t) \rangle_x}{C} (\langle V(t) \rangle_x - V_i) + \frac{I_{DC}}{C}, \end{aligned} \quad (3.3)$$

$$\frac{d\langle g_s(t) \rangle_x}{dt} = -\frac{1}{\tau_s} (\langle g_s(t) \rangle_x - g_{s0}) + \sqrt{\frac{2\sigma_s^2}{\tau_s}} \langle \xi_s(t) \rangle_x, \quad (3.4)$$

where $\tau_L = C/g_L$ and $\langle \cdot \rangle_x$ denotes the ensemble average. In other words, the time evolution Eqs (3.1) and (3.2) also hold in terms of ensemble averages. In the following, we drop the bracket notation for legibility, but assume we are dealing with ensemble averaged quantities unless otherwise stated.

We discretize Eq. (3.3) in time with a step-size Δt and solve for g_i^k ,

$$g_i^k = -\frac{C}{V^k - V_i} \left\{ \frac{V^k - V_L}{\tau_L} + \frac{g_e^k(V^k - V_e)}{C} + \frac{V^{k+1} - V^k}{\Delta t} - \frac{I_{DC}}{C} \right\}. \quad (3.5)$$

Since the series V^k for the voltage STA is known, g_i^k has become a function of g_e^k . In the same way, we solve Eq. (3.4) for ξ_s^k , which have become Gaussian distributed random numbers,

$$\xi_s^k = \frac{1}{\sigma_s} \sqrt{\frac{\tau_s}{2\Delta t}} \left(g_s^{k+1} - g_s^k \left(1 - \frac{\Delta t}{\tau_s} \right) - \frac{\Delta t}{\tau_s} g_{s0} \right). \quad (3.6)$$

There is a continuum of combinations $\{g_e^{k+1}, g_i^{k+1}\}$ that can advance the mem-

3.4. RESULTS

brane potential from V^{k+1} to V^{k+2} , each pair occurring with a probability

$$p^k := p(g_e^{k+1}, g_i^{k+1} | g_e^k, g_i^k) = \frac{1}{2\pi} e^{-\frac{1}{2}(\xi_e^{k2} + \xi_i^{k2})} = \frac{1}{2\pi} e^{-\frac{1}{4\Delta t} X^k}, \quad (3.7)$$

$$\begin{aligned} X^k = & \frac{\tau_e}{\sigma_e^2} \left(g_e^{k+1} - g_e^k \left(1 - \frac{\Delta t}{\tau_e} \right) - \frac{\Delta t}{\tau_e} g_{e0} \right)^2 \\ & + \frac{\tau_i}{\sigma_i^2} \left(g_i^{k+1} - g_i^k \left(1 - \frac{\Delta t}{\tau_i} \right) - \frac{\Delta t}{\tau_i} g_{i0} \right)^2, \end{aligned} \quad (3.8)$$

where we have used Eq. (3.6). Note that because of Eq. (3.5), g_e^k and g_i^k are not independent and p^k is, thus, a unidimensional distribution only. Given initial conductances g_s^0 , we can now write down the probability p for certain series of conductances $\{g_s^j\}_{j=0,\dots,n}$ to occur that reproduce a given voltage trace $\{V^l\}_{l=1,\dots,n+1}$:

$$p = \prod_{k=0}^{n-1} p^k. \quad (3.9)$$

Due to the symmetry of the distribution p , the average paths of the conductances coincide with the most likely ones, so the cumbersome task of solving nested Gaussian integrals can be circumvented. Instead, in order to determine the conductance series with extremal likelihood, we solve the n -dimensional system of linear equations

$$\left\{ \frac{\partial X}{\partial g_e^k} = 0 \right\}_{k=1,\dots,n}, \quad (3.10)$$

where $X = \sum_{k=0}^{n-1} X^k$, for the vector $\{g_e^k\}$. This is equivalent to solving $\{\frac{\partial p}{\partial g_e^k} = 0\}_{k=1,\dots,n}$ and involves the numerical inversion of an $n \times n$ -matrix. Since the system of equations is linear, if there is a solution for $\{g_e^k\}$, plausibility arguments suggest that it is the most likely (rather than the least likely) excitatory conductance time course. The series $\{g_i^k\}$ is then obtained from Eq. (3.5).

3.4.2 Test of the accuracy of the method using numerical simulations

To test this method, we first considered numerical simulations of the IF model in four different situations. We distinguished high-conductance states, where the total conductance is dominated by inhibition, from low-conductance states, where both synaptic conductances are of comparable magnitude. We also varied the standard deviations of the conductances such that for both high- and low-conductance states we have the cases $\sigma_i > \sigma_e$ as well as $\sigma_e > \sigma_i$. The results are summarized in Fig. 3.1, where the STA traces of excitatory and inhibitory conductances

recorded from simulations are compared to the most likely (equivalent to the average) conductance traces obtained from solving Eq. (3.10). In general, the plots demonstrate a very good agreement.

To quantify our results, we investigated the effect of the statistics as well as of the broadness of the conductance distributions on the quality of the estimation. The latter is crucial, because the derivation of the most likely conductance time course allows for negative conductances, whereas in the simulations negative conductances lead to numerical instabilities, and conductances are bound to positive values. We thus expect an increasing error with increasing ratio SD/mean of the conductance distributions. We estimated the root-mean-square (RMS) of the difference between the recorded and the estimated conductance STAs. The results, summarized in Fig. 3.2, are as expected. Increasing the number of spikes enhances the match between theory and simulation (Fig. 3.2A shows the RMS deviation for excitation, 3.2B for inhibition) up to the point where the effect of negative conductances becomes dominant. In this example, where the ratio SD/mean was fixed at 0.1, the RMS deviation enters a plateau at about 7000 spikes. The plateau values can also be recovered from the neighboring plots (i.e., the RMS deviations at SD/mean = 0.1 in Fig. 3.2 C and D correspond to the plateau values in A and B). On the other hand, a broadening of the conductance distribution yields a higher deviation between simulation and estimation. However, at SD/mean = 0.5, the RMS deviation is still as low as $\sim 2\%$ of the mean conductance for excitation and $\sim 4\%$ for inhibition.

To assess the effect of dendritic filtering on the reliability of the method, we used a two-compartment model based on that of Pinsky and Rinzel (1994), from which we removed all active channels and replaced them by an integrate-and-fire mechanism at the soma. We repeatedly injected the same 100 s sample of fluctuating excitatory and inhibitory conductances in the dendritic compartment and performed two different recording protocols at the soma (Fig. 3.3A). First, we recorded in current-clamp in order to obtain the V_m time course as well as the spike times. In this case, the leak conductance g_L^{so} and the capacitance C^{so} were obtained from current pulse injection at rest. Second, we simulated an “ideal” voltage-clamp (no series resistance) at the soma using two different holding potentials (we chose the reversal potentials of excitation and inhibition, respectively). Then, from the currents I_{V_e} and I_{V_i} , one can calculate the conductance time courses as

$$g_{e,i}^{so}(t) = \frac{I_{V_{i,e}}(t) - g_L(V_{i,e} - V_L)}{V_{i,e} - V_{e,i}}, \quad (3.11)$$

where the superscript *so* indicates that these are the conductances seen at the soma (in the following referred to as somatic conductances). From these, we determined the parameters g_{e0}^{so} , g_{i0}^{so} , σ_e^{so} and σ_i^{so} , the conductance means and standard deviations. In contrast to $g_e(t)$ and $g_i(t)$, the distributions of $g_e^{so}(t)$ and $g_i^{so}(t)$ are not Gaussian (not shown), and have lower means and variances. We compared the

3.4. RESULTS

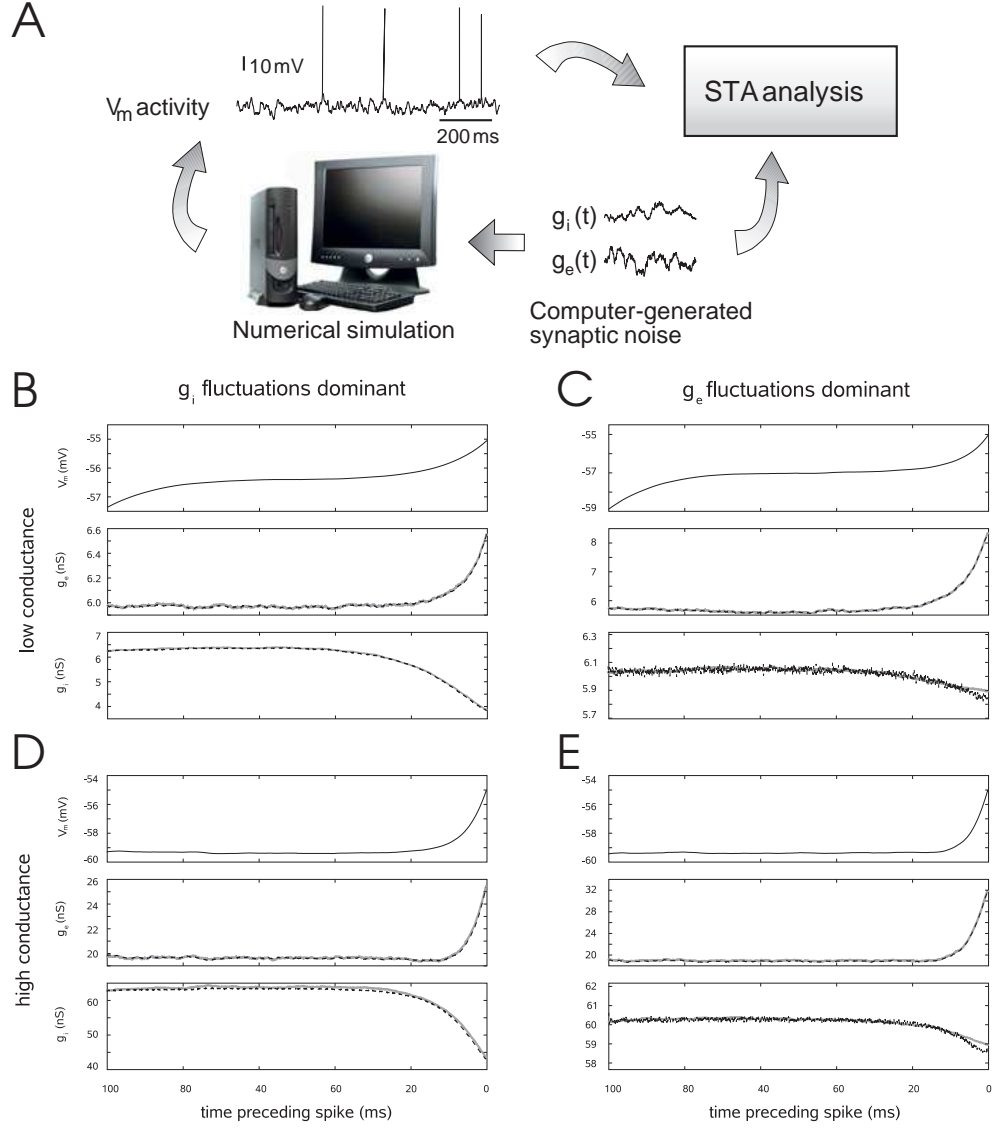


Figure 3.1: Test of the STA analysis method using an IF neuron model subject to colored conductance noise. **A**. Scheme of the procedure used. An IF model with synaptic noise was simulated numerically (bottom) and the procedure to estimate STA was applied to the V_m activity (top). The estimated conductance STAs from V_m were then compared to the actual conductance STA in this model. Bottom panels: STA analysis for different conditions, low-conductance states (**B,C**), high-conductance states (**D,E**), with fluctuations dominated by inhibition (**B,D**) or by excitation (**C,E**). For each panel, the upper graph shows the voltage STA, the middle graph the STA of excitatory conductance, and the lower graph the STA of inhibitory conductance. Solid lines (grey) show the average conductance recorded from the simulation, while the dashed line (black) represents the conductance estimated from the V_m . Parameters in **B**: $g_{e0}=6$ nS, $g_{i0}=6$ nS, $\sigma_e=0.5$ nS, $\sigma_i=1.5$ nS; **C**: $g_{e0}=6$ nS, $g_{i0}=6$ nS, $\sigma_e=1.5$ nS, $\sigma_i=0.5$ nS; **D**: $g_{e0}=20$ nS, $g_{i0}=60$ nS, $\sigma_e=4$ nS, $\sigma_i=12$ nS; **E**: $g_{e0}=20$ nS, $g_{i0}=60$ nS, $\sigma_e=6$ nS, $\sigma_i=3$ nS

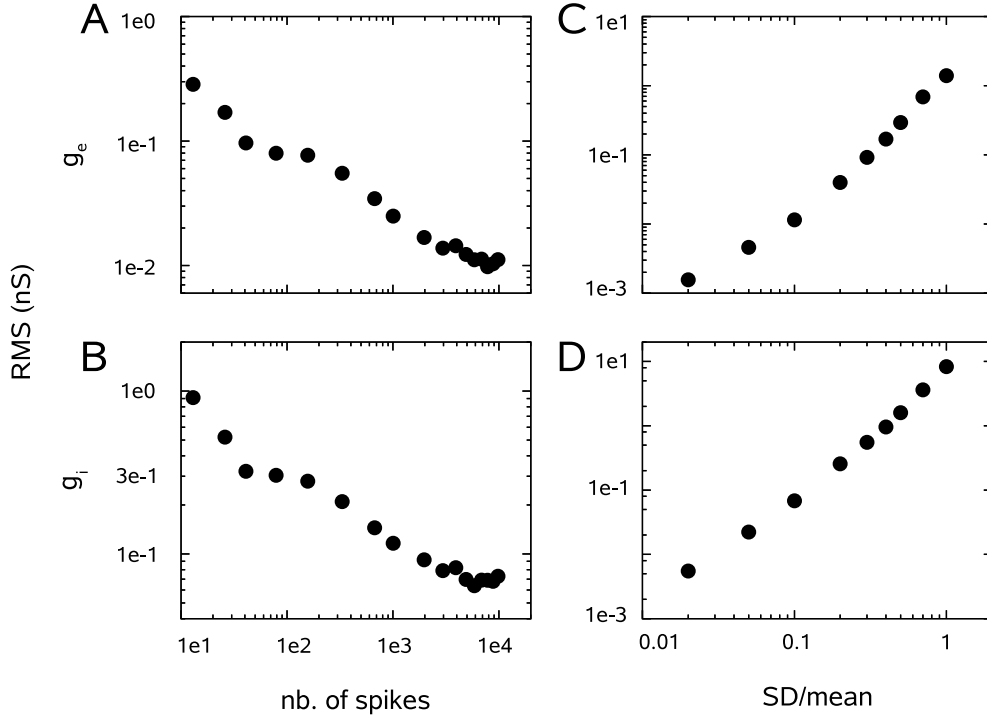


Figure 3.2: The root-mean-square (RMS) of the deviation of the estimated from the recorded STAs. A: RMS deviation as a function of the number of spikes for the STA of excitatory conductance, where the SD of the conductance distribution was 10% of its mean. The RMS deviation first decreases with the number of spikes, but saturates at ~ 7000 spikes. This is due to the effect of negative conductances, which are excluded in the simulation (cf. C). B: Same as A for inhibition. C: RMS deviation for excitation as a function of the ratio SD/mean of the conductance distribution. The higher the probability of negative conductances, the higher the discrepancy between theory and simulation. However, at $SD/mean = 0.5$, the mean deviation is as low as $\sim 2\%$ of the mean conductance for excitation and $\sim 4\%$ for inhibition. D: Same as C for inhibition.

3.4. RESULTS

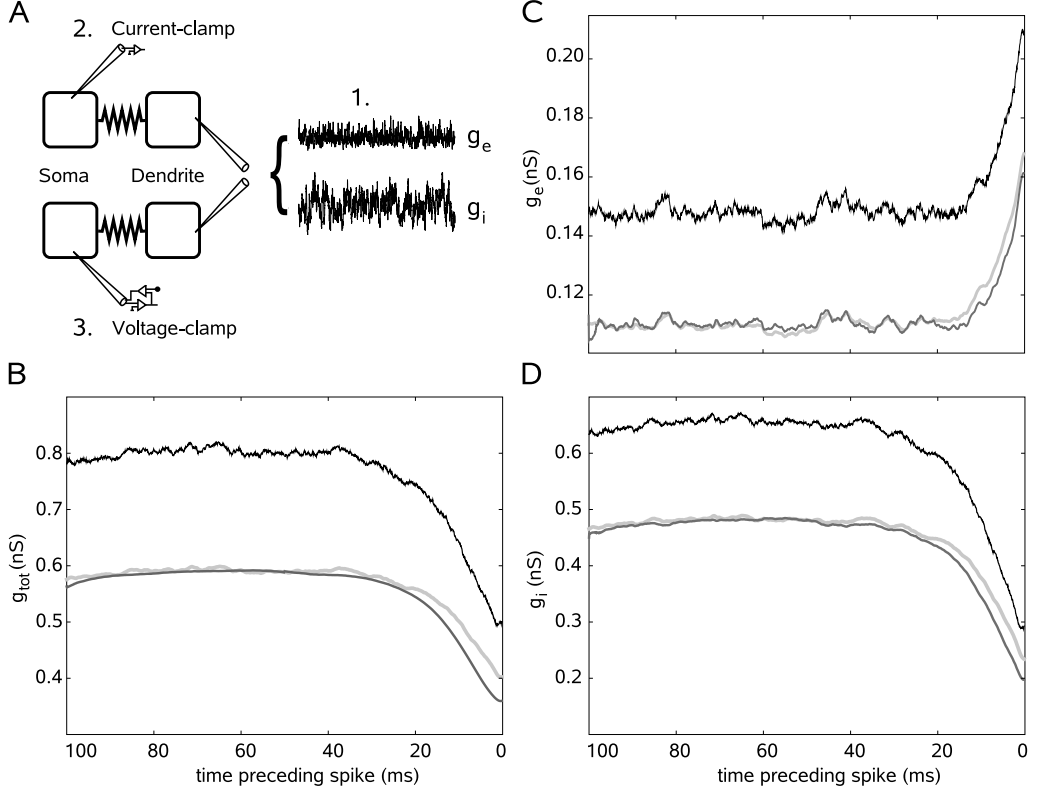


Figure 3.3: Test of the method using dendritic conductances. A. Simulation scheme: A 100 s sample of excitatory and inhibitory (frozen) conductance noise was injected into the dendrite of a 2-compartment model (1). Then, two different recording protocols were performed at the soma. First, the V_m time course was recorded in current-clamp (2), second, the currents corresponding to two different holding potentials were recorded in voltage-clamp (3). From the latter, the excitatory and inhibitory conductance time courses were extracted using Eq. 3.11. B. STA of total conductance inserted at the dendrite (black), compared with the estimate obtained in voltage-clamp (light gray) and with that obtained from somatic V_m activity using the method (dark gray). Due to dendritic attenuation, the total conductance values measured are lower than the inserted ones, but the variations of conductances preceding the spike are conserved. C. Same as B, for excitatory conductance. D. Same as B, for inhibitory conductance. Parameters: $g_{e0} = 0.15$ nS, $g_{i0} = 0.6$ nS, $\sigma_e = 0.05$ nS, $\sigma_i = 0.2$ nS, $g_{e0}^{so} = 0.113$ nS, $g_{i0}^{so} = 0.45$ nS, $\sigma_e^{so} = 0.034$ nS, $\sigma_i^{so} = 0.12$ nS, where the superscript *so* denotes quantities as seen at the soma.

STA of the injected (dendritic) conductance, the STA obtained from the somatic V_m using our method and the STA obtained using a somatic “ideal” voltage-clamp (see Fig. 3.3B-D), which demonstrated the following points: (1) as expected, due to dendritic attenuation, all somatic estimates were attenuated compared to the actual conductances injected in dendrites (compare light and dark gray curves, soma, with black curve, dendrite, in Fig. 3.3B-D); (2) the estimate obtained by applying the present method to the somatic V_m (dark gray curves in Fig. 3.3B-D) was very similar to that obtained using an “ideal” voltage-clamp at the soma (light gray curves). The difference close to the spike may be due to the non-Gaussian shape of the somatic conductance distributions, whose tails then become important; (3) despite attenuation, the qualitative shape of the conductance STA was preserved. We conclude that the STA estimate from V_m activity captures rather well the conductances as seen by the spiking mechanism.

3.4.3 Test of the method in real neurons

We also tested the method on voltage STAs obtained from dynamic-clamp recordings of guinea-pig cortical neurons in slices. In real neurons, a problem is the strong influence of spike-related voltage-dependent (presumably sodium) conductances on the voltage time course. Since we maximize the *global* probability of $g_e(t)$ and $g_i(t)$, the voltage in the vicinity of the spike has an influence on the estimated conductances at all times. As a consequence, without removing the effect of sodium, the estimation fails (see Fig. 3.4). Fortunately, it is rather simple to correct for this effect by excluding the last 1–2 ms before the spike from the analysis. The corrected comparison between the recorded and the estimated conductance traces is shown in Fig. 3.5.

Finally, to check for the applicability of this method to *in vivo* recordings, we assessed the sensitivity of the estimates with respect to the different parameters by varying the values describing passive properties and synaptic activity. We assume that the total conductance can be constrained by input resistance measurements, and that time constants of the synaptic currents can be estimated by power spectral analyses (Destexhe and Rudolph 2004). This leaves g_L , C , g_{e0} , σ_e and σ_i as the main parameters. The impact of these parameters on STA conductance estimates is shown in Fig. 3.6. Varying these parameters within $\pm 50\%$ of their nominal value led to various degrees of error in the STA estimates. The dominant effect of a variation in the mean conductances is a shift in the estimated STAs, whereas a variation in the SDs changes the curvature just before the spike.

To address this point further, we fitted the estimated conductance STAs with an exponential function:

$$f_s(t) = G_s \left(1 + K_s e^{\frac{t-t_0}{T_s}} \right),$$

where s again takes the values e, i for excitation and inhibition, respectively. t_0 is

3.4. RESULTS

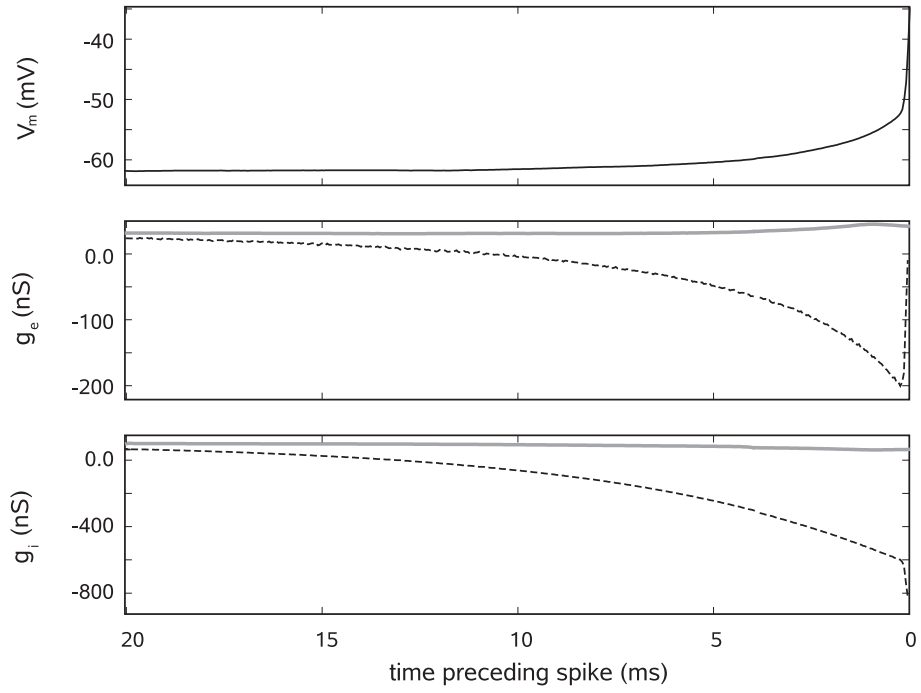


Figure 3.4: The effect of the presence of additional voltage-dependent conductances on the estimation of the synaptic conductances. Gray, solid lines indicate recorded conductances; black, dotted lines indicate estimated conductances. In this case, the estimation fails. The sharp rise of the voltage in the last ms before the spike requires very fast changes in the synaptic conductances, which introduces a considerable error in the analysis. Parameters used: $g_{e0}=32$ nS, $g_{i0}=96$ nS, $\sigma_e=8$ nS, $\sigma_i=24$ nS.

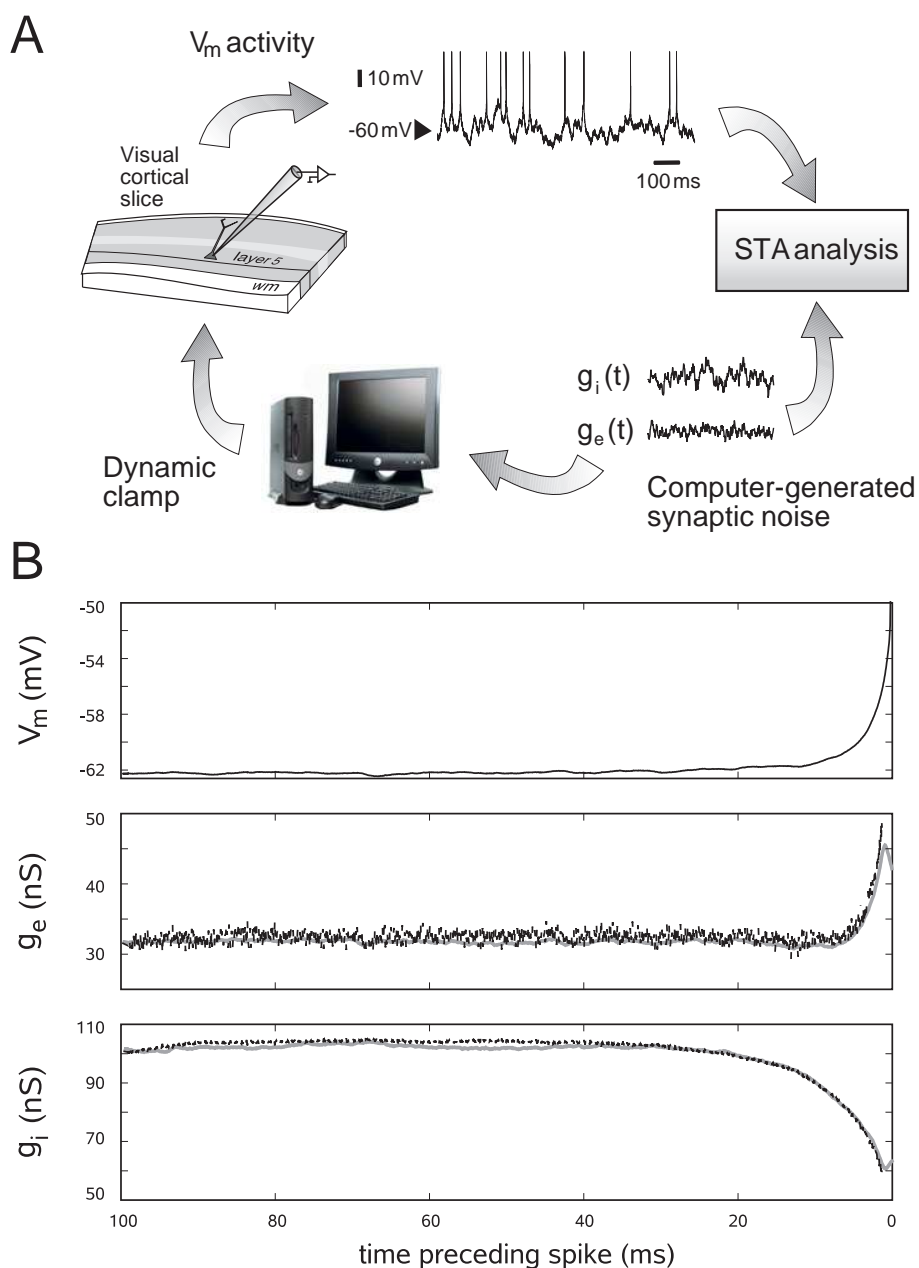


Figure 3.5: Test of the method in real neurons using dynamic-clamp in guinea-pig visual cortical slices. **A.** Scheme of the procedure. Computer-generated synaptic noise was injected in the recorded neuron under dynamic-clamp (bottom). The V_m activity obtained (top) was then used to extract the STA of conductances, which was compared to the STA directly obtained from the injected conductances. **B.** Results of this analysis in a representative neuron. Black lines show the estimated STA of conductances from V_m activity, grey lines show the STA of conductances that were actually injected into the neuron. The analysis was made by excluding the data from the 1.2 ms before the spike to avoid contamination by voltage-dependent conductances. Parameters for conductance noise were as in Fig. 3.4.

3.4. RESULTS

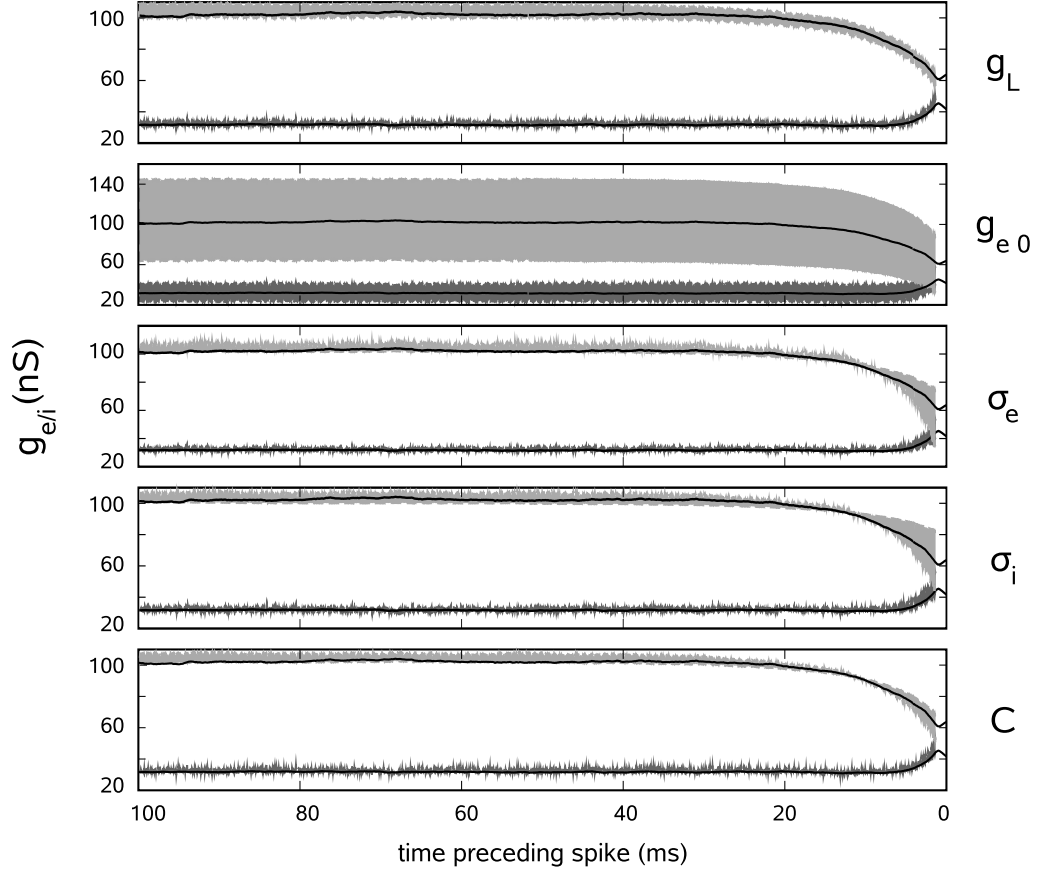


Figure 3.6: Deviation in the estimated conductance STAs in real neurons using dynamic-clamp due to variations in the parameters. The black lines represent the conductance STA estimates using the correct parameters, the gray areas are bound by the estimates that result from variation of a single parameter (indicated on the right) by $\pm 50\%$. Light gray areas represent inhibition, dark gray areas represent excitation. The total conductance (leak plus synaptic conductances) was assumed to be fixed. A variation in the mean values of the conductances evokes mostly a shift in the estimate, while a variation in the SDs influences the curvature just before the spike.

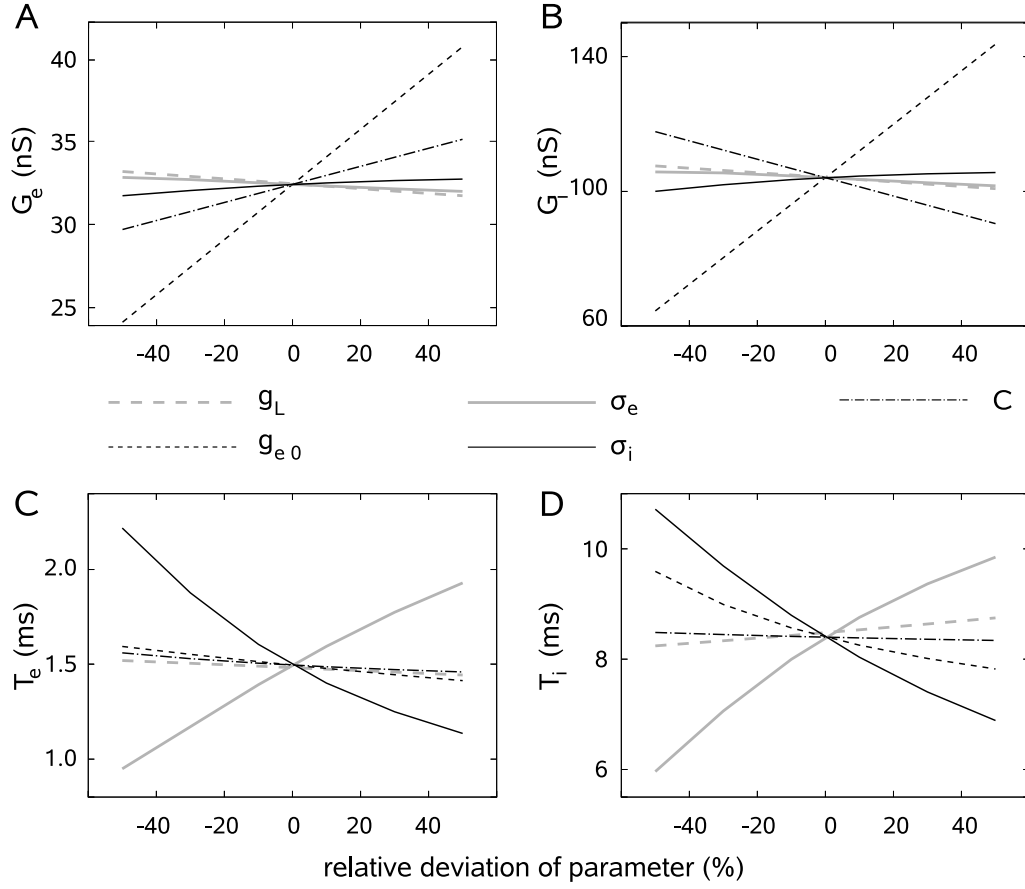


Figure 3.7: Detailed evaluation of the sensitivity to parameters. The conductance STAs were fitted with an exponential function $f_s(t) = G_s(1 + K_s \exp((t - t_0)/T_s))$, $s = e, i$. t_0 is chosen to be the time at which the analysis stops. Each plot shows the estimated value of G_e , G_i , T_e or T_i from this experiment, each curve represents the variation of a single parameter (see legend).

chosen to be the time at which the analysis stops. Fig. 3.7 gives an overview of the dependence of the fitting parameters G_e , G_i , T_e and T_i on the relative change of g_L , g_{e0} , σ_e , σ_i and C . For example, a variation of g_{e0} has a strong effect on G_e and G_i , but affects to a lesser extent T_e and T_i , while the opposite was seen when varying σ_e and σ_i .

3.5 Discussion

Understanding the transfer function of a neuron from synaptic input to spike output would ideally require the simultaneous monitoring of both the synaptic conductances and the cell's firing. Current methods for extracting synaptic conductances rely on intracellular recordings performed at different holding potentials

3.5. DISCUSSION

(in voltage-clamp) or different current levels (in current-clamp; e.g. Borg-Graham et al. 1998) and, as a consequence, they do not allow the establishment of a direct correspondence between synaptic conductances and spikes. Although these methods have been very useful, for example in establishing the synaptic structure of sensory receptive fields in a variety of systems (Monier et al. 2003; Wehr and Zador 2003; Wilent and Contreras 2005), they do not distinguish between trials that effectively produce spikes at a given latency and those that do not.

Here, we have presented a method to extract the average excitatory and inhibitory conductance patterns directly related to spike initiation. As illustrated in Fig. 3.8, this method can extract spike-related conductances based solely on the knowledge of V_m activity. First, the STA of the V_m is computed from the intracellular recordings. Next, by discretizing the time axis, one estimates the “most likely” conductance time courses that are compatible with the observed STA of V_m . Due to the symmetry of their distribution, the average conductance time courses coincide with the most likely ones, so integration over the entire stimulus space (whose dimension depends on the STA interval as well as on the temporal resolution) can be replaced by a differentiation and subsequent solution of a system of linear equations. Solving this system gives an estimate of the average conductance time courses. We demonstrated that this estimation gives reasonably accurate estimates for the leaky IF model, as well as in real neurons under dynamic-clamp.

Like any other method, this method suffers from several sources of error. Errors can result from nonlinearities in the I-V curve of the neuron, e.g. those due to voltage-dependent conductances. In agreement with this, we have shown that the subthreshold activation of spike-generating currents close to threshold can lead to severe misestimations of the conductances (Fig. 3.4). This problem can be circumvented by excluding a short period (1–2 ms) preceding the spike. To avoid contamination by voltage-dependent currents, this method should be complemented by a check for I-V curve linearity in the range of V_m considered. Note that a linear I-V curve does not guarantee the absence of voltage-dependent conductances. For example, if the mean interspike interval of the cell becomes too short, spike-related potassium currents might be present during a substantial fraction of the STA interval and could affect the estimation. This might diminish the applicability of the method to neurons spiking at high frequency, in particular to fast-spiking interneurons. Also, strong subthreshold dendritic conductances that are very remote from the soma could influence the STA estimate without being visible in the I-V curve. On the other hand, in cases where it is possible to parameterize these nonlinearities, they can be included in Eq. 3.5. It should thus be possible to extend the method in order to apply it to more complex models, for example the exponential integrate-and-fire model (Fourcaud-Trocme et al. 2003). Another possible extension would be to include voltage-dependent terms such as N-methyl-D-aspartate (NMDA) receptor-mediated synaptic currents, although

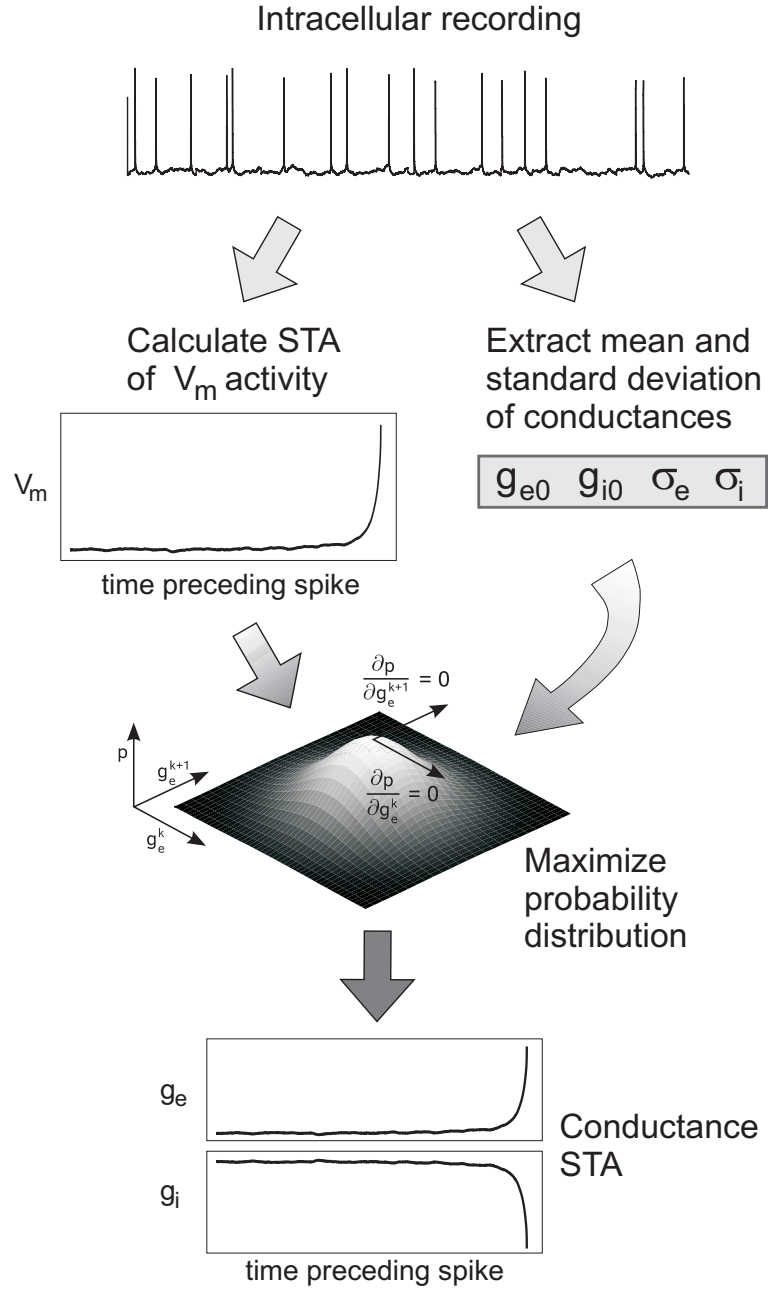


Figure 3.8: Scheme of the method to extract spike-triggered average conductances from membrane potential activity. Starting from an intracellular recording (top), the spike-triggered average (STA) membrane potential (V_m) is computed (leftmost panel). From the STA of the V_m , by discretizing the time axis, it is possible to estimate the STA of conductances (bottom) by maximizing a probability distribution (see text). This step requires knowledge of the values of the average conductances and their standard deviations (g_{e0} , g_{i0} , σ_e , σ_i , respectively), which must be extracted independently (rightmost panel).

3.6. ACKNOWLEDGMENTS

such currents probably have a limited contribution at the range of V_m considered here (below -50 mV).

Another source of error may arise from “negative conductances”. The present model of synaptic noise assumes that conductances are Gaussian-distributed, but if the standard deviation becomes comparable to the mean value of the conductances, the Gaussian distribution will include negative conductances, which are unrealistic. This is an important limitation of representing synaptic conductances by Gaussian-distributed noise (“diffusion approximation”). However, this type of approximation seems to apply well to cortical neurons *in vivo*, which receive a large number of inputs (Destexhe et al. 2001). *In vivo* measurements so far indicate that the standard deviation is much smaller than the mean for both excitatory and inhibitory conductances (Haider et al. 2006; Rudolph et al. 2005), which also indicates that the diffusion approximation is valid in this case. Such a check for consistency is a prerequisite for applying the present method.

Previous work related to the question of spike-triggered stimuli was mainly focused on white noise current inputs, and showed that no stable finite input average exists in the limit $dt \rightarrow 0$ (Paninski 2006a). Other contributions shed light on the question of membrane voltage STAs, for the leaky IF neuron as well as for biophysically more plausible models. However, so far no procedure was proposed to solve this problem of reverse correlation for conductance noise inputs. The method we propose here attempts to fill this gap, and directly provides a procedure that can be applied to real neurons. To this end, the present method must be complemented by measurements of the mean and standard deviation of excitatory and inhibitory conductances. Such measurements can be obtained either by voltage-clamp (Haider et al. 2006), or by current-clamp, as recently proposed (Rudolph et al. 2004, 2005). Combining the latter method with the present method, it should now be possible to directly extract conductance patterns from V_m recordings *in vivo*, and thus obtain estimates of the conductance variations related to spikes during natural network states.

3.6 Acknowledgments

We thank Romain Brette for discussions and Andrew Davison for comments on the manuscript. Research supported by the CNRS, the ANR (HR-CORTEX project), the Human Frontier Science Program, and the European Community (FACETS project IST 015879).

3.7 References

Agüera y Arcas B. and Fairhall A. L. What causes a neuron to spike? *Neural Computation* **15**: 1789-1807, 2003.

- Badel L., Gerstner W. and Richardson M.J.E. Dependence of the spike-triggered average voltage on membrane response properties. *Neurocomputing* **69**, 1062-1065, 2006.
- Borg-Graham L., Monier C. and Frégnac Y. Visual input evokes transient and strong shunting inhibition in visual cortical neurons. *Nature* **393**: 369-373, 1998.
- de Boer F. and Kuypers P. Triggered Correlation. *IEEE Trans. Biomed. Eng.* **15**: 169-197, 1968.
- Destexhe A. and Rudolph M. Extracting information from the power spectrum of synaptic noise. *J. Computational Neurosci.* **17**: 327-345, 2004.
- Destexhe A., Rudolph M. and Paré D. The high-conductance state of neocortical neurons *in vivo*. *Nature Reviews Neurosci.* **4**: 739-751, 2003.
- Destexhe A., Rudolph M., Fellous J.-M. and Sejnowski T. J. Fluctuating synaptic conductances recreate in-vivo-like activity in neocortical neurons. *Neuroscience* **107**: 13-24, 2001.
- Fourcaud-Trocme N., Hansel D., van Vreeswijk C., Brunel N. How spike generation mechanisms determine the neuronal response to fluctuating inputs. *J. Neurosci.* **23**(37): 11628-11640, 2003.
- Haider B., Duque A., Hasenstaub A.R. and McCormick D.A. Network activity in vivo is generated through a dynamic balance of excitation and inhibition. *J. Neurosci.* **26**: 4535-4545, 2006.
- Hines M. L. and Carnevale N. T. (1997) The NEURON simulation environment. *Neural Computation* **9**: 1179-1209, 1997
- Monier C., Chavane F., Baudot P., Borg-Graham L. and Frégnac Y. Orientation and direction selectivity of synaptic inputs in visual cortical neurons: a diversity of combinations produces spike tuning. *Neuron* **37**(4): 663-680, 2003.
- Paninski L. The spike-triggered average of the integrate-and-fire cell driven by Gaussian white noise. *Neural Computation* **18**: 2592-2616, 2006a.
- Paninski L. The most likely voltage path and large deviations approximations for integrate-and-fire neurons. *J. Comput. Neurosci.* **21**: 71-87, 2006b.
- Paninski L. , Pillow J. and Simoncelli E. Maximum likelihood estimation of a stochastic integrate-and-fire neural model. *Neural Computation* **16**: 2533-2561, 2004.

3.7. REFERENCES

- Pillow J. and Simoncelli E. Biases in white noise analysis due to non-Poisson spike generation. *Neurocomputing* **52**: 109-155, 2003.
- Pinsky P. F. and Rinzel J. Intrinsic and network rhythmogenesis in a reduced Traub model for CA3 neurons. *J. Comput. Neurosci.* **1**(1-2): 39-60, 1994.
- Robinson H. P. and Kawai N. Injection of digitally synthesized synaptic conductance transients to measure the integrative properties of neurons. *J. Neurosci. Methods* **49**(3): 157-165, 1993.
- Rudolph M., Pelletier J.-G., Par D. and Destexhe A. Characterization of synaptic conductances and integrative properties during electrically-induced EEG-activated states in neocortical neurons in vivo. *J. Neurophysiol.* **94**: 2805-2821, 2005.
- Rudolph M., Piwkowska Z., Badoual M., Bal T. and Destexhe A. A method to estimate synaptic conductances from membrane potential fluctuations. *J. Neurophysiol.* **91**: 2884-2896, 2004.
- Sharp A. A., O'Neil M. B., Abbott L. F. and Marder E. The dynamic clamp: artificial conductances in biological neurons. *Trends Neurosci.* **16**: 389-394, 1993.
- Wehr M. and Zador A. Balanced inhibition underlies tuning and sharpens spike timing in auditory cortex. *Nature* **426** (6965):442-446, 2003.
- Wilent W. and Contreras D. Dynamics of excitation and inhibition underlying stimulus selectivity in rat somatosensory cortex. *Nature Neurosci.* **8** (10):1364-1370, 2005.

Chapter 4

Inhibition determines membrane potential dynamics and controls action potential generation in awake and sleeping cat cortex

Michelle Rudolph, Martin Pospischil, Igor Timofeev and Alain Destexhe. Inhibition determines membrane potential dynamics and controls action potential generation in awake and sleeping cat cortex. *J Neurosci* **27**(20):5280-5290, 2007.

Résumé

Introduction

Les enregistrements intracellulaires chez le chat éveillé démontrent une activité intense et fluctuante, mais il n'est pas clair comment les neurones traitent l'information pendant ces états apparemment stochastiques. Afin de déterminer les conductances sous-jacentes à cette activité, nous appliquons plusieurs méthodes d'estimation de conductances aux neurones du cortex associatif, enregistrés chez le chat éveillé.

Résultats obtenus

A partir d'enregistrements intracellulaires chez le chat éveillé et en sommeil naturel (sommeil lent et paradoxal), nous estimons les conductance sous-jacentes par la technique "VmD". Cette analyse révèle une grande diversité de conductances dans les neurones, parfois dominés par l'excitation, mais le plus souvent dominés par l'inhibition. En effet, les conductances inhibitrices (moyenne et variance) sont en général plus fortes que leurs homologues excitatrices.

Ensuite, nous analysons ces mêmes neurones en utilisant la méthode STA exposée au chapitre précédant. Cette analyse démontre que les deux modes de PAs sont présents, mais les PAs évoqués par l'inhibition sont vus dans la majorité des neurones. Finalement, nous montrons que les deux estimations sont corrélées, c'est-à-dire que les neurones montrant une inhibition forte (états de haute conductance) sont aussi ceux dont les PAs sont évoqués par l'inhibition. Ils forment la majorité des neurones analysés pendant l'éveil et le sommeil lent.

Conclusions

En conclusion, cette étude démontre que les états "activés", comme l'éveil, sont définis au niveau de la conductance membranaire par (1) une grande diversité de combinaisons excitation-inhibition; (2) en général une inhibition dominante (états de haute conductance); (3) la variance de l'inhibition est presque toujours plus grande que celle de l'excitation, ce qui suggère que ce sont les fluctuations d'inhibition qui génèrent les PAs.

En accord avec cette analyse, les STA des conductances démontrent directement que les PAs sont en général liés à une diminution d'inhibition, comme nous l'avons montré précédemment en dynamic-clamp (Chapitre 2). Ces résultats suggèrent que les processus inhibiteurs jouent un rôle prépondérant dans les états activés du cortex cérébral associatif.

4.1 Abstract

Intracellular recordings of cortical neurons in awake cat and monkey show a depolarized state, sustained firing and intense subthreshold synaptic activity. It is not known what conductance dynamics underlies such activity, and how neurons process information in such highly stochastic states. Here, we combine intracellular recordings in awake and naturally sleeping cats with computational models to investigate subthreshold dynamics of conductances and how conductance dynamics determine spiking activity. We show that during both wakefulness and the “up-states” of natural slow-wave sleep, membrane potential activity stems from a diversity of combinations of excitatory and inhibitory synaptic conductances, with dominant inhibition in most of the cases. Inhibition also provides the largest contribution to membrane potential fluctuations. Computational models predict that in such inhibition-dominant states, spikes are preferentially evoked by a drop of inhibitory conductance, and that its signature is a transient drop of membrane conductance prior to the spike. This pattern of conductance change is indeed observed in estimates of spike-triggered averages of synaptic conductances during wakefulness and slow-wave sleep up-states. These results show that activated states are defined by diverse combinations of excitatory and inhibitory conductances with pronounced inhibition, and that the dynamics of inhibition is particularly effective on spiking, suggesting an important role for inhibitory processes in both conscious and unconscious cortical states.

4.2 Introduction

Intracellular recordings of cortical neurons in awake, conscious cats and monkeys show a depolarized membrane potential (V_m), sustained firing and intense subthreshold synaptic activity (Matsumara et al. 1988; Baranyi et al. 1993; Steriade et al. 2001; Timofeev et al. 2001). It is presently unclear how neurons process information in such active and irregular states. An important step to investigate this problem is to obtain a precise characterization of the conductance variations during activated electroencephalogram (EEG) states. Input resistance measurements indicate that during such activated states, cortical neurons can experience periods of high conductance, which may have significant consequences for their integrative properties (Destexhe and Paré 1999; Kuhn et al. 2004; reviewed in Destexhe et al. 2003). In anesthetized animals, several studies have provided measurements of the excitatory and inhibitory conductance contributions to the state of the membrane, using various paradigms (e.g., see Borg-Graham et al. 1998; Hirsch et al. 1998; Paré et al. 1998; Anderson et al. 2000; Wehr and Zador 2003; Priebe et al. 2005; Haider et al. 2006). However, no such conductance measurements have been made so far in awake and naturally sleeping animals.

4.3. MATERIALS AND METHODS

In the present paper, we provide such estimates using a combination of intracellular recordings and computational models. Intracellular recordings were performed in the association cortex of non-anesthetized cats, across wake or sleep states, according to a technique described previously (Steriade et al. 2001; Timofeev et al. 2001). Intracellularly-recorded neurons display a highly complex and irregular subthreshold synaptic activity, from which we estimate the conductances (and their variances) by matching stochastic models to the intracellular data. We also use the same approach to estimate the time course of relative conductance changes during the transition between depolarized and hyperpolarized phases (up and down states), as seen intracellularly during slow-wave sleep (SWS). We next introduce computational models with stochastic conductances reproducing the above measurements, in order to infer the type of conductance variations that underlie spiking activity in such states. Part of these results were published as conference abstracts (Destexhe et al., *COSYNE Conference*, 2005; Pospischil et al. 2005).

4.3 Materials and Methods

4.3.1 Intracellular recordings in awake and naturally sleeping animals

Intracellular recordings were performed in cat association cortex (areas 5, 7 and 21 of parietal cortex) using a technique described in detail previously (see Methods in Steriade et al. 2001; Timofeev et al. 2001). Briefly, a chamber specially designed for chronic intracellular recordings, local field potential (LFP), electromyogram (EMG) and electrooculogram (EOG) electrodes as well as head fixation screws, were implanted under anesthesia. Electrodes for LFP recordings were inserted in cortical depth and their tips were located at a depth of 0.8-1.0 mm. The animals were gradually habituated to the recording setup and the head-fixed position. After 3-4 days of training the cats started to display normal sleep-waking cycles and could move their limbs.

Intracellular recordings were performed under current-clamp using standard borosilicate glass micropipettes 1.5/0.84 mm (OD/ID) filled with 2.5 mM potassium acetate. Initially, pipettes were pulled to a resistance of 120-150 M Ω and under visual guidance their tips were broken to obtain a resistance of 50-70 M Ω . The pipettes descended in the recording chamber. After insertion in the brain the resistance of some of the pipettes further decreased. The intracellular electrodes with resistance lower than 30 M Ω were discarded because intracellular recordings obtained with these electrodes often revealed signs of deterioration appearing as unstable membrane potential, which becomes progressively depolarized, and broadening of action potential duration. Typically the recording sessions lasted up

to 3 hours. Only recordings showing stable V_m (no drift) and overshooting action potentials were considered here. To correctly estimate the membrane potential, we recorded the potential drop during penetration of the recorded neuron, and after pulling out of the neuron. If the difference in the estimation of recorded membrane potential at the beginning and at the end of recording exceeded 2 mV, these data were discarded. A total of 118 neurons were recorded during the wake/sleep cycle, including 96 presumed excitatory cells and 22 presumed inhibitory interneurons (see Results).

To accumulate sufficient statistics for the analysis (see below), recordings needed to last typically more than 30 min, and be conducted using several levels of injected DCs. A total of 15 neurons were obtained satisfying these criteria and were used for conductance analysis. In some cases, the recording was long enough to span across several states of vigilance (quiet wakefulness, slow-wave sleep and REM sleep). Experiments were conducted in agreement with ethics guidelines of the Canadian Council on Animal Care and were approved by the committee for animal care of Laval University.

4.3.2 Analysis and computational models

The basis of the analysis was to match the V_m of the intracellularly-recorded neurons to a stochastic model of synaptic background activity. This model was used for estimating synaptic conductances, to perform spike-triggered averages of synaptic conductance variations related to spikes, as well as for simulating membrane dynamics based on those estimates. The methods related to these different approaches are described below.

The basis of the analysis was a *fluctuating conductance model*, which approximates the highly complex synaptic activity as a random process, using global synaptic conductances described by the following stochastic equation (Destexhe et al. 2001):

$$\frac{dg_e(t)}{dt} = -\frac{1}{\tau_e} [g_e(t) - g_{e0}] + \sqrt{\frac{2\sigma_e^2}{\tau_e}} \xi_e(t) , \quad (4.1)$$

where $g_e(t)$ is the global excitatory conductance, fluctuating around the mean value g_{e0} and with variance σ_e^2 , τ_e is the excitatory time constant, and $\xi_e(t)$ is a Gaussian white noise source with zero mean and unit standard deviation. The global inhibitory conductance $g_i(t)$ is described by an equivalent equation with parameters g_{i0} , σ_i^2 , τ_i and noise source $\xi_i(t)$. These conductances determine the subthreshold variations of the membrane potential $V(t)$, according to the membrane equation:

$$C \frac{dV(t)}{dt} = -G_L [V(t) - E_L] - g_e(t) [V(t) - E_e] - g_i(t) [V(t) - E_i] + I_{ext} , \quad (4.2)$$

4.3. MATERIALS AND METHODS

where C denotes the membrane capacitance, I_{ext} a stimulation current, G_L the leak conductance, E_L the leak reversal potential, while E_e and E_i are the reversal potentials of $g_e(t)$ and $g_i(t)$, respectively.

The advantage of this stochastic model is that different analytic approximations are available for the steady-state V_m distribution. The VmD method consists in matching this analytic expression to V_m distributions obtained experimentally, leading to estimates of excitatory and inhibitory conductances, as well as their variance, solely from current-clamp recordings (for a detailed discussion and testing of this method, see Rudolph et al. 2004). The method is based on the assumption of Gaussian distribution for synaptic conductances. The validity of this approximation was tested in numerical simulations (Destexhe et al. 2001; Rudolph and Destexhe 2003, 2005), theoretical investigations (Rudolph and Destexhe 2006) as well as experimental studies (Rudolph et al. 2004, 2005). V_m distributions must be obtained at different holding current (DC) levels, and using multiple current levels allows one to identify the linear range of the voltage-current (V-I) relations (see Fig. 4.3A). This is an important check to limit the possible contamination of subthreshold voltage-dependent conductances. To insure that only subthreshold activity is used for the analysis, action potentials – if present – were removed by excluding all V_m activity within a window of 5 ms before and 10 ms after the spike. To avoid the possible bias caused by removing compound EPSPs before spikes, the VmD estimates were performed in hyperpolarized segments with little spiking activity; the testing of this method using dynamic-clamp experiments indicates that such a bias is negligible (see Rudolph et al. 2004).

As two DC levels are necessary to estimate conductances, $n > 2$ levels provides multiple estimates corresponding to different ranges of V_m . Up to $n = 8$ current levels were used here, which leads up to 28 possible pairings. For each pairing, the fitting of the V_m distributions with the analytic expression (in particular its Gaussian approximation given in Rudolph et al. 2004) yields estimates of the synaptic conductances and their variances, provided a number of other parameters are kept fixed. These parameters are the synaptic reversal potentials ($E_e = 0$ mV and $E_i = -75$ mV) and the decay time constants ($\tau_e = 3$ ms and $\tau_i = 10$ ms) of synaptic conductances, as well as the leak conductance (G_L ; see Results) and reversal potential ($E_L = -80$ mV). The values of $\tau_e = 3$ ms and $\tau_i = 10$ ms were obtained from the power spectra of V_m activity (Rudolph et al. 2005). The leak parameters were estimated based on previous intracellular experiments realized on neurons of the same area of cat cortex (area 5-7) following application of tetrodotoxin (Paré et al. 1998): after suppression of network activity, the membrane conductance was reduced by approximately five times, and the resting V_m was of -80 mV on average. The “optimal values” of conductance presented here (e.g., Fig. 4.3C) were based on the assumption that the up-states of these experiments (ketamine-xylazine anesthesia) have the same relative impact on the mem-

brane as the up-states of natural slow-wave sleep analyzed here. This assumption is supported by the fact that the absolute values of input resistance during up-states are similar in the two preparations (Paré et al. 1998; Steriade et al. 2001). We performed variations around this estimate (see Results), in order to check that the results obtained do not qualitatively depend on this assumption. Note that the values of the conductance variances are not affected by the particular choice of the leak conductances (Rudolph et al. 2004; see Results).

We also performed a spike-triggered average (STA) conductance analysis from V_m activity. The average conductance time course related to spikes was estimated using a method outlined recently, and which was tested in real neurons with dynamic-clamp (Pospischil et al. 2007). The STA of the voltage is calculated first, and the method searches for the “most likely” spike-related conductance time courses ($g_e(t)$, $g_i(t)$) that are compatible with the observed voltage STA. This estimation is made by discretizing the time axis in equations (4.1) and (4.2), which leads to a discretized system from which one can evaluate the probability distribution for the spike-related conductance time courses. Since this distribution is symmetric, the STAs of the synaptic conductances can be determined by maximizing its probability distribution, which amounts to differentiating the distribution and subsequently solving a system of algebraic equations (Pospischil et al. 2007). The system of algebraic equations is solved using standard numerical methods (Press et al. 1986).

To quantify the conductance STA, we fitted the conductance time course using the following exponential template:

$$g_e(t) = g_{e0} \left(1 + k_e \exp\left(\frac{t - t_0}{T_e}\right) \right), \quad (4.3)$$

for excitation, and an equivalent equation for inhibition. Here, t_0 stands for the time of the spike, k_e quantifies the maximal increase/decrease of conductance prior to the spike, with time constant T_e (and similarly for inhibition). We also calculated the *relative conductance change* before the spike:

$$r_g = \frac{g_{e0} k_e - g_{i0} k_i}{g_{e0} + g_{i0}}. \quad (4.4)$$

Here, the terms $g_{e0} k_e$ and $g_{i0} k_i$ quantify the absolute excitatory and inhibitory conductance change before the spike, respectively. The difference between these two contributions is normalized to the total synaptic conductance. A negative value indicates an overall drop of total membrane conductance before the spike (as in Fig. 4.9A), while a positive value indicates an increase of total conductance (as in Supplementary Fig. 4).

To relate the STA analysis to the VmD analysis, we quantified the *relative excess conductance* by calculating the quantity:

$$e_g = \frac{g_{e0} - g_{i0}}{g_{e0} + g_{i0}}. \quad (4.5)$$

4.4. RESULTS

Here, a negative value indicates a membrane dominated by inhibitory conductance, while a positive value indicates dominant excitatory conductance.

Similarly, we calculated the *relative excess conductance fluctuations* by evaluating the quantity:

$$s_g = \frac{\sigma_e - \sigma_i}{g_{e0} + g_{i0}}. \quad (4.6)$$

Finally, the fluctuating conductance model (Eq. 4.2) was simulated numerically together with voltage-dependent Na^+ and K^+ conductances responsible for generating action potentials (Hodgkin-Huxley type models with parameters identical as described in Destexhe et al. 2001, and references therein). The conductance values obtained from intracellular data were integrated in this model to verify that the V_m activity and firing behavior obtained match the recordings of the corresponding cell. Simulations were performed on LINUX workstations using the NEURON simulation environment (Hines and Carnevale 1997).

4.4 Results

4.4.1 Intracellular recordings in awake and naturally sleeping animals

Intracellular recordings of cortical neurons were performed in parietal cortex of awake and naturally-sleeping cats (see Materials and Methods). Intracellular recordings were done simultaneously with the local field potential (LFP), electromyogram (EMG) and electrooculogram (EOG) to identify behavioral states. With pipettes filled with K^+ -Acetate (KAc), we recorded and electrophysiologically identified activities of 96 presumed excitatory neurons during the waking state. Of them, 47 neurons revealed a regular-spiking (RS) firing pattern, with significant spike-frequency adaptation in response to depolarizing current pulses, and spike width of 0.69 ± 0.20 ms (range 0.4-1.5 ms). The V_m of RS neurons varied in a range between -56 mV and -76 mV (mean -64.0 ± 5.9 mV). 26 of these RS neurons were “wake-active” cells, in which the firing was sustained all through the wake state, as described previously (Matsumara et al. 1988; Baranyi et al. 1993; Steriade et al. 2001; Timofeev et al. 2001). In these “wake-active” neurons (Fig. 4.1A), the V_m was depolarized (around -65 mV) and showed high-amplitude fluctuations and sustained irregular firing (3.1 Hz on average; range 1 to 11 Hz) during wakefulness. During slow-wave sleep, all neurons always showed up and down states in the V_m activity in phase with the slow-waves (Fig. 4.1A, SWS), as described previously (Steriade et al. 2001).

Almost half of the RS neurons recorded (21 out of 47), were “wake-silent” cells, which systematically ceased firing during periods of quiet wakefulness (cf. Fig. 4.1B). Note that during the transition from slow-wave sleep to waking, these

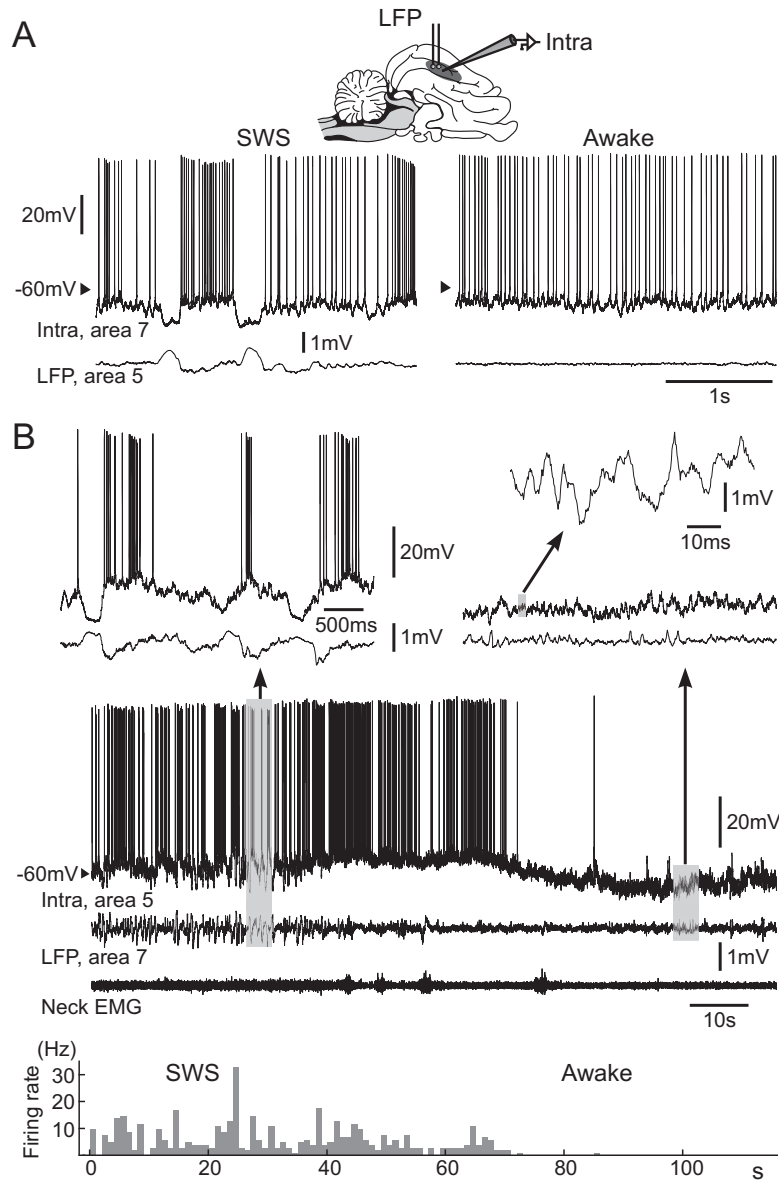


Figure 4.1: Activity of regular-spiking neurons during slow-wave sleep and wakefulness. **A.** "Wake active" regular-spiking neuron recorded simultaneously with local field potentials (LFP; see scheme) during slow-wave sleep (SWS) and wakefulness (Awake) condition. **B.** "Wake-silent" regular-spiking neuron recorded simultaneously with LFPs and EMG during slow-wave sleep to wake transition. Slow-wave sleep was characterized by high-amplitude low-frequency field potentials, cyclic hyperpolarizations, and stable muscle tone (expanded in upper left panel). Low-amplitude and high-frequency fluctuations of field potentials and muscle tone with periodic contractions characterized the waking state. This neuron was depolarized and fired spikes during initial 30 s of waking, then hyperpolarized spontaneously and stopped firing. A fragment of spontaneous V_m oscillations is expanded in the upper right panel. A period with barrages of hyperpolarizing potentials is further expanded as indicated by the arrow.

4.4. RESULTS

wake-silent neurons continued to fire for 10-60 s, and after that period, their V_m hyperpolarized by several mV and they stopped to fire action potentials as long as the animal remained in the state of quiet wakefulness. Figure 4.1B illustrates one example of a wake-silent cell which upon awakening had a V_m of -53.0 ± 4.9 mV and fired with frequency 10.1 ± 7.9 Hz for about 30 s. Thereafter, the V_m hyperpolarized to -62.5 ± 2.6 mV and the same neuron stopped firing. The hyperpolarization during waking state was not due to K^+ load because on 2 occasions, we were able to obtain intracellular recordings from wake-silent neurons during waking state that was preceded and followed by other states of vigilance (see Supplementary Fig. 1). In this case, the recorded neuron was relatively depolarized and fired action potentials during REM sleep. Upon awakening, this neuron was hyperpolarized by about 10 mV and stopped firing. After 3 min of waking state the animal went to slow-wave sleep state and the same neuron was depolarized and started to fire action potentials. On one occasion (not shown) we recorded extracellularly spikes from two units. One of the units stopped firing during waking state lasting about 10 min while another unit continued to emit action potentials. This observation suggests that it is a particular set of neurons and not local networks that stop firing during quiet wakefulness. The mean firing rates for RS neurons were 6.1 ± 6.7 Hz (silent neurons included; 10.1 ± 5.6 Hz with silent neurons excluded). No wake-silent cells were observed for other neuronal classes than RS cells, and all together, wake-silent neurons represented about 25% of the total number of recorded cells in the wake state. This large proportion of wake-silent neurons constitutes a first hint for an important role for inhibitory conductances during waking.

In contrast, no silent neuron was found for presumed interneurons. During quiet wakefulness, 22 neurons were electrophysiologically identified as fast-spiking (FS). They displayed virtually no adaptation and had action potential width of 0.27 ± 0.08 ms (range 0.15-0.45 ms). Upon awakening, FS neurons tended to increase firing (Fig. 4.2A-B), and none of them was found to cease firing ($n=9$). Interestingly, the increase of firing of FS neurons seems to follow the steady hyperpolarization of RS “wake-silent” neurons (Fig. 4.2A). The mean firing frequency of FS neurons was 28.8 ± 20.4 Hz (Range 1-88 Hz; only 2 neurons fired with frequency less than 2 Hz), which was significantly higher than that of RS neurons ($p<0.001$; see Fig. 4.2C). The mean V_m of FS neurons was -61.3 ± 4.5 mV, which is not significantly different from the V_m of RS neurons ($p=0.059$).

To check for the contribution of K^+ conductances during quiet wakefulness, we recorded activities of 3 RS neurons with Cs^+ -filled pipettes (data not shown). The presence of cesium greatly affected the repolarizing phase of action potentials, demonstrating that Cs^+ was effective in blocking K^+ conductances, but the V_m distribution was marginally affected by the presence of cesium. The action of intracellular Cs^+ may overlap with the blocking action of neuromodulators

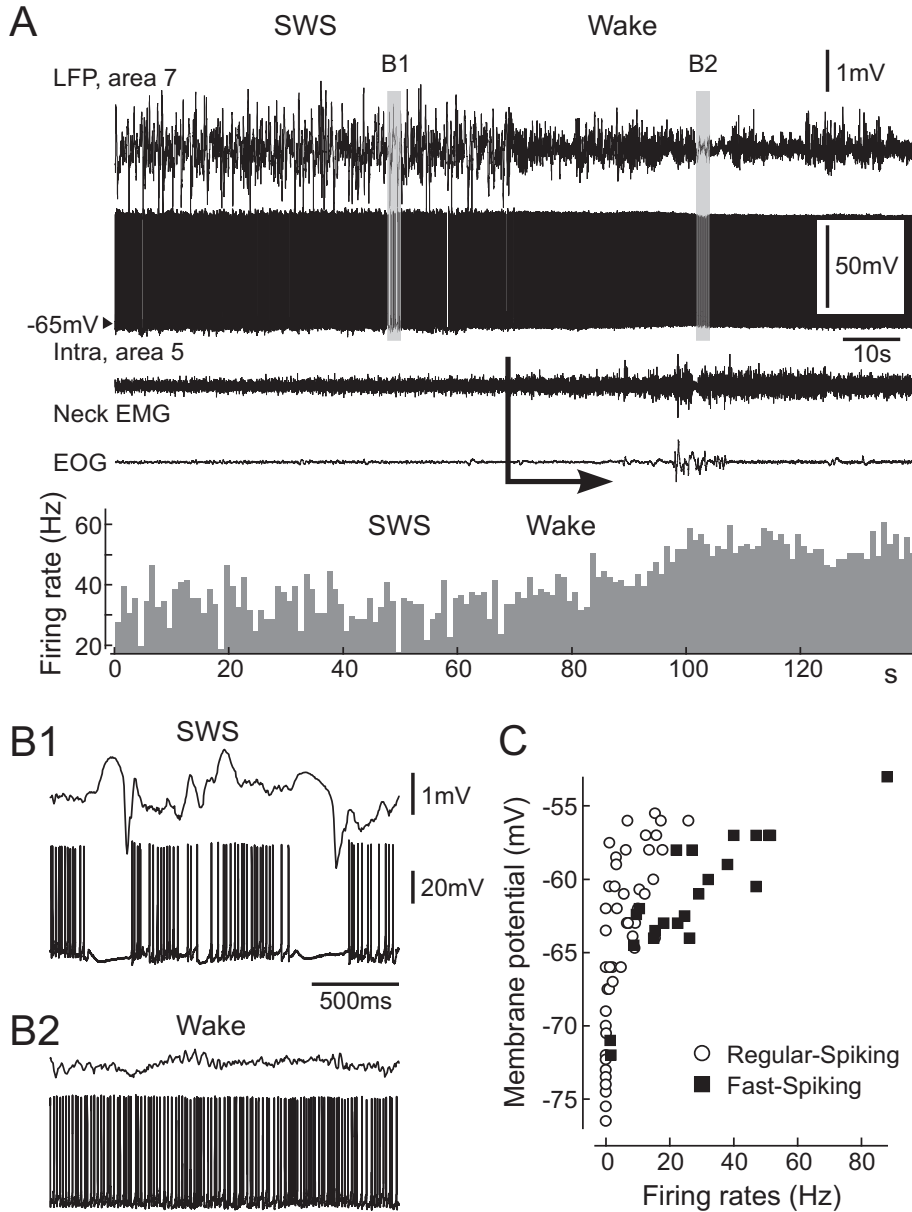


Figure 4.2: Activity of fast-spiking interneurons upon awakening. **A.** Intracellular activity of a fast-spiking neuron recorded simultaneously with LFPs, EMG and EOG during the transition from slow-wave sleep to wake state. The onset of the waking state is indicated by the arrow. Upon awakening, the mean firing rate initially remained the same as during sleep (for about 20 s), then slightly increased (see firing rate histogram at bottom). **B.** Fragments of LFP and neuronal activities during slow-wave sleep and waking states are expanded as indicated in A by B1 and B2. **C.** Comparison of firing rates of regular-spiking and fast-spiking neurons in wake states. Pooled results showing the mean firing rate of RS (open circles) and FS (filled squares), represented against the mean V_m during waking.

4.4. RESULTS

on other K^+ conductances (McCormick 1992; Metherate and Ashe 1993), which may explain the absence of effect of Cs^+ on the V_m . This preliminary evidence for a limited effect of cesium during wakefulness indicates that leak and K^+ conductances have no major effect on the V_m distribution, suggesting that it is mainly determined by synaptic conductances.

4.4.2 Synaptic conductances in wakefulness and natural sleep

To determine the relative contribution of excitatory and inhibitory conductances, we have analyzed the intracellular recordings described above using the recently proposed VmD method (Rudolph et al. 2004). This method assumes that the V_m fluctuations are due to the combined action of two synaptic conductances, excitatory (g_e) and inhibitory (g_i ; see Materials and Methods). Instead of modeling explicitly the activity of thousands of synapses, one considers the V_m and synaptic conductances as stochastic variables, which are described by probability densities. Using this formalism, it is possible to obtain an analytic expression for the steady-state probability distribution of the V_m , which is expressed as a function of the synaptic conductance parameters (Rudolph and Destexhe 2003, 2005). Because the steady-state V_m distribution is observable experimentally, fitting the analytic expression to experimental V_m distributions provides estimates of the underlying synaptic conductances. This method was tested using dynamic-clamp methods and was shown to provide consistent estimates of synaptic conductances and their fluctuations (Rudolph et al. 2004).

We computed V_m distributions for periods of stationary activity during wakefulness and slow-wave sleep up-states. Fig. 4.3B (Awake) shows V_m distributions of two different but representative cells obtained from periods of wakefulness, in which the cat and the LFPs did not show any sign of drowsiness. The V_m distribution was approximately Gaussian, centered around $\bar{V} = -63.1$ mV, and the standard deviation of the V_m (σ_V) was about 3.6 mV. During slow-wave sleep, we calculated the V_m distribution specifically during up-states (Fig. 4.3B, SWS). It had an approximately similar shape as during wakefulness ($\bar{V} = -62.7$ mV; $\sigma_V = 3.3$ mV). Similar distributions were also observed during rapid eye movement (REM) sleep (not shown). The V_m distributions were computed using several pairs of DC levels, which were selected in the linear portion of the V-I relation (Fig. 4.3A). The conductance estimates obtained for several of such pairings (see Materials and Methods) are represented in Fig. 4.3C. In this example, during both wakefulness and slow-wave sleep up-states, the inhibitory conductances were several-fold larger than excitatory conductances. Variations of different parameters, such as the leak conductances (Fig. 4.3D), or the parameters of synaptic conductances (see Materials and Methods), affected the absolute values of conductance estimates, but always pointed to the same qualitative effect of dominant inhibition. The sole exception was when considering high leak conductances, larger than the

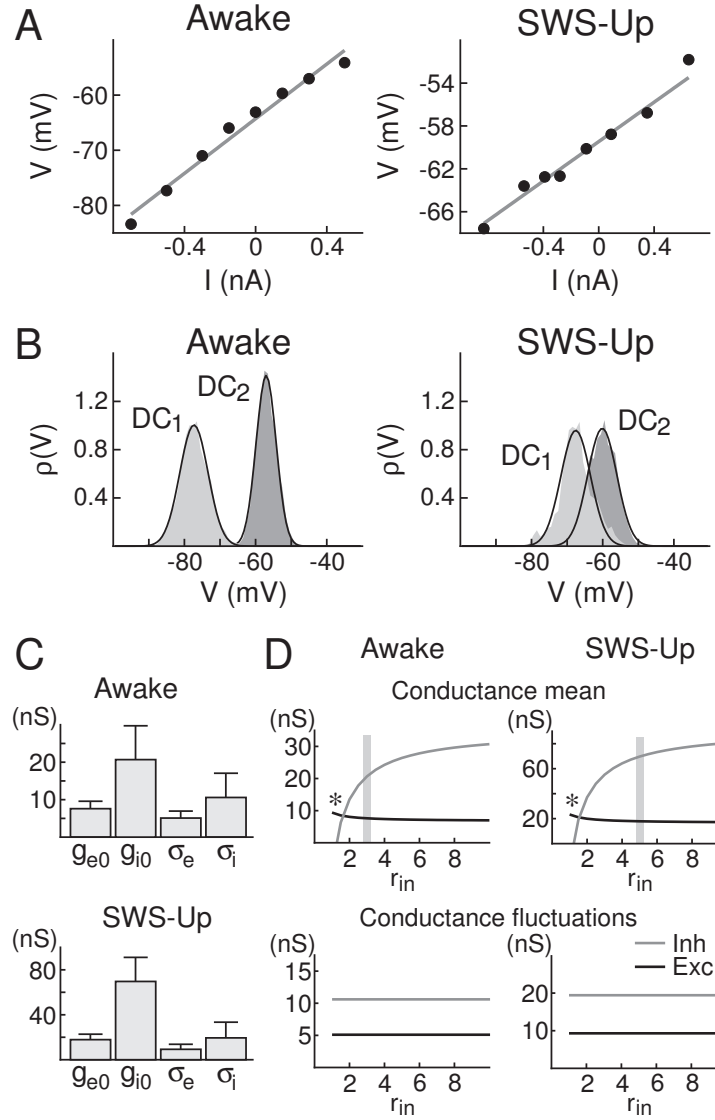


Figure 4.3: Estimation of conductances from intracellular recordings in awake and naturally sleeping cats. **A.** Voltage-current (V-I) relations obtained in two different cells during wakefulness (Awake) and the up-states of slow-wave sleep (SWS-Up). The average subthreshold voltage (after removing spikes) is plotted against the value of the holding current. **B.** Examples of V_m distributions $\rho(V)$ obtained in the same neurons as in **A.** The continuous lines show Gaussian fits of the experimental distributions. **C.** Conductance values (mean and standard deviation) estimated by decomposing synaptic activity into excitatory and inhibitory components using the VmD method (applied to 28 and 26 pairings of V_m recordings at different DC levels for Awake and SWS up-states, respectively). **D.** Variations of the value for conductance mean (top panels) and conductance fluctuations (bottom panels) as a function of different choices for the leak conductance. $r_{in} = R_{in}(\text{quiescent})/R_{in}(\text{active})$; * indicates the region with high leak conductances where excitation is larger than inhibition; the gray area shows the r_{in} values used for the conductance estimates in **C.**

4.4. RESULTS

synaptic activity itself, in which case the excitatory and inhibitory conductance were of comparable magnitude (Fig. 4.3D, *).

The VmD method also provides estimates of the variance of synaptic conductances. Similar to absolute conductance estimates, conductance variances were generally larger for inhibition (Fig. 4.3C). However, in contrast to absolute conductance estimates, the estimates of conductance variance do not depend on the particular choice of leak conductances (Fig. 4.3D, bottom panels; Fig. 4.5C for population result). These results suggest that inhibition provides a major participation to the V_m fluctuations.

This pattern was observed in the majority of cells analyzed, although a diversity of conductance combinations was present when considering the different states of vigilance, including periods of REM sleep. In cells for which synaptic conductances were estimated ($n=11$ for Awake, wake-active cells only, $n=7$ for SWS up-states, $n=2$ for REM), the average V_m and fluctuation amplitude was comparable in all states ($\bar{V} = -54.2 \pm 7.5$ mV, $\sigma_V = 2.4 \pm 0.7$ mV for Awake; $\bar{V} = -58.3 \pm 4.9$ mV, $\sigma_V = 2.7 \pm 0.5$ mV for SWS-Up; $\bar{V} = -67.0 \pm 6.9$ mV, $\sigma_V = 1.9 \pm 0.6$ mV for SWS-Down; $\bar{V} = -58.5 \pm 5.2$ mV, $\sigma_V = 2.1 \pm 0.9$ mV for REM; see Fig. 4.4A). However, the total input resistance showed important variations (16.1 ± 14.5 M Ω for Awake; 12.3 ± 19.6 M Ω for SWS-Up; 22.4 ± 31.7 M Ω for SWS-Down; 8.5 ± 12.1 M Ω for REM), possibly caused by differences in the passive properties and cellular morphologies. The estimated synaptic conductances spread over a large range of values for both mean (ranging from 5 to 70 nS and 5 to 170 nS for excitation and inhibition; Fig. 4.4B; medians: 21 nS and 55 nS for excitation and inhibition during SWS-Up, 13 nS and 21 nS for excitation and inhibition for Awake; Fig. 4.4C) and standard deviation (ranging from 1.5 to 22 nS and 3.5 to 83 nS for excitation and inhibition; Fig. 4.5A) and standard deviation (ranging from 1.5 to 22 nS and 3.5 to 83 nS for excitation and inhibition; Fig. 4.5A; medians: 7.6 nS and 9.3 nS for excitation and inhibition for SWS-Up, 4.3 nS and 7.7 nS for excitation and inhibition for Awake; Fig. 4.5B). In all states and for reasonable assumptions for the leak conductance (Fig. 4.4D, grey), dominant inhibition was found in more than half of the cells analyzed ($n=6$ for Awake and $n=7$ for SWS-Up had $>40\%$ larger mean inhibitory conductance; $n=6$ for Awake and $n=4$ for SWS-Up had $>40\%$ larger inhibitory standard deviation). In the remaining cells, inhibitory and excitatory conductance values were of comparable magnitude, with a tendency for a slight dominance of inhibition (except for $n=2$ cells in Awake). Moreover, in all cells analyzed, inhibition was more pronounced during the up-states of SWS (estimated ratios between inhibition and excitation were 2.7 ± 1.4 and 3.0 ± 2.2 for conductance mean and standard deviation; medians: 1.9 and 1.4, respectively) compared to wakefulness (ratios of 1.8 ± 1.1 and 1.9 ± 0.9 for conductance mean and standard deviation; medians: 1.4 and 1.4, respectively; see Fig. 4.4C and Fig. 4.5B, respectively). Renormalizing the conductance values to the leak conductance for each cell in the wake state led

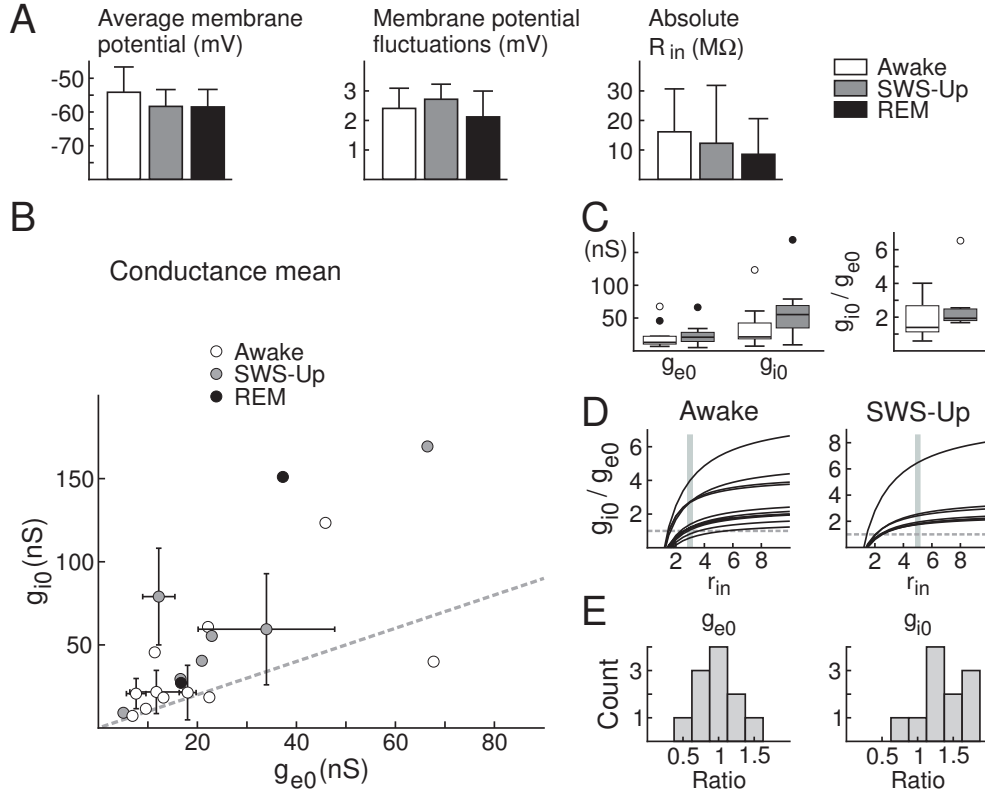


Figure 4.4: Conductance estimates in cortical neurons during wake and sleep states. **A**. Average V_m , V_m fluctuation amplitude and absolute input resistance R_{in} during wakefulness (Awake), slow-wave sleep up-states (SWS-Up) and REM sleep periods, computed from all cells for which synaptic conductances were estimated. **B**. Spread of excitatory (g_{e0}) and inhibitory (g_{i0}) conductance mean during wakefulness and slow-wave sleep up-states. Estimated conductance values show a high variability among the investigated cells, but in almost all states, a dominance of inhibition was observed. **C**. Box plots of mean excitatory and inhibitory conductance estimates (left) and average ratio between inhibitory and excitatory mean (right) observed during wakefulness and slow-wave sleep up-states for the population shown in **B**. In both states, dominant inhibition was observed, an effect which was more pronounced during SWS-Up. **D**. Variations of the ratio between inhibitory and excitatory mean conductance values as a function of different choices for the leak conductance. $r_{in} = R_{in}(\text{quiescent})/R_{in}(\text{active})$; the gray area indicates the values used for conductance estimation plotted in **B** and **C**. **E**. Histograms of conductance values relative to the leak conductance during the wake state.

4.4. RESULTS

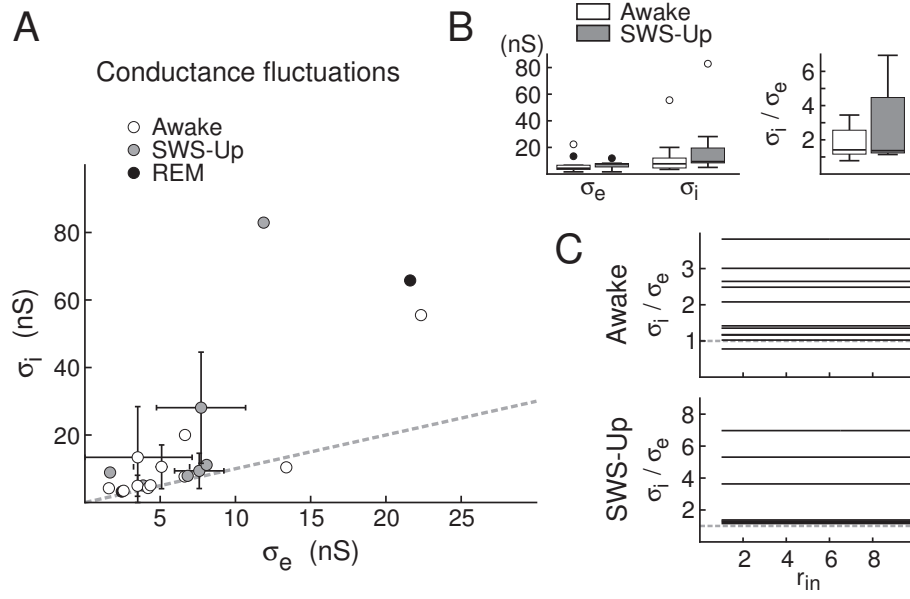


Figure 4.5: Estimates of conductance fluctuations from cortical neurons during wake and sleep states. **A.** Spread of excitatory (σ_e) and inhibitory (σ_i) conductance fluctuations during wakefulness and slow-wave sleep up-states. Estimated conductance values show a high variability among the investigated cells, but in all states, a dominance of inhibition was observed. **B.** Box plots of excitatory and inhibitory conductance fluctuation amplitude (left) and average ratio between inhibitory and excitatory standard deviation (right) observed during wakefulness (Awake) and slow-wave sleep up-states (SWS-Up) for population shown in **A**. In all cases, dominant inhibition was observed. **C.** In the VmD method, estimated values for the ratio between inhibitory and excitatory conductance fluctuations do not depend on different choices for the leak conductance. $r_{in} = R_{in}(\text{quiescent})/R_{in}(\text{active})$.

to values which were more homogeneous (Fig. 4.4E). In this case, the excitatory conductance was of the order of the leak conductance (Fig. 4.4E, left; 0.81 ± 0.26), while inhibition was about 1.5 times larger (Fig. 4.4E, right; 1.26 ± 0.31).

These results were also checked using the classic “Ohmic” conductance analysis (see Supplementary Methods). By integrating the V_m measurements in the various active states into the membrane equation (see Eq. 4.8 in Supplementary Methods), we obtained estimates for the ratio between mean inhibitory (excitatory) conductances and the leak conductance for each cell (Supplementary Fig. 2A). This and the pooled results for all available cells (Supplementary Fig. 2B), also indicate that the relative contribution of inhibition is several-fold larger than that of excitation for both wakefulness and SWS up-states. Average values are $\bar{g}_i/\bar{g}_e = 3.2 \pm 1.3$ for SWS-Up and $\bar{g}_i/\bar{g}_e = 1.7 \pm 1.1$ during wakefulness. Here also, these values were relatively robust against the choice of the leak conductance (Supplementary Fig. 2C).

In a small subset of cells ($n=3$), the recording was long enough to span across several wake and sleep states, so that SWS and wakefulness could be directly compared. In agreement with the reduction of the average firing rate of RS neurons during the transition from SWS to wakefulness, we observed a reduction of the mean excitatory conductance (values during wakefulness were between 40 and 93% of those during SWS-Up) and its fluctuation amplitude (between 45 and 85% of those observed during SWS-Up). In contrast to the observed increase of the firing rate of interneurons during sleep-wake transitions, the inhibitory conductances also decreased markedly (values during wakefulness were between 35 and 60% for the mean conductance, and between 10 and 71% for the standard deviation compared to corresponding values during SWS-Up; see Discussion).

4.4.3 Conductance time course during up and down state transitions

We next estimated the time evolution of conductances during up and down states of slow-wave sleep. We performed a similar analysis as above, with the difference that V_m distributions were not calculated by accumulating statistics only over time, but also over repeated trials. Several up-states ($n=1$, between 6 and 36 slow-wave oscillation cycles at 8 DC levels) were selected and aligned with respect to the “down to up” transition as determined by the sharp LFP negativity (Fig. 4.6, left panels). The V_m distributions were then calculated within small (10 ms) windows before and after the transition. This procedure led to estimates of the time course of the conductances and their variances, as a function of time during “down-up” state transitions, and similarly for “up-down” transitions (Fig. 4.6, right panels). It is important to note that conductance changes were estimated here relative to the down state, and not with respect to rest, as above. This analysis showed that, for this particular cell, the onset of the up state is driven by

4.4. RESULTS

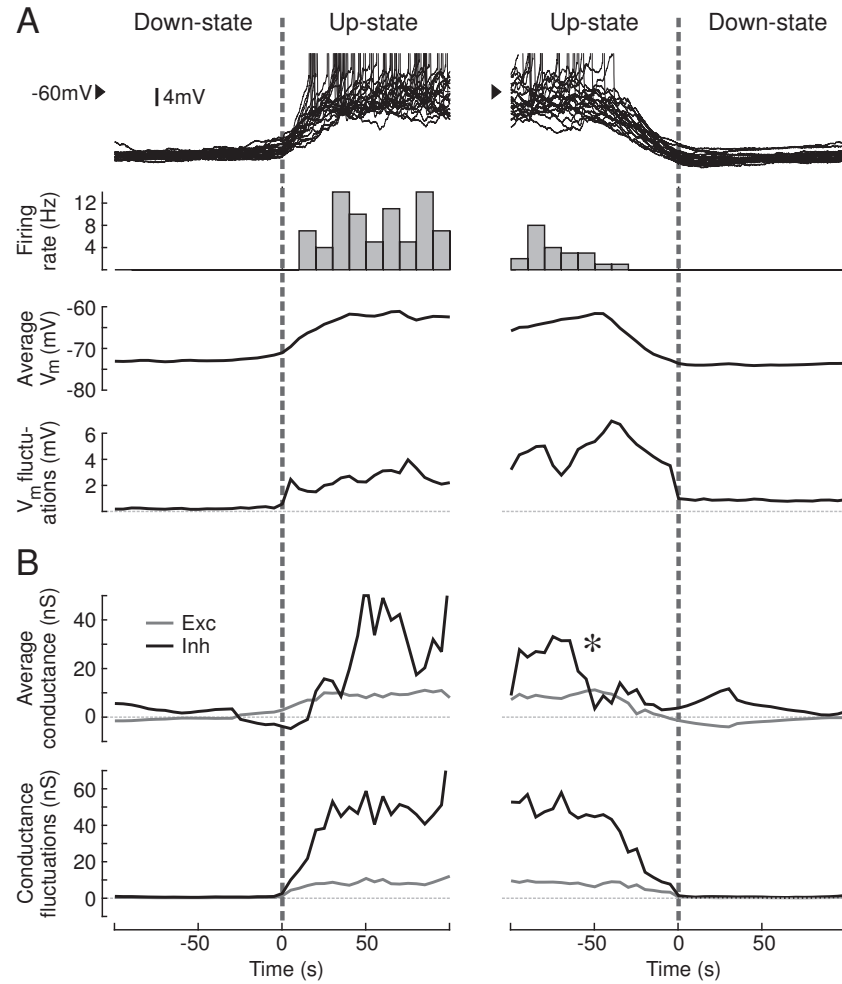


Figure 4.6: Conductance time course during up and down states during slow-wave sleep. **A.** Superimposed intracellular traces during transitions from down- to up-states (left panels), and up- to down-states (right panels). **B.** Time course of global synaptic conductances during down-up and up-down transitions. Conductance changes were evaluated relative to the average conductance of the down state. Top: excitatory (g_e , gray) and inhibitory (g_i , black) conductances; * indicates a drop of inhibitory conductance prior to the up-down transition. Bottom: standard deviation of the conductances for excitation (σ_e , gray) and inhibition (σ_i , black). Both are shown at the same time reference as for **A**.

excitation, while inhibitory conductances activate with a delay of about 20 ms, after which they tend to dominate over excitation. Note that in this case, inhibition is only slightly larger than excitation, presumably because the reference state is here the down state, which does not represent the true resting state. In this cell, the end of the up state was preceded by a drop of inhibition (Fig. 4.6B, *). The variance of inhibitory conductances was always larger than that of excitatory conductances (see Fig. 4.6B, bottom).

4.4.4 Dynamics of spike initiation during activated states

To investigate how excitatory and inhibitory conductance dynamics affect spike initiation, we first simulated the above results using computational models. We used a spiking model with stochastic conductances (see Eq. 4.2 in Materials and Methods) whose parameters are given by the above estimates. Integrating the particular values of conductances shown in Fig. 4.3C led the model to generate V_m activity in excellent agreement with the intracellular recordings (Fig. 4.7A,C, Awake). All the present conductance measurements during the waking state were simulated in a similar way and yielded V_m activity consistent with the recordings (two more examples, with clearly dominant excitation or inhibition are shown in Supplementary Fig. 3). Similarly, integrating the conductance variations, given in Fig. 4.6B, generated V_m activity consistent with the up-down state transitions seen experimentally (Fig. 4.7B,C, SWS and SWS-Up). These results show that the conductance estimates obtained above are consistent with the V_m activity recorded experimentally.

We next evaluated the optimal conductance changes related to spike initiation in the simulated wake state. Fig. 4.8A shows that the STA shows opposite variations for excitatory and inhibitory conductances preceding the spike. As expected, spikes were correlated to an increase of excitation (Fig. 4.8, Excitatory). Less expected was that spikes were also correlated with a decrease of inhibitory conductance (Fig. 4.8, Inhibitory), so that the total synaptic conductance decreases before the spike (Fig. 4.8, Total). Such a drop of total conductance was not present in simulated states when inhibition was not dominant (Fig. 4.8B). These results were checked using different combinations of parameters, and a drop of total conductance was always associated with inhibition-dominant states, except when the variance of inhibition was very small (not shown). Such a drop of total conductance before the spike therefore constitutes a good predictor for inhibition-dominant states, given that conductance fluctuations are roughly proportional to their means.

This prediction was tested using intracellular recordings of electrophysiologically identified RS cells. We performed STAs of the V_m during wakefulness and the up-states of SWS (Fig. 4.9A, AvgVm). The corresponding STA conductances were estimated by discretizing the time axis and solving the membrane equation

4.4. RESULTS

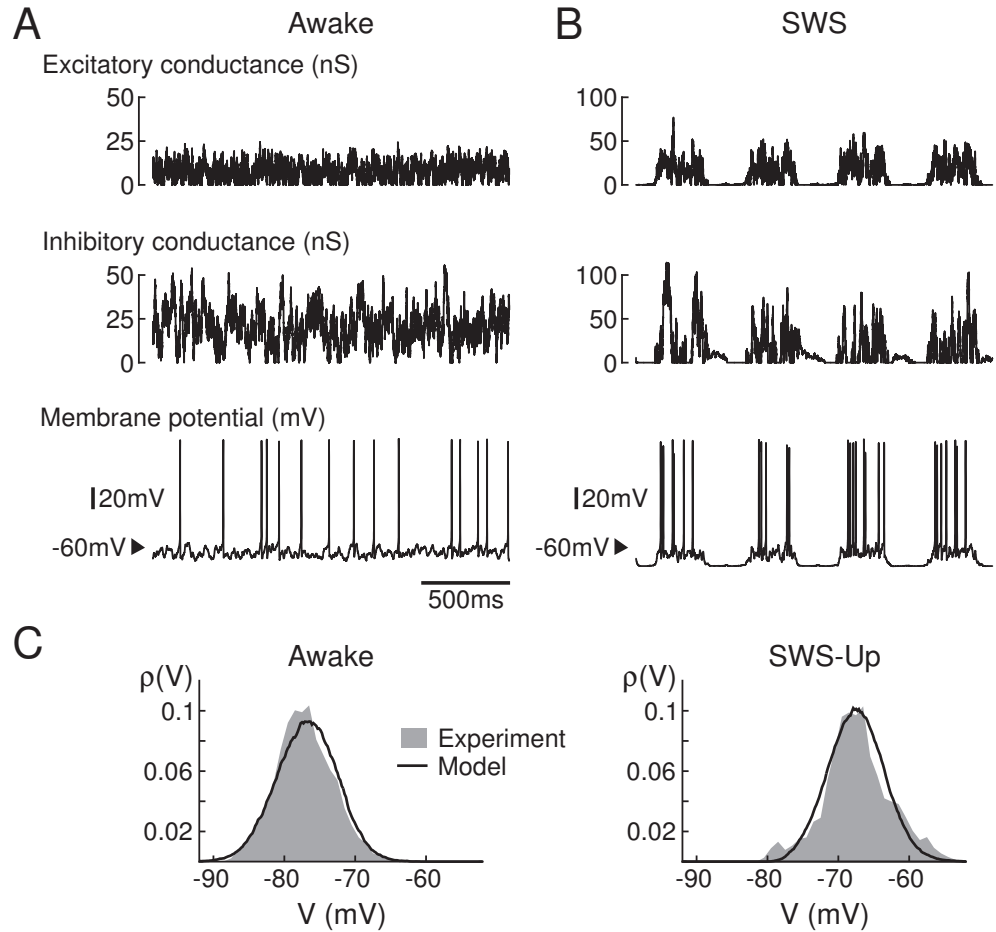


Figure 4.7: Model of conductance interplay during wakefulness and the up-states of slow-wave sleep. **A.** Simulated intracellular activity corresponding to measurements in the wake state (based on conductance values shown in Fig. 4.3C; leak conductance of 13.4 nS). **B.** Simulated up and down states transitions (based on the values given in Fig. 4.6B). **C.** V_m distributions obtained in the model (solid lines) compared to that of the experiments (gray) in the same conditions (DC injection of -0.5 and -0.43 nA, respectively).

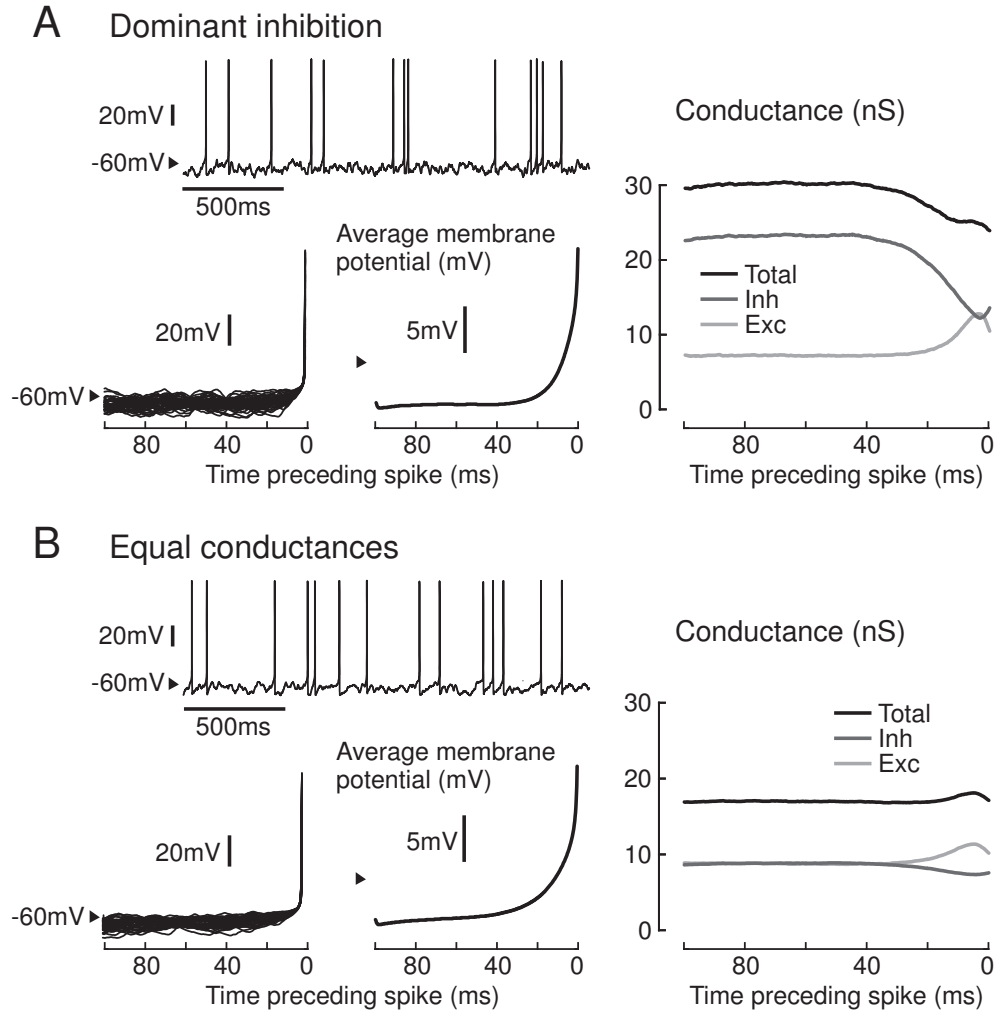


Figure 4.8: Model prediction of conductance variations preceding spikes. **A.** Simulated waking state with dominant inhibition as in Fig. 4.7A (top). Left: selection of 40 spikes; middle: spike-triggered average (STA) of the V_m ; Right: STAs of excitatory, inhibitory and total conductance. Spikes were correlated with a prior increase of excitation, a decrease of inhibition, and a decrease of the total conductance. **B.** Same STA procedure from a state which displayed comparable V_m fluctuations and spiking activity as in **A**, but where excitatory and inhibitory conductances had the same mean value. The latter state was of lower overall conductance as compared to **A**, and spikes were correlated with an increase of membrane conductance.

4.4. RESULTS

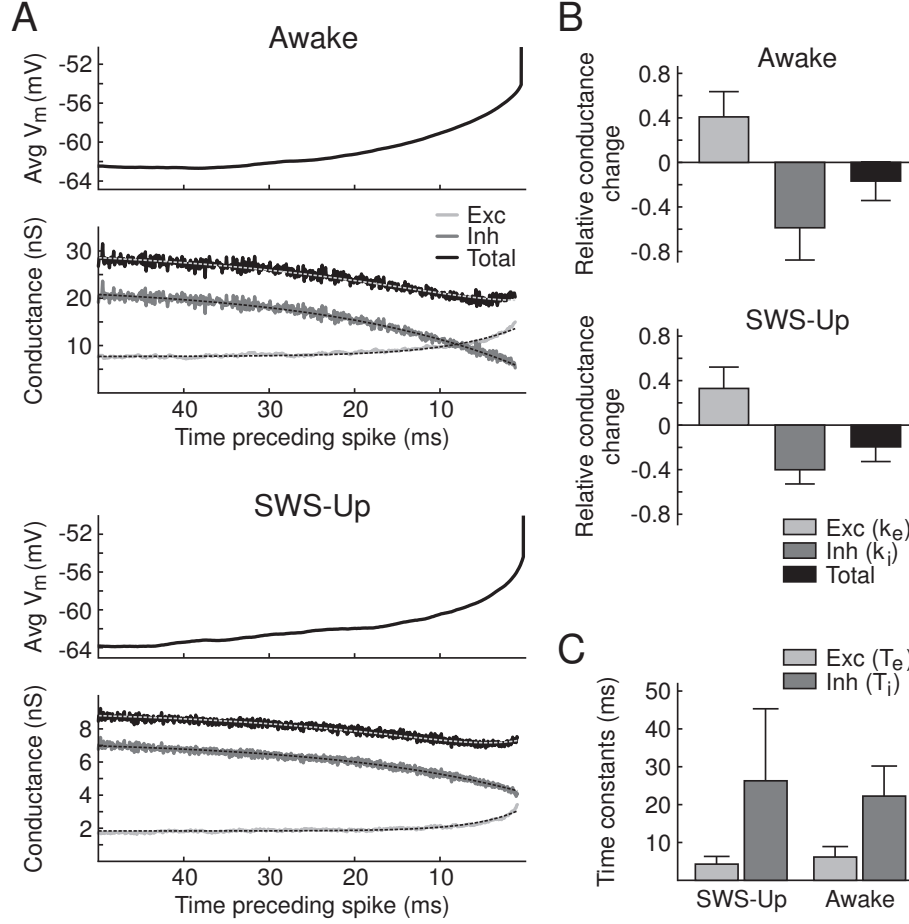


Figure 4.9: Decrease of membrane conductance preceding spikes in wake and sleep states. **A**. STA for the membrane potential (Avg V_m) as well as excitatory, inhibitory and total conductances obtained from intracellular data of regular-spiking neurons in an awake (top) and sleeping (SWS-Up, bottom) cat. The estimated conductance time courses showed in both cases a drop of the total conductance caused by a marked drop of inhibitory conductance within about 20 ms before the spike. **B**. Average value for the relative conductance change (k_e and k_i) triggering spikes during wakefulness (top) and up-states during SWS (bottom) obtained from exponential fits of the STA conductance time-course (using Eq. 4.3), for all investigated cells. A decrease of the total membrane conductance and of the inhibitory conductance is correlated with spike generation, similar to the model (Fig. 4.8A). Estimated values: $k_e = 0.41 \pm 0.23$, $k_i = -0.59 \pm 0.29$, total change: -0.17 ± 0.18 for Awake; $k_e = 0.33 \pm 0.19$, $k_i = -0.40 \pm 0.13$, total change: -0.20 ± 0.13 for SWS-Up. **C**. Time constants of average excitatory and inhibitory conductance time course ahead of a spike in SWS and wake states. Estimated values: $T_e = 4.3 \pm 2.0$ ms, $T_i = 26.3 \pm 19.0$ ms for SWS; $T_e = 6.2 \pm 2.8$, $T_i = 22.3 \pm 7.9$ ms for Awake.

(see Materials and Methods). The STA conductances demonstrated a drop of total membrane conductance preceding the spike (Fig. 4.9A, Total), which occurred on a similar time scale compared to the model (compare with Fig. 4.8A). The decomposition of this conductance into excitatory and inhibitory components shows that the inhibitory conductance drops before the spike, while the excitatory conductance shows a steeper increase just prior to the spike (Fig. 4.9A; note that the latter increase is probably contaminated by voltage-dependent currents associated with spike generation). Such a pattern was observed in most of the cells tested (7 out of 10 cells in Awake, 6 out of 6 cells in SWS-Up and 2 out of 2 cells in REM; see Fig. 4.9B-C). An example of a neuron which did not show such a drop of total conductance is given in Supplementary Fig. 4. Most of the cells, however, yielded STAs qualitatively equivalent to that of the model when inhibition is dominant (Fig. 4.8A).

Finally, we investigated whether the dominance of inhibition (as deduced from conductance analysis) and the drop of conductance (from STA analysis) are related, by including all cells for which both analyses could be done (Fig. 4.10). The total conductance change before the spike was clearly related to the difference of excitatory and inhibitory conductance deduced from VmD analysis (gray area in Fig. 4.10A), indicating that cells dominated by inhibition generally gave rise to a drop of total conductance prior to the spike. However, there was no quantitative relation between the amplitude of those changes. Such a quantitative relation was obtained for conductance fluctuations (Fig. 4.10B), which indicates that the magnitude and sign of the conductance change prior to the spike is strongly related to the relative amount of excitatory and inhibitory conductance fluctuations. The clear correlation between the results of these two independent analyses therefore confirms that most neurons have strong and highly fluctuating inhibitory conductances during wake and sleep states.

4.5 Discussion

We have presented here a combination of intracellular recordings and computational models of cortical neurons, which points to the following conclusions: (i) V_m activity during wake and sleep states results from diverse combinations of excitatory and inhibitory conductances, with dominant inhibition in most of the cases; (ii) inhibitory conductance fluctuations are generally larger than for excitation; (iv) spike initiation is in most cases correlated with a decrease of inhibition, which appears as a transient drop of membrane conductance prior to the spike. We discuss below the significance of these findings.

It is important to note that the excitatory and inhibitory conductances were estimated here from somatic recordings. The values obtained therefore reflect the overall conductances as seen from the soma, after dendritic integration, and

4.5. DISCUSSION

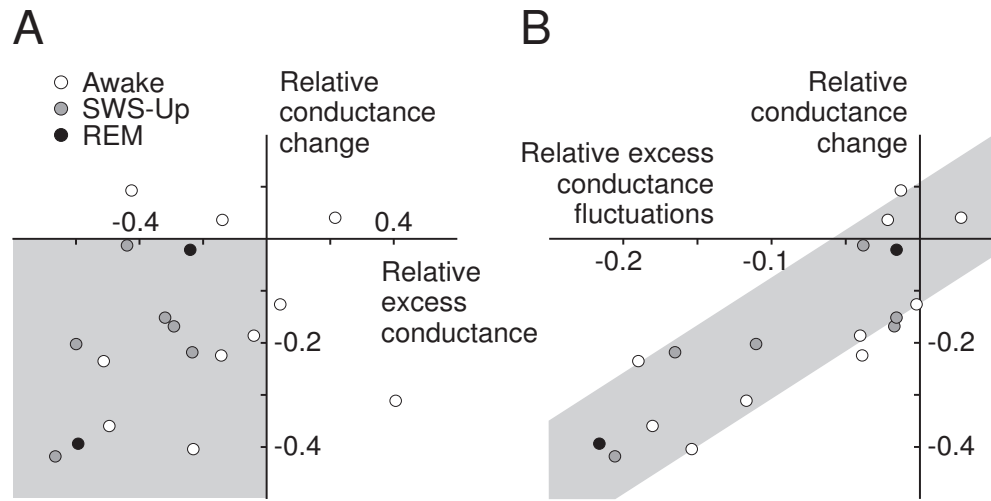


Figure 4.10: Relation between conductance STA and the estimates of conductance and variances. **A.** Relation between total membrane conductance change before the spike (“relative conductance change”, Eq. 4.4) obtained from STA analysis, and the difference of excitatory and inhibitory conductance (“relative excess conductance”, Eq. 4.5) estimated using the VmD method. Most cells are situated in the lower-left quadrant (gray), indicating a relation between inhibitory-dominant states and a drop of membrane conductance prior to the spike. **B.** Relation between relative conductance change before the spike and conductance fluctuations, expressed as the difference between excitatory and inhibitory fluctuations (“relative excess conductance fluctuations”, Eq. 4.6). Here, a clear correlation (gray area) shows that the magnitude of the conductance change before the spike is related to the amplitude of conductance fluctuations. Symbols: wake = open circles, SWS-Up = gray circles, REM = black circles. See Materials and Methods for definitions.

are necessarily different than the “total” conductance present in the soma and dendrites of the neuron. However, these somatic estimates are close to the conductance interplay underlying spike generation because the spike initiation zone (presumably in the axon; see Stuart et al. 1997) is electrotonically close to the soma.

Using such somatic estimates, dominant inhibition was seen in all cells during the up-states of slow-wave sleep ($n=7$ cells had more than 40% larger inhibitory conductance), and in the majority of neurons recorded in the wake state ($n=6$ cells showed clear dominant inhibitory conductances). This conclusion is robust to a number of parameter variations, including different hypotheses about the leak conductance. A notable exception is when high leak conductances (larger than synaptic activity) are assumed, in which case excitatory and inhibitory conductances are of comparable magnitude. However, this possibility is very unlikely in cats, because high leak conductances would predict dramatic effects of cesium on the V_m distribution, which is not what we observed (unpublished observations). Moreover, intracellular measurements in cats show that the total conductance resulting from intense synaptic activity is several-fold larger than the leak conductance (Borg-Graham et al. 1998; Paré et al. 1998). Nevertheless, some neurons were found to have roughly equal excitatory and inhibitory conductances during waking for reasonable values of the leak conductance (Fig. 4.4D). These results suggest that there exists a diversity of combinations of excitation and inhibition, which varies from cell to cell in the same network, as also shown previously for visual responses in anesthetized cats (Monier et al. 2003).

On the other hand, with the exception of one cell, the variance of inhibition was always larger than that of excitation, for all parameters tested. In contrast to conductance estimates, the VmD estimate of conductance variance does not depend on any hypothesis about the leak conductance. This high level of inhibitory fluctuations is consistent with previous measurements in cortical neurons under anesthesia (Rudolph et al. 2005; Hasenstaub et al. 2005). It suggests that a major part of V_m fluctuations are due to variations of inhibitory conductances. Because variations of V_m are most effective on evoking spikes, rather than the absolute V_m level (Mainen and Sejnowski 1995), these results suggest that inhibition is particularly effective in evoking spikes (see below).

Interestingly, we also found that a significant proportion of excitatory neurons cease firing during the wake state. Such wake-silent cells were also observed in motor cortex of young rats using whole-cell recordings (Brecht et al. 2004). The high proportion of these wake-silent cells (44.6%) suggests that there should be less excitatory conductance during wakefulness compared to slow-wave sleep, which is indeed what we observed. Interneurons also show diverse behaviors: the majority of FS cells recorded show an increase of firing in the wake state, while a minority shows the opposite (not shown). In contrast, all excitatory cells analyzed in the sleep-wake transition ($n=3$) show a decrease of inhibition

4.5. DISCUSSION

at the transition to waking. This discrepancy can be explained by bias in our sampling of different populations of interneurons, which are known to display opposite sensitivity to neuromodulators (Xiang et al. 1998), or by a different state of depression/potential at inhibitory synapses depending on behavioral state. In agreement with a previous study under anesthesia (Rudolph et al. 2005), these differences also suggest that up-states and EEG-activated states stem from similar, but non-identical network states.

In contrast with the present results, recent conductance measurements showed that, paradoxically, up and down states have a comparable input resistance in rat barrel cortex *in vivo* (Zou et al. 2005; Waters and Helmchen 2006). The difference is not due to contamination by action-potential related Na^+ currents, as suggested by Waters and Helmchen (2006), because the spikes are removed in our VmD analysis and the V-I relations were linear. Indeed, applying the VmD method to barrel cortex *in vivo* also gave the same paradoxical results (Zou et al. 2005), which were radically different than in association cortex of cats using the same method (Rudolph et al. 2005; present results). High-conductance states have also been observed *in vivo* in cat visual cortex (Borg-Graham et al. 1998; Hirsch et al. 1998; Anderson et al. 2000), in cat association cortex (Paré et al. 1998; Rudolph et al. 2005), and in ferret visual cortex (Haider et al. 2006), which suggests fundamental differences of network dynamics in different cortical regions.

The present evidence for dominant inhibition also contrasts with the roughly equal conductances measured in voltage-clamp during spontaneous up-states in ferret cortical slices (Shu et al. 2003) or *in vivo* (Haider et al. 2006). Although we also observed neurons with roughly equal conductances ($n=5$ for Wake, none for SWS-Up), this does not explain the differences. A possible explanation is that those voltage-clamp measurements were performed in the presence of Na^+ and K^+ channel blockers (QX314 and cesium), and these drugs affect somatodendritic attenuation by reducing the resting conductance. Consequently, excitatory events located in dendrites have a more powerful impact on the soma compared to the intact neuron, which may explain the discrepancy. Another possible explanation is that, in voltage-clamp experiments, when the voltage-clamp is applied from the soma, the more distal regions of the cell are unlikely to be clamped, which may result in errors in estimating conductances and reversal potentials. Moreover, in this case, the presence of uncompensated electrode series resistance may worsen the estimates or affect the ratio between excitation and inhibition (see simulations in Supplementary Table 1). Further conductance measurements should be performed in non-anesthetized animals to address these issues. On the other hand, our results are in agreement with conductance measurements performed in cortical neurons *in vivo* under anesthesia, which also show evidence for dominant inhibitory conductances (Borg-Graham et al 1998; Hirsch et al. 1998; Destexhe et al. 2003; Rudolph et al. 2005).

Not only inhibition seems to provide a major contribution to the conductance

state of the membrane, but also the conductance variations are larger for inhibition compared to excitation. This suggests that inhibition largely contributes to setting the V_m fluctuations, and therefore it presumably has a strong influence on action potential firing. This hypothesis was tested in computational models, which predicted that when inhibition is dominant, spikes are correlated with a prior decrease of inhibition, rather than an increase of excitation. This decrease of inhibition should be visible as a membrane conductance decrease prior to the spike, which is indeed what we observed in most neurons analyzed in wake and sleep states (Fig. 4.9). A prominent role for inhibition is also supported by previous intracellular recordings demonstrating a time locking of inhibitory events with action potentials in awake animals (Timofeev et al. 2001), and the powerful role of inhibitory fluctuations on spiking in anesthetized states (Hasenstaub et al. 2005). Taken together, these results suggest that strong inhibition is not a consequence of anesthesia, but rather represents a property generally seen in awake and natural sleep states, pleading for a powerful role for interneurons in determining neuronal selectivity and information processing.

4.5.1 Supplementary Information

Supplementary Methods

The classic “Ohmic” method to estimate synaptic conductances from intracellular data is based on temporal averaging of the passive membrane equation (Eq. 4.2). Under the assumption that the average membrane potential \bar{V} remains stationary, Eq. 4.2 yields

$$\bar{V} = \frac{E_L + (\bar{g}_e/G_L)E_e + (\bar{g}_i/G_L)E_i}{1 + \bar{g}_e/G_L + \bar{g}_i/G_L}, \quad (4.7)$$

where \bar{g}_e and \bar{g}_i denote the average excitatory and inhibitory conductance, respectively. Denoting the ratio between the total membrane input resistance in states without network activity and in active states with $r_{in} = R_{in}(\text{quiescent})/R_{in}(\text{active})$, one obtains

$$\frac{\bar{g}_{\{e,i\}}}{G_L} = \frac{r_{in}\bar{V} - E_L + E_{\{i,e\}}(1 - r_{in})}{E_{\{e,i\}} - E_{\{i,e\}}}. \quad (4.8)$$

This relation allows one to estimate the average relative contribution of inhibitory excitatory synaptic inputs in activated states. The value of r_{in} was 3 for the wake state, it was $r_{in} = 4$ for SWS up-states and $r_{in} = 5$ for REM sleep.

Conductance estimates in morphologically-reconstructed neurons

To compare the conductance analysis using the VmD method with other methods, we have performed additional simulations using models of reconstructed pyrami-

4.5. DISCUSSION

dal neurons. In a previous study (Rudolph et al., 2004), we showed using models of pyramidal neurons that the VmD method provides conductance estimates which are identical to those obtained using a “perfect” (zero series resistance) voltage-clamp in the soma. We extend here these simulations by comparing VmD and voltage-clamp estimates for different parameter variations (see Supplementary Table 1). A Layer VI pyramidal cell from cat was simulated with AMPA and GABA_A synapses distributed in soma and dendrites and which released randomly such as to reproduce *in vivo*-like activity (model from Destexhe and Paré, 1999). Different situations were considered: (a) the presence of a 10 nS somatic shunt to represent sharp-electrode impalement (same parameters as in Destexhe and Paré, 1999); (b) Cesium recordings by reducing 95% of the leak conductance in soma and dendrites; (c) Different values of the series resistance of the electrode (R_s). The presence of a somatic shunt had little effect on conductance estimates, while cesium leads to larger conductances, but the largest effect was that of series resistance: not only the amplitude of the measured conductances, but also the conductance variance, and the ratio between excitatory and inhibitory conductances.

Supplementary table

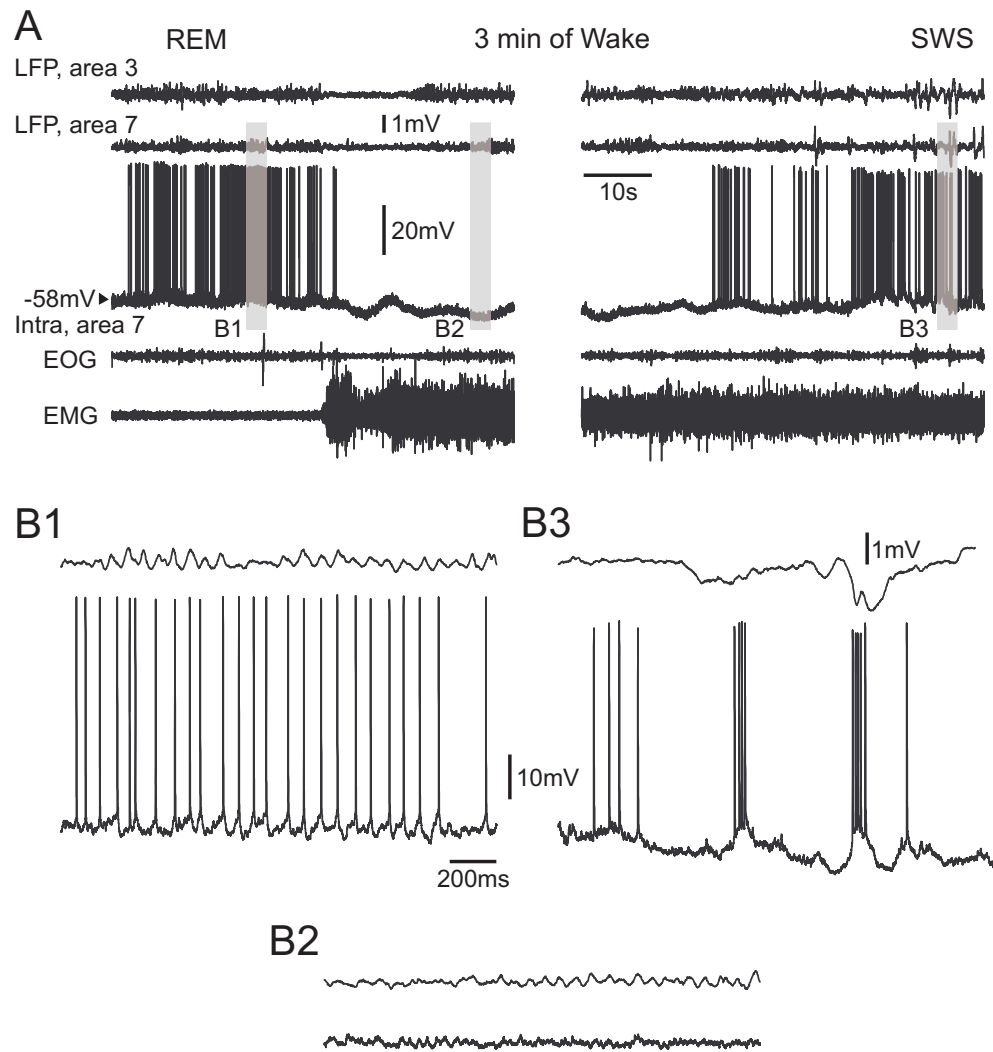
	g_{e0} (nS)	σ_e (nS)	g_{i0} (nS)	σ_i (nS)	g_{i0}/g_{e0}
Control, $R_s=0$	13.41	2.68	40.66	2.79	3.03
10 nS shunt, $R_s=0$	13.44	2.68	40.66	2.78	3.03
10 nS shunt, $R_s=3 \text{ M}\Omega$	11.3	2.05	30.0	2.02	2.65
10 nS shunt, $R_s=10 \text{ M}\Omega$	8.31	1.32	15.6	1.24	1.87
10 nS shunt, Cesium, $R_s=0$	13.57	2.70	43.9	2.83	3.23
10 nS shunt, Cesium, $R_s=3 \text{ M}\Omega$	11.36	2.07	33.97	2.07	2.99
10 nS shunt, Cesium, $R_s=10 \text{ M}\Omega$	8.32	1.34	20.3	1.28	2.44
10 nS shunt, Cesium, $R_s=15 \text{ M}\Omega$	7.04	1.07	14.6	1.01	2.07
10 nS shunt, Cesium, $R_s=25 \text{ M}\Omega$	5.46	0.76	7.46	0.71	1.36

Supplementary Table 1:

Table 4.1: Conductance estimates in voltage-clamp using a morphologically-reconstructed cortical pyramidal neuron. A model of background activity in a spatially distributed neuron (Layer VI pyramidal cell), with AMPA/GABA_A currents in soma and dendrites, was used (same model parameters as given in Destexhe and Paré, 1999). The “Control” conditions correspond to a perfect voltage-clamp (series resistance $R_s=0$), which was used to estimate the excitatory and inhibitory conductances visible from the somatic electrode. A 10 nS shunt was added in the soma, and the series resistance was varied. To simulate recordings in the presence of Cesium, the leak resistance was reduced by 95%, but the shunt was unaffected. The last column indicates the ratio between inhibitory and excitatory conductances. Both the amplitude of the measured conductance, and the ratio of excitation/inhibition, were highly dependent on series resistance.

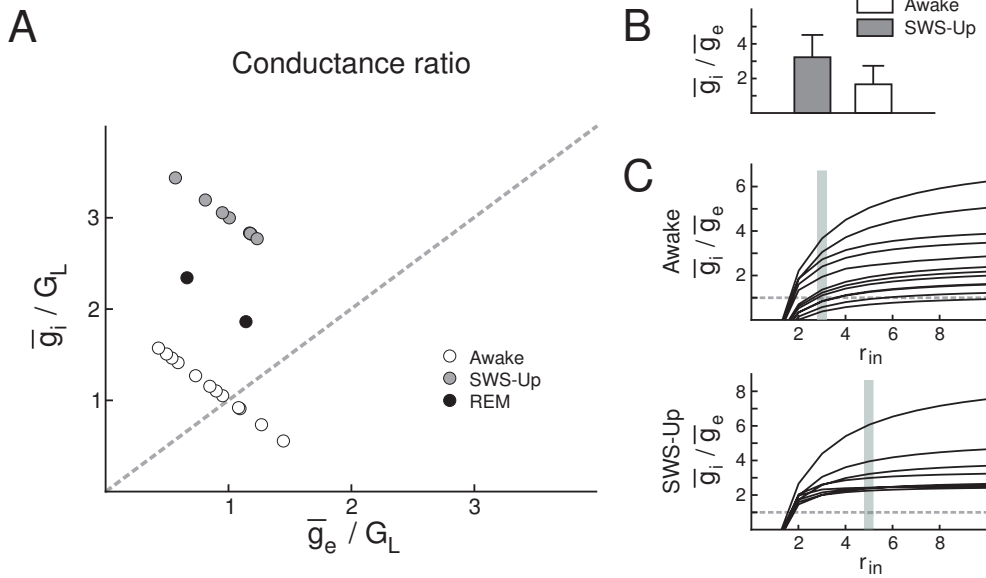
4.5. DISCUSSION

Supplementary figures



Supplementary Figure 1:

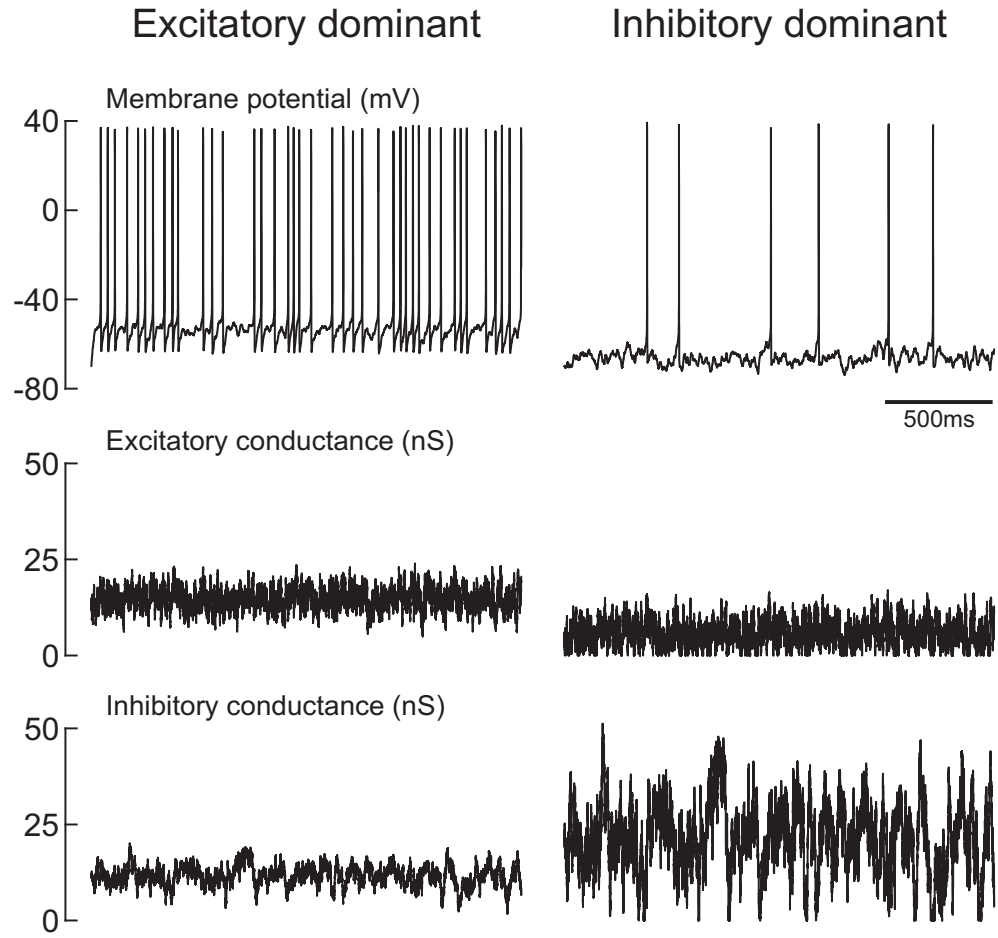
Figure 4.11: Example of wake-silent neuron recorded through different behavioral states. This neuron ceased firing during the REM to Wake transition (top left panel) and restarted firing as the animal drifted towards slow-wave sleep (top right panel). The bottom panels indicate the membrane potential and LFPs in those different states at higher resolution.



Supplementary Figure 2:

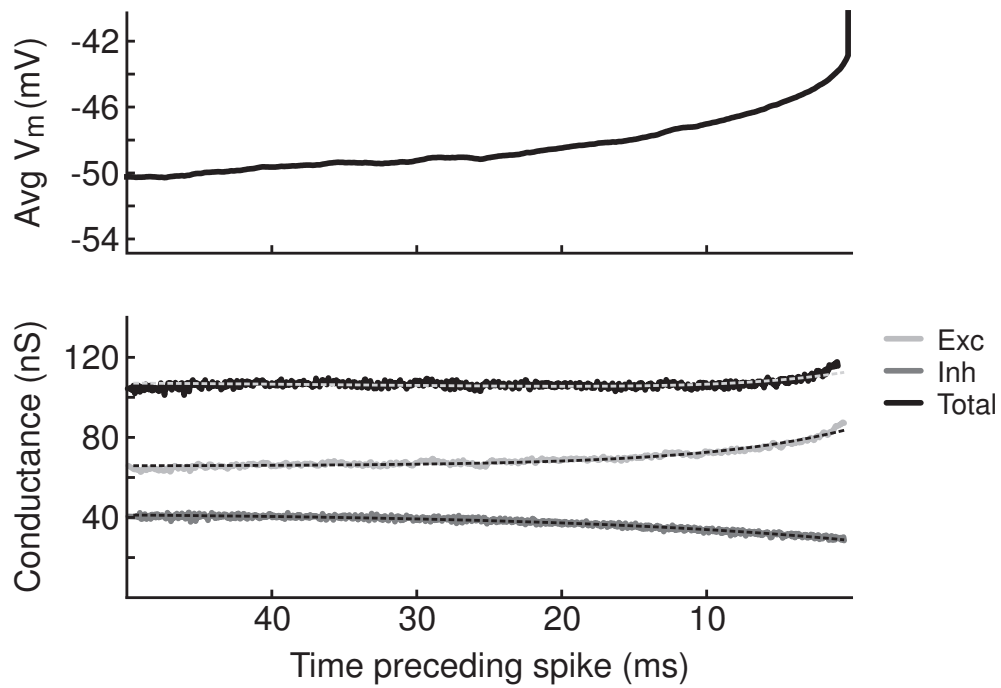
Figure 4.12: Estimation of relative conductances from intracellular recordings using the Ohmic method. **A.** Contribution of average excitatory (\bar{g}_e) and inhibitory (\bar{g}_i) conductances relative to the leak conductance G_L during wakefulness (Awake), slow-wave sleep up-states (SWS-Up) and REM sleep periods. Estimates were obtained by incorporating measurements of the average membrane potential (spikes excluded) into the passive membrane equation (Ohmic method, see Supplementary Methods). Estimated relative conductance values show a high variability among the investigated cells, but a general dominance of inhibition. **B.** Average ratio between inhibitory and excitatory mean conductances observed during wakefulness (Awake) and slow-wave sleep up-states (SWS-Up). Dominant inhibition was observed in both states, and more pronounced during SWS. **C.** Variations of the ratio between average inhibitory and excitatory conductance values as a function of different choices for the leak conductance. $r_{in} = R_{in}(\text{quiescent})/R_{in}(\text{active})$; the gray area indicates the values used for conductance estimation used in **A** and **B**.

4.5. DISCUSSION



Supplementary Figure 3:

Figure 4.13: Computational models of two different conductance dynamics in the wake state. Two examples similar to Fig. 4.7A are shown for conductance measurements in two other cells. Left panel: neuron where the excitatory conductance was larger than the inhibitory conductance (“Excitatory dominant”). Right panel: neuron for which the inhibition was more pronounced (“Inhibitory dominant”; this type of cell represented the majority of cells in the waking state). Same parameters as in Fig. 4.7A and Methods, except $g_{e0} = 14.6$ nS, $g_{i0} = 12.1$ nS, $\sigma_e = 2.7$ nS, $\sigma_i = 2.8$ nS (left panel); $g_{e0} = 5.7$ nS, $g_{i0} = 22.8$ nS, $\sigma_e = 3.3$ nS, $\sigma_i = 10.0$ nS (right panel).



Supplementary Figure 4:

Figure 4.14: Example of cell showing an increase of total membrane conductance preceding spikes during the wake state. For this particular neuron recorded during the wake state, the STA showed an increase of total membrane conductance prior to the spike. Same description of panels and curves as in Fig. 4.9A, Awake.

4.6 References

- Anderson J. S., Carandini M., Ferster D. Orientation tuning of input conductance, excitation and inhibition in cat primary visual cortex. *J. Neurophysiol.* **84**: 909-926, 2000.
- Baranyi A., Szente M. B., Woody C. D. Electrophysiological characterization of different types of neurons recorded in vivo in the motor cortex of the cat. II. Membrane parameters, action potentials, current-induced voltage responses and electrotonic structures. *J. Neurophysiol.* **69**: 1865-1879, 1993.
- Borg-Graham L. J., Monier C., Frégnac Y. Visual input evokes transient and strong shunting inhibition in visual cortical neurons. *Nature* **393**: 369-373, 1998.
- Brecht M., Schneider M., Sakmann B., Margrie T. W. Whisker movements evoked by stimulation of single pyramidal cells in rat motor cortex. *Nature* **427**: 704-710, 2004.
- Destexhe A. and Paré D. Impact of network activity on the integrative properties of neocortical pyramidal neurons in vivo. *J. Neurophysiol.* **81**: 1531-1547, 1999.
- Destexhe A., Rudolph M., Fellous J.-M., Sejnowski T.J. Fluctuating synaptic conductances recreate in vivo-like activity in neocortical neurons. *Neuroscience* **107**: 13-24, 2001.
- Destexhe A., Rudolph M. and Paré D. The high-conductance state of neocortical neurons in vivo. *Nature Reviews Neurosci.* **4**: 739-751, 2003.
- Haider B., Duque A., Hasenstaub A. R., McCormick D.A. Neocortical network activity in vivo is generated through a dynamic balance of excitation and inhibition. *J. Neurosci.* **26**: 4535-4545, 2006.
- Hasenstaub A., Shu Y., Haider B., Kraushaar U., Duque A. and McCormick D.A. Inhibitory postsynaptic potentials carry synchronized frequency information in active cortical networks. *Neuron* **47**: 423-435, 2005.
- Hines M.L., Carnevale N.T. The NEURON simulation environment, *Neural Computation* **9**: 1179-1209, 1997.
- Hirsch J. A., Alonso J. M, Clay Reid R., Martinez L. M. Synaptic integration in striate cortical simple cells. *J. Neurosci.* **18**: 9517-9528, 1998.
- Kuhn A., Aertsen A., Rotter S. Neuronal integration of synaptic input in the fluctuation-driven regime. *J. Neurosci.* **24**: 2345-2356, 2004.

- Mainen Z. F., Sejnowski T. J. Reliability of spike timing in neocortical neurons. *Science* **268**: 1503-1506, 1995.
- Matsumura M., Cope T., Fetz E. E. Sustained excitatory synaptic input to motor cortex neurons in awake animals revealed by intracellular recording of membrane potentials. *Exp. Brain Res.* **70**: 463-469, 1988.
- McCormick D. A. Neurotransmitter actions in the thalamus and cerebral cortex and their role in neuromodulation of thalamocortical activity. *Prog. Neurobiol.* **39**: 337-388, 1992.
- Metherate R., Ashe J. H. Ionic flux contributions to neocortical slow waves and nucleus basalis-mediated activation: whole-cell recordings in vivo. *J Neurosci* **13**: 5312-5323, 1993.
- Monier C., Chavane F., Baudot P., Graham L. J., Frégnac Y. Orientation and direction selectivity of synaptic inputs in visual cortical neurons: a diversity of combinations produces spike tuning. *Neuron* **37**: 663-680, 2003.
- Paré D., Shink E., Gaudreau H., Destexhe A., Lang E. J. Impact of spontaneous synaptic activity on the resting properties of cat neocortical neurons in vivo. *J. Neurophysiol.* **79**: 1450-1460, 1998.
- Pospischil M., Piwkowska Z., Rudolph M., Bal T. and Destexhe A. Calculating event-triggered average synaptic conductances from the membrane potential. *J. Neurophysiol.*, in press, 2007.
- Pospischil M., Rudolph M., Shulz D., Timofeev I., Destexhe A. Are we inhibited when we are awake ? A combined intracellular and computational analysis of membrane potential dynamics in cortical neurons of awake and naturally sleeping animals. *Soc. Neurosci. Abstracts* **31**: 276.15, 2005
- Priebe N. J., Ferster D. Direction selectivity of excitation and inhibition in simple cells of the cat primary visual cortex. *Neuron* **45**: 133-145, 2005.
- Press W. H., Flannery B. P., Teukolsky S. A., Vetterling W. T. *Numerical Recipes. The Art of Scientific Computing*. Cambridge University Press, Cambridge, MA, 1986.
- Rudolph M., Destexhe A. Characterization of subthreshold voltage fluctuations in neuronal membranes. *Neural Computation* **15**: 2577-2618, 2003.
- Rudolph M., Destexhe A. An extended analytic expression for the membrane potential distribution of conductance-based synaptic noise. *Neural Computation* **17**: 2301-2315, 2005.

4.6. REFERENCES

- Rudolph M., Destexhe A. Multichannel shot noise approach to describe synaptic background activity in neurons. *Eur. Phys. J. B* **52**: 125-132, 2006.
- Rudolph M., Piwkowska Z., Badoual M., Bal T., Destexhe A. A method to estimate synaptic conductances from membrane potential fluctuations. *J. Neurophysiol.* **91**: 2884-2896, 2004.
- Rudolph M., Pelletier J.-G., Paré D., Destexhe A. Characterization of synaptic conductances and integrative properties during electrically-induced EEG-activated states in neocortical neurons in vivo. *J. Neurophysiol.* **94**: 2805-2821, 2005.
- Shu Y., Hasenstaub A., McCormick D. A. Turning on and off recurrent balanced cortical activity. *Nature* **423**: 288-293, 2003.
- Steriade M., McCarley R.W. *Brainstem Control of Wakefulness and Sleep*. Plenum Press, New York, 1990.
- Steriade M., Timofeev I., Grenier F. Natural waking and sleep states: a view from inside neocortical neurons. *J. Neurophysiol.* **85**: 1969-1985, 2001.
- Stuart G., Spruston N., Sakmann B., Hausser M. Action potential initiation and backpropagation in neurons of the mammalian CNS. *Trends Neurosci.* **20**: 125-131, 1997.
- Timofeev I., Grenier F., Steriade M. Disfacilitation and active inhibition in the neocortex during the natural sleep-wake cycle: an intracellular study. *Proc. Natl. Acad. Sci. USA* **98**: 1924-1929, 2001.
- Wehr M., Zador A. M. Balanced inhibition underlies tuning and sharpens spike timing in auditory cortex. *Nature* **426**: 442-446, 2003.
- Xiang Z., Huguenard J. R., Prince D. A. Cholinergic switching within neocortical inhibitory networks. *Science* **281**: 985-988, 1998.
- Waters J., Helmchen F. Background synaptic activity is sparse in neocortex. *J. Neurosci.* **26**: 8267-8277, 2006.
- Zou Q., Rudolph M., Roy N., Sanchez-Vives M., Contreras D., Destexhe A. Reconstructing synaptic background activity from conductance measurements in vivo. *Neurocomputing* **65**: 673-678, 2005.

Chapter 5

Characterizing synaptic conductance fluctuations in cortical neurons and their influence on spike generation

Zuzanna Piwkowska, Martin Pospischil, Romain Brette, Julia Sliwa, Michelle Rudolph-Lilith, Thierry Bal and Alain Destexhe. Characterizing synaptic conductance fluctuations in cortical neurons and their influence on spike generation. *submitted*, 2007.

Résumé

Introduction

Les neurones du cortex cérébral sont sujets à une activité très intense et irrégulière. Une série de méthodes ont été introduites basées sur une représentation stochastique de l'activité synaptique, le modèle d'Ornstein-Uhlenbeck (1930). Cet article réalise une revue de ces différentes méthodes en les comparant pour la première fois à partir des mêmes données.

Résultats obtenus

La première méthode est l'estimation "VmD" de conductance à partir de la distribution du potentiel de membrane. Nous montrons l'application de cette méthode à partir de modèles numériques et à partir de neurones du cortex visuel *in vitro*. Des estimations sont également réalisées *in vivo* (cfr Chapitre 4).

La deuxième méthode est l'estimation des constantes de temps synaptiques par la densité spectrale (PSD) du potentiel membranaire. Nous analysons l'applicabilité de cette méthode par simulation numérique, enregistrements en dynamic-clamp dans des neurones du cortex visuel *in vitro* et du cortex associatif du chat *in vivo*.

La troisième méthode analysée est la méthode STA exposée au Chapitre 3. Nous comparons les simulations numériques avec les données obtenues en dynamic-clamp *in vitro* et chez le chat *in vivo*. Nous donnons également une nouvelle version de cette méthode qui contient un paramètre additionnel de corrélation entre excitation et inhibition.

En particulier, nous donnons une interprétation géométrique qui explique pourquoi la variance forte de l'inhibition implique d'observer une diminution de conductance liée aux PAs. Cette corrélation est observée lors d'expériences récentes réalisées en dynamic-clamp *in vitro*.

Conclusions

En conclusion, cet article procure une revue des différentes méthodes pour caractériser l'activité synaptique lors d'enregistrements intracellulaires, à partir du seul V_m . Une analyse critique de ces méthodes est donnée, et nous concluons que ces méthodes procurent un ensemble d'analyse très puissant, mais qui connaît certaines limitations dont l'utilisateur doit être conscient.

5.1 Abstract

Cortical neurons are subject to sustained and irregular synaptic activity which causes important fluctuations of the membrane potential (V_m). We review here different methods to characterize this activity and its impact on spike generation. The simplified, fluctuating point-conductance model of synaptic activity provides the starting point of a variety of methods for the analysis of intracellular V_m recordings. In this model, the synaptic excitatory and inhibitory conductances are described by Gaussian-distributed stochastic variables, or “colored conductance noise”. The matching of experimentally recorded V_m distributions to an invertible theoretical expression derived from the model allows the extraction of parameters characterizing the synaptic conductance distributions. This analysis can be complemented by the matching of experimental V_m power spectral densities (PSDs) to a theoretical template, even though the unexpected scaling properties of experimental PSDs limit the precision of this latter approach. Building on this stochastic characterization of synaptic activity, we also propose methods to qualitatively and quantitatively evaluate spike-triggered averages of synaptic time-courses preceding spikes. This analysis points to an essential role for synaptic conductance variance in determining spike times. The presented methods are evaluated using controlled conductance injection in cortical neurons *in vitro* with the dynamic-clamp technique. We review their applications to the analysis of *in vivo* intracellular recordings in cat association cortex, which suggest a predominant role for inhibition in determining both sub- and supra-threshold dynamics of cortical neurons embedded in active networks.

5.2 Introduction

Cerebral cortical networks can generate states of intense and irregular activity, which are characterized by low-amplitude “desynchronized” fast activity in the electroencephalogram (EEG), a defining feature of the awake state. Intracellular measurements in awake animals (Woody and Gruen, 1978; Matsumura et al., 1988; Baranyi et al., 1993; Steriade et al., 2001; Timofeev et al., 2001; Rudolph et al., 2007) have shown that cortical neurons are depolarized (about -60 mV), have a low input resistance, their membrane potential fluctuates, and they fire irregularly and sustainedly. During slow-wave sleep, or under several types of anesthetics (such as urethane or ketamine-xylazine), the membrane potential displays “up-” (depolarized) and “down-” (hyperpolarized) states, which are paralleled with EEG slow waves (Metherate and Ashe, 1993; Steriade et al., 1993; Steriade et al., 2001; Timofeev et al., 2001). During the up-state, the EEG is desynchronized and the membrane potential of cortical neurons is depolarized and highly fluctuating, similar to the sustained activity found in awake animals (Destexhe et al., 2007).

5.2. INTRODUCTION

Up- and down-states have also been found in ferret cortical slices using high-potassium and low-calcium extracellular media (Sanchez-Vives and McCormick, 2000) and in rat entorhinal slices as a function of the metabolic state (Cunningham et al., 2006): these experiments indicate that intracortical circuits are able to generate such states, presumably through recurrent excitation and inhibition. TTX block of action potentials *in vivo* (Paré et al., 1998) and CNQX block of excitatory synapses *in vitro* (Cunningham et al., 2006) abolish the depolarized, fluctuating states, which confirms their synaptic origin.

The recurrent activity of cortical networks has been investigated using computational models at different levels and including various degrees of biological detail. Large networks of formal (or simple spiking) neurons allow the analytic derivation (or numerical confirmation) of conditions for different classes of network activity, such as oscillations or deterministic chaos (Van Vreeswijk and Sompolinsky, 1996; Roxin et al., 2005; Barak and Tsodyks, 2007). Network models incorporating a realistic diversity of cell types and details of cortical connectivity allow quantitative predictions to be obtained through numerical simulations (Compte et al., 2003; Hill and Tononi, 2005). At the single neuron level, detailed models can include the cell's morphology, a variety of intrinsic ion channels and distributed synaptic inputs: studies of such models assess the impact of massive input from the cortical network on dendritic processing, spike train statistics, neuronal responsiveness and integrative properties (Bernander et al., 1991; Destexhe and Paré, 1999; Rudolph and Destexhe 2003b,c; Destexhe et al., 2003). However, the parameterization of all those models requires a large amount of information that cannot be obtained from any single experiment, which complicates the comparison of simulation results with biological data.

A complementary approach consists in developing and studying models that are relatively simple, but contain variables and parameters that can all be related to quantities directly measured in experiments. The point-conductance model is one such example (Destexhe et al., 2001): it describes the evolution of the subthreshold V_m of a single-compartment neuron by a passive membrane equation with two additional stochastic conductance variables, $g_e(t)$ and $g_i(t)$. These variables, modeled as Ornstein-Uhlenbeck (Brownian-motion-like) processes, represent the effective impact at the soma of thousands of single synapses, respectively excitatory and inhibitory, activated by Poisson spike trains. We present here how this model can be used in close combination with electrophysiological experiments to investigate the properties and the impact of cortical recurrent activity at the single neuron level.

More specifically, we critically review, on the basis of new as well as already published data, applications of the point-conductance model of synaptic activity to the analysis of intracellular recordings in cortical neurons: in each case, we first briefly describe the method of analysis, then we show how it can be validated experimentally by using controlled “conductance injection” in biological neurons

with dynamic-clamp, and finally we present the application of the method to the analysis of real synaptic activity. We especially focus on recently developed approaches for determining which of the conductance configurations occurring in the fluctuating synaptic activity trigger spikes.

5.3 Methods

5.3.1 Computational methods

Computational models were based on single-compartment neurons described by the following membrane equation:

$$C \frac{dV}{dt} = -G_L (V - E_L) - g_e (V - E_e) - g_i (V - E_i) + I_{ext} , \quad (5.1)$$

where C denotes the membrane capacitance, I_{ext} a stimulation current, G_L the leak conductance and E_L the leak reversal potential. $g_e(t)$ and $g_i(t)$ are stochastic excitatory and inhibitory conductances, with respective reversal potentials E_e and E_i .

These effective synaptic conductances were described by the following Ornstein-Uhlenbeck model (Destexhe et al., 2001):

$$\frac{dg_e(t)}{dt} = -\frac{1}{\tau_e} [g_e(t) - g_{e0}] + \sqrt{\frac{2\sigma_e^2}{\tau_e}} \xi_e(t) \quad (5.2)$$

$$\frac{dg_i(t)}{dt} = -\frac{1}{\tau_i} [g_i(t) - g_{i0}] + \sqrt{\frac{2\sigma_i^2}{\tau_i}} \xi_i(t) , \quad (5.3)$$

where g_{e0} and σ_e^2 are, respectively, the mean value and variance of the excitatory conductance, τ_e is the excitatory time constant, and $\xi_e(t)$ is a Gaussian white noise source with zero mean and unit standard deviation. The inhibitory conductance $g_i(t)$ is described by an equivalent equation (Eq. 5.3) with parameters g_{i0} , σ_i^2 , τ_i and noise source $\xi_i(t)$.

In some simulations, the voltage-dependent conductances responsible for action potentials, g_{Na} and g_{Kd} (with respective reversals E_{Na} and E_K), were included. They were described by Hodgkin-Huxley type models (with equations and parameters identical as described in Destexhe et al., 2001, and references therein), resulting in the following equation:

$$C \frac{dV}{dt} = -G_L (V - E_L) - g_{Na} (V - E_{Na}) - g_{Kd} (V - E_K) - g_e (V - E_e) - g_i (V - E_i) + I_{ext} . \quad (5.4)$$

Simulations were performed on LINUX workstations using the NEURON simulation environment (Hines and Carnevale, 1997).

5.3. METHODS

5.3.2 Biological preparation

In vitro experiments were performed on 380-400 μm thick coronal or sagittal slices from the lateral portions of pentobarbital-anesthetized adult ferret (Marshall Europe, Lyon) and guinea-pig (CPA, Olivet, France) occipital cortex, as described previously (Rudolph et al., 2004; Pospischil et al., 2007). Slices were maintained in an interface style recording chamber at 33-35 $^{\circ}\text{C}$ in slice solution containing (in mM) 124 NaCl, 2.5 KCl, 1.2 MgSO_4 , 1.25 NaHPO_4 , 2 CaCl_2 , 26 NaHCO_3 , and 10 dextrose and aerated with 95% O_2 -5% CO_2 to a final pH of 7.4. In some experiments on ferret cortical slices, after approximately 1 hour, the solution was modified to contain 1 mM MgSO_4 , 1 mM CaCl_2 and 3.5 mM KCl (Sanchez-Vives and McCormick, 2000) in order to obtain up-states. Intracellular recordings following two hours of recovery were performed in all cortical layers on electrophysiologically identified regular spiking and intrinsically bursting cells.

All research procedures concerning the experimental animals and their care adhered to the American Physiological Society's Guiding Principles in the Care and Use of Animals, to the European Council Directive 86/609/EEC and to European Treaties series no. 123, and was also approved by the local ethics committee "Ile-de-France Sud" (certificate no. 05-003).

We also review data from intracellular recordings in cat association cortex *in vivo*, which were described in detail elsewhere (Rudolph et al., 2005; Steriade et al., 2001; Rudolph et al., 2007).

5.3.3 Electrophysiology

Sharp electrodes for intracellular recordings were made on a Sutter Instruments P-87 micropipette puller from medium-walled glass (WPI, 1BF100) and beveled on a Sutter Instruments beveler (BV-10M). Micropipettes were filled with 1.2-2 M potassium acetate - 4 mM potassium chloride and had resistances of 65-110 $\text{M}\Omega$ after beveling. An Axoclamp 2B amplifier (Axon Instruments) was used for V_m recording and current injection. A Digidata 1322A card (Axon Instruments) was used for data acquisition at 20 kHz.

The dynamic-clamp technique (Robinson et al., 1993; Sharp et al., 1993) was used to inject computer-generated conductances in real neurons. Dynamic-clamp experiments were run as described previously (Rudolph et al., 2004, Pospischil et al., 2007) using the hybrid RT-NEURON environment (developed by G. Le Masson, INSERM 358, Université Bordeaux 2), which is a modified version of NEURON (Hines and Carnevale, 1997) running in real-time under the Windows 2000 operating system (Microsoft Corp.). In these experiments, the injected current I_{DynClamp} was determined from the fluctuating conductances $g_e(t)$ and $g_i(t)$ modeled with Ornstein-Uhlenbeck processes (Eqs. 5.2-5.3) as well as from the difference between the recorded membrane voltage V and the respective reversal

potentials:

$$I_{DynClamp} = -g_e(V - E_e) - g_i(V - E_i) . \quad (5.5)$$

The contamination of measured membrane voltage by electrode artefacts was avoided either through the use of the discontinuous current-clamp mode (in which current injection and voltage recording alternate at frequencies of 2-3 kHz with our electrodes) or with Active Electrode Compensation, a novel, high-resolution digital on-line compensation technique we have recently developed (Brette et al., 2005; Rudolph et al., 2005).

5.3.4 Data analysis

The PC-based software ELPHY (developed by G. Sadoc, CNRS Gif-sur-Yvette, ANVAR and Biologic), Statview, Excel, custom-written C-code and Neuron-code were used for analyses. All values are given as average \pm standard deviation.

VmD analysis

In dynamic-clamp experiments re-creating up-states with conductance injection, two approaches were used. In 3 cells, conductance estimates were computed for different, realistic values of leak conductance and cell capacitance, and were then tested against the real up-states in dynamic-clamp. In 2 cells, leak conductance and cell capacitance were estimated from the response to short current pulses, and those values were then used for conductance estimation: the estimated conductance parameters, when used for dynamic-clamp injection, proved to allow successful matching of the real up-state in terms of Vm distributions. In all cases, conductance estimation was done during the recording using ELPHY.

VmD analysis of the *in vivo* data reviewed here is described in Rudolph et al., 2005 and Rudolph et al., 2007.

PSD analysis

Power spectra of V_m activity were fit to an analytic template (see Results) using a simplex fitting algorithm (Press et al., 1986). Different initial conditions (“first guesses”) were given to the fitting procedure to ensure that there was no convergence to local minima. Some fits were realized by fitting both the amplitude of excitatory and inhibitory components (A_e and A_i ; see Results), as well as the time constants (τ_e and τ_i). In other cases, it was not possible to fit 4 parameters from the experimental PSD. In such cases (typically from *in vivo* data), the fit was performed with a single amplitude component ($A_e = A_i$). In all cases, the effective membrane time constant ($\tilde{\tau}_m$) was fixed to the value estimated from the recordings.

5.4. RESULTS

STA analysis

For each conductance injection, spikes were detected using a threshold at -30 mV. Inter-spike-intervals (ISIs) were computed and for further analysis, a stable region in terms of ISI distribution was used (as assessed by a non-significant Spearman correlation test between ISI duration and time), including 673 ± 493 spikes. When investigating the impact of frequency on the accuracy of the estimates, the same number of spikes (52) was used for all analyzed injections. Spikes following ISIs of at least 100 ms were then selected. 50-ms-long pieces of V_m , g_e and g_i preceding each selected spike were averaged to obtain the “measured STAs”. We checked that excluding spikes following ISIs shorter than 100 ms did not affect the STAs in an important way: the difference in measured conductance variation before the spike was of -0.14 ± 0.35 nS for excitation, and of 0.5 ± 0.7 nS for inhibition. In order to compare with the STA extraction method based on the V_m STA, it is important to exclude short ISIs from the analysis to avoid contamination of the V_m STA by preceding spikes or by their after-hyperpolarizations.

For conductance STAs extraction based on the V_m STA, parameters were obtained in the following way: responses to depolarizing current pulses were used to estimate the membrane capacitance from the time constant of exponential fits to the decay of the V_m , and the leak conductance was obtained by dividing the average voltage during conductance injection, relative to rest, by the average injected current. When analyzing *in vivo* recordings, the leak conductance obviously cannot be obtained in this way. However, *in vivo*, the total membrane conductance was estimated each time, which was not done *in vitro* since most conductance injections were performed at only one current level: the chosen procedure for leak conductance estimation is meant to get as close as possible to the situation where the total conductance is constrained. More information about the STA analysis of the *in vivo* data reviewed here can be found in Rudolph et al. (2007).

To quantify both the measured and the extracted conductance STAs, we fitted the conductance time courses using the exponential template

$$g_e(t) = g_{e0}^{STA} \left[1 + k_e \exp \frac{(t - t_0)}{\tau_{g_e}^{STA}} \right], \quad (5.6)$$

for excitation, and an equivalent equation for inhibition. Here, t_0 stands for the time of the spike, k_e quantifies the maximal increase/decrease of conductance prior to the spike ($\Delta g_e = g_{e0} k_e$), with time constant $\tau_{g_e}^{STA}$, and g_{e0}^{STA} is the average baseline conductance (see Results).

5.4 Results

The point-conductance model of recurrent cortical activity describes the evolution of the subthreshold V_m of a point neuron based on two effective fluctuating

conductances g_e and g_i (Destexhe et al., 2001; see Methods for equations). The basic assumption of this model is that the synaptic conductances can be described as Gaussian-distributed stochastic variables. It was shown that the well-known Ornstein-Uhlenbeck model of Brownian noise (Uhlenbeck and Ornstein, 1930) approximates very well the total synaptic conductances resulting from a large number of conductance-based synaptic inputs (Destexhe et al., 2001; Destexhe and Rudolph, 2004). A fitting of this simple model to the results of numerical simulations using realistic cortical neuron morphologies and distributed synaptic inputs indicates the following correspondences between variables: the time constants (τ_e , τ_i) are identical to the decay time constants of synaptic currents. The average conductance (g_{e0} , g_{i0}) is related to the overall (integrated) conductance, which depends on the release frequency of the corresponding Poisson inputs, the quantal conductance and the decay time of synaptic currents. The variance of the conductances (σ_e^2 , σ_i^2) is related to the same parameters, as well as to the synchrony between inputs of the same type.

The theoretical and numerical analysis of the point-conductance model has led to various useful derivations: an invertible expression for the steady-state distribution of V_m fluctuations (Rudolph and Destexhe, 2003, 2005), an expression for the power spectral density of V_m fluctuations (Destexhe and Rudolph, 2004), a geometrical analysis of the configuration of conductances directly preceding spikes, and a probabilistic method for calculating the most likely conductance time course preceding spikes given an average V_m time course (Pospischil et al., 2007). We now proceed to examine in more detail the applications of these computational results to the analysis of intracellular recordings in cortical neurons.

5.4.1 The VmD method for extracting synaptic conductance parameters

Outline of the VmD method

The model described by Eqs. 5.1–5.3 has been thoroughly studied theoretically and numerically. This model describes the subthreshold V_m fluctuations of a neuron subject to fluctuating conductances g_e and g_i . Different analytic approximations have been proposed to describe the steady-state distribution of these V_m fluctuations (Rudolph and Destexhe, 2003, 2005; Richardson, 2004; Lindner and Longtin, 2006; for a comparative study, see Rudolph and Destexhe, 2006). One of these expressions is invertible (Rudolph and Destexhe, 2003, 2005), which enables one to directly estimate the parameters (g_{e0} , g_{i0} , σ_e , σ_i) from experimentally calculated V_m distributions. This constitutes the basis of the VmD method (Rudolph et al., 2004), which we outline below.

The essential idea behind the VmD method is to fit an analytic expression to the steady-state subthreshold V_m distribution obtained experimentally, and yield

5.4. RESULTS

estimates of the parameters (mean, variance) of the underlying synaptic conductances. Among the different analytic expressions outlined above, we consider the following Gaussian approximation of the steady-state V_m distribution:

$$\rho(V) \sim \exp \left[-\frac{(V - \bar{V})^2}{2\sigma_V^2} \right], \quad (5.7)$$

where \bar{V} is the average V_m and σ_V its standard deviation. This expression provides an excellent approximation of the V_m distributions obtained from models and experiments (Rudolph et al., 2004), because the V_m distributions obtained experimentally show little asymmetry (for up-states and activated states; for specific examples, see Figs. 5.1 and 5.2, and Rudolph et al., 2004, 2005, 2007).

One main advantage of this Gaussian approximation is that it can be inverted, which leads to expressions of the synaptic noise parameters as a function of the V_m measurements, \bar{V} and σ_V . By fixing the values of τ_e and τ_i , which are related to the decay time of synaptic currents and can be estimated from voltage-clamp data and/or current-clamp by using power spectral analysis (see Section 5.4.2), we remain with four parameters to estimate: the means (g_{e0} , g_{i0}) and standard deviations (σ_e , σ_i) of excitatory and inhibitory synaptic conductances. To extract these four conductance parameters from the membrane probability distribution, Eq. 5.7 is, however, insufficient because it is characterized by only two parameters (\bar{V} , σ_V). To solve this problem, one possibility is to consider two V_m distributions obtained at two different constant levels of injected current I_{ext1} and I_{ext2} . In this case, the Gaussian approximation (Eq. 5.7) of the two distributions gives two mean V_m values, \bar{V}_1 and \bar{V}_2 , and two standard deviation values, σ_{V1} and σ_{V2} . The resulting system of four equations relating V_m parameters with conductance parameters can now be solved for four unknowns:

$$g_{\{e,i\}0} = \frac{(I_{ext1} - I_{ext2}) \left[\sigma_{V2}^2 (E_{\{i,e\}} - \bar{V}_1)^2 - \sigma_{V1}^2 (E_{\{i,e\}} - \bar{V}_2)^2 \right]}{\left[(E_e - \bar{V}_1)(E_i - \bar{V}_2) + (E_e - \bar{V}_2)(E_i - \bar{V}_1) \right] (E_{\{e,i\}} - E_{\{i,e\}}) (\bar{V}_1 - \bar{V}_2)^2} - \frac{(I_{ext1} - I_{ext2})(E_{\{i,e\}} - \bar{V}_2) + [I_{ext2} - G_L(E_{\{i,e\}} - E_L)] (\bar{V}_1 - \bar{V}_2)}{(E_{\{e,i\}} - E_{\{i,e\}}) (\bar{V}_1 - \bar{V}_2)}, \quad (5.8)$$

$$\sigma_{\{e,i\}}^2 = \frac{2C (I_{ext1} - I_{ext2}) \left[\sigma_{V1}^2 (E_{\{i,e\}} - \bar{V}_2)^2 - \sigma_{V2}^2 (E_{\{i,e\}} - \bar{V}_1)^2 \right]}{\tilde{\tau}_{\{e,i\}} \left[(E_e - \bar{V}_1)(E_i - \bar{V}_2) + (E_e - \bar{V}_2)(E_i - \bar{V}_1) \right] (E_{\{e,i\}} - E_{\{i,e\}}) (\bar{V}_1 - \bar{V}_2)^2}. \quad (5.9)$$

Here, $\tilde{\tau}_{\{e,i\}}$ are effective time constants given by (Rudolph and Destexhe, 2005):

$$\tilde{\tau}_{\{e,i\}} = \frac{2\tau_{\{e,i\}}\tilde{\tau}_m}{\tau_{\{e,i\}} + \tilde{\tau}_m}, \quad (5.10)$$

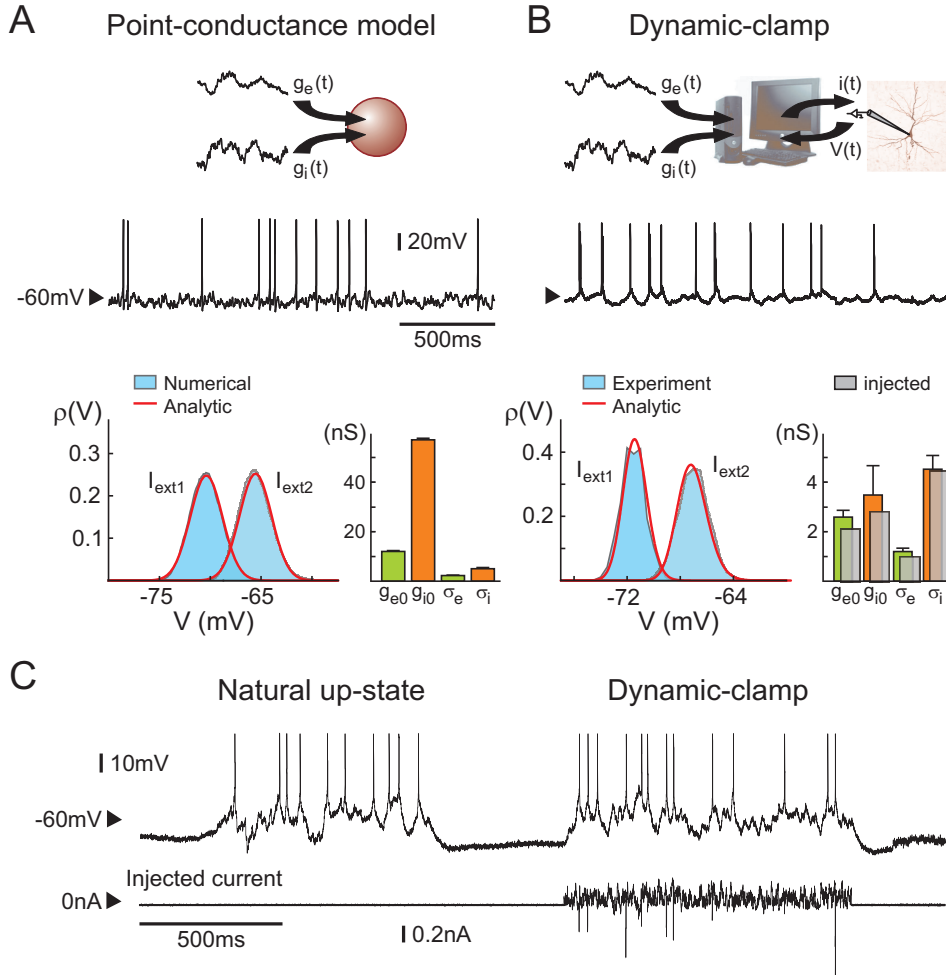


Figure 5.1: Conductance extraction from V_m distributions: numerical and dynamic-clamp test of the method. A. Simulation of the point-conductance model (top trace) and comparison between numerically computed V_m distributions (bottom; blue) and the analytic expression (red curves; conductance values shown in the bar graph). B. Dynamic-clamp injection of the point-conductance model in a real neuron. (Right) Conductance parameters are re-estimated (back, colored; error bars are standard deviations obtained when the same injected conductance parameters are re-estimated in different cells) from the V_m distributions and compared to the known parameters of the injected conductances (front, grey). (Left) The experimental V_m distributions are compared to the analytic distributions calculated using the re-estimated conductance parameters. C. Comparison of a spontaneous up-state (Natural up-state) with an artificial up-state recreated using conductance injection (Dynamic-clamp). Modified from Rudolph et al., 2004.

5.4. RESULTS

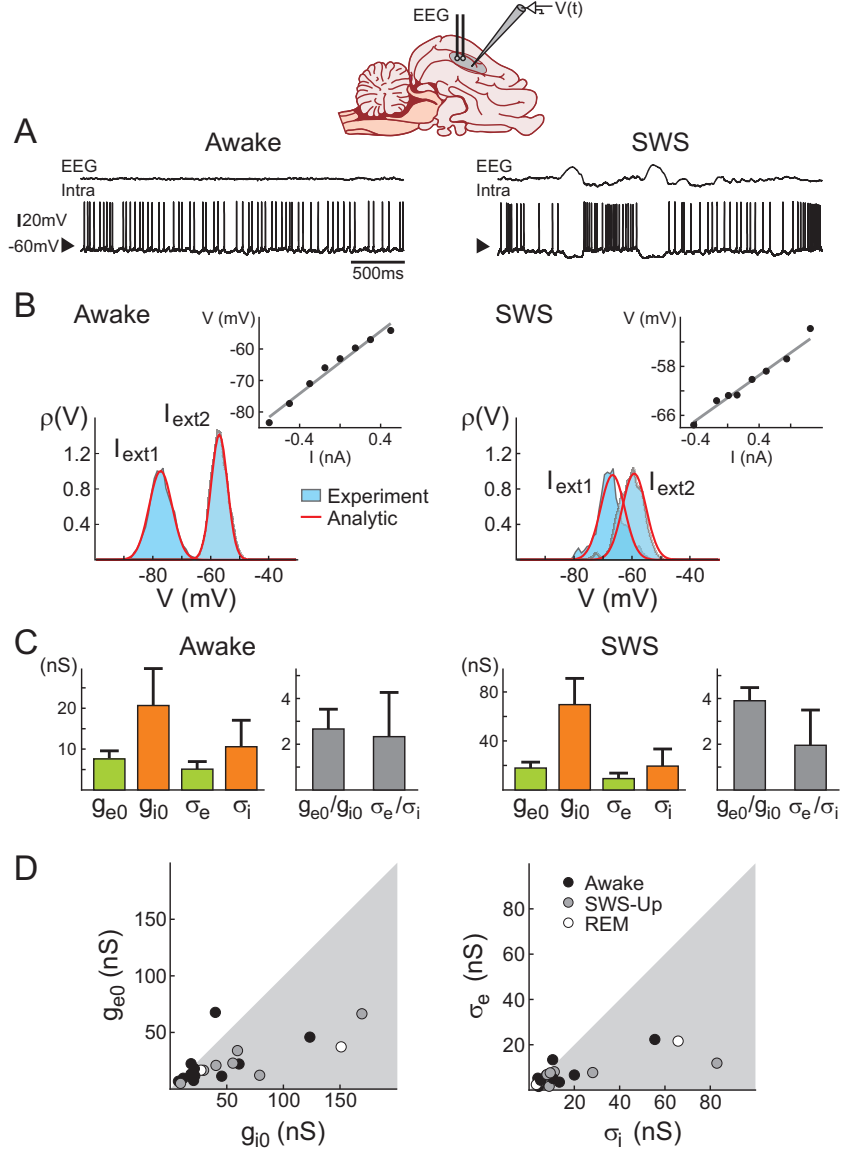


Figure 5.2: VmD estimation of conductances from intracellular recordings in awake and naturally sleeping cats. A. Intracellular recordings in awake and naturally sleeping (SWS) cats. Recordings were made in association cortex (area 5-7). B. Examples of Vm distributions computed during wakefulness (Awake) and slow-wave sleep up-states (SWS). The continuous lines show Gaussian fits of the experimental distributions. Insets: current-voltage relations obtained for these particular neurons. C. Conductance values estimated using the VmD method. Results for the means (g_{e0} , g_{i0}) and standard deviations (σ_e , σ_i) of excitatory and inhibitory conductances, respectively, as well as their ratios are shown (error bars: standard deviations obtained by repeating the analysis using different pairs of injected current levels). D. Grouped data showing the means and standard deviations of the conductances for different cells across different behavioral states (REM = Rapid Eye Movement sleep). Figure modified from Rudolph et al., 2007.

where $\tilde{\tau}_m = C/(G_L + g_{e0} + g_{i0})$ is the effective membrane time constant.

These relations enable us to estimate global characteristics of network activity, such as mean excitatory (g_{e0}) and inhibitory (g_{i0}) synaptic conductances, as well as their respective variances (σ_e^2 , σ_i^2), from the sole knowledge of the V_m distributions obtained at two different levels of injected current. This VmD method was tested using computational models and dynamic-clamp experiments (Rudolph et al., 2004) and was also used to extract conductances from different experimental conditions *in vivo* (Rudolph et al., 2005, 2007; Zou et al., 2005).

Testing the VmD method with dynamic-clamp

Taking advantage of the possibility, given by the dynamic-clamp technique (see Methods), to mimic in a finely controlled way the fluctuating conductances g_e and g_i in biological neurons, we performed *in vitro* tests of the VmD method (Rudolph et al., 2004; Piwkowska et al., 2004). In a first test (in 5 neurons), we computed V_m distributions selectively during periods of subthreshold activity collected within up-states recorded in ferret cortical slices, we subsequently extracted conductance parameters from Gaussian fits to these distributions, and finally we used the estimated parameters to inject fluctuating conductances in dynamic-clamp in the same cell, during down-states. Fig 5.1C shows a typical example of a real up-state and, shortly after, an up-state re-created in dynamic-clamp. We confirmed that the V_m distributions are very similar in the two cases (see Rudolph et al., 2004 for more details). This test shows that the V_m distributions observed experimentally *in vitro* during recurrent cortical activity can be accounted for by the proposed point-conductance model. We also re-estimated known parameters of synaptic conductances (g_{e0} , g_{i0} , σ_e , σ_i) injected in dynamic-clamp from the resulting V_m distributions: the match between actual and estimated values is shown in Fig. 5.1B. This second test indicates that the passive approximation for the membrane behavior holds in the studied case. In these tests, we did not consider the issue of the estimation of τ_e and τ_i and assumed these values are known.

Analysis of intracellular recordings of cortical neurons *in vivo*

The VmD method was then applied to analyze intracellular recordings in anesthetized (Rudolph et al., 2005), as well as naturally sleeping and awake cats (Rudolph et al., 2007).

In the first study, recordings were performed in cat association cortex under ketamine-xylazine anesthesia, during the slow oscillation typical of this anesthetic and resembling slow-wave-sleep, as well as during prolonged periods of activity, triggered by brain stem (PPT) stimulation, and with activity similar to that of the aroused brain. The VmD method was used to extract synaptic conductance

5.4. RESULTS

parameters underlying the V_m fluctuations of the up-states of the slow oscillation, as well as those underlying the continuous fluctuations following PPT stimulation. In both cases, the average estimated inhibitory conductance g_{i0} was markedly higher than the average estimated excitatory conductance g_{e0} , and similarly the estimated variance of inhibition σ_i^2 was higher than the variance of excitation σ_e^2 .

The second study shows similar results across the natural wake-sleep cycle of the cat (Fig. 5.2): for a majority of cells, especially during slow-wave-sleep up-states, inhibition dominated in terms of both mean and variance. At the population level, the ratio of inhibition to excitation was higher during slow-wave-sleep up-states compared to the wake state. In 3 neurons that were recorded across several states, both average conductances together with their variances decreased in the wake state compared to slow-wave-sleep up-states. In addition, especially during the wake state, some cells displayed comparable excitation and inhibition or even a dominant excitation (2 out of 11 cells in the wake state). The study also reports an important diversity in the absolute values of the estimated conductance parameters.

An important concern in this type of studies is the estimation of the leak parameters of the recorded neurons. The down-states of the slow oscillation, when the local network is presumably silent, are too short for properly estimating these parameters, since these brief periods immediately following prolonged up-states are likely to include after-hyperpolarizing currents (Sanchez-Vives et al., 2000) that would bias the estimate of the leak. In both cases, values obtained from previous work (Paré et al, 1998; Destexhe and Paré, 1999) were used for the up-states: these studies evaluated that the ratio of input resistance after TTX block of synaptic activity to the total input resistance during up-states was about 4 to 6-fold. The total input resistance was estimated in all cells studied from the linear portion of the I-V curve obtained during up-states. During wake or wake-like states, the mean total input resistance, as compared to the mean total input resistance during up-states, was taken into account to predict the ratio of input resistance with and without synaptic activity. The underlying hypothesis for these assumptions is that the ratio of leak conductance to synaptic conductance is similar in all cells during comparable network states, implying that the leak conductance and the total synaptic conductance covary in a strong way across cells. In the natural wake-sleep cycle study, the dependence of the conductance estimates on this important ratio was systematically evaluated: this analysis showed that the estimated domination of inhibition was qualitatively robust, and that this prediction failed only when the leak conductance and the total synaptic conductance were assumed to be approximately equal.

On the other hand, the variance estimates do not depend on the leak conductance, provided that the total conductance is known, as is the case in the cited studies. They are, however, dependent on the membrane capacitance C (see Eqs. 5.9 and 5.10). This value was assumed to be constant across the cells analyzed *in vivo*

(supposing a specific membrane capacitance of $1 \mu\text{F}/\text{cm}^2$ and a membrane area of around $30000 \mu\text{m}^2$). In future studies, it could possibly be estimated using short current pulse injection during the spontaneous activity, where the capacitance can be extracted from the time constant of exponential fits to the V_m decay. Synaptic conductance variances are useful parameters that can be related to spike initiation (see Sections 5.4.3 and 5.4.4). The VmD method provided the first published estimates for these parameters *in vivo* (for a different approach, see Monier et al., this issue).

5.4.2 Estimating time constants from V_m power spectral density

Outline of the method

The point-conductance model given by Eqs. 5.1–5.3 was studied further, and recently we showed that the power spectral density (PSD) of the V_m fluctuations described by this model can be well approximated by the following expression (Destexhe and Rudolph, 2004):

$$S_V(\omega) = \frac{4}{G_T^2} \frac{1}{1 + \omega^2 \tilde{\tau}_m^2} \left[\frac{\sigma_e^2 \tau_e (E_e - \bar{V})^2}{1 + \omega^2 \tau_e^2} + \frac{\sigma_i^2 \tau_i (E_i - \bar{V})^2}{1 + \omega^2 \tau_i^2} \right], \quad (5.11)$$

where $\omega = 2\pi f$, f is the frequency, $G_T = G_L + g_{e0} + g_{i0}$ is the total membrane conductance, $\tilde{\tau}_m = C/G_T$ is the effective time constant, and $\bar{V} = (G_L E_L + g_{e0} E_e + g_{i0} E_i)/G_T$ is the average membrane potential. The “effective leak” approximation used to derive this equation consisted in incorporating the average synaptic conductances into the total leak conductance, and then considering that fluctuations around the obtained mean voltage are subjected to a constant driving force (Destexhe and Rudolph, 2004).

As mentioned above, the synaptic time constant parameters, τ_e and τ_i , need to be estimated in order to extract precise values of the conductance variances with the VmD method. As those two parameters appear in the theoretical expression of the V_m PSD, we explored the possibility of evaluating them from the analysis of the PSD of experimentally recorded V_m fluctuations. To this end, the following simplified expression can be fitted:

$$S_V(\omega) = \frac{1}{1 + \omega^2 \tilde{\tau}_m^2} \left[\frac{A_e \tau_e}{1 + \omega^2 \tau_e^2} + \frac{A_i \tau_i}{1 + \omega^2 \tau_i^2} \right], \quad (5.12)$$

where A_e and A_i are amplitude parameters. This five parameter template is used to provide estimates of the parameters τ_e and τ_i (supposing that $\tilde{\tau}_m$ has been measured). A further simplification consists in assuming that $A_e = A_i$, which was used for fitting *in vivo* data (see Methods).

5.4. RESULTS

These analytic expressions were tested by comparing the prediction to numerical simulations of a single-compartment model subject to fluctuating synaptic conductances (Eqs. 5.1–5.3). The matching between the analytic expression and the PSD obtained numerically was nearly perfect, as shown in Fig. 5.3A and as reported in detail previously (Destexhe and Rudolph, 2004).

Testing synaptic time constants estimates with dynamic-clamp

We applied the procedure described above to the PSD of V_m fluctuations obtained by controlled, dynamic-clamp fluctuating conductance injection in cortical neurons *in vitro* (using a new, high resolution electrode compensation technique, Brette et al., 2005; Rudolph et al., 2005). In this case, the scaling of the PSD conforms to the prediction (Fig. 5.3B): the theoretical template (Eq. 5.12) can provide a very good fit of the experimentally obtained PSD, up to around 400 Hz, where recording noise becomes important. The template used was according to Eq. 5.11 or Eq. 5.12, both of which provided equally good fits (not shown). This shows that the analytic expression for the PSD is consistent not only with models, but also with conductance injection in real neurons *in vitro*.

PSD Analysis of V_m fluctuations *in vitro* and *in vivo*

We have also attempted to apply the same procedure to V_m fluctuations resulting from real synaptic activity, during up-states recorded *in vitro* (Fig. 5.3C) and during sustained network activity *in vivo* (Fig. 5.3D). In this case, however, it is apparent that the experimental PSDs cannot be fitted with the theoretical template as nicely as for dynamic-clamp data (Fig. 5.3B). The PSD presents a frequency scaling region at high frequencies, and scales as $1/f^\alpha$ with a different exponent α as predicted by the theory (see Figs. 5.3C-D). The analytic expression (Eq. 5.11) predicts that the PSD should scale as $1/f^4$ at high frequencies, but the experiments show that the exponent α is obviously lower than that value (see Discussion for possible reasons for such a difference). This difference of course compromises the accuracy of the method to estimate τ_e and τ_i in situations of real synaptic bombardment. Nevertheless, including the values of $\tau_e = 3$ ms and $\tau_i = 10$ ms provided acceptable fits to the low-frequency (<100 Hz) part of the spectrum (Fig. 5.3C-D, red curves). However, in this case, small variations (around 20-30%) around these values of τ_e and τ_i yielded equally good fits (not shown; see also Rudolph et al., 2005). Thus, the method cannot be used to precisely estimate those parameters, but can nevertheless be used to broadly estimate them with an error of the order of 30 %.

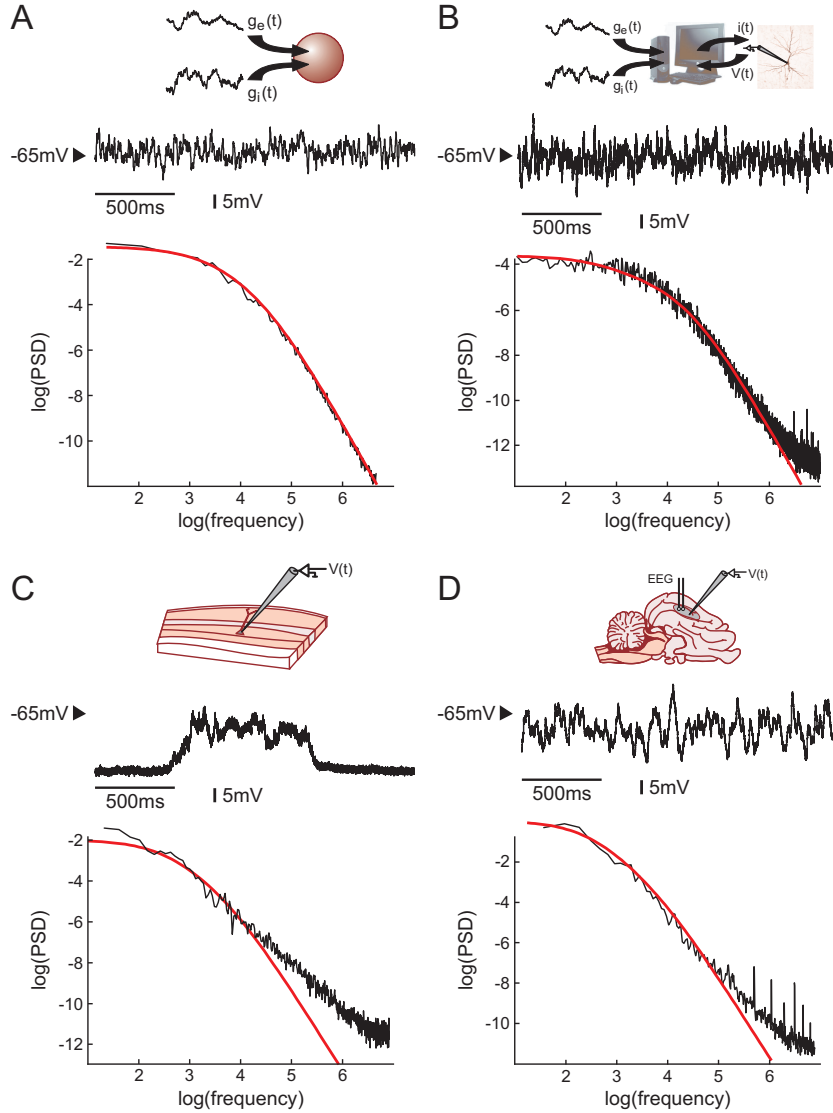


Figure 5.3: Fit of the synaptic time constants to the power spectrum of the membrane potential. A. Comparison between the analytic prediction (Eq. 5.11; red) and the PSD of the V_m for a single-compartment model (Eq. 5.1; black) subject to excitatory and inhibitory fluctuating conductances (Eqs. 5.2-5.3; $\tau_e = 3$ ms and $\tau_i = 10$ ms). B. PSD of the V_m activity in a guinea-pig visual cortex neuron (black), where the same model of fluctuating conductances as in A was injected using dynamic-clamp. The red curve shows the analytic prediction using the same parameters as the injected conductances ($\tau_e = 2.7$ ms and $\tau_i = 10.5$ ms). C. PSD of V_m activity obtained in a ferret visual cortex neuron (black) during spontaneously occurring up-states. The PSD was computed by averaging PSDs calculated for each up-state. The red curve shows the best fit of the analytic expression with $\tau_e = 3$ ms and $\tau_i = 10$ ms. D. PSD of V_m activity recorded in cat association cortex during activated states *in vivo*. The red curve shows the best fit obtained with $\tau_e = 3$ ms and $\tau_i = 10$ ms. Panel A modified from Destexhe and Rudolph, 2004; Panel D modified from Rudolph et al., 2005.

5.4.3 Estimating spike-triggering conductance configurations

A preliminary investigation

The conductance measurements outlined above show that there is a diversity of combinations of g_e and g_i that underlies the genesis of subthreshold activity in different preparations. We used a computational model based on the point-conductance model, but including a spiking mechanism (see Eq. 5.5), to reproduce those measurements and try to infer what different properties such states may have in terms of spike selectivity. Indeed, an infinite number of combinations of g_e and g_i can give similar V_m activity. Figure 5.4A illustrates two extreme examples out of this continuum: first a state where both excitatory and inhibitory conductances are of comparable magnitude (Fig. 5.4A, left; “Equal conductances”). In this state, both conductances are lower than the resting conductance of the cell and the V_m is fluctuating around -60 mV. Second, similar V_m fluctuations can be obtained when both conductances are of larger magnitude, but in this case, inhibition has to be augmented several-fold to maintain the V_m around -60 mV (Fig. 5.4A, right; “Inhibition-dominated”). Such conductance values are more typical of what is usually measured *in vivo*. Both conductances are larger than the resting conductance, a situation which can be described as a “high-conductance state”.

To determine how these two states differ in their spike selectivity, we evaluated the spike-triggering conductances by averaging the conductance traces collected in 50 ms windows preceding spikes. This average pattern of conductance variations leading to spikes is shown in Fig. 5.4B. For equal-conductance states, there is an increase of total conductance preceding spikes (purple curve in Fig. 5.4B, left), as can be expected from the fact that excitation increases (g_e curve in Fig. 5.4B, left). In contrast, for inhibition-dominated states, the total conductance decreases prior to the spike (purple curve in Fig. 5.4B, right), and this decrease necessarily comes from a similar decrease of inhibitory conductance, which is, in this case, stronger than the increase of excitatory conductance (g_i curve in Fig. 5.4B, right). Thus, in such states the spike seems primarily caused by a drop of inhibition.

This pattern was seen not only in the average, but also at the level of single spikes. Using a vector representation to display the conductance variation preceding spikes (each vector links the conductance state in a window of 30-40 ms before the spike with that in the 10 ms preceding the spike) shows that the majority of spikes follow the average pattern (Fig. 5.4C). The same features were also present when the integrate-and-fire model was used (not shown), and thus do not seem to depend on the spike generating mechanisms.

These patterns of conductance variations preceding spikes were also investigated in real neurons by using dynamic-clamp experiments to inject fluctuating conductances *in vitro*. In this case, performing the same analysis as above revealed similar features: spike-triggered averages (STAs) of the injected conductances displayed either increase or decrease in total conductance, depending on

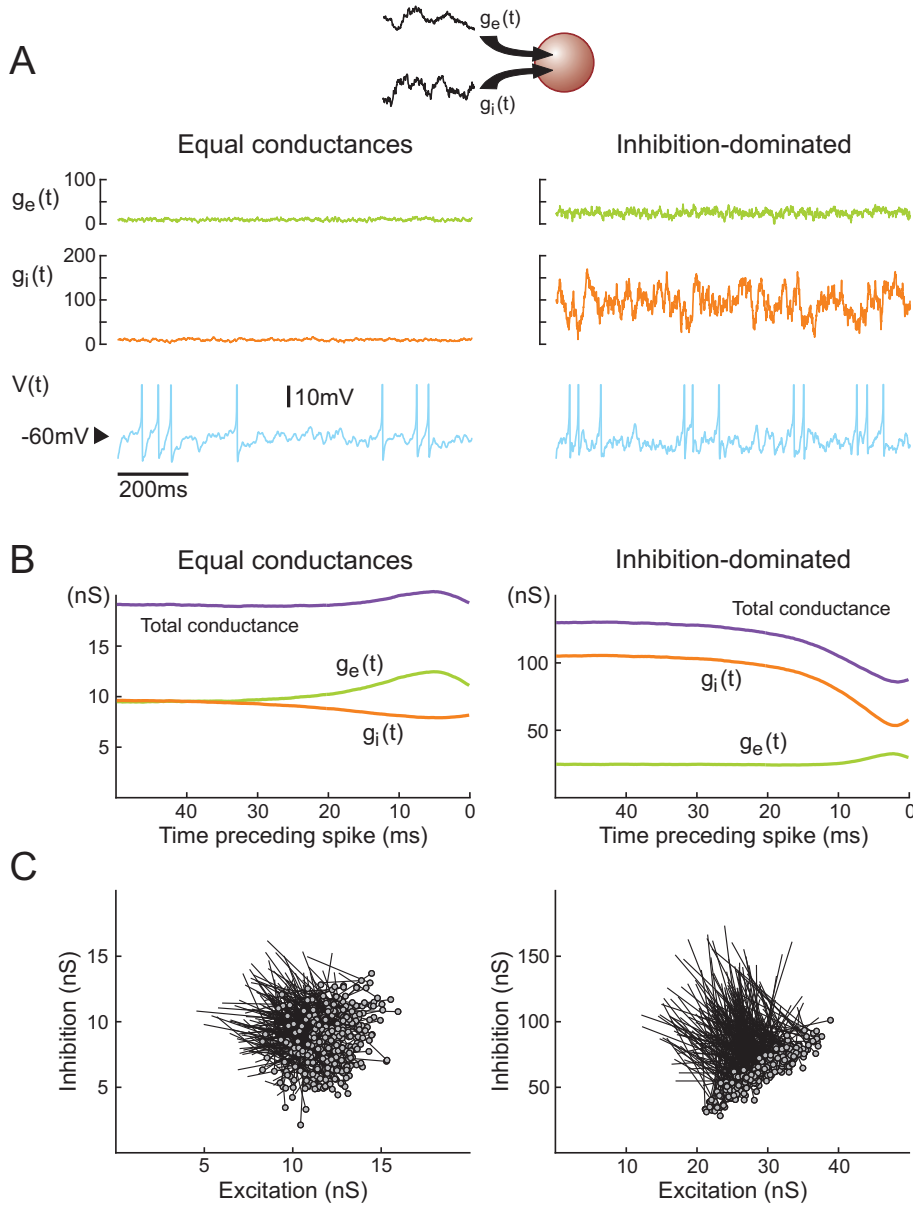


Figure 5.4: Comparison between equal conductances and inhibition-dominated states in a computational model. A. Equal conductance (left; $g_{e0} = g_{i0} = 10$ nS, $\sigma_e = \sigma_i = 2.5$ nS) and inhibition-dominated states (right; $g_{e0} = 25$ nS, $g_{i0} = 100$ nS, $\sigma_e = 7$ nS and $\sigma_i = 28$ nS) in the point-conductance model. Excitatory and inhibitory conductances, and the membrane potential, are shown from top to bottom. Action potentials (truncated here) were described by Hodgkin-Huxley type models (Destexhe et al., 2001; Eq. 5.5). B. Average conductance patterns triggering spikes. Spike-triggered averages (STAs) of excitatory, inhibitory and total conductance were computed in a window of 50 ms before the spike. C. Vector representation showing the variation of synaptic conductances preceding each spike. The excitatory and inhibitory conductances were averaged in two windows of 30-40 ms and 0-10 ms (circle) before the spike, and a vector was drawn between the obtained values.

5.4. RESULTS

the conductance parameters used (Fig. 5.5A), and the vector representations were also similar (Fig. 5.5B). It suggested that these features are independent of the spike generating mechanism but rather are caused by subthreshold Vm dynamics.

A geometrical interpretation based on the point-conductance model

The configuration of synaptic conductances just before spikes can be explained qualitatively by considering that the total current must be positive at spike time, i.e., $g_e(E_e - V_t) + g_i(E_i - V_t) + G_L(E_L - V_t) > 0$, where V_t is the spike threshold (using an integrate-and-fire approximation).

This inequality defines a half-plane in which (g_e, g_i) must lie at spike time. Fig. 5.6A shows graphically how this inequality affects the synaptic conductances. The variable (g_e, g_i) is normally distributed, so that isoprobability curves are ellipses in the plane (plotted in red). In that plane, the line $\{g_e + g_i = g_{e0} + g_{i0}\}$ going through the center of the ellipses defines the points for which the total conductance equals the mean conductance, and the line $\{g_e(E_e - V_t) + g_i(E_i - V_t) + G_L(E_L - V_t) = 0\}$ defines the border of the half-plane in which conductances lie at spike time. In the equal conductances regime (Fig. 5.6A, left), synaptic conductances are small and have similar variances, so that isoprobability curves are circular; the intersection of the half-plane with those circles is mostly above the mean total conductance line, so that the total conductance is higher than average at spike time.

In the inhibition-dominated regime (Fig. 5.6A, right), synaptic conductances are large and the variance of g_i is larger than the variance of g_e , so that isoprobability curves are vertically elongated ellipses; the intersection of the half-plane with those ellipses is essentially below the mean total conductance line, so that the total conductance is lower than average at spike time.

More precisely, when isoprobability curves are circular (equal variances), then the expected total conductance is unchanged at spike time when the lines $\{g_e(E_e - V_t) + g_i(E_i - V_t) + G_L(E_L - V_t) = 0\}$ and $\{g_e + g_i = g_{e0} + g_{i0}\}$ are orthogonal, i.e., when $E_e - V_t + E_i - V_t = 0$. Spikes are associated with increases in conductance when the first line has a higher slope, i.e., when $E_e - V_t > V_t - E_i$ (which is typically the case).

When isoprobability curves are not circular, we can look at the graph in the space $(\frac{g_e}{\sigma_e}, \frac{g_i}{\sigma_i})$ where isoprobability curves are circular. Then the orthogonality condition between the lines

$$\left\{ \frac{g_e}{\sigma_e} \sigma_e (E_e - V_t) + \frac{g_i}{\sigma_i} \sigma_i (E_i - V_t) + G_L(E_L - V_t) = 0 \right\}$$

and

$$\left\{ \frac{g_e}{\sigma_e} \sigma_e + \frac{g_i}{\sigma_i} \sigma_i = g_{e0} + g_{i0} \right\}$$

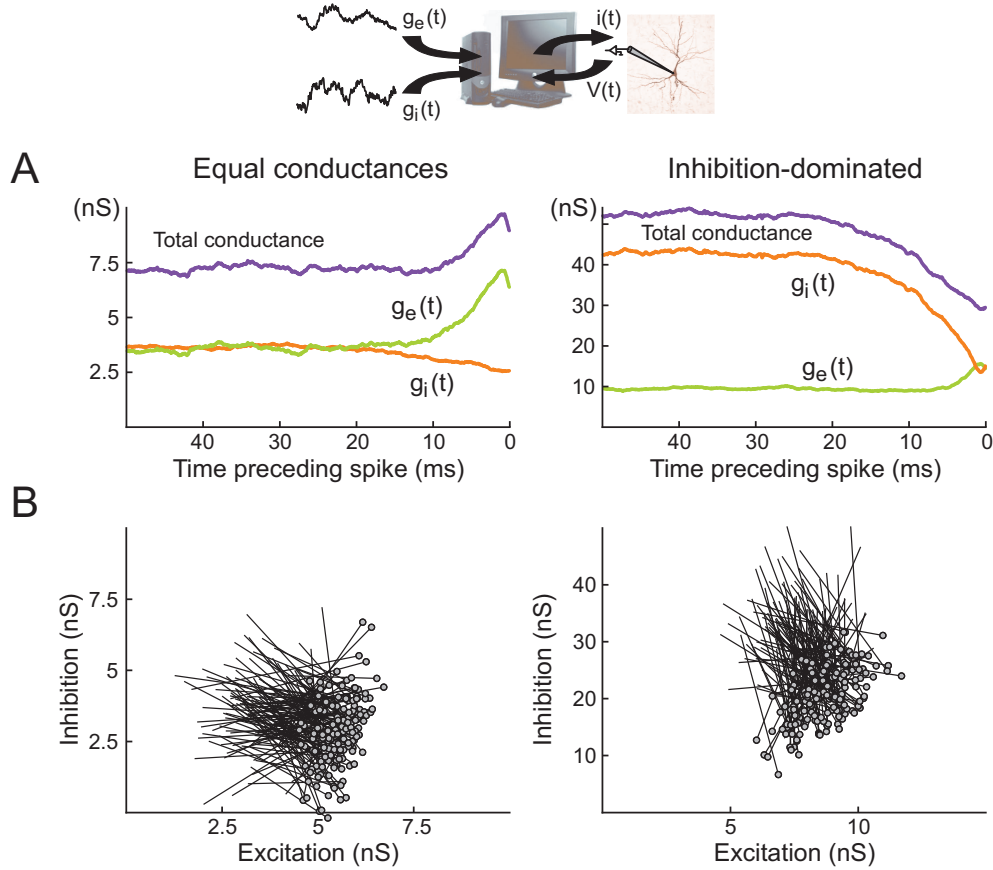


Figure 5.5: Average conductance patterns triggering spikes in dynamic-clamp experiments. A. Spike-triggered averages of excitatory, inhibitory and total conductance in a window of 50 ms before the spike in a cortical neuron subject to fluctuating conductance injection. The two states, equal conductances (left) and inhibition-dominated (right), were recreated similar to the model of Fig. 5.4. Conductance STAs showed qualitatively similar patterns. B. Vector representation showing the variation of synaptic conductances preceding each spike (as in Fig. 5.4C).

5.4. RESULTS

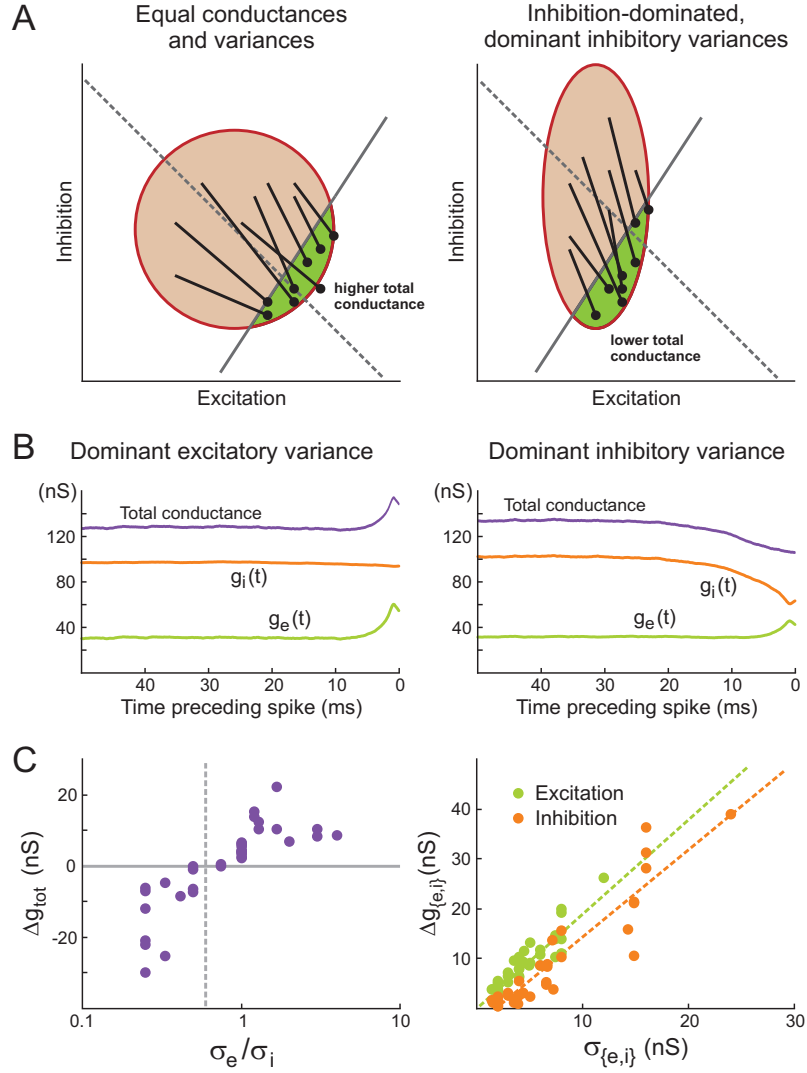


Figure 5.6: Geometrical interpretation of the average conductance patterns preceding spikes and test in dynamic-clamp. A. Red ellipses: isoprobable conductance configurations. Green area: conductance configurations for which the total synaptic current is positive at spike threshold. The vector representations of Figs. 5.4–5.5 are schematized here, and compared to the lines defined by $\{g_e(E_e - V_t) + g_i(E_i - V_t) + G_l(E_L - V_t) = 0\}$ and $\{g_e + g_i = g_{e0} + g_{i0}\}$. The angle between the two lines determines whether spikes are preceded, on average, by total conductance increase (left) or decrease (right) (see text for further explanations). B. Spike-triggered average conductances obtained in dynamic-clamp, illustrating that for the same average conductances, the variances determine whether spikes are preceded by total conductance increase (left) or decrease (right). C. Geometrical prediction tested in dynamic-clamp (left): grouped data showing total conductance change preceding spikes as a function of the ratio σ_e/σ_i . The dashed line ($\sigma_e/\sigma_i=0.6$) visualizes the predicted value separating total conductance increase cases from total conductance decrease cases. In addition (right), dynamic-clamp data indicates that the amplitude of change of each of the conductances before a spike is linearly correlated with the standard deviation parameter used for this conductance.

reads

$$\sigma_e^2(E_e - V_t) + \sigma_i^2(E_i - V_t) = 0 .$$

It follows that spikes are associated with increases in total conductance when the following condition is met:

$$\frac{\sigma_e}{\sigma_i} > \sqrt{\frac{V_t - E_i}{E_e - V_t}} .$$

One can also recover this result by calculating the expectation of the conductance change conditionally to the fact that the current at spike threshold is positive (implicitly, we are neglecting the correlation time constants of the synaptic conductances). Using typical values ($V_t = -55$ mV, $E_e = 0$ mV, $E_i = -75$ mV), we conclude that spikes are associated with increases in total conductance when $\sigma_e > 0.6\sigma_i$. This inequality is indeed satisfied in the equal conductances regime and not in the inhibition-dominated regime investigated above.

Testing the geometrical prediction with dynamic-clamp

The geometrical reasoning predicts that the sign of the total synaptic conductance change triggering spikes depends only on the ratio of synaptic variances, and not on the average conductances. We have systematically tested this prediction using dynamic-clamp injection of fluctuating conductances *in vitro*. In 8 regular spiking cortical neurons, we scanned different parameter regimes in a total of 36 fluctuating conductance injections. Fig. 5.6B shows two examples from the same cell: both correspond to an average “high conductance” regime, dominated by inhibition, but in one case it is the variance of excitation, in the other case the variance of inhibition, that is higher. We can see that the total conductance before the spike increases in the first case, but decreases in the second. Fig. 5.6C (left) shows the average total conductance change preceding spikes as a function of σ_e/σ_i , for all the 36 injections: the vertical dashed line represents the predicted value of $\sigma_e/\sigma_i=0.6$, which indeed separates all the “conductance drop” configurations from the “conductance increase” configurations. Even though the prediction is based on a simple integrate-and-fire extension of the point-conductance model, we can see that the ratio of synaptic variances can predict the sign of the total conductance change triggering spikes in biological cortical neurons subjected to fluctuating excitatory and inhibitory conductances.

In addition (Fig. 5.6C, right), the dynamic-clamp data shows that the average amplitude of change ($\Delta g_e = g_{e0} k_e$, see Methods) of each synaptic conductance preceding a spike is related, in a linear way, to the standard deviation of this conductance. For a fixed value of standard deviation, there was no significant influence of the average conductance (not shown). This observation is consistent with the idea that in all the cases studied here, the firing of the cell was driven by fluctuations in the V_m , rather than by a high mean V_m value (not shown).

5.4. RESULTS

Taken together, these theoretical and experimental analyses indicate that the average total conductance drop preceding spikes, as seen in the “high conductance” case we initially considered (Fig. 5.4), is not a direct consequence of the “high conductance” state of the membrane, but is in fact related to the high inhibitory variance, which is indeed to be expected especially when the mean inhibitory conductance is also high (as confirmed by the studies presented in the first part of this article).

5.4.4 Estimating spike-triggered averages of synaptic conductances from the V_m

In order to extend the analysis of spike-triggering conductance configurations to real recurrent cortical activity observed *in vivo*, we recently developed a procedure to extract the spike-triggered averages (STAs) of conductances from recordings of the V_m (Fig. 5.7; Pospischil et al., 2007). The STA of the V_m is calculated first, and the method searches for the “most likely” spike-related conductance time courses ($g_e(t)$, $g_i(t)$) that are compatible with the observed voltage STA. The procedure is based on a discretization of the time axis in Eqs. 5.1–5.3, which, rearranged, lead to the following relations:

$$g_i^k = -\frac{C}{V^k - E_i} \left\{ \frac{V^k - E_L}{\tau_L} + \frac{g_e^k(V^k - E_e)}{C} + \frac{V^{k+1} - V^k}{\Delta t} - \frac{I_{ext}}{C} \right\}, \quad (5.13)$$

$$\xi_e^k = \frac{1}{\sigma_e} \sqrt{\frac{\tau_e}{2\Delta t}} \left(g_e^{k+1} - g_e^k \left(1 - \frac{\Delta t}{\tau_e} \right) - \frac{\Delta t}{\tau_e} g_{e0} \right), \quad (5.14)$$

$$\xi_i^k = \frac{1}{\sigma_i} \sqrt{\frac{\tau_i}{2\Delta t}} \left(g_i^{k+1} - g_i^k \left(1 - \frac{\Delta t}{\tau_i} \right) - \frac{\Delta t}{\tau_i} g_{i0} \right), \quad (5.15)$$

where $\tau_L = C/G_L$ is the resting membrane time constant. Note that $\xi_e(t)$ and $\xi_i(t)$ have become Gaussian-distributed random numbers ξ_e^k and ξ_i^k . There is a continuum of combinations $\{g_e^{k+1}, g_i^{k+1}\}$ that can advance the membrane potential from V^{k+1} to V^{k+2} , each pair occurring with a probability

$$p^k := p(g_e^{k+1}, g_i^{k+1} | g_e^k, g_i^k) = \frac{1}{2\pi} e^{-\frac{1}{2}(\xi_e^{k2} + \xi_i^{k2})} = \frac{1}{2\pi} e^{-\frac{1}{4\Delta t} X^k}, \quad (5.16)$$

$$X^k = \frac{\tau_e}{\sigma_e^2} \left(g_e^{k+1} - g_e^k \left(1 - \frac{\Delta t}{\tau_e} \right) - \frac{\Delta t}{\tau_e} g_{e0} \right)^2 + \frac{\tau_i}{\sigma_i^2} \left(g_i^{k+1} - g_i^k \left(1 - \frac{\Delta t}{\tau_i} \right) - \frac{\Delta t}{\tau_i} g_{i0} \right)^2. \quad (5.17)$$

Because of Eq. 5.13, g_e^k and g_i^k are not independent and p^k is, thus, a unidimensional distribution only. Given initial conductances $\{g_e^0, g_i^0\}$, one can write down

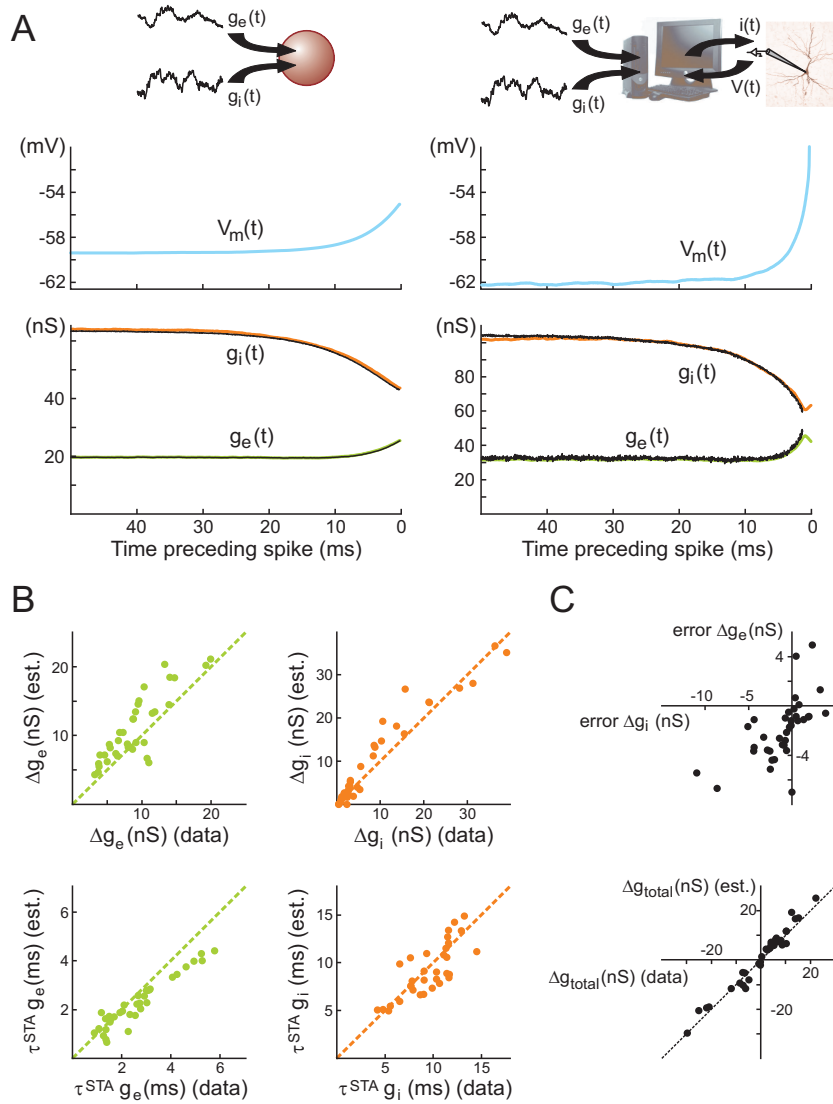


Figure 5.7: Spike-triggered conductance extraction from intracellular recordings of the V_m and test in dynamic-clamp. A. Left: spike-triggered average (STA) of the V_m in an integrate-and-fire extension of the point-conductance model (top trace). The numerically obtained conductance STAs (orange, green) are compared to the conductance STAs extracted from the V_m (black) (bottom trace). Right: test of the STA method using dynamic-clamp. The STA of the V_m is obtained following injection of fluctuating conductances (top trace). The measured conductance STAs (orange, green) are compared to the conductance STAs extracted from the V_m (black) (bottom trace). B. Grouped data comparing conductance STAs extracted using the method with the conductance STAs measured following dynamic-clamp injection: amplitude of conductance change preceding the spike (top graphs) and time constant of this change (bottom graphs), for both excitation and inhibition. C. Top: correlation between errors for excitation and inhibition on the absolute value of conductance variation. Bottom: total conductance change preceding spikes; comparison between extracted and measured STAs. Dashed lines: $Y = X$.

5.4. RESULTS

the probability p for certain series of conductances $\{g_e^j, g_i^j\}_{j=0, \dots, n}$ to occur that reproduce a given voltage trace $\{V^l\}_{l=1, \dots, n+1}$:

$$p = \prod_{k=0}^{n-1} p^k. \quad (5.18)$$

Due to the symmetry of the distribution p , the average paths of the conductances coincide with the most likely ones. It is thus sufficient to determine the conductance series with extremal likelihood by solving the n -dimensional system of linear equations

$$\left\{ \frac{\partial X}{\partial g_e^k} = 0 \right\}_{k=1, \dots, n}, \quad (5.19)$$

where $X = \sum_{k=0}^{n-1} X^k$, for the vector $\{g_e^k\}$. This is equivalent to solving $\{\frac{\partial p}{\partial g_e^k} = 0\}_{k=1, \dots, n}$ and involves the numerical inversion of an $n \times n$ -matrix, which can be done using standard numeric methods (Press et al., 1986). The series $\{g_i^k\}$ is subsequently obtained from Eq. 5.13. Details of this procedure as well as an evaluation of its performance can be found in Pospischil et al., 2007.

The method requires first an estimation of the parameters describing the distribution of each of the conductances, which can be obtained by the VmD method. The leak parameters of the cell, or alternatively the effective parameters during V_m fluctuations (effective conductance and effective time constant), also have to be estimated prior to this analysis. The method was successfully tested using computational models: conductance STAs extracted from the V_m of an integrate-and-fire point-conductance model are nearly identical to the numerically obtained conductance STAs (Fig. 5.7A, left; Pospischil et al., 2007).

During response to sensory stimuli, there can be a substantial degree of correlation between excitatory and inhibitory synaptic input (Monier et al., 2003; Wehr and Zador, 2003; Wilent and Contreras, 2005). Since this situation has not been addressed in Pospischil et al., 2007, we would like to sketch a possible extension of the method. To this end, we reformulate the discretized versions of Eqs. 5.2, 5.3 in the following way:

$$\frac{g_e^{k+1} - g_e^k}{\Delta t} = -\frac{g_e^k - g_{e0}}{\tau_e} + \sigma_e \sqrt{\frac{2\Delta t}{\tau_e(1+c)}} (\xi_1^k + \sqrt{c} \xi_2^k), \quad (5.20)$$

$$\frac{g_i^{k+1} - g_i^k}{\Delta t} = -\frac{g_i^k - g_{i0}}{\tau_i} + \sigma_i \sqrt{\frac{2\Delta t}{\tau_i(1+c)}} (\xi_2^{k-d} + \sqrt{c} \xi_1^{k-d}). \quad (5.21)$$

Here, instead of having one “private” white noise source feeding each conductance channel, now the same two noise sources ξ_1 and ξ_2 contribute to both inhibition and excitation. The amount of correlation is tuned by the parameter c . Also, since there is evidence that the peak of the g_e - g_i -crosscorrelation is not

always centered at 0 during stimulus-evoked responses (“delayed inhibition”; see Wehr and Zador, 2003; Wilent and Contreras, 2005), we allow a non-zero delay d : for a positive parameter d , the inhibitory channel receives the input that the excitatory channel received d time steps before. Eqs. 5.20 and 5.21 can be solved for ξ_1^k and ξ_2^k , thus replacing Eqs. 5.14 and 5.15. It is then possible to proceed as in the uncorrelated case, where now, due to the delay, the matrix describing Eq. 5.19 has additional subdiagonal entries.

However, the application of this extended method requires the estimation of the usual leak parameters, of conductance distribution parameters – for which the VmD method cannot be directly used in its current form since it is based on uncorrelated noise sources – as well as knowledge of the parameters c and d . At present, we can only speculate on how c and d could be evaluated in experiments: extracellularly recorded spike trains could perhaps be used to this end, provided that simultaneously recorded single units could be classified as excitatory or inhibitory. Alternatively, different plausible c and d values could be scanned to examine how they could potentially influence the conductance STAs extracted from a given V_m STA.

Testing STA estimation with dynamic-clamp

The dynamic-clamp data presented above was used to evaluate the accuracy of the conductance STA estimation method (for the uncorrelated case only): indeed, the conductance STAs estimated from the V_m STAs could be compared to conductance STAs obtained directly by averaging conductance traces, since in dynamic-clamp the injected conductances are perfectly controlled by the experimentalist. For the 36 injections analyzed, a good match was observed between the two (see one example in Fig. 5.7A, right panel). Since we intended to evaluate the STA method specifically, we assumed that conductance distribution parameters were known. In addition, we estimated the cell’s leak parameters (see Methods). To quantify the comparison on a population basis, we did the following analyses: exponential functions (see Methods) were fitted to each conductance STA (estimated and directly measured) starting at 1 ms before the spike and decaying to baseline backwards in time. We then compared the asymptotic values (i.e., the average baseline conductances) and the time constants of these fits, as well as the amplitude of conductance change from the start of the fit to the asymptote (i.e., the amplitude of conductance change preceding the spike). In all cases but one, the exponential functions provided excellent fits to the conductance STAs. It was necessary to exclude the 1 ms time window preceding the spike to avoid severe contamination of the analyses by intrinsic conductances. Excluding a broader time window did not improve the analyses for these neurons.

The average baseline conductances always matched very well (error of -0.1 ± 0.25 nS, or -0.8 ± 2.6 %, for excitation; 0.8 ± 1.5 nS, or 0.6 ± 4.5 %, for inhi-

5.4. RESULTS

bition; not shown). More importantly, the estimates of the average conductance patterns leading to spikes were also in good correspondence with the measured patterns, in terms of both the amplitude of conductance change (Fig. 5.7C, top; error of -1.2 ± 3 nS, or -26 ± 28.8 %, for excitatory amplitude change, and -2.0 ± 2.5 nS, or -10.7 ± 47 %, for inhibitory amplitude change) and the time constant (Fig. 5.7C, bottom; error of 0.39 ± 0.48 ms, or 11.2 ± 21.1 % for excitatory time constant, and 0.36 ± 1.71 , or 2.6 ± 18.8 %, for inhibitory time constant). For excitation, the error on the estimate of the amplitude is correlated with the error on the estimate of the time constant (not shown): this suggests that, in most cases, a slightly too fast rise of the excitatory conductance results in a slightly too high amplitude of conductance change. The lack of correlation between the two error measures in the case of the inhibitory conductance points to a more complex origin for the observed errors. Moreover, the errors on the amplitude of the two conductance changes are positively correlated (Fig. 5.7D, top). This dependency actually ensures that the error on the estimated total conductance change (excitation-inhibition) remains small (-0.8 ± 2.4 nS; Fig. 5.7D, bottom).

Finally, we have investigated the dependency of the estimate errors on a diversity of variables, and found a correlation of amplitude errors with the average V_m during the fluctuating conductance injection (not shown): this dependency points to a possible contamination by intrinsic conductances activated differentially at different average V_m levels. However, we found no dependency of the error on average firing rate (for the rates up to around 30 Hz studied here), suggesting no important contamination by spike-dependent conductances like the ones underlying the after-hyperpolarization (when care is taken to compute STAs using spikes preceded by at least 100 ms of silence, see Methods).

We have also verified that conductance STA estimates can be relied on to investigate what factors determine the average conductance variations preceding spikes. Fig. 5.8 shows that the analyses performed previously on dynamic-clamp data (i.e., on STAs obtained directly by averaging the conductance traces, Fig. 5.6B-C), can also be successfully performed using the conductance STAs estimated from the corresponding V_m STAs: Fig. 5.8A shows the estimated STAs in the two different “high conductance” states, dominated by either excitatory or inhibitory variance (compare to Fig. 5.6B). Fig. 5.8B shows, for the population data, the (significant) correlations between total conductance change and σ_e/σ_i , as well as between the change of each of the conductances and the corresponding standard deviation. Note the similarity between Fig. 5.6B-C and Fig. 5.8A-B, even though the correlations at the population level are more noisy when the estimated STAs are used.

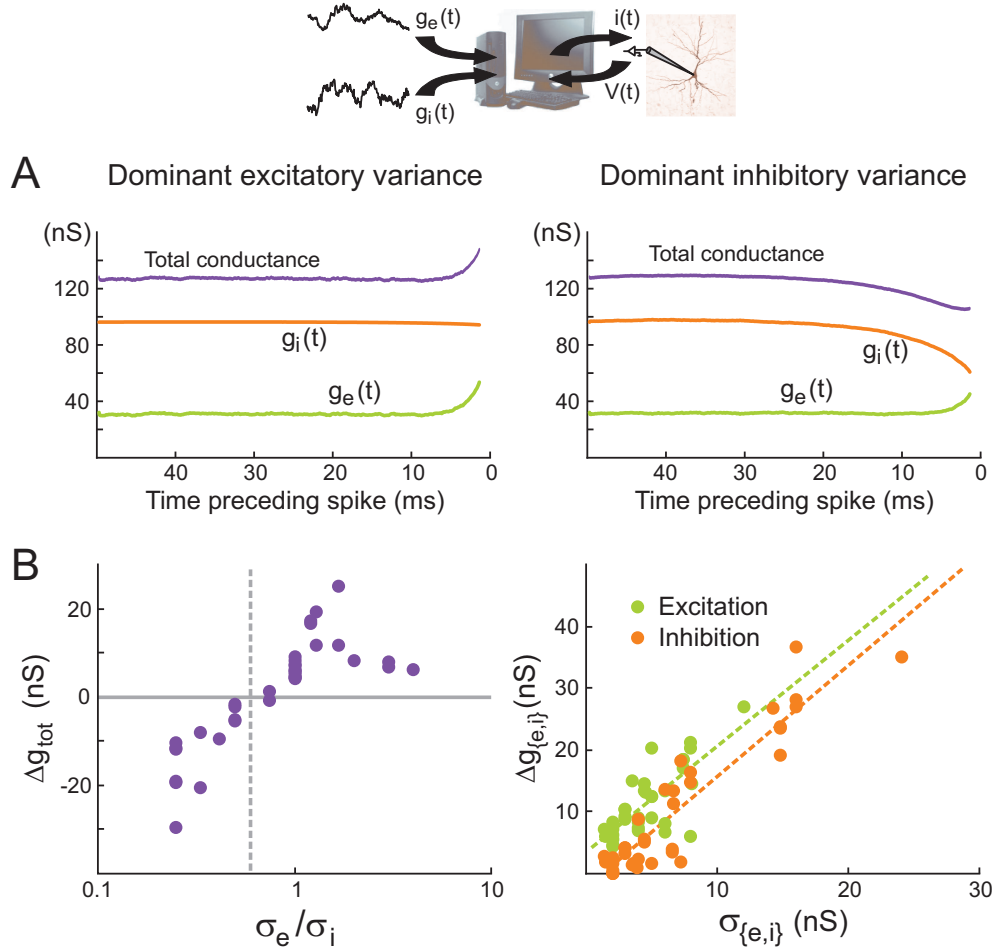


Figure 5.8: Analysis of the average conductance patterns preceding spikes, same analysis as Fig. 5.6B-C, but using conductance STAs extracted from the V_m , instead of the measured ones. A. Example conductance STAs extracted from the V_m STAs of the same cell and the same conductance injections as Fig. 5.6B. B. Left: test of the geometrical prediction (dashed line) using conductance STAs extracted from the V_m , and showing total conductance change preceding spikes as a function of the ratio σ_e/σ_i (as in Fig. 5.6C, left). Right: correlation between the amplitude of change of each conductance preceding a spike, as extracted from the V_m , and the standard deviation parameter for this conductance (compare to Fig. 5.6C, right).

5.5. DISCUSSION

STA Analysis of intracellular recordings of cortical neurons *in vivo*

The conductance STA estimation method was used to determine conductance variations preceding spikes during V_m fluctuations *in vivo* (Rudolph et al., 2007). Starting from V_m recordings of spontaneous spiking activity in awake or naturally sleeping cats, we computed the spike-triggered average of the V_m (Fig. 5.9). Using values of g_{e0} , g_{i0} , σ_e , σ_i estimated using the VmD method (see above), we computed the most likely conductance traces yielding the observed V_m averages. Most of these analyses (7 out of 10 cells for awake, 6 out of 6 for slow-wave-sleep, 2 out of 2 for REM) revealed conductance dynamics consistent with states dominated by inhibitory variance: there was a drop of the total conductance preceding spikes, due to a strong decrease of the inhibitory conductance (Fig. 5.9, right). However, a few cases, in the wake state (3 out of 10 cells), displayed the opposite configuration with the total synaptic conductance increasing before the spike (Fig. 5.9, left).

We also checked how the geometrical prediction relating the sign of total conductance change preceding spikes and the ratio σ_e/σ_i performed for this data (Fig. 5.9B). We have seen that the critical value of σ_e/σ_i for which the total conductance change shifts from positive to negative depends on the spike threshold. This parameter was quite variable in the recorded cells, and so a critical σ_e/σ_i value was calculated for each cell. Fig. 5.9B shows the lowest and highest critical values obtained (dashed lines), and also displays in white the cells which do not conform to the prediction based on their critical value. This is the case for only 4 out of 18 cells, for three of which the total conductance change is close to zero.

The extraction of conductance STAs depends on the accuracy of the synaptic conductance parameters estimated with the VmD method, which means that assumptions made about the leak conductance and the cell capacitance will influence the results (see Section 5.4.1). We have shown that the ratio σ_e/σ_i should determine whether, on average, the total conductance increases or decreases prior to the spike. This ratio is independent of the leak conductance, but it depends on the capacitance C . However, it appears in both the numerator and the denominator of the ratio. Fig. 5.9C shows the dependency of σ_e/σ_i on this parameter for different values of total input resistance and two sets of realistic values for the V_m distribution parameters. This analysis indicates that a reasonable error on C produces a limited error on the ratio σ_e/σ_i , and suggests that conclusions drawn from the *in vivo* data about the respective contributions of excitation and inhibition in triggering spikes are valid.

5.5 Discussion

We presented how the simple point-conductance model of cortical synaptic activity can provide a basis for the analysis of experimental data, essentially through

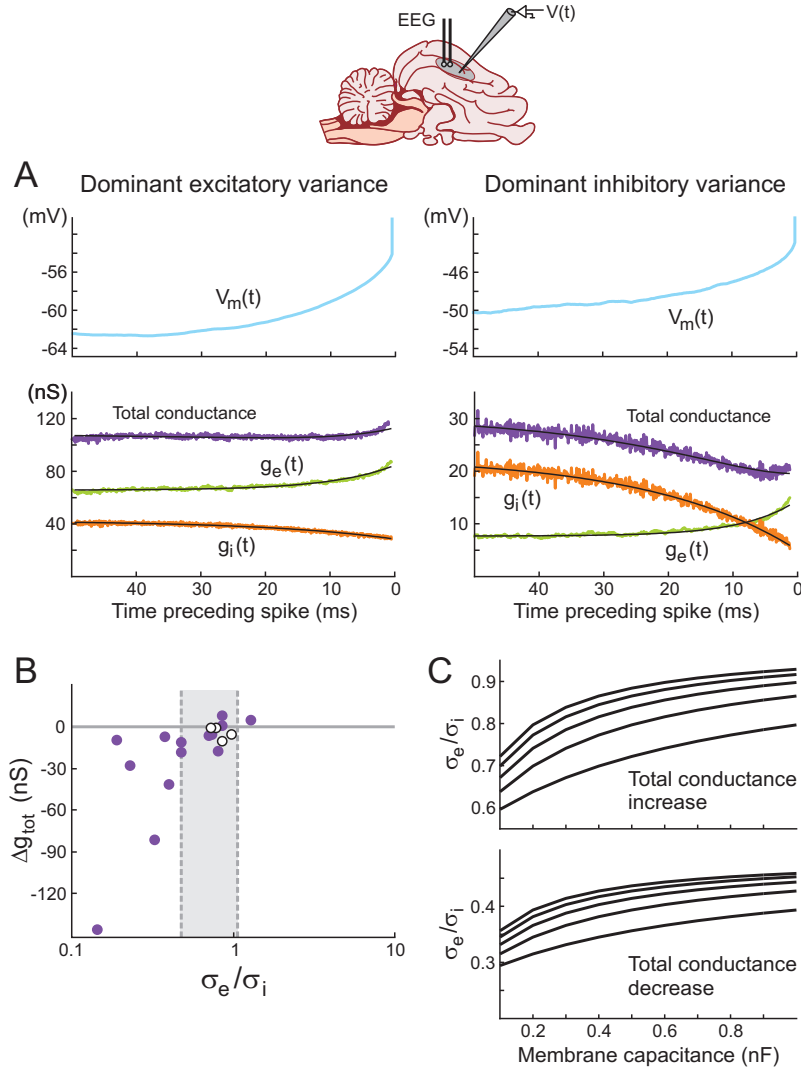


Figure 5.9: Spike-triggered conductance analysis *in vivo*. **A**. STA conductance analysis from intracellular recordings in awake and sleeping cats. Two example cells are shown during wakefulness, and for each, the V_m STA (top) and the extracted conductance STAs (bottom) are shown. In the first cell (left), the total conductance increases before the spike. In the second example cell (right), the total conductance decreases before the spike (black traces are exponential fits to the extracted STAs). **B**. Total conductance change preceding spikes as a function of the ratio σ_e/σ_i . Given the cell-to-cell variability of observed spike thresholds, each cell has a different predicted ratio separating total conductance increase cases from total conductance decrease cases. The two dashed lines ($\sigma_e/\sigma_i=0.48$ and $\sigma_e/\sigma_i=1.07$) visualize the two extreme predicted ratios. Cells in white are the ones not conforming to the prediction. **C**. Dependency of the ratio σ_e/σ_i estimated by the VmD method on the value of the membrane capacitance C . Two sets of realistic V_m distribution parameters were used as input for the estimation, one leading to $\sigma_e/\sigma_i > 0.6$ (left), another leading to $\sigma_e/\sigma_i < 0.6$ (right). For each set, the total input resistance was varied from 10 M Ω (bottom curves) to 50 M Ω (top curves), in steps of 10 M Ω . Panel A modified from Rudolph et al., 2007.

5.5. DISCUSSION

the matching of expressions derived from the model to intracellular V_m recordings of cortical neurons. This approach has been used for extracting different parameters from the recurrent cortical activity *in vivo*: the averages and variances of excitatory and inhibitory conductances, their decay time and the optimal conductance waveform underlying spike selectivity. These analyses were possible because the point conductance model represents in a compact and mathematically tractable way the activity resulting from several thousand synapses. In turn, the analysis provides a characterization of synaptic activity in simple terms (average conductance, level of fluctuations). Such parameters can readily be incorporated in computational models to yield the membrane potential and conductance state corresponding to *in vivo* activity with just a few variables. This approach has been used for example in network simulations to obtain realistic conductance states in neurons even with small networks (Haeusler and Maass, 2007). It is also directly usable in dynamic-clamp experiments to investigate the impact of synaptic background activity on signal processing by single cortical or thalamic neurons (Fellous et al., 2003; Shu et al., 2003; Wolfart et al., 2005; Desai and Walcott, 2006).

Beyond the matching of experimental V_m distributions to a theoretical expression (VmD method), we have also attempted to match the PSDs of V_m fluctuations. This approach provides some validation for assumptions made about synaptic time constants on the basis of published studies (Destexhe and Paré, 1999; Destexhe et al., 2001). However, the fact that the point-conductance model does not account for the scaling properties of experimental PSDs (Fig. 5.3C-D) limits the accuracy of the method and yields only broad estimates of the synaptic time constants (approximately 30% error). A parallel study (Bedard and Destexhe, 2007) has shown that the frequency scaling observed experimentally cannot be accounted for by standard cable theory, and modifications of cable equations are required to match those values. We hope to obtain a more accurate fitting template, which would allow more precise PSD analyses in the future.

In the second part of the paper, we focused on a question that we recently started addressing, making use of the point-conductance model: what are the patterns of excitation and inhibition triggering spikes under different conditions of network activity? A preliminary study pointed to the fact that these patterns depend on the statistics of synaptic conductances, and that spikes could be preceded, on average, either by increases in total synaptic conductance, indicating a predominant role for excitation, or by decreases in total synaptic conductance, indicating a predominant role for inhibition. Other authors (Hasenstaub et al., 2005) have recently suggested that drop of inhibition can play an important role in determining spike timing in cortical neurons, based on dynamic-clamp injection of specific synaptic conductances with parameters matched to their *in vivo* recordings. Here we explored this issue further and showed, first by a theoretical reasoning, and second by scanning different parameter regimes using dynamic-clamp con-

ductance injection, that the sign of the total conductance change before a spike does not directly depend on the average synaptic conductances, but is solely determined by the ratio of synaptic conductance variances. The variance of synaptic conductances in the Ornstein-Uhlenbeck model is related to the degree of correlation between Poisson input trains of each type in a detailed biophysical model (Destexhe et al., 2001): the level of synchrony among inhibitory neurons could thus be determining for spike timing whenever it significantly exceeds the level of synchrony among excitatory neurons. This result stresses the importance of evaluating the variances of synaptic conductances, in addition to their averages, when analyzing V_m fluctuations recorded *in vivo*. To our knowledge, the two reviewed studies using the VmD method are the only ones (together with Monier et al., 2007, in this issue) explicitly providing estimates of synaptic conductance variances.

Other studies proposed synaptic conductance estimates *in vivo* derived from I-V curves (in current-clamp) or V-I curves (in voltage-clamp) obtained at different points in time following a stimulus (Borg-Graham et al., 1998; Anderson et al., 2000; Monier et al., 2003; Wehr and Zador, 2003; Wilent and Contreras, 2005) or the onset of an up-state (Haider et al., 2006). An exhaustive comparison of these studies is beyond the scope of the present article (see Monier et al., 2007 in this issue), but a few points can be stressed. The fact that the VmD method applies to current-clamp data obtained at a few levels of constant injected current circumvents technical problems with voltage-clamp due to high series resistance of patch electrodes *in vivo* (but see Borg-Graham et al., 1998; Monier et al., 2003; Wehr and Zador, 2005) or the need for discontinuous voltage-clamp with sharp electrodes (Haider et al., 2006). The fact that it relies on a strong assumption about the stochasticity of synaptic inputs and the independence of excitation and inhibition allows the analysis of spontaneous cortical activity with no “zero” time point. However, this assumption also makes it unsuited, in its present form, for the analysis of stimulus-evoked activity with important temporal structure.

The VmD method suffers from one common limitation with other approaches for synaptic conductance estimation: the need to separate synaptic currents from leak currents. The fact that it is used for the analysis of on-going, spontaneous activity in cortical networks poses, however, an additional complication: indeed, when synaptic inputs evoked by sensory stimulation are analyzed, it is with reference to the pre-stimulus activity, which includes the leak current and any other baseline currents, including on-going synaptic activity (Borg-Graham et al., 1998; Anderson et al., 2000; Monier et al., 2003; Wehr and Zador, 2003; Wilent and Contreras, 2005). When we attempt to analyze the spontaneous activity itself, there is no straightforward reference that can be used. As mentioned above, the short down-states do not seem a good candidate since they include after-hyperpolarizing currents consecutive to the up-states (Sanchez-Vives et al., 2000), although a down-state-referenced analysis (as in Haider et al., 2006) could perhaps

5.5. DISCUSSION

be compared to the analysis performed in the reviewed studies. However, in the wake state, the continuous on-going activity does not even present down-states. The only precise approach to evaluate the leak conductance for each studied cell is to block all synaptic activity with TTX, but that also means recording only one or two cells per animal for this protocol, which is an extremely constraining experimental situation. The compromise chosen in the reviewed *in vivo* studies consisted in using published average values obtained in previous TTX experiments in a similar preparation (Paré et al., 1998) and checking the robustness of the estimates to the assumed leak conductance parameter. The estimates should be re-evaluated in the light of any future experimental data providing information about the leak parameters of cortical cells *in vivo* in the absence of synaptic activity. Optimally, such future studies would include the simple, classical protocol required for a subsequent VmD analysis: several-second-long current-clamp recordings of the V_m at different levels of steady injected current.

Building on the possibility to evaluate synaptic conductance statistics with the VmD method, and in order to be able to study average spike-triggering patterns of conductances *in vivo*, we have developed a probabilistic method for extracting the STAs of conductances from STAs of the V_m (Pospischil et al., 2007). We are not aware of any other method currently allowing this analysis for spontaneous activity: in voltage-clamp, no spikes are recorded and so, obviously, conductances leading to spikes cannot be extracted directly. Voltage-clamp can only be used for extracting plausible conductance STAs when the precise times of spikes are known and reproducible (for example, at a given delay after a sensory stimulation), so that the estimated, stimulus-locked conductance dynamics can be reasonably expected to lead to spikes in the current-clamp configuration (Monier et al., 2003; Wehr and Zador, 2003). The application of the probabilistic method to *in vivo* recordings in awake and naturally sleeping cats led to the observation of both types of firing regimes described above - average total conductance increase and average total conductance drop - with a majority of cases displaying the inhibition-dominated, conductance-drop pattern.

The result of the STA analysis is, however, dependent on the estimates of synaptic averages and variances, so that we may ask to what extent this result depends on the accuracy of the VmD method. In general, the average baseline conductances will reflect the estimates of average synaptic conductances (since both analyses are constrained by the same total input resistance measure and the same leak conductance assumption), unless the total input resistance changes markedly between the current levels used for the VmD analysis and the zero-current level at which STAs are extracted, due to activation of intrinsic conductances: in this case, since the conductances (G_L , $g_e(t)$, $g_i(t)$) have to be compatible with the voltage $V_m(t)$, the conductance STA baselines can be considerably shifted away from the mean conductance values tens of ms before the spike. The same effect is seen in *in vitro* dynamic-clamp experiments when a wrong leak conductance value is

used (not shown). This distortion could be used as an indication for important activation of intrinsic conductances and suggest that the result should be discarded.

As to the estimation of the amplitudes of average conductance change preceding a spike, we have seen that this change seems to be mainly determined by the variances of synaptic conductances. The estimation of synaptic conductance variances is independent of the assumption made about the leak conductance, which excludes this source of potential error. It is dependent on the membrane capacitance C , which should be evaluated on a cell-by-cell basis whenever possible in future studies. However, we have also shown that the ratio of synaptic conductance variances is only weakly dependent on the precise value of C : this ratio seems to determine the sign of total conductance change preceding a spike, and so the conclusion about a majority of cases *in vivo* displaying an important role for inhibition in controlling spikes seems robust.

Finally, we illustrated how and to what extent the validity of different approaches for conductance analysis can be tested using dynamic-clamp. This electrophysiological technique is an attractive tool to evaluate methods of conductance analysis, since it allows to mimic the activation of known conductances in a biological neuron: the results of an analysis method based on V_m recordings can be directly compared to measures of the actual conductances controlled by the experimentalist. In all the dynamic-clamp applications presented here, we have used the same description for the synaptic conductances - the Ornstein-Uhlenbeck stochastic model - as in the theoretical analyses. This means that we could compare how the analysis methods perform if the stochastic conductances are inserted at the soma of a real cortical neuron, with a complex structure and a variety of intrinsic channels, instead of a passive single compartment. As we have seen, potential dendritic effects solicited only during distributed synaptic stimulation, like, possibly, the unexpected scaling of the V_m PSDs during real synaptic activity (Bedard and Destexhe, 2007), cannot be addressed with this somatic injection technique. They could perhaps be investigated in the future using dendritic patch-clamp.

The comparison was performed most extensively for the conductance STA estimation method: it indicates that if the window of analysis is chosen properly (by excluding a window of about 1 ms before the spike, and also excluding inter-spike-intervals shorter than around 100 ms), the estimations perform well, and that the estimation errors, correlated with the average V_m , are presumably linked to V_m -dependent intrinsic channels. However, we did not systematically compare how the methods perform if the synaptic conductances deviate from the Ornstein-Uhlenbeck model: such an approach could constitute another application of the dynamic-clamp tool to the evaluation of conductance analysis methods. We have also not attempted yet to evaluate in dynamic-clamp the extended STA analysis method sketched above, which incorporates a known correlation between excitation and inhibition (Eqs. 5.20–5.21).

Acknowledgments

We thank Igor Timofeev for giving us permission to use some of his data. Research supported by CNRS, ANR, ACI, HFSP and the European Community (FACETS grant FP6 15879). Z.P. gratefully acknowledges the support of the FRM.

5.6 References

- Anderson J. S., Carandini M., Ferster D. Orientation tuning of input conductance, excitation, and inhibition in cat primary visual cortex. *J Neurophysiol* **84**:909-926, 2000.
- Barak O., Tsodyks M. Persistent activity in neural networks with dynamic synapses. *PLoS Comput Biol* **3**:e35, 2007.
- Baranyi A., Szenté M. B., Woody C. D. Electrophysiological characterization of different types of neurons recorded in vivo in the motor cortex of the cat. II. Membrane parameters, action potentials, current-induced voltage responses and electrotonic structures. *J Neurophysiol* **69**:1865-1879, 1993.
- Bedard C., Destexhe A. A modified cable formalism for modeling neuronal membranes at high frequencies. Manuscript under review, 2007; preprint available at <http://arxiv.org/abs/0705.3759>.
- Bernander O., Douglas R. J., Martin K. A., Koch C. Synaptic background activity influences spatiotemporal integration in single pyramidal cells. *Proc Natl Acad Sci USA* **88**:11569-11573, 1991.
- Borg-Graham L. J., Monier C., Frégnac Y. Visual input evokes transient and strong shunting inhibition in visual cortical neurons. *Nature* **393**:369-373, 1998.
- Brette R., Rudolph M., Piwkowska Z., Bal T., and Destexhe A. How to emulate double-electrode recordings with a single electrode? A new method of active electrode compensation. *Soc Neurosci Abstracts* 688.2, 2005.
- Compte A., Sanchez-Vives M. V., McCormick D. A., Wang X. J. Cellular and network mechanisms of slow oscillatory activity (<1 Hz) and wave propagations in a cortical network model. *J Neurophysiol* **89**:2707-2725, 2003.
- Cunningham M. O., Pervouchine D. D., Racca C., Kopell N. J., Davies C. H., Jones R. S., Traub R. D., Whittington M. A. Neuronal metabolism governs cortical network response state. *Proc Natl Acad Sci USA* **103**:5597-5601, 2006.

- Desai N. S., Walcott E. C. Synaptic bombardment modulates muscarinic effects in forelimb motor cortex. *J Neurosci* **26**:2215-2226, 2006.
- Destexhe A. and Paré D. Impact of network activity on the integrative properties of neocortical pyramidal neurons in vivo. *J Neurophysiol* **81**:1531-1547, 1999.
- Destexhe A., Rudolph M. Extracting information from the power spectrum of synaptic noise. *J Comput Neurosci* **17**:327-345, 2004.
- Destexhe A., Hughes S. W., Rudolph M., Crunelli V. Are corticothalamic “up” states fragments of wakefulness? *Trends Neurosci* doi:10.1016/j.tins.2007.04.006, 2007.
- Destexhe A., Rudolph M., Fellous J.-M., Sejnowski T. J. Fluctuating synaptic conductances recreate in vivo-like activity in neocortical neurons. *Neuroscience* **107**:13-24, 2001.
- Destexhe A., Rudolph M. and Paré D. The high-conductance state of neocortical neurons in vivo. *Nature Reviews Neurosci* **4**:739-751, 2003.
- Fellous J. M., Rudolph M., Destexhe A., Sejnowski T. J. Synaptic background noise controls the input/output characteristics of single cells in an in vitro model of in vivo activity. *Neuroscience* **122**:811-829, 2003.
- Haider B., Duque A., Hasenstaub A. R., McCormick D. A. Neocortical network activity in vivo is generated through a dynamic balance of excitation and inhibition. *J Neurosci* **26**:4535-4545, 2006.
- Hasenstaub A., Shu Y., Haider B., Kraushaar U., Duque A., McCormick D. A. Inhibitory postsynaptic potentials carry synchronized frequency information in active cortical networks. *Neuron* **47**:423-435, 2005.
- Haeusler S. and Maass W. A statistical analysis of information-processing properties of lamina-specific cortical microcircuit models. *Cereb Cortex* **17**:149-62, 2007.
- Hill S., Tononi G. Modeling sleep and wakefulness in the thalamocortical system. *J Neurophysiol* **93**:1671-1698, 2005.
- Hines M. L., Carnevale N. T. The NEURON simulation environment, *Neural Computation* **9**:1179-1209, 1997.
- Lindner B., Longtin A. Comment on “Characterization of subthreshold voltage fluctuations in neuronal membranes”, by M. Rudolph and A. Destexhe. *Neural Comput* **18**:1896-1931, 2006.

5.6. REFERENCES

- Matsumura M., Cope T., Fetz E. E. Sustained excitatory synaptic input to motor cortex neurons in awake animals revealed by intracellular recording of membrane potentials. *Exp Brain Res* **70**:463-469, 1988.
- Metherate R., Ashe J. H. Ionic flux contributions to neocortical slow waves and nucleus basalis-mediated activation: whole-cell recordings in vivo. *J Neurosci* **13**:5312-5323, 1993.
- Monier C., Chavane F., Baudot P., Graham L. J., Frégnac Y. Orientation and direction selectivity of synaptic inputs in visual cortical neurons: a diversity of combinations produces spike tuning. *Neuron* **37**:663-680, 2003.
- Paré D., Shink E., Gaudreau H., Destexhe A., Lang E. J. Impact of spontaneous synaptic activity on the resting properties of cat neocortical neurons in vivo. *J Neurophysiol* **79**:1450-1460, 1998.
- Piwkowska Z., Rudolph M., Badoual M., Destexhe A., Bal T. Re-creating active states in vitro with a dynamic-clamp protocol. *Neurocomputing* **65-66**:55-60, 2005.
- Pospischil M., Piwkowska Z., Rudolph M., Bal T., Destexhe A. Calculating event-triggered average synaptic conductances from the membrane potential. *J Neurophysiol* **97**:2544-2552, 2007.
- Press W. H., Flannery B. P., Teukolsky S. A., Vetterling W. T. Numerical Recipes. The Art of Scientific Computing. Cambridge, MA: Cambridge University Press, 1986.
- Richardson M. J. Effects of synaptic conductance on the voltage distribution and firing rate of spiking neurons. *Phys Rev E Stat Nonlin Soft Matter Phys* **69**:051918, 2004.
- Robinson H. P., Kawai N. Injection of digitally synthesized synaptic conductance transients to measure the integrative properties of neurons. *J Neurosci Methods* **49**:157-165, 1993.
- Roxin A., Brunel N., Hansel D. Role of delays in shaping spatiotemporal dynamics of neuronal activity in large networks. *Phys Rev Lett* **94**:238103, 2005.
- Rudolph M., Destexhe A. Characterization of subthreshold voltage fluctuations in neuronal membranes. *Neural Computation* **15**:2577-2618, 2003a.
- Rudolph M., Destexhe A. The discharge variability of neocortical neurons during high-conductance states. *Neuroscience* **119**:855-873, 2003b.

- Rudolph M., Destexhe A. A fast-conducting, stochastic integrative mode for neocortical neurons in vivo. *J. Neurosci* **23**:2466-2476, 2003c.
- Rudolph M., Destexhe A. An extended analytic expression for the membrane potential distribution of conductance-based synaptic noise. *Neural Computation* **17**:2301-2315, 2005.
- Rudolph M., Destexhe A. On the use of analytic expressions for the voltage distribution to analyze intracellular recordings. *Neural Comput.* **18**: 2917-2922, 2006.
- Rudolph M., Piwkowska Z., Badoual M., Bal T., Destexhe A. A method to estimate synaptic conductances from membrane potential fluctuations. *J Neurophysiol* **91**:2884-2896, 2004.
- Rudolph M., Piwkowska Z., Brette R., Destexhe A., and Bal T. Precise dynamic-clamp injection of stochastic conductances using active electrode compensation. *Soc Neurosci Abstracts* 687.13, 2005.
- Rudolph M., Pelletier J.-G, Paré D., Destexhe A. Characterization of synaptic conductances and integrative properties during electrically-induced EEG-activated states in neocortical neurons in vivo. *J Neurophysiol* **94**:2805-2821, 2005.
- Sanchez-Vives M. V., McCormick D. A. Cellular and network mechanisms of rhythmic recurrent activity in neocortex. *Nat Neurosci* **3**:1027-1034, 2000.
- Sanchez-Vives M. V., Nowak L. G., McCormick D. A. Cellular mechanisms of long-lasting adaptation in visual cortical neurons in vitro. *J Neurosci* **20**:4286-4299, 2000.
- Sharp A. A., O'Neil M. B., Abbott L. F., Marder E. Dynamic clamp: computer-generated conductances in real neurons. *J Neurophysiol* **69**:992-995, 1993.
- Shu Y., Hasenstaub A., Badoual M., Bal T., McCormick D. A. Barrages of synaptic activity control the gain and sensitivity of cortical neurons. *J Neurosci* **23**:10388-10401, 2003.
- Steriade M., Nunez A., Amzica F. A novel slow (< 1 Hz) oscillation of neocortical neurons in vivo: depolarizing and hyperpolarizing components. *J Neurosci* **13**:3252-3265, 1993.
- Steriade M., Timofeev I., Grenier F. Natural waking and sleep states: a view from inside neocortical neurons. *J Neurophysiol* **85**:1969-1985, 2001.

5.6. REFERENCES

- Timofeev I., Grenier F., Steriade M. Disfacilitation and active inhibition in the neocortex during the natural sleep-wake cycle: an intracellular study. *Proc Natl Acad Sci USA* **98**:1924-1929, 2001.
- Uhlenbeck G. E. and Ornstein L. S., On the theory of the Brownian motion. *Phys Rev* **36**:823-841, 1930.
- van Vreeswijk C., Sompolinsky H. Chaos in neuronal networks with balanced excitatory and inhibitory activity. *Science* **274**:1724-1726, 1996.
- Wehr M., Zador A. M. Balanced inhibition underlies tuning and sharpens spike timing in auditory cortex. *Nature* **426**:442-446, 2003.
- Wehr M., Zador A. M. Synaptic mechanisms of forward suppression in rat auditory cortex. *Neuron* **47**:437-445, 2005.
- Wilent W., Contreras D. Dynamics of excitation and inhibition underlying stimulus selectivity in rat somatosensory cortex. *Nature Neurosci* **8**:1364-1370, 2005.
- Wolfart J., Debay D., Le Masson G., Destexhe A., Bal T. Synaptic background activity controls spike transfer from thalamus to cortex. *Nat Neurosci* **8**:1760-1767, 2005.
- Woody C. D., Gruen E. Characterization of electrophysiological properties of intracellularly recorded neurons in the neocortex of awake cats: a comparison of the response to injected current in spike overshoot and undershoot neurons. *Brain Res* **158**:343-357, 1978.
- Zou Q., Rudolph M., Roy N., Sanchez-Vives M., Contreras D., Destexhe A. Reconstructing synaptic background activity from conductance measurements in vivo. *Neurocomputing* **65**:673-678, 2005.

Chapter 6

Which model best captures the spiking response of cortical neurons to excitatory inputs?

Martin Pospischil, Zuzanna Piwkowska, Thierry Bal and Alain Destexhe. Which model best captures the spiking response of cortical neurons to excitatory inputs? *submitted*, 2007.

Résumé

Introduction

Une grande diversité de modèles ont été proposés pour représenter les potentiels d’actions (PAs) des neurones. Ces modèles sont les “intégrer-et-tire (IF)”, et ses variantes quadratique et exponentielle, le modèle d’Izhikevich (IZ) et le modèle de Hodgkin & Huxley (HH) par exemple. Ces modèles capturent différents aspects de l’excitabilité des neurones mais il n’existe pas de comparaison de leur performance. Dans cet article nous réalisons une telle comparaison à partir de données expérimentales, en particulier pendant les états de haute conductance.

Résultats obtenus

Les expériences réalisées consistent en une injection d’entrée excitatrice (EPSC) en dynamic-clamp dans des neurones du cortex visuel du cochon d’Inde *in vitro*. L’amplitude de la conductance est contrôlée, et la réponse des PAs est enregistrée et moyennée sur un grand nombre d’essais, ce qui donne un “post-stimulus time histogram” (PSTH). La famille de PSTH (pour différentes amplitudes) est obtenue, pour deux états de bruit synaptique, basse conductance (LC) et haute conductance (HC).

Ensuite les différents modèles sont ajustés à ces données expérimentales et sont comparés. La comparaison est réalisée soit en considérant les deux états LC et HC, ou bien en considérant un seul état et en utilisant l’autre comme test du modèle.

Conclusions

Ces résultats indiquent que le modèle HH, le plus complexe, donne le meilleur accord, de façon attendue. Par contre, des modèles beaucoup plus simples, comme le IF exponentiel, donnent un accord extrêmement proche de HH. Ce type de modèle devrait se révéler très utile pour les simulations de réseaux de neurones.

6.1 Abstract

A wide diversity of models have been proposed to account for the spiking response of central neurons, such as the integrate-and-fire (IF) model and its quadratic and exponential variants, to multiple-variable models such as the Izhikevich (IZ) model and the well-known Hodgkin-Huxley (HH) type models. Such models can capture different aspects of the spiking response of neurons, but there is no objective comparison of their performance. In this paper, we provide a comparison of such models in the context of a well-defined stimulation protocol consisting of excitatory conductance injection, arising in the presence of synaptic background activity. We use the dynamic-clamp technique to characterize the response of regular-spiking neurons from guinea-pig visual cortex by computing families of post-stimulus time histograms (PSTH), for different stimulus intensities, and for two different background activities (low- and high-conductance states). The data obtained are then used to fit different classes of models such as the IF, IZ or HH types. This analysis shows that HH models are generally more accurate to fit the details of experimental PSTH, but their performance is almost equaled by much simpler models, such as the exponential IF model. Similar conclusions were also reached by performing partial fitting of the data, and examining the ability of different models to “predict” responses that were not used for the fitting. Although such results must be qualified by more sophisticated stimulation protocols, they suggest that simple IF models capture surprisingly well the response of cortical regular-spiking neurons and should be useful candidates for network simulations.

6.2 Introduction

Since the early days of computational neuroscience, a plurality of different neuron models have been proposed, among which the leaky integrate-and-fire (leaky IF, Lapicque 1907) and the Hodgkin-Huxley (HH, Hodgkin and Huxley 1952) models are probably the best known and most used ones. They also constitute a sort of frame, with on the one hand the leaky IF model rather being a sketch of a spiking model, compared to the detailed analogy between state variables in the HH model and ion channels in biological neurons on the other hand. A multitude of other models have been developed over the years that fall within this frame. The extension of the leaky IF model has lead to a whole family of nonlinear IF models (e.g. the quadratic or the exponential IF models, Ermentrout 1996, Latham et al. 2000, Fourcaud et al. 2003), whereas the reduction of the HH model gave rise to a different type of models, where spikes result from the interplay of two coupled state variables (e.g. the FitzHugh–Nagumo or the Morris–Lecar models, FitzHugh 1961, Nagumo et al. 1962, Morris and Lecar 1981). Recently, the two concepts have been unified: in the Izhikevich model and the adaptive exponential IF model

6.2. INTRODUCTION

(Izhikevich 2003, Brette and Gerstner 2005), subthreshold dynamics are described by two coupled state variables, but spiking is realised in terms of thresholds and reset values.

Clearly, the models differ in their capability to qualitatively reproduce firing types seen in cortical neurons, and usually (though not always) are the more elaborate models also the ones that cover a broader range (cf. Izhikevich 2004 for a summary). A different question, however, is the following: given a, say, regular spiking neuron, how well do the models reproduce a particular firing pattern *quantitatively*? Different approaches have been followed in order to address this question. Some consist in assuming that a given detailed model represents a good candidate for biological behavior, which then serves as a benchmark in the attempt to match one or several simpler models to it (cf. e.g. Fourcaud et al. 2003, Jolivet et al. 2004, Brette and Gerstner 2005). Another approach consists in directly matching models to data obtained in experiments (e.g. Jolivet et al. 2006, Clopath et al. 2007). Sometimes, one and the same model is matched to itself for the purpose of exploring the underlying “parameter landscape” (Achard and DeSchutter 2006) or comparing the capacity of different optimisation techniques (Weaver and Wearne 2006). The protocols used in these cases are diverse. They comprise both current and conductance injections, where the waveforms range from simple square pulses to stochastically fluctuating traces.

But also the matching itself can be accomplished along various lines. Besides the widely used, straight forward “hand tuning”, more unbiased techniques have been employed. In some cases it is possible to determine model parameters from standard electrophysiological protocols. It is e.g. conventional to extract input resistance and capacitance of a neuron from current pulse injections. But while for some models it is possible to obtain all parameter values in such a direct way, for others it is not and automated optimisation techniques have to be applied. A comparative study of four such techniques has been given in Vanier and Bower 1999. For the problem treated therein, it clearly favours the simulated annealing algorithm. However, the performance of an optimization technique also depends on the objective function. While for a fit of subthreshold properties it might be sufficient of the membrane potential, in general this is not a good choice for spiking neurons. Here, shifts in spike times of the order of the spike width will introduce large jumps in the assigned error. A different approach has been taken in Vanier and Bower 1999, where the objective function is basically composed as a sum over differences in spike time between model and target, normalized by the time of the respective spike in the model. In the cases, where a neuron model constitutes its own target, it is possible to use more sophisticated objective functions by either taking into account the spike shape (Weaver and Wearne 2006), or by using the neurons probability density in the $(V_m - dV_m/dt)$ -plane (Achard and DeSchutter 2006, LeMasson and Maex 2001). It is not clear, however, how the latter performs when model and data are based on different dynamical systems.

In this article, we compare the capacity of seven different neuron models, spanning the complexity spectrum between the leaky IF and the HH model, to quantitatively reproduce the behavior of four different cortical neurons, that were recorded *in vitro* using dynamic clamp. Since the neurons are regular spiking (RS), we include an adaptation channel in all models. The protocol used is intended to recreate conditions that are close to natural network states. The neuron (and the models) are injected with two channels of fluctuating conductances (point-conductance model, Destexhe et al. 2001) intended to represent the input of excitatory and inhibitory presynaptic neurons, respectively. In addition, an AMPA-shaped stimulus is injected. The peri-stimulus time histograms (PSTHs) of the models are then compared to the ones of the target cells, where we contrast two different background states: The first is a “low conductance” (LC) state, where the mean values of excitatory and inhibitory conductances are approximately equal and comparable in magnitude to the leak conductance. The other is a “high conductance” (HC) state, characterized by dominant inhibition and a leak conductance that is small compared to the synaptic conductances. We fit the models either to one state at a time and predict the PSTH for the respective other state, or we fit the PSTHs obtained in both states simultaneously.

6.3 Materials and Methods

6.3.1 *In vitro* experiments

In vitro experiments were performed on 0.4 mm thick coronal or sagittal slices from the lateral portions of guinea-pig occipital cortex. Guinea-pigs, 4-12 weeks old (CPA, Olivet, France), were anesthetized with sodium pentobarbital (30 mg/kg). The slices were maintained in an interface style recording chamber at 33-35°C. Slices were prepared on a DSK microslicer (Ted Pella Inc., Redding, CA) in a slice solution in which the NaCl was replaced with sucrose while maintaining an osmolarity of 307 mOsm. During recording, the slices were incubated in slice solution containing (in mM): NaCl, 124; KCl, 2.5; MgSO₄, 1.2; NaHPO₄, 1.25; CaCl₂, 2; NaHCO₃, 26; dextrose, 10, and aerated with 95% O₂, 5% CO₂ to a final pH of 7.4. Intracellular recordings following two hours of recovery were performed in deep layers (layer IV, V and VI) in electrophysiologically identified regular spiking and intrinsically bursting cells. Electrodes for intracellular recordings were made on a Sutter Instruments P-87 micropipette puller from medium-walled glass (WPI, 1BF100) and beveled on a Sutter Instruments beveler (BV-10M). Micropipettes were filled with 1.2 to 2 M potassium acetate and had resistances of 80-100 MΩ after beveling.

The dynamic-clamp technique (Robinson et al., 1993; Sharp et al., 1993) was used to inject computer-generated conductances in real neurons. Dynamic-clamp

6.3. MATERIALS AND METHODS

experiments were run using the hybrid RT-NEURON environment (developed by G. Le Masson, Université de Bordeaux), which is a modified version of NEURON (Hines and Carnevale, 1997) running under the Windows 2000 operating system (Microsoft Corp.). NEURON was augmented with the capacity of simulating neuronal models in real time, synchronized with the intracellular recording. To achieve real-time simulations as well as data transfer to the PC for further analysis, we used a PCI DSP board (Innovative Integration, Simi Valley, USA) with 4 analog/digital (inputs) and 4 digital/analog (outputs) 16 bits converters. The DSP board constrains calculations of the models and data transfers to be made with a high priority level by the PC processor. The DSP board allows input (for instance the membrane potential of the real cell incorporated in the equations of the models) and output signals (the synaptic current to be injected into the cell) to be processed at regular intervals (time resolution = 0.1 ms). A custom interface was used to connect the digital and analog inputs/outputs signals of the DSP board with the intracellular amplifier (Axoclamp 2B, Axon Instruments) and the data acquisition systems (PC-based acquisition software ELPHY, developed by G. Sadoc, CNRS Gif-sur-Yvette, ANVAR and Biologic). The dynamic-clamp protocol was used to insert the fluctuating conductances underlying synaptic noise in cortical neurons using the point-conductance model, similar to a previous study (Destexhe et al., 2001). The injected current is determined from the fluctuating conductances $g_e(t)$ and $g_i(t)$ as well as from the difference of the membrane voltage from the respective reversal potentials, $I_{DynClamp} = -g_e(V - V_e) - g_i(V - V_i)$.

All research procedures concerning the experimental animals and their care adhered to the American Physiological Society’s Guiding Principles in the Care and Use of Animals, to the European Council Directive 86/609/EEC and to European Treaties series no. 123, and was also approved by the local ethics committee “Ile-de-France Sud” (certificate no. 05-003).

6.3.2 Models

For the simulations, we use single compartment models of varying complexity in an attempt to reproduce the PSTHs obtained during experiments. During some simulations, a mechanism that accounts for spike rate adaptation was included, the details of which depend on the type of model. We assume that the capacitance of the cell as well as its leak conductance and leak reversal potential can be deduced from the experiment, hence these parameters are kept fixed during the optimisation. All other parameters are allowed to vary freely, except for the HH model, where only a subset of parameters was adjusted. We describe the models in the following in ascending order of complexity.

6.3.3 Integrate-and-fire models

We use four different integrate-and-fire (IF) models, that are distinguished by their I-V relation. First, we use the linear or leaky IF model (Lapicque 1907). It is described by the membrane equation

$$C \frac{dV}{dt} = -g_L(V - V_L) - g_K(V - V_K) + I_{ext}, \quad (6.1)$$

which in addition to the classic definition contains a conductance g_K , that accounts for spike rate adaptation. Further parameters are the leak conductance and reversal potential g_L and V_L as well as the capacitance C . The model can be driven by an additional input current I_{ext} . It is said to fire a spike whenever the voltage reaches a fixed threshold V_{th} , after which the integration restarts at the reset potential V_R . Modifications to this model have been suggested, in order to obtain biophysically more plausible behavior. The most prominent among these so called nonlinear IF models are maybe the quadratic (Ermentrout 1996, Latham et al. 2000) as well as the exponential IF model (Fourcaud et al. 2003). We slightly vary the definition given in Fourcaud et al. 2003:

$$C \frac{dV}{dt} = -g_L(V - V_L) + \psi(V) - g_K(V - V_K) + I_{ext}. \quad (6.2)$$

The nonlinearity $\psi(V)$ is given by

$$\psi(V) = \begin{cases} \frac{g_L}{2\Delta_T}(V - V_T)^2 + g_L(V - V_L) - I_T & \text{quadratic IF model} \\ g_L\Delta_T \exp(\frac{V - V_T}{\Delta_T}) & \text{exponential IF model} \end{cases}. \quad (6.3)$$

In both cases, a spike is said to be fired when the membrane potential diverges to infinity, and it is subsequently set to the reset potential V_R . There are three additional parameters: V_T is the *threshold voltage*, i.e. the largest voltage at which the neuron can be maintained during constant current injection without firing a spike. Δ_T is the *spike slope factor*, which controls the rapidity of spike initiation; for $\Delta_T \rightarrow 0$ the exponential IF model degenerates to its linear analogue. For the quadratic IF model I_T is the *threshold current*, i.e. a constant injected current of amplitude I_T depolarises the neuron voltage to V_T .

We also used a hybrid IF model that is identical to the linear IF model for voltages below a fixed value V_C , and whose I-V curve rises quadratically whenever the voltage exceeds V_C . This model was called the “linear-quadratic IF” (lqIF) model in the following and is described by Eq. (6.2), where

$$\psi(V) = \begin{cases} 0 & V < V_C \\ \frac{g_L}{2\Delta_T}(V - V_T)^2 + g_L(V - V_L) - I_T & V \geq V_C \end{cases}. \quad (6.4)$$

V_C as well as I_T are determined from the condition that $\psi(V)$ as well as its first derivative be continuous for $V \rightarrow V_C$. They are given by $V_C = V_T - \Delta_T$ and $I_T =$

6.3. MATERIALS AND METHODS

$-g_L(\frac{\Delta_T}{2} + V_L - V_T)$. Spiking is realised in the same way as for the other nonlinear IF models.

6.3.4 The 2-state-variable models

We use two models of intermediate complexity, the Izhikevich model (Izhikevich 2003) as well as the adaptive exponential IF (aEIF) model (Brette and Gerstner 2005). In addition to the membrane potential, both models comprise a second state variable that is responsible for subthreshold and suprathreshold adaptation. The defining equations of the Izhikevich model are

$$C \frac{dV}{dt} = k(V - V_L)(V - V_T) - w + I_{ext}, \quad (6.5)$$

$$\frac{dw}{dt} = a(b(V - V_L) - w). \quad (6.6)$$

A spike is released when the voltage exceeds 30 mV, after which it is reset to V_R and a fixed value d is added to the adaptation variable ($w \rightarrow w + d$). The aEIF model is defined in a similar way, except that the subthreshold I–V–relation contains an exponential nonlinearity rather than a quadratic one:

$$C \frac{dV}{dt} = -g_L(V - V_L) + g_L \Delta_T \exp\left(\frac{V - V_T}{\Delta_T}\right) - w + I_{ext} \quad (6.7)$$

$$\tau_w \frac{dw}{dt} = a(V - V_L) - w \quad (6.8)$$

If $V_m > 20$ mV a spike is released, after which the voltage is reset to V_R and the adaptation variable augmented by b ($w \rightarrow w + b$). During the simulations where no adaptation current was included, in both models we skipped the update of the adaptation variable following a spike, i.e. we set $d = 0$ in the Izhikevich model and $b = 0$ in the aEIF model. Again, we assumed that the capacitance C as well as the leak conductance and reversal potential g_L and V_L are extracted from the experiment, all other parameters are adjusted during the fit in order to obtain optimal behaviour. However, while the parameters C and V_L in the models directly represent the respective physiological quantities, this is not the case for the leak conductance: writing Eqs. 6.5 and 6.7 as $C dV/dt = -f(V) + I_{ext}$, the physiological leak conductance is given by

$$g_L^{physiol} = \left. \frac{df(V)}{dV} \right|_{V=V_L}. \quad (6.9)$$

Thus for the Izhikevich model we obtain the relation $g_L^{physiol} = b - k(V_L - V_T)$, for the aEIF model it reads $g_L^{physiol} = g_L(1 - \exp(\frac{V_L - V_T}{\Delta_T})) + a$. For typical parameter values the exponential term can be neglected, so during the simulations we used $g_L^{physiol} = g_L + a$.

6.3.5 The Hodgkin-Huxley model

Finally, we use a Hodgkin-Huxley (HH) model consisting of two channels, a fast sodium channel (g_{Na}) and a delayed rectifier potassium channel (g_{Kd} , details can be found in Traub and Miles 1991), specified by the following membrane equation:

$$C \frac{dV}{dt} = -g_L(V - V_L) - g_{Na}(V - V_{Na}) - g_{Kd}(V - V_K) - g_M(V - V_K) + I_{ext}. \quad (6.10)$$

Also, a muscarinic conductance (g_M) has been included, that accounts for adaptation. The conductances g_{Na} and g_{Kd} are governed by the three state variables m , h and n and respective maximal conductances \bar{g}_{Na} , \bar{g}_{Kd} :

$$g_{Na} = \bar{g}_{Na} m^3 h, \quad (6.11)$$

$$g_{Kd} = \bar{g}_{Kd} n^4. \quad (6.12)$$

The state variables evolve according to the time evolution equations

$$\frac{ds}{dt} = \frac{s_\infty(V) - s(t)}{\tau_s(V)}, \quad s = \{m, h, n\}, \quad (6.13)$$

where the functions $s_\infty(V)$ and $\tau_s(V)$ are composed of the respective forward- and backward rates between open and closed states, α_s and β_s :

$$s_\infty(V) = \frac{\alpha_s(V)}{\alpha_s(V) + \beta_s(V)} \quad (6.14)$$

$$\tau_s(V) = \frac{1}{\alpha_s(V) + \beta_s(V)} \quad (6.15)$$

For the state variable m , α and β are parameterized as

$$\alpha_m(V) = -\frac{f_a(V - V_{0,a})}{\exp(-\frac{V - V_{0,a}}{d_a}) - 1} \quad (6.16)$$

$$\beta_m(V) = \frac{f_b(V - V_{0,b})}{\exp(\frac{V - V_{0,b}}{d_b}) - 1} \quad (6.17)$$

The muscarinic conductance g_M is described by similar equations, details can be found in Mainen and Sejnowski 1996. During optimisation, we vary all parameters describing the sodium activation curve, i.e. f_a , $V_{0,a}$, d_a , f_b , $V_{0,b}$ and d_b , as well as a parameter introducing a relative voltage shift between sodium activation and inactivation. The shape of the latter as well as the potassium activation curve are kept fixed. In addition, we adjust the maximal conductances of the spike-related sodium and potassium channels, \bar{g}_{Na} and \bar{g}_K , and of the muscarinic current, \bar{g}_M .

6.3. MATERIALS AND METHODS

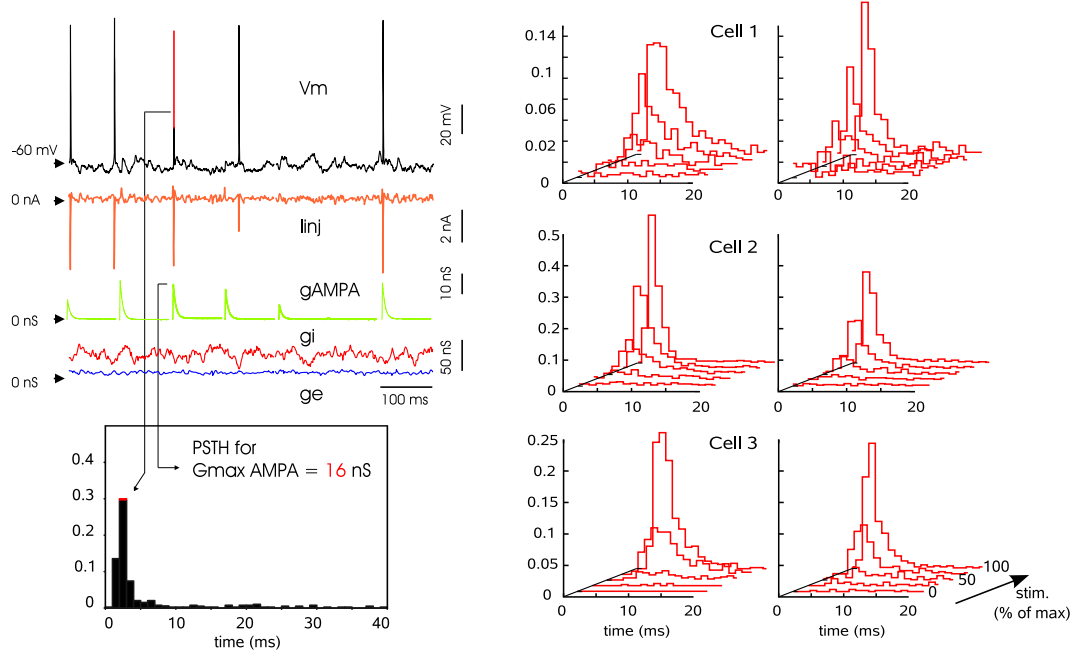


Figure 6.1: Experimental protocol and resulting PSTHs. Left: Dynamic-clamp experiment in which two fluctuating conductances (excitation, blue and inhibition, red) were injected to recreate *in vivo*-like activity states. In addition, AMPA-shaped excitatory conductance stimulus (green) with varying strength was injected into the cell using dynamic clamp. Stimulus amplitudes were randomized, and collected for each stimulus strength separately, to compute PSTHs. Right panels: PSTHs calculated for three different cells (a fourth cell is shown in Fig. 6.2). The x-axis shows time after stimulus onset, the y-axis labels stimulus strength, and the z-axis the probability for generating an action potential (time bin of 1 ms).

6.3.6 The protocol

We applied the same stimulation protocol to cortical neurons *in vitro* and to the models described above (cf. Fig. 6.1). It consisted of a background stimulation provided by the “point-conductance model” (Destexhe et al. 2001), supposed to simulate synaptic input. The model creates two channels of fluctuating conductances, one excitatory ($g_e(t)$) and one inhibitory ($g_i(t)$), that are described by Ornstein-Uhlenbeck equations. For the excitatory channel, the time evolution equation reads

$$\frac{dg_e(t)}{dt} = -\frac{1}{\tau_e}(g_e(t) - g_{e0}) + \sqrt{\frac{2\sigma_e^2}{\tau_e}}\xi_e(t). \quad (6.18)$$

We use g_{e0} and σ_e to indicate the mean and standard deviation (SD) of the excitatory conductance distribution, $\xi_e(t)$ is a Gaussian white noise process with zero

mean and unit standard deviation and τ_e is the excitatory correlation time constant. The inhibitory channel is described by an equivalent equation with parameters g_{i0} , σ_i , $\xi_i(t)$ and τ_i . Throughout this article we use the correlation times $\tau_e = 2.728$ ms and $\tau_i = 10.49$ ms. In particular, we consider two possible background states: a “low-conductance (LC) state”, where excitatory and inhibitory conductances have roughly the same mean value and their sum is smaller or of the same order as the leak conductance, and a “high-conductance (HC) state”, which is characterised by a dominant inhibitory conductance and a leak conductance that constitutes only a fraction of the total conductance. In addition to the background conductance, an AMPA-stimulus of varying strength is injected in intervals of 100 ms, where the strength can take one of the five values 1 nS and 1–4 times a base strength \bar{g}_S , whose value depends on the cell under consideration. Subsequently, the stimulus-triggered spiking response (post-stimulus time histogram, PSTH) is calculated with a bin width of 1 ms for each stimulus strength separately. The recording time during the experiments was about 300 s for each background state (corresponds to about 600 repetitions per stimulus strength), in the models the simulated time was 100 s per background state and stimulus strength (1000 repetitions per stimulus strength).

6.3.7 The optimisation

The optimisation has been done using a NEURON (Hines and Carneval 1997) implementation of the simulated annealing method based on a simplex algorithm (Press et al. 1992, Davison 2004). The strategy consists of a simplex (an assembly of n points, where n is the number of parameters) that moves in parameter space, where uphill steps are accepted with a certain probability depending on a slowly decreasing variable E (the ‘temperature’). For very low temperature, the method becomes identical to the simplex algorithm, but during optimisation it is less likely to be caught in local minima. A comparative survey showed (Vanier and Bower 1999), that for an intermediate number of parameters, the simulated annealing procedure was superior to other methods. For the fitting of the PSTH, the error function consisted of the RMS (root mean square) of the difference between the experimental and the simulated PSTHs in the first 20 ms taken across all background states and stimulus strength under consideration, normalised by the RMS of the experimental PSTH:

$$e = \sqrt{\frac{\sum_{b,s,i} (psth_i^{exp} - psth_i^{sim})^2}{\sum_{b,s,i} (psth_i^{exp})^2}}, \quad (6.19)$$

with the subscript b indicating the background state, s the stimulus strength and i the bin number. Simulations were performed on Linux PCs using the NEURON simulation environment (Hines and Carneval 1997) (for the HH model) or custom C++ programs (for the other models).

6.4 Results

Recordings were taken from four different cells. Their properties as well as stimulation details are summarised in Tab. 6.1. The conductance parameters for the LC state were chosen such that spontaneous activity was low (up to 6 Hz), for the HC state they were chosen such that they roughly reproduced the mean voltage and its fluctuations. For each cell, the PSTH was calculated during either LC or HC states for five different stimulus amplitudes (cf. Figs. 6.1 and 6.2). In general, during LC states PSTHs are broader and their peaks occur later after stimulus onset than during HC states. Also, the number of spikes per stimulus is higher in the LC state, though the stimulus strength was the same in both states. Fig. 6.3 shows

Table 6.1: Cell parameters

	C (nF)	g_L (nS)	V_L (mV)	\bar{g}_S (nS)		g_{e0} (nS)	σ_e (nS)	g_{i0} (nS)	σ_i (nS)
cell 1	0.34	13.6	-93.1	5.0	LC	6.0	3.0	3.0	1.0
					HC	15.0	5.0	50.0	17.0
cell 2	0.39	10.9	-99.0	9.0	LC	6.9	3.0	5.1	2.5
					HC	10.1	4.0	25.9	10.0
cell 3	0.33	24.9	-81.7	7.0	LC	4.0	1.7	3.0	1.5
					HC	7.5	3.0	34.0	15.0
cell 4	0.412	20.8	-86.0	12.0	LC	5.9	2.9	2.6	1.3
					HC	11.6	5.0	39.4	17.0

the quality (cf. Eq. 6.19) of the fits to the four cells for all seven models in ascending order of model complexity. We first fitted the six PSTHs that correspond to the stimulus strengths 1 nS, 2 \bar{g}_S and 4 \bar{g}_S during LC as well as HC states. In all models, spike-related adaptation mechanisms were disabled by setting the appropriate parameters to zero (cf. Section “Materials and Methods”). We would like to highlight several points: First, the HH model, which is the computationally most costly model, shows the best performance, both for each cell separately as well as on average. This might not be too surprising given the large number of parameters that are adjusted. However, the model with the worst performance (again separately for each cell and on average) is the quadratic IF model rather than the linear one, as one might have expected. But also the Izhikevich model, with spike-related adaptation disabled, shows an unsatisfactory behaviour. An explanation for this observation might be the constraints we put on the models, namely to reflect the experimental leak conductance and its reversal potential. This fixes the shape of the quadratic nonlinearity at the leak reversal, but due to its inherent symmetry also to a large extent in the spike initiation region. For the quadratic IF model, the only freedom left is the position of the second root of the parabola. For the Izhikevich model, there are three free parameters left, and its performance also depends on the shape of the PSTH. Cell 3 shows a later onset of spikes following the stimulus, which better suits a quadratic I–V–curve (cf. Fourcaud et al. 2003). The latter exactly contrasts the preferences of the linear IF model, and in fact here

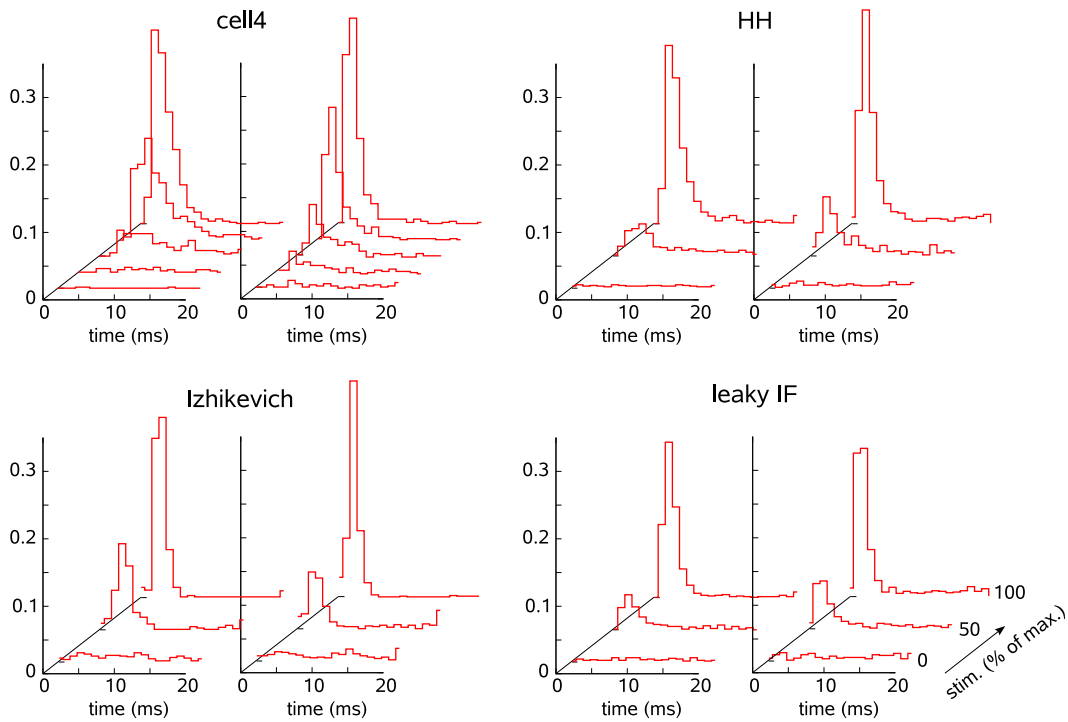


Figure 6.2: Comparison between experimental PSTHs and best model fits during LC and HC states simultaneously, adaptation included. Upper left: Experimental PSTH obtained for cell 4. Upper right: PSTH of the best-fitted HH model. Lower left: PSTH of the best-fitted Izhikevich model. Lower right: PSTH of the best-fitted leaky IF model. For this particular error cell, all three models show acceptable to good agreement with the experiments (cf. error values in Fig. 6.4).

6.4. RESULTS

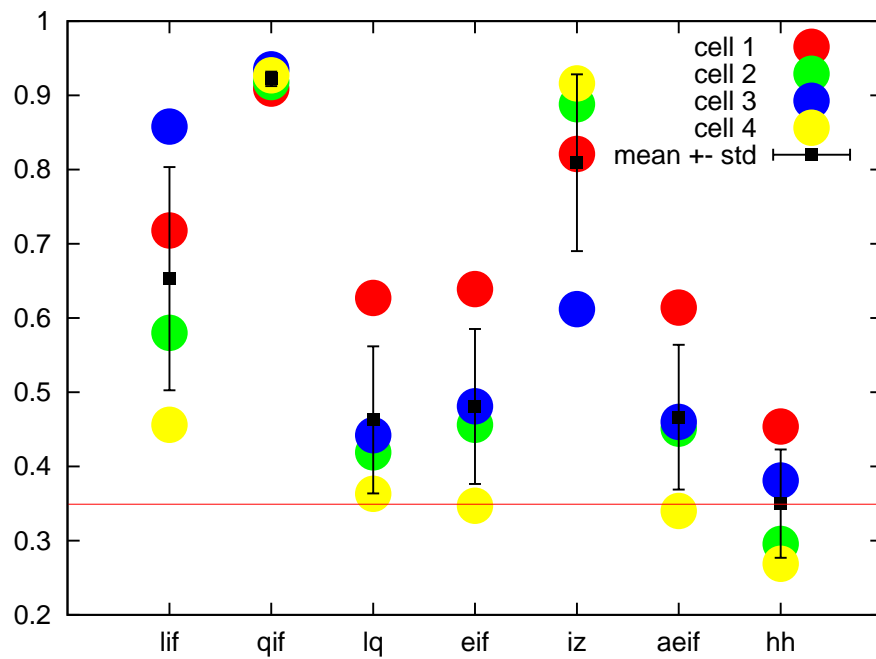


Figure 6.3: RMS error for the best fits of all models to all cells without spike-related adaptation. The red line shows the average RMS of the best model (HH). The performance of the leaky IF model strongly depended on the cell, the match of the quadratic IF and the Izhikevich model with experiment was generally unsatisfactory. All other models showed good performance.

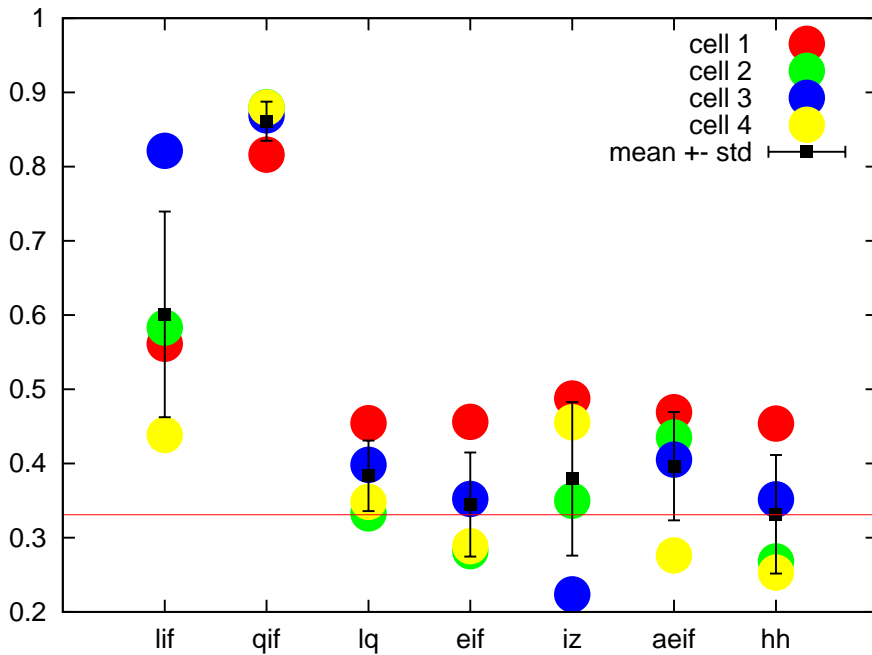


Figure 6.4: RMS error for the best fits of all models to all cells with spike-related adaptation. The red line shows the average RMS of the best model (HH). Generally, all fits were better compared to Fig. 6.3, the increase in performance is most remarkable for the Izhikevich model.

the order of goodness of fit for single cells is reversed compared to the Izhikevich model (no real order is apparent in the case of the quadratic IF model). In the absence of noise, the linear IF model can emit spikes only during the rising phase of the EPSP, whereas the nonlinear IF models are able to spike at any time after the stimulus (provided the V_m is sufficiently depolarised, i.e. beyond the second root of the I–V-curve). The presence of synaptic noise slightly blurs this effect, but the principal behaviour remains. Finally, the lq and exponential IF as well as the aEIF model display a very homogenous performance in reproducing the experimental PSTHs. All three combine the advantages of the quadratic IF model (no sharp spike initiation) and the linear IF model (separation of the behaviour at rest and at threshold). Apparently, the exact realisation of the nonlinearity (quadratic or exponential) is not crucial here. Also, it seems that the presence of an adaptation state variable (with spike-related adaptation disabled) in the aEIF model does not improve the match significantly in this particular context.

We repeated the fit, now allowing all models their own way of spike-related adaptation (cf. Section “Materials and Methods”). The results are displayed in Fig. 6.4. The most apparent difference is clearly the far better match for the Izhikevich model. The fit of cell 3 even yields the best fit in the ensemble. Still, the HH model shows the best match, for each cell separately and on average. However,

6.4. RESULTS

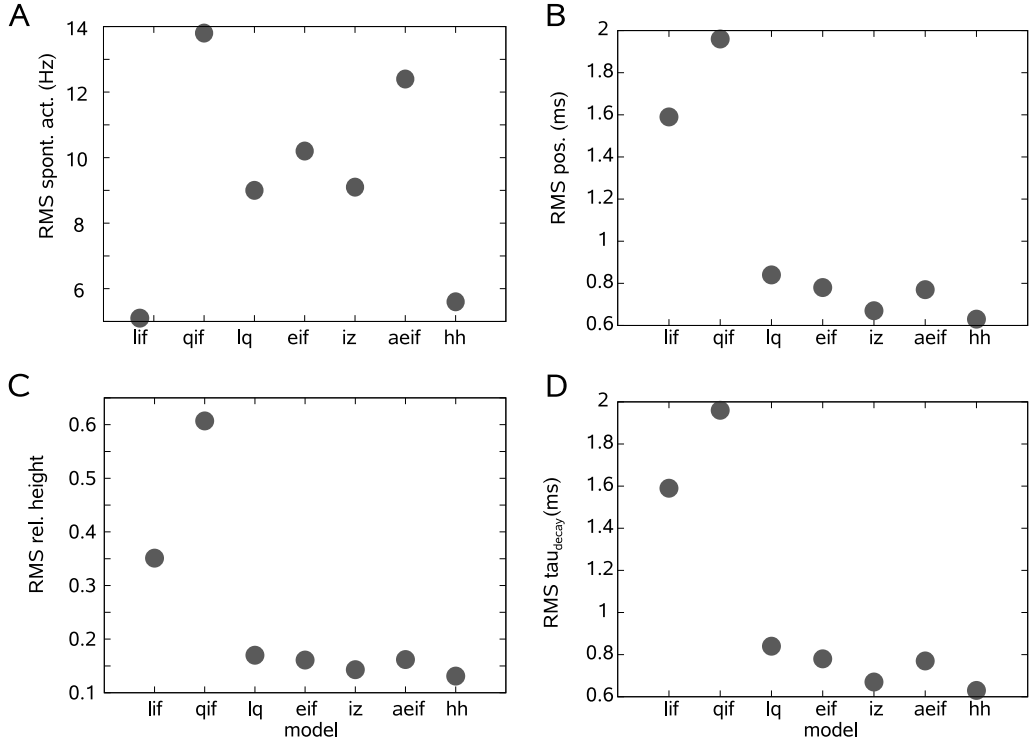


Figure 6.5: Comparison of different characteristics of the PSTH. The RMS error of the difference between the experimental and the model PSTHs are given. **A:** spontaneous activity. **B:** PSTH peak position. **C:** relative peak height. **D:** PSTH decay time constant. With exception of spontaneous activity, the model performance followed the ranking of Fig. 6.4.

the exponential IF model comes surprisingly close, and for two cells (cells 1 and 3) the advantage of the HH model is only marginal. On average, the exponential IF model with adaptation even performs better than its more elaborate counterpart, the aEIF model. Roughly speaking, all models except the linear and the quadratic IF models, show an acceptable match with the experiments, although each model has its particular strengths and weaknesses depending on the cell.

For the latter fit, we looked at the results in more detail. We wanted to see, which features of the PSTHs were reproduced accurately and which were not, depending on the model. To this end, we fitted gamma distributions to both the experimental and the simulated PSTHs, from which we extracted the position and the height of the peaks as well as the “decay time constant” of the falling flanks. In addition we fitted a constant to the PSTH for lowest stimulus strength (which is basically flat) in order to get an idea of the spontaneous activity.

For the data, the spontaneous activity was around 0–6 Hz. Fig. 6.5 A shows the RMS of the difference in spontaneous activity with respect to the different models. The difference is smallest for the HH and the linear IF model. However,

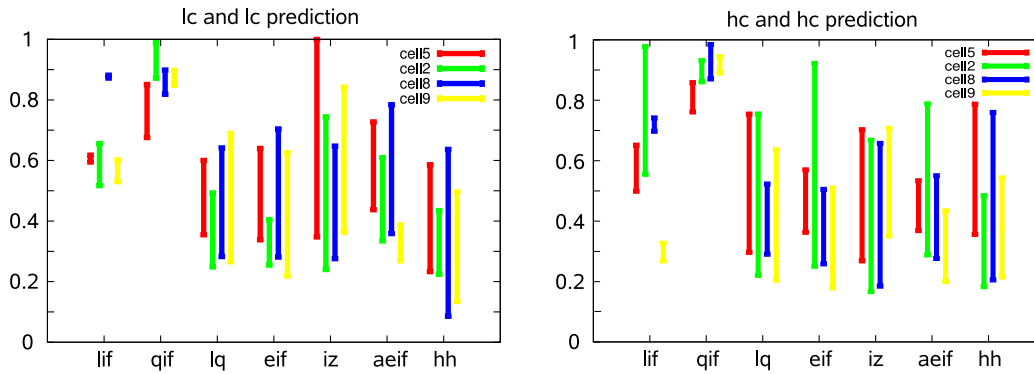


Figure 6.6: Quality of model predictions to data not used in the fitting. Left: all models were fit to PSTHs only for the LC state, and the optimal fits were used to predict the responses obtained for the HC state. Each bar joins the RMS error of the fit (lower end of the bar) to the RMS error of the prediction (higher end of the bar). Different colors correspond to different cells, as shown in the inset.

the contribution of this feature to the error function is minor, so one cannot really expect a good match between simulation and experiment. Fig. 6.5 B shows the RMS of the difference in the time of the PSTH peak after stimulus onset. Here, the plot more or less reproduces the order in performance of Fig. 6.4. The only exception is maybe the Izhikevich model, which fits slightly better with the data than would be expected from the previous plot. The same observations hold for the RMS of the difference in relative peak height (Fig. 6.5 C) and the decay time constant (Fig. 6.5 D).

Finally, we tested whether fitting the model response to the LC and HC background at the same time added constraints, or if a fit using each background separately would have yielded similar results. To this end, we first ran a fit (adaptation included) of the PSTHs obtained during either LC or HC background (using the same sequence of stimulus strengths as before). With the model parameters obtained in this manner, we subsequently computed the PSTH during the respective other background state. We termed the PSTHs obtained during a LC state, but using the parameters corresponding to a fit in the HC state, the “LC prediction” and vice versa. Fig. 6.6 summarises the results: The lower end of each vertical bar indicates the minimal error obtained during a fit during either LC (left) or HC (right) state, the upper end represents the error of the respective prediction. The length of the bar thus represents the discrepancy between the best fit and the prediction. With only a few exceptions (e.g. the leaky IF, LC, cell3), all fits to a single background state have lower error values than the fits to both states at the same time. Note, that the exceptions are justified, since only the “mean” (roughly speaking) should be lower or equal to the error from the fit to both states at the same time. The mismatch between a PSTH and its respective prediction does not seem to be related to a specific model or cell with the exception of the two worst

behaving models, the linear and the quadratic IF model. Since there is an upper limit for the minimal error during the fit (no response at all corresponds to an error of 1), chances are high (although not unity) that as soon as there is a response, the corresponding error is lower than 1.

6.5 Discussion

We have presented a study that compares the ability of seven neuron models to reproduce *in vitro* recordings in a quantitative way. The complexity of the models span a range between very simple (leaky IF) and detailed (HH). In choosing the protocol, we took care to reproduce a situation that is likely to be encountered for neurons in natural networks. The specific setting should be able to assess the sensitivity of neurons to “signals”, e.g. correlated synaptic input, transmitted in networks. We contrasted two different scenarios of synaptic input, a LC and a HC state. The analysis revealed that, in general, additional complexity yields a better match with experiments, as expected. However, the surplus in accuracy can be very costly computationally. This observation was valid for the fits to either LC or HC state separately or to both at the same time. The HH model, for example, performed best of all models, with and without adaptation included. However, the relatively simple exponential IF model came surprisingly close. We conclude that the latter model constitutes a very good candidate for simulations of networks of RS neurons.

We also found that the best fit for a model does depend on the state (LC or HC) that the neuron is in. Fitting the response to stimuli during one state at a time usually entailed a bad match during the respective other state. In Herrmann and Gerstner 2001, 2002, an analytical derivation of the PSTH shape has been given during conditions that are comparable though not exactly the same as here. The authors used current-based inputs and an escape noise model. One of their results is the description of the PSTH shape as a superposition of the stimulus waveform and its first derivative, the relative importance of the two depending on the level of noise. Given the low level of spontaneous activity in our recordings, the comparison to their results is difficult. However, conforming with their results and our choice of noise parameters ($0.3 \leq \sigma/g_0 \leq 0.5$) the absence of secondary peaks and a strong trough after the main peak indicates that our recordings were done in a high-noise regime.

It must be stressed that the particular protocol that we choose here is just one possibility among many others in order to characterize neuronal behavior. Another very relevant approach is the exact reproduction of spike times in response to noisy stimuli (Jolivet et al. 2006; Clopath et al. 2007). Also, future work should consider not only responses to isolated excitatory inputs, but complex responses to streams of several excitatory and inhibitory inputs. This approach should provide

much more severe constraints on models and is also closer to the situation of input integration in real networks. However, for such complex stimuli, there is a combinatorial explosion of the number of possible combinations, and realizing them experimentally would necessitate several hours of stable recording, which certainly constitutes the most challenging aspect of this type of experiments.

6.6 References

- Achard P., De Schutter E. Complex parameter landscape for a complex neuron model. *PLoS Comput Biol.* **2**(7):794-804, 2006.
- Brette R., Gerstner W. Adaptive exponential integrate-and-fire model as an effective description of neuronal activity. *J. Neurophysiol.* **94**(5):3637-3642, 2005.
- Clopath C., Jolivet R., Rauch A., Lüscher H. R., Gerstner W. Predicting neuronal activity with simple models of the threshold type: Adaptive Exponential Integrate-and-Fire model with two compartments. *Neurocomputing* **70**(10-12):1668-1673, 2007.
- Davison A. P. *Private communications*.
- Destexhe A., Rudolph M., Fellous J. M., Sejnowski T. J. Fluctuating synaptic conductances recreate in-vivo-like activity in neocortical neurons. *Neuroscience* **107**:13-24, 2001.
- Ermentrout G. B.. Type i membranes, phase resetting curves, and synchrony. *Neural Comput.*, **8**:979-1001, 1996.
- FitzHugh R. Impulses and physiological states in models of nerve membrane. *Biophys. J.*, **1**:445-466, 1961.
- Fourcaud-Trocmé N., Hansel D., van Vreeswijk C., Brunel N. How Spike Generation Mechanisms Determine the Neuronal Response to Fluctuating Inputs. *J. Neurosci* **23**(37): 11628-11640, 2003.
- Herrmann A., Gerstner W. Noise and the PSTH response to current transients: I. General theory and application to the integrate-and-fire neuron. *J Comput Neurosci.*, **11**(2):135-151, 2001.
- Herrmann A., Gerstner W. Noise and the PSTH response to current transients: II. Integrate-and-fire model with slow recovery and application to motoneuron data. *J Comput Neurosci.*, **12**(2):83-95, 2002.
- Hines M. L., Carnevale N. T. The NEURON simulation environment. *Neural Computation* **9**: 1179-1209, 1997
- Hodgkin A. L. and Huxley A. F. A quantitative description of membrane current and its application to conduction and excitation in nerve. *J. Physiol.* **117**, 500-544, 1952.
- Izhikevich E. M. Simple Model of Spiking Neurons *IEEE Transactions on Neural Networks* **14**(6): 1569-1572, 2003.

- Izhikevich E. M. Which Model to Use for Cortical Spiking Neurons? *IEEE Transactions on Neural Networks* **15**(5): 1063-1070, 2004.
- Jolivet R., Lewis T. J., Gerstner W. Generalized integrate-and-fire models of neuronal activity approximate spike trains of a detailed model to a high degree of accuracy. *J. Neurophysiol.* **92**(2):959-976, 2004.
- Jolivet R., Rauch A., Lscher H. R., Gerstner W. Predicting spike timing of neocortical pyramidal neurons by simple threshold models. *J. Comput. Neurosci.* **21**:35-49, 2006.
- Lapicque L. Recherches quantitatives sur l'excitation électrique des nerfs traitée comme une polarisation. *J. Physiol. Pathol. Gen.*, **9**:620-635, 1907.
- Latham P. E., Richmond B. J., Nelson PG, Nirenberg S. Intrinsic dynamics in neuronal networks. I. Theory. *J. Neurophysiol.*, **83**:808-827, 2000.
- LeMasson G., Maex R. Introduction to equation solving and parameter fitting. In: De Schutter E, editor. Computational neuroscience: Realistic modeling for experimentalists. London: CRC Press. 347 p.
- Mainen Z. F., Sejnowski T. J. Influence of dendritic structure on firing pattern in model neocortical neurons. *Nature*, **382**(6589):363-366, 1996.
- Morris C., Lecar H.. Voltage oscillations in the barnacle giant muscle fiber. *Biophys. J.*, pages 193-213, 1981.
- Nagumo J. S., Arimoto S., Yoshizawa S. An active pulse transmission line simulating nerve axon. *Proc. IRE*, **50**:2061-2070, 1962.
- Press W. H., Flannery B. P., Teukolsky S. A. Numerical Recipes in C: The Art of Scientific Computing. Cambridge University Press, Second Edition, 1992.
- Traub R. D., Miles R. Neuronal networks of the hippocampus. Cambridge, MA: Cambridge UP.
- Vanier M. C., Bower J. M. A Comparative Survey of Automated Parameter-Search Methods for Compartmental Neural Models. *J. Comput. Neurosci.* **7**:149-171, 1999.
- Weaver C. M., Wearne S. L. The role of action potential shape and parameter constraints in optimization of compartment models. *Neurocomputing* **69**:1053-1057, 2006.

6.6. REFERENCES

Chapter 7

General Conclusions

7.1 Summary

Neurons, the central processing units of the brain, are in a particular state during periods of intense network activity, as it is the case e.g. in the awake state or during slow-wave sleep up-states. In these conditions, cortical neurons receive a barrage of excitatory and inhibitory synaptic inputs. As an effect, their membrane potential depolarizes and strongly fluctuates, giving rise to irregular firing activity at high discharge rates. Furthermore, the share of inhibitory conductance exceeds the excitatory one, and also the amount of fluctuations is mainly contributed by inhibition. Since in such states spikes are mainly triggered by voltage fluctuations, these observations suggest an important role for interneurons in information processing. However, how information is integrated, processed and passed on in these states is still an open question, and may very well be different during different behavioral states.

In the course of my thesis, the aim was to shed light on the process of signal integration during states that were characterized by the amount of synaptic input received. More concrete, we compared two states that are very similar on a level of voltage means and fluctuations as well as spike rates and irregularity, but differ markedly in the synaptic background activity. One of these states we called “low-conductance state”, identified by an overall low synaptic input, where excitation and inhibition were of about the same magnitude. This state was set in contrast with a “high-conductance state”, where synaptic conductances dominate over the leak conductance and inhibition provides the largest share. The amount of conductance fluctuations was assumed to be roughly proportional to the respective mean. This resembles the situation of neurons in highly active networks.

The tool of choice for the analysis of such states was the spike-triggered average (STA), applied to excitatory as well as inhibitory conductances. A primary investigation in computational models showed, that there are principle differences in the STAs depending on the background. Not very surprisingly, in the last few tens

7.1. SUMMARY

of milliseconds before spikes, on average one observes a drop in inhibitory and a rise in excitatory conductance in both states. However, during low-conductance states the rise in excitation surpasses the drop in inhibition such that there is a net rise in the sum of the two. This conforms to the idea that spikes are primarily evoked by additional excitatory synaptic events. In contrast, during high-conductance states, the drop in inhibition is much more pronounced, amounting to a drop in total conductance. The same protocol has been repeated in *in vitro* preparations using dynamic clamp, and the same prespike conductance patterns have been identified. This observation points to an important role of inhibition in signal integration during activated states.

It is difficult to conduct a similar analysis *in vivo*. While in models and during dynamic clamp the conductance time course is known and the STA can thus be readily calculated, only the membrane potential time course is observable during intracellular recordings *in vivo*. At the beginning of my thesis, no method had been reported in the literature, that could extract average conductances related to spikes from the membrane potential. A complicacy with traditional methods used for conductance estimation is the fact that the conductance STA shows a dependency on an injected constant current. Therefore, the passive membrane equation can not be solved anymore, since assuming that the conductances be the same at both current levels leads to erroneous results. On the other hand, there are infinitely many solutions for the conductance time courses, when they are constrained by only one voltage time course. Nonetheless, it is possible to assign a probability of occurrence to any one of these solutions, based on the stochastic nature of the synaptic conductances. Making use of basic calculus, the most likely conductance traces can then be extracted which, due to the symmetry of the conductance distributions, at the same time are the average traces. Knowing the means and standard deviations of the synaptic conductances (for the estimation of which methods exist) the method can be applied to intracellular recordings *in vivo*.

Subsequently, we presented a conductance analysis of recordings from awake and naturally sleeping cat. This kind of data is still very rare, and no such analysis has been done before. It was interesting to observe, how certain cells change their firing behavior upon awakening of the animal. Regular-spiking cells showed up–down–state cycles during slow–wave sleep, but while some showed pronounced firing upon awakening, a considerable share ($\sim 45\%$) initially depolarized, but hyperpolarized briefly afterwards and stopped firing. In contrast, most interneurons increased their discharge activity when the animal woke up. A conductance analysis using the VmD-method revealed diverse combinations of synaptic conductances in regular spiking neurons during these states, but in most of the cases inhibition was stronger than excitation. On average, inhibitory conductances were 2-3 times larger than excitatory ones. This tendency was even more pronounced during slow–wave sleep up–states than during the wake state. Similar observa-

tions hold for the respective conductance fluctuations. Using these conductance estimates, model simulations of intracellular activity were in accordance with the observations. Finally, we estimated the STA conductances using the method outlined before. We found, that most cells in the awake state (7/10) and all cells in slow-wave sleep up-states (6/6) and during REM sleep (2/2) showed a drop in total conductance prior to spikes. In brief, the recorded cells showed all characteristics of neurons in high-conductance states.

In Chapter 5, we reviewed and partially extended analysis techniques based on the point-conductance model, that can be readily applied to intracellular recordings *in vivo*. We first outlined the VmD-method, which has the capacity to extract the mean values and the amount of fluctuations of excitatory and inhibitory conductances from the voltage distributions obtained at two DC levels. The method was successfully employed to re-estimate known injected conductances as well as to analyse and recreate spontaneous up-states during *in vitro* recordings using dynamic clamp. The method depends on a couple of parameters, two of which are hard to constrain: the correlation time constants of synaptic conductances. We presented a method based on the power spectral density (PSD) of the membrane potential, that can provide estimates for these time constants. While the performance is very good in models and during dynamic clamp, it suffers from an unexpected scaling of the PSD for high frequencies in *in vivo* recordings. Nevertheless, it can provide evidence that the assumed time constants are reasonable. Eventually, the STA-method was reviewed, further tested and extended in the concluding section. The testing was done on a pool of 36 recordings, the estimated conductance STAs were compared to the injected ones on the basis of the parameters of an exponential template that was fitted to the traces. The agreement was very good for all three parameters. The study also revealed, that the change in total conductance just before spikes is mainly determined by the ratio of the standard deviations of excitation and inhibition, and that the standard deviations also largely control the change in their respective conductance. It is thus through a correlation between the means and fluctuations of a conductance channel, that neurons in inhibition-dominated states display a drop in the STA of the total conductance. Furthermore, the method was extended for the case of a non-vanishing crosscorrelation between synaptic conductances as well as a possible shift in their timing in order to account for the situation reported during response to sensory stimuli.

Finally, we presented a comparison of the ability of different computational models to reproduce the behavior of biological neurons. We chose a protocol that was intended to closely resemble the situation of cortical neurons imbedded in active networks. It consisted of a background of fluctuating synaptic conductances (realized by means of the point-conductance model) and an additional AMPA-shaped stimulus, intended to represent an excitatory signal composed of correlated input. We tried to reproduce the experimental PSTH using models of very differ-

7.2. OUTLOOK

ent complexity, including the linear IF model, nonlinear IF models, Izhikevich-type models with two state-variables and finally a model using HH-type sodium and potassium channels. Roughly speaking, the quality of reproduction increased with model complexity, and not too surprisingly the HH model performed best. However, the rather simple exponential IF model came very close and, given its low computational demand, represents a sound model e.g. for network simulations. Again, we compared low- as well as high-conductance states and fitted the models either to each state separately or to both states at the same time. It turned out that the models optimally adjusted to one state usually showed an unsatisfactory behavior during the other. Both states thus add different constraints to the models.

7.2 Outlook

In this thesis we have shown how a simple model of synaptic activity can be used for the analysis of intracellular recordings *in vivo* by matching observable quantities to model parameters. Important insights have been gained concerning the structure of synaptic conductances in cortical neurons during different behavioral states, and their impact on the average spike-triggering conductance patterns. Concerning the method to extract the latter, several improvements could be envisaged.

A source of ambiguity is the length of the prespike window that has to be cut in order to avoid contamination through voltage dependent ion (sodium) channels. The mathematical structure is such that the voltage time course, milliseconds before the spike, shapes the estimated conductance STA throughout the whole interval under consideration. Fortunately, in the case of sodium contamination, the estimated trace converges quickly to a rather stable state, but it is impossible to determine a precise cut. A way around could consist in the application of the exponential rather than the leaky IF model, since the exponential term is exactly intended to model the increase in sodium conductance. A drawback would be the appearance of two more parameters (V_T and Δ_T , cf. Chapter 6, Eq. 6.2) that have to be estimated from the data, but this could be done using a deconvolution of the voltage trace (Richardson & Badel 2007). Using the exponential IF model as basis, it may be possible to drastically shorten or completely omit the prespike window.

Furthermore, it would be nice to acquire direct evidence that the method works well *in vivo*. For this to succeed, an independent and reliable estimation of synaptic conductances is necessary. A way to do this in models or in dynamic clamp would be to use “frozen noise”, i.e. to inject the exact same fluctuating conductance time courses twice at different DC levels. The conductances (during inter-spike intervals) can then be estimated from the membrane potential using

the inversion of a membrane equation; in order to minimize the perturbation due to spike-related sodium conductances, the exponential IF model would be the model of choice. While it is probably impossible to realize a frozen noise situation for periods of spontaneous spiking activity *in vivo*, it was shown (Monier et al. 2003; Wehr & Zador 2003; Wilent & Contreras 2005a) that the voltage response to sensory stimuli (and thus presumably the underlying synaptic input) can be very reliable. One could think of a protocol e.g. in rat barrel cortex, where recordings are taken from a neuron while it is excited via colored noise stimulation applied to its principal whisker (or to several whiskers at a time). As mentioned before, the synaptic input induced in a neuron in this way is likely to display correlations between excitatory and inhibitory events. This was one of the reasons to extend the STA analysis in the way described in Chapter 5. Using this protocol would allow to compare the estimates obtained with the STA method to the STAs computed from the estimation of the conductance time courses, thus validating (or disproving) its application to *in vivo* recordings.

Another possible amelioration concerns the fact that the solution is obtained by the numerical inversion of a matrix, whose dimension depends on the number of datapoints in the STA. Though this hardly puts practical limits on the duration or resolution of the STA, it may be worth the effort to translate Eq. 3.7 (Chapter 3) back to continuous time (cf. Badel et al. 2006) and attempt an analytic solution to the thereby emerging variational problem, which would highlight the interplay between voltage and conductance STA waveforms. However, since this amounts to the solution of a second order differential equation with time-dependent coefficients, success is everything but guaranteed. Instead, one could attempt to represent the voltage STA by an exponential function (which usually seems to be a good approximation) thus simplifying the analytical solution. The conductance STAs could then directly be expressed as a function of three parameters, thus considerably simplifying the application of the method.

However, the simplicity of the point-conductance model also entails certain limitations. As mentioned before, conductances are to be understood as being effective ones at the level of the soma. While it makes perfect sense to study this situation, since the site of action potential generation is assumed to be situated close to the soma (Stuart et al. 1997), the effect of dendritic filtering is completely neglected and thus the link to input arriving at synapses distributed across the dendritic tree is hard to establish. The simple simulation in Chapter 3, exploring the effect of dendritic filtering, shows that already in a passive two compartment model the somatic conductances can look very different from the dendritic ones. The effect of a synaptic input on the conductance at the soma should thus strongly depend on its electrotonic distance. On the other hand, it has been shown in a detailed biophysical model (Rudolph & Destexhe 2003c) that during high-conductance states the efficacy of synaptic inputs to evoke action potentials is approximately location-independent, if the dendrites dispose of active (Na^+)

7.2. OUTLOOK

conductances. A way to assess distributed synaptic input in biological neurons has been suggested recently (Huys et al. 2006). It relies on high-quality voltage-sensitive imaging and in principle constitutes a way to trace the impact of synaptic input in the dendrites on the voltage at the soma. Clearly, further electrophysiological investigation of dendritic channel densities and their effect on signal filtering during different synaptic input scenarios is needed in order to better understand the input–output function of single neurons.

Appendix A

Estimating conductance parameters from the membrane potential time course

A.1 Synopsis

The mathematical framework of Chapter 3 can also be used in a different context. There, we mention that in order to extract the conductance STA from a single voltage trace, one needs to know the parameters of the respective conductance distributions. We give reference to a method that is able to do exactly this (Rudolph and Destexhe 2003, Rudolph et al. 2005). However, recordings at minimally two different current levels are necessary in order to apply the technique. Several drawbacks come with this requirement. First and maybe least crucial, repeating a protocol at two or more DC levels requires that the cell be stable for a multiple of the time necessary to apply the protocol once. Second and maybe more importantly, injecting a constant current into a cell during an *in vivo* recording shifts the membrane potential away from its natural level. This in turn may affect the fraction of open channels for a particular ion type and thus influence the conductance state of the cell. Last, and maybe most crucial in practice, it is simply impossible to analyse data that has been recorded at an earlier time without anticipating the possibility of such an analysis, and thus recordings are only available at a single (zero) current level. In this Appendix, we sketch and test a method that can extract the mean and variance of synaptic conductances from a single voltage trace. The method is based on a maximum likelihood estimation of the respective parameters.

A.2 The Method

We use the model described in Chapter 3, i.e. Eqs. 3.1 and 3.2. Unlike described in the respective Section, for the current approach it is not necessary to formulate the equations in terms of ensemble averaged quantities. In discrete time and slightly rearranged they read (cf. Eqs. 3.5 and 3.6):

$$g_i^k = -\frac{C}{V^k - V_i} \left\{ \frac{V^k - V_L}{\tau_L} + \frac{g_e^k(V^k - V_e)}{C} + \frac{V^{k+1} - V^k}{\Delta t} - \frac{I_{DC}}{C} \right\}, \quad (\text{A.1})$$

$$\xi_s^k = \frac{1}{\sigma_s} \sqrt{\frac{\tau_s}{2\Delta t}} \left(g_s^{k+1} - g_s^k \left(1 - \frac{\Delta t}{\tau_s} \right) - \frac{\Delta t}{\tau_s} g_{s0} \right). \quad (\text{A.2})$$

We start from Eqs. 3.7 and 3.8 (they are repeated here for convenience), only that this time no implicit average is assumed:

$$p^k := p(g_e^{k+1}, g_i^{k+1} | g_e^k, g_i^k) = \frac{1}{2\pi} e^{-\frac{1}{2}(\xi_e^{k2} + \xi_i^{k2})} = \frac{1}{2\pi} e^{-\frac{1}{4\Delta t} X^k}, \quad (\text{A.3})$$

$$\begin{aligned} X^k &= \frac{\tau_e}{\sigma_e^2} \left(g_e^{k+1} - g_e^k \left(1 - \frac{\Delta t}{\tau_e} \right) - \frac{\Delta t}{\tau_e} g_{e0} \right)^2 \\ &\quad + \frac{\tau_i}{\sigma_i^2} \left(g_i^{k+1} - g_i^k \left(1 - \frac{\Delta t}{\tau_i} \right) - \frac{\Delta t}{\tau_i} g_{i0} \right)^2. \end{aligned} \quad (\text{A.4})$$

As before, p^k has the following meaning: at time $k + 1$, the membrane voltage takes the value V^{k+1} as a result of the synaptic conductances present at time k (cf. Eq. 3.5 for the dependence of V^{k+1} on V^k , g_e^k and g_i^k). Going one step further in time, a continuum of pairs (g_e^{k+1}, g_i^{k+1}) is possible in order to reach the (known) voltage V^{k+2} . The quantity p^k assigns to all such pairs a probability of occurrence, depending on the previous pair and the voltage history. Ultimately, it is the probability of occurrence of the appropriate random numbers ξ_e^k and ξ_i^k that relate the respective conductances at subsequent time steps. It is then straightforward to write down the probability p for certain conductance series to occur, that reproduce the voltage time course. This is just the probability for successive conductance steps to occur, namely the product of the probabilities p^k :

$$p = \prod_{k=0}^{n-1} p^k, \quad (\text{A.5})$$

given initial conductances g_e^0, g_i^0 . However, again, there is a continuum of conductance series $\{g_e^l, g_i^l\}_{l=1, \dots, n+1}$, that are all compatible with the observed voltage trace. We define a likelihood function $f(V^k, \theta)$, $\theta = (g_{e0}, g_{i0}, \sigma_e, \sigma_i)$, that takes into account all of them with appropriate weight. We thus integrate Eq. A.5 over the unconstrained conductances g_e^k and normalise by the volume of configuration space:

$$f(V^k, \theta) = \frac{\int \prod_{k=0}^{n-1} dg_e^k p}{\int \prod_{k=0}^{n-1} dg_e^k dg_i^k p}, \quad (\text{A.6})$$

where only in the nominator g_i^k has been replaced by Eq. A.1. This expression reflects the likelihood that a specific voltage series $\{V^k\}$ occurs, normalized by the probability, that *any* trace occurs. The most likely parameters θ giving rise to $\{V^k\}$ are obtained by maximising (or minimising the negative of) $f(V^k, \theta)$ using standard optimization schemes.

A.3 Application to model data

We tested the method in detail in its applicability to voltage traces, that were created using the same model (IF model). To this end, we performed simulations scanning the (g_{e0}, g_{i0}) -plane and subsequently tried to re-estimate the conductance parameters used. The method was applied to ten samples of 5000 data points (corresponding to 250 ms each) and the average was taken subsequently. The conductance standard deviations (SDs) were chosen to be one third of the respective mean values, other parameters were assumed to be known during re-estimation ($C = 0.4$ nF, $g_L = 13.44$ nS, $V_L = -80$ mV, $\tau_e = 2.728$ ms, $\tau_i = 10.49$ ms), the time step was $dt = 0.05$ ms. Also, we assumed that the total conductance

A.3. APPLICATION TO MODEL DATA

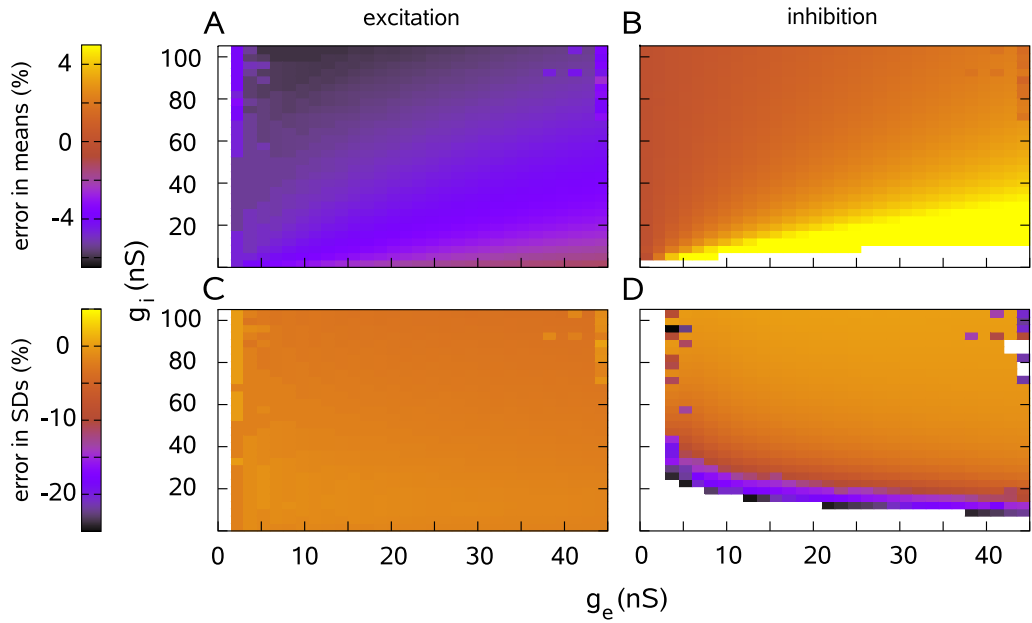


Figure A.1: Test of the method for the IF model. Each panel presents a scan in the (g_{e0}, g_{i0}) -plane. Color codes the relative deviation between model parameters and their estimates using the method (note the different scales for means/SDs). **A**: deviation in the mean of excitatory conductance (g_{e0}). **B**: Same as **A** for inhibition. **C**: deviation in the SD of excitatory conductance **D**: Same as **C** for inhibition. In general the method works fine, except for a small band in the case of inhibitory SD.

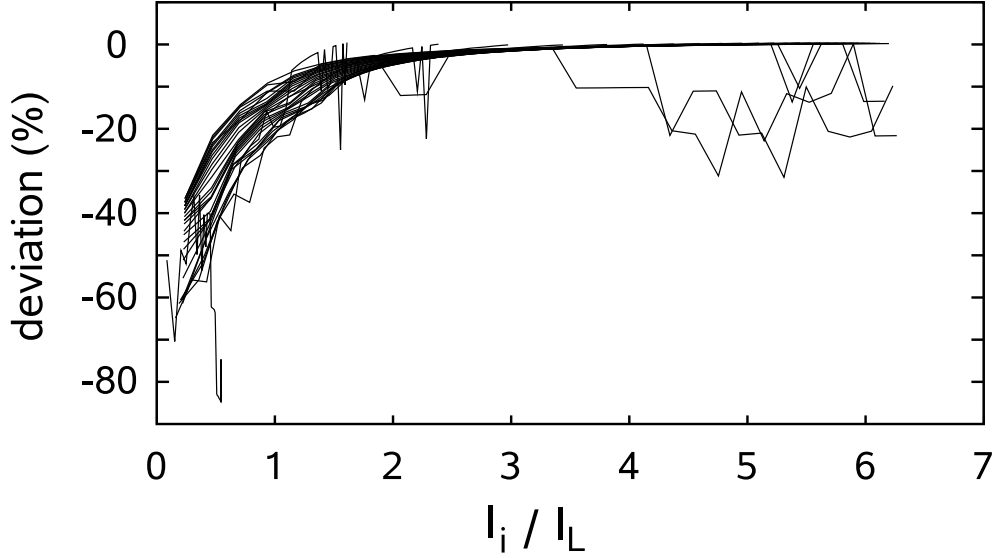


Figure A.2: Relative deviation between the parameter σ_i in the simulations and its re-estimated value depending on the ratio of the currents due to inhibitory and leak conductance. The estimation fails, when the inhibitory component becomes too small.

g_{tot} was known, the likelihood function A.6 was thus only maximized with respect to g_{e0} , σ_e and σ_i . Fig. A.1 summarizes the results. The mean conductances are well reproduced over the entire scan region. An exception is the estimation of g_{i0} for a situation, where the mean excitation exceeds inhibition severalfold, a situation which is hardly found in real neurons. The situation for the SDs is different. While the excitatory SD is reproduced very well in the whole area under consideration, the situation is different for inhibition. Here, the estimation is good for most parts of the scanned region, but shows a considerable deviation along the left and lower boundaries. These are regions, where the transmembrane current due to inhibition is weak, either because the inhibitory conductance is weak (lower boundary) or because it is strong and excitation is weak (left boundary), such that the mean voltage is close to the inhibitory reversal potential and the driving force is small. In these conditions it seems that the effect of inhibition on the membrane voltage cannot be distinguished from that of the leak conductance. Fig. A.2 illustrates this point. It shows the relative deviation between σ_i in the model and its re-estimation depending on the ratio of the transmembrane current due to inhibitory (I_i) and leak (I_L) conductance. All curves correspond to a fixed excitatory and varying inhibitory conductance. Apart from fluctuations, there is a clear tendency. The estimation is simply wrong when the inhibitory current is smaller or comparable to the leak current, but it becomes very reliable as soon as the ratio I_i/I_L becomes larger than 1.5-2.

A.4 Application to *in vitro* data

The unavoidable presence of recording noise presents a certain problem in the application of the method to recordings from real neurons. Fig. A.3 shows, how low amplitude white noise added to the voltage trace of an IF model impairs the reliability of the method. There, Gaussian-distributed random numbers have been added to the voltage trace at every time step, scaled by the amplitude given in the abscissa. Different curves correspond to different pairs (g_{e0}, g_{i0}) . The noise has an opposite effect on the estimation of the conductance mean values. While the estimate of excitation exceeds the real parameter value, for inhibition the situation is inversed. However, one has to keep in mind that both parameters are not estimated independently, but their sum is kept fixed. In contrast, the estimates for the conductance SDs always exceed the real values, and they can deviate by almost 500% for a noise amplitude of $10 \mu\text{V}$. Clearly, in order to apply the method to recordings from real neurons, one needs to get rid of the noise. We chose to preprocess the original voltage trace with a Gaussian filter with a SD of 3 data points.

We tested the method on *in vitro* recordings using dynamic clamp (for details on the experiments cf. the “Materials and Methods”-Sections in Chapters 3 and 6). As in the model, the stimulus consisted in two channels of fluctuating conductances representing excitation and inhibition. We chose a high-conductance (HC, $g_{e0} = 32.1 \text{ nS}$, $g_{i0} = 96.2 \text{ nS}$, $\sigma_e = 8.0 \text{ nS}$, $\sigma_i = 24.0 \text{ nS}$) as well as a low-conductance (LC, $g_{e0} = 12.4$, $g_{i0} = 7.6$, $\sigma_e = 6.0$, $\sigma_i = 3.6$) stimulus. The method was applied to subsequent inter-spike intervals (ISIs) of a minimum duration of 2000 datapoints (corresponding to $\sim 100 \text{ ms}$). For the HC stimulus, the result was as follows: The estimates for the mean conductances during successive ISIs fluctuated with low amplitude and close to the target values. On the other hand, the estimates for the SDs showed a bimodal distribution. They either took a value close to the target, or the result was far off. In the latter case, the estimate for the inhibitory SD was between 130 and 170 nS, whereas at the same time the estimate for the excitatory SD was zero. This bimodality made it easy to separate the successful estimates from the clear failures. Fitting a constant to the successful trials gave the following parameter estimates: $g_{e0} = 28.0 \text{ nS}$, $g_{i0} = 100.1 \text{ nS}$, $\sigma_e = 6.6 \text{ nS}$, $\sigma_i = 25.9 \text{ nS}$, which is in good agreement with the real values. For the LC stimulus, the situation was different. On the one hand, now also for the estimates of the mean values there were outliers, positive ones for excitation, negative ones for inhibition. On the other hand, the outliers for the excitatory SD now also were positive. However, it was still possible to separate successful trials from failures. The estimates for LC stimulus were: $g_{e0} = 10.7 \text{ nS}$, $g_{i0} = 9.3 \text{ nS}$, $\sigma_e = 6.8 \text{ nS}$, $\sigma_i = 7.4 \text{ nS}$. Except for σ_i , this might qualify as acceptable agreement. Regarding the latter, for the parameters chosen the ratio I_i/I_L is ~ 0.15 . So in view of Fig. A.2 the bad performance is not surprising.

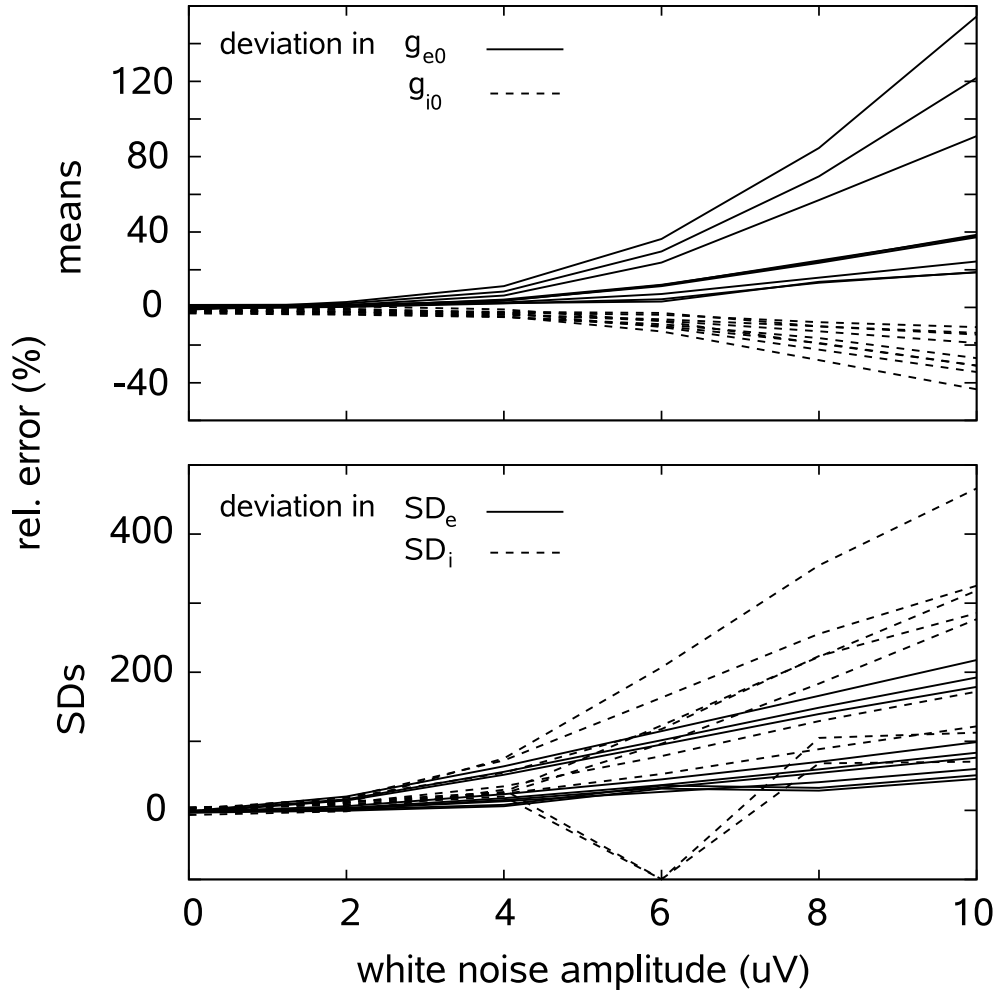


Figure A.3: White noise in the voltage trace significantly impairs the reliability of the method. The relative deviation in the estimation of g_{e0} and g_{i0} (upper panel) as well as σ_e and σ_i is given as a function of the white noise amplitude. Different curves correspond to different pairs (g_{e0}, g_{i0}) . While the noise has an opposite effect on the estimation of the mean conductance values, the estimates of the SDs increase with the noise.

A.5 Discussion

We have introduced a method that can extract conductance parameters from the voltage time course at a single current level. The method does not rely on static properties of the membrane voltage, like mean and standard deviation, in order to determine the shape of the conductance distributions. Instead, it exploits the dynamical information hidden in the V_m time course. Not only the step sizes are important, but also at which voltage level they occur. The likelihood function is highly sensitive to the conductance fluctuations and, constraining the total conductance, also to the conductance mean values. Tests on model data were encouraging, but also pointed to weaknesses of the method in a regime where the transmembrane current due to inhibitory conductances is small compared to the leak current. There, the inhibitory fluctuations are not reliably resolved. A test of the method on data obtained *in vitro* using dynamic clamp confirmed the weakness in this regime, but also displayed the good performance during a HC state. Since in cortical neurons *in vivo* the membrane potential is usually well above the inhibitory reversal potential and inhibitory conductances tend to dominate excitatory ones, this method should be applicable to *in vivo* recordings.

Acknowledgements

During the past four years, a lot of people have contributed to the progress of my thesis, either directly by providing support in scientific questions, or in a less apparent fashion. I would like to express my gratefulness towards all of them.

Above all, I would like to thank my parents, Gitte and Ewald Pospischil. Without their support throughout the entire duration of my studies, I would probably never have come to the point of even starting a doctoral thesis.

Just as much, I would like to thank my supervisor Alain Destexhe. Through his deliberate choice of subject I had the opportunity to work on very interesting questions at the interface of theoretical and experimental neuroscience. His profound knowledge of the field was a great help and inspiration, and it was a pleasure to interact in such an uncomplicated manner.

My work would have been less fruitful without the possibility to collaborate with a number of people. Most of the results in my thesis have been tested on experimental recordings. In this regard, cordial thanks go to Zuzanna Piwowska, Julia Sliwa and Thierry Bal, as well as to Igor Timofeev for providing really unique data. In the same line I would like to thank Michelle Lilith for her continuous support in various directions, especially during my first steps in neuroscience. Also, I'm grateful to Andrew Davison for lots of help with one of my projects, as well as to Romain Brette for inspiring discussions.

Thanks to all those who take part in maintaining the UNIC a place, where active research is conducted. This includes first and foremost the lab director Yves Frégnac, but also the senior scientists Jean-Pierre Denizot, Kirsty Grant, Marc Pananceau and Daniel E. Shulz, as well as the people taking care of administrative concerns, Loredana Focsa, Paul Galloux, Michèle Gautier, Irina Kopysova, Mélanie Lapoumeyroulie, Sylvie L'amour, Yann Le Franc and Gérard Sadoc.

I'm grateful to all adherent to the UNIC, Postdocs, doctoral and master students, trainees, for enjoyable hours spent inside and outside the lab. Thanks for conversations about science, about science-related topics, about topics not related to science whatsoever, thanks for playing tennis, for exploring beautiful Paris, for patience and assistance during my attempts to learn the French language, for smoking cigarillos, for company in the opera, for help with small as well as severe computer problems, for ordering pizza at night and a plurality of other things that made my life in Paris richer.

A.5. DISCUSSION

Finally, I want to thank my wife Joy Aquino-Beiderbeck for her patience and comprehension, for accepting a period of time that had its difficulties. Her support and compassion were indispensable.

Bibliography

- [1] Achard P. & De Schutter E. Complex parameter landscape for a complex neuron model. *PLoS Comput. Biol.* **2**(7):794-804, 2006.
- [2] Agüera y Arcas B. & Fairhall A. L. What causes a neuron to spike? *Neural Computation* **15**:1789-1807, 2003.
- [3] Anderson J. S., Carandini M., Ferster D. Orientation tuning of input conductance, excitation, and inhibition in cat primary visual cortex. *J. Neurophysiol.* **84**:909-926, 2000.
- [4] Azouz R. & Gray C.M. Dynamic spike threshold reveals a mechanism for synaptic coincidence detection in cortical neurons *in vivo*. *Proc. Natl. Acad. Sci. USA* **97**:8110-8115, 2000.
- [5] Badel L., Gerstner W., Richardson M.J.E. Dependence of the spike-triggered average voltage on membrane response properties. *Neurocomputing* **69**:1062-1065, 2006.
- [6] Badoual M., Rudolph M., Piwkowska Z., Destexhe A., Bal T. High discharge variability in neurons driven by current noise. *Neurocomputing* **65-66**:493-498, 2005.
- [7] Barak O. & Tsodyks M. Persistent activity in neural networks with dynamic synapses. *PLoS Comput. Biol* **3**:e35, 2007.
- [8] Baranyi A., Szenté M. B., Woody C. D. Electrophysiological characterization of different types of neurons recorded *in vivo* in the motor cortex of the cat. II. Membrane parameters, action potentials, current-induced voltage responses and electrotonic structures. *J. Neurophysiol.* **69**:1865-1879, 1993.
- [9] Bedard C. & Destexhe A. A modified cable formalism for modeling neuronal membranes at high frequencies. Manuscript under review, 2007; preprint available at <http://arxiv.org/abs/0705.3759>.

BIBLIOGRAPHY

- [10] Bernander O., Douglas R. J., Martin K. A., Koch C. Synaptic background activity influences spatiotemporal integration in single pyramidal cells. *Proc. Natl. Acad. Sci. USA* **88**:11569-11573, 1991.
- [11] Borg-Graham L. J., Monier C., Frégnac Y. Visual input evokes transient and strong shunting inhibition in visual cortical neurons. *Nature* **393**:369-373, 1998.
- [12] de Boer F. & Kuypers P. Triggered Correlation. *IEEE Trans. Biomed. Eng.* **15**:169-197, 1968.
- [13] Brecht M., Schneider M., Sakmann B., Margrie T. W. Whisker movements evoked by stimulation of single pyramidal cells in rat motor cortex. *Nature* **427**:704-710, 2004.
- [14] Brette R. & Gerstner W. Adaptive exponential integrate-and-fire model as an effective description of neuronal activity. *J. Neurophysiol.* **94**(5):3637-3642, 2005.
- [15] Brette R., Piwkowska Z., Rudolph-Lilith M., Bal T., Destexhe A. How to emulate double-electrode recordings with a single electrode? A new method of active electrode compensation. *Soc. Neurosci. Abstracts* 688.2, 2005.
- [16] Brette R., Rudolph M., Piwkowska Z., Bal T., Destexhe A. High-resolution intracellular recordings using a real-time interaction between the neuron and a computational model of the electrode. *submitted*, 2007.
- [17] Bryant H.L. & Segundo J.P. Spike initiation by transmembrane current: a white-noise analysis. *J. Physiol.* **260**:279-314, 1976.
- [18] Clopath C., Jolivet R., Rauch A., Lüscher H. R., Gerstner W. Predicting neuronal activity with simple models of the threshold type: Adaptive Exponential Integrate-and-Fire model with two compartments. *Neurocomputing* **70**(10-12):1668-1673, 2007.
- [19] Compte A., Sanchez-Vives M. V., McCormick D. A., Wang X. J. Cellular and network mechanisms of slow oscillatory activity (<1 Hz) and wave propagations in a cortical network model. *J. Neurophysiol.* **89**:2707-2725, 2003.
- [20] Cunningham M. O., Pervouchine D. D., Racca C., Kopell N. J., Davies C. H., Jones R. S., Traub R. D., Whittington M. A. Neuronal metabolism governs cortical network response state. *Proc. Natl. Acad. Sci. USA* **103**:5597-5601, 2006.

- [21] Cymbalyuk G.S., Gaudry Q., Masino M.A., Calabrese R.L. Bursting in leech heart interneurons: cell-autonomous and network-based mechanisms. *J. Neurosci.* **22**(24):10580-10592, 2002.
- [22] Dayan P. and Abbott L.F. Theoretical Neuroscience: Computational And Mathematical Modeling of Neural Systems. *MIT Press*, 2001.
- [23] Desai N. S. & Walcott E. C. Synaptic bombardment modulates muscarinic effects in forelimb motor cortex. *J. Neurosci.* **26**:2215-2226, 2006.
- [24] Davison A. P. *Private communications*.
- [25] Destexhe A. & Paré D. Impact of network activity on the integrative properties of neocortical pyramidal neurons in vivo. *J. Neurophysiol.* **81**:1531-1547, 1999.
- [26] Destexhe A. & Rudolph M. Extracting information from the power spectrum of synaptic noise. *J. Comput. Neurosci.* **17**:327-345, 2004.
- [27] Destexhe A., Mainen Z.F., Sejnowski T.J. An efficient method for computing synaptic conductances based on a kinetic model of receptor binding. *Neural Computation* **6**:14-18, 1994.
- [28] Destexhe A., Rudolph M., Fellous J.-M., Sejnowski T. J. Fluctuating synaptic conductances recreate in vivo-like activity in neocortical neurons. *Neuroscience* **107**:13-24, 2001.
- [29] Destexhe A., Rudolph M., Paré D. The high-conductance state of neocortical neurons in vivo. *Nat. Rev. Neurosci.* **4**:739-751, 2003.
- [30] Destexhe A., Hughes S. W., Rudolph M., Crunelli V. Are corticothalamic “up–” states fragments of wakefulness? *Trends Neurosci.* doi:10.1016/j.tins.2007.04.006, 2007.
- [31] Ermentrout G. B.. Type i membranes, phase resetting curves, and synchrony. *Neural Computation*, **8**:979-1001, 1996.
- [32] Fellous J. M., Rudolph M., Destexhe A., Sejnowski T. J. Synaptic background noise controls the input/output characteristics of single cells in an in vitro model of in vivo activity. *Neuroscience* **122**:811-829, 2003.
- [33] FitzHugh R. Impulses and physiological states in models of nerve membrane. *Biophys. J.*, **1**:445-466, 1961.
- [34] Fourcaud-Trocme N., Hansel D., van Vreeswijk C., Brunel N. How spike generation mechanisms determine the neuronal response to fluctuating inputs. *J. Neurosci.* **23**(37):11628-11640, 2003.

BIBLIOGRAPHY

- [35] Gerstner W. & Kistler W. M. Spiking Neuron Models. Single Neurons, Populations, Plasticity. *Cambridge University Press*, 2002.
- [36] Gillespie D. T. The mathematics of Brownian motion and Johnson noise. *Am. J. Phys.* **64**:225-240, 1996.
- [37] Haider B., Duque A., Hasenstaub A. R., McCormick D. A. Neocortical network activity in vivo is generated through a dynamic balance of excitation and inhibition. *J Neurosci* **26**:4535-4545, 2006.
- [38] Hasenstaub A., Shu Y., Haider B., Kraushaar U., Duque A., McCormick D. A. Inhibitory postsynaptic potentials carry synchronized frequency information in active cortical networks. *Neuron* **47**:423-435, 2005.
- [39] Haeusler S. & Maass W. A statistical analysis of information-processing properties of lamina-specific cortical microcircuit models. *Cereb Cortex* **17**:149-162, 2007.
- [40] Herrmann A. & Gerstner W. Noise and the PSTH response to current transients: I. General theory and application to the integrate-and-fire neuron. *J. Comput. Neurosci.* **11**(2):135-151, 2001.
- [41] Herrmann A. & Gerstner W. Noise and the PSTH response to current transients: II. Integrate-and-fire model with slow recovery and application to motoneuron data. *J. Comput. Neurosci.* **12**(2):83-95, 2002.
- [42] Hill S. & Tononi G. Modeling sleep and wakefulness in the thalamocortical system. *J. Neurophysiol.* **93**:1671-1698, 2005.
- [43] Hines M. L. & Carnevale N. T. The NEURON simulation environment, *Neural Computation* **9**:1179-1209, 1997.
- [44] Hirsch J. A., Alonso J. M., Clay Reid R., Martinez L. M. Synaptic integration in striate cortical simple cells. *J. Neurosci.* **18**:9517-9528, 1998.
- [45] Hodgkin A. L. & Huxley A. F. A quantitative description of membrane current and its application to conduction and excitation in nerve. *J. Physiol.* **117**:500-544, 1952.
- [46] Huys Q.J., Ahrens M.B., Paninski L. Efficient estimation of detailed single-neuron models. *J. Neurophysiol.* **96**(2):872-890, 2006.
- [47] Izhikevich E. M. Simple Model of Spiking Neurons *IEEE Transactions on Neural Networks* **14**(6):1569-1572, 2003.
- [48] Izhikevich E. M. Which Model to Use for Cortical Spiking Neurons? *IEEE Transactions on Neural Networks* **15**(5):1063-1070, 2004.

- [49] Jolivet R., Lewis T. J., Gerstner W. Generalized integrate-and-fire models of neuronal activity approximate spike trains of a detailed model to a high degree of accuracy. *J. Neurophysiol.* **92**(2):959-976, 2004.
- [50] Jolivet R., Rauch A., Lüscher H. R., Gerstner W. Predicting spike timing of neocortical pyramidal neurons by simple threshold models. *J. Comput. Neurosci.* **21**:35-49, 2006.
- [51] Kuhn A., Aertsen A., Rotter S. Neuronal integration of synaptic input in the fluctuation-driven regime. *J. Neurosci.* **24**:2345-2356, 2004.
- [52] Lapicque L. Recherches quantitatives sur l'excitation électrique des nerfs traitée comme une polarisation. *J. Physiol. Pathol. Gen.* **9**:620-635, 1907.
- [53] Latham P. E., Richmond B. J., Nelson P. G., Nirenberg S. Intrinsic dynamics in neuronal networks. I. Theory. *J. Neurophysiol.* **83**:808-827, 2000.
- [54] LeMasson G. & Maex R. Introduction to equation solving and parameter fitting. In: De Schutter E, editor. Computational neuroscience: Realistic modeling for experimentalists. London: CRC Press. 347 p, 2001.
- [55] Le Masson G., Renaud-Le Masson S., Debay D., Bal T. Feedback inhibition controls spike transfer in hybrid thalamic circuits. *Nature* **417**:854-858, 2002.
- [56] Lindner B. & Longtin A. Comment on "Characterization of subthreshold voltage fluctuations in neuronal membranes", by M. Rudolph and A. Destexhe. *Neural Computation* **18**:1896-1931, 2006.
- [57] Ma M. & Koester J. The role of potassium currents in frequency-dependent spike broadening in *Aplysia* R20 neurons: a dynamic clamp analysis. *J. Neurosci.* **16**:4089-4101, 1996.
- [58] Mainen Z. F. & Sejnowski T. J. Reliability of spike timing in neocortical neurons. *Science* **268**:1503-1506, 1995.
- [59] Mainen Z. F. & Sejnowski T. J. Influence of dendritic structure on firing pattern in model neocortical neurons. *Nature* **382**(6589):363-366, 1996.
- [60] Matsumura M., Cope T., Fetz E. E. Sustained excitatory synaptic input to motor cortex neurons in awake animals revealed by intracellular recording of membrane potentials. *Exp. Brain Res.* **70**:463-469, 1988.
- [61] McCormick D. A. Neurotransmitter actions in the thalamus and cerebral cortex and their role in neuromodulation of thalamocortical activity. *Prog. Neurobiol.* **39**:337-388, 1992.

BIBLIOGRAPHY

- [62] Metherate R. & Ashe J. H. Ionic flux contributions to neocortical slow waves and nucleus basalis-mediated activation: whole-cell recordings in vivo. *J. Neurosci.* **13**:5312-5323, 1993.
- [63] Monier C., Chavane F., Baudot P., Graham L. J., Frégnac Y. Orientation and direction selectivity of synaptic inputs in visual cortical neurons: a diversity of combinations produces spike tuning. *Neuron* **37**:663-680, 2003.
- [64] Morris C. & Lecar H. Voltage oscillations in the barnacle giant muscle fiber. *Biophys. J.* **35**:193-213, 1981.
- [65] Nagumo J. S., Arimoto S., Yoshizawa S. An active pulse transmission line simulating nerve axon. *Proc. IRE* **50**:2061-2070, 1962.
- [66] Paninski L. The spike-triggered average of the integrate-and-fire cell driven by gaussian white noise. *Neural Computation* **18**:2592-2616, 2006a.
- [67] Paninski L. The most likely voltage path and large deviations approximations for integrate-and-fire neurons. *J. Comput. Neurosci.* **21**:71-87, 2006b.
- [68] Paninski L., Pillow J. Simoncelli E. Maximum likelihood estimation of a stochastic integrate-and-fire neural model. *Neural Computation* **16**:2533-2561, 2004.
- [69] Paré D., Shink E., Gaudreau H., Destexhe A., Lang E. J. Impact of spontaneous synaptic activity on the resting properties of cat neocortical neurons in vivo. *J. Neurophysiol.* **79**:1450-1460, 1998.
- [70] Pillow J. & Simoncelli E. Biases in white noise analysis due to non-Poisson spike generation. *Neurocomputing* **52**:109-155, 2003.
- [71] Pinsky P. F. & Rinzel J. Intrinsic and network rhythmogenesis in a reduced Traub model for CA3 neurons. *J. Comput. Neurosci.* **1**(1-2):39-60, 1994.
- [72] Piwkowska Z., Rudolph M., Badoual M., Destexhe A., Bal T. Re-creating active states in vitro with a dynamic-clamp protocol. *Neurocomputing* **65-66**:55-60, 2005.
- [73] de Polavieja G.G., Harsch A., Kleppe I., Robinson H.P.C., Juusola M. Stimulus history reliably shapes action potential waveforms of cortical neurons. *J. Neurosci.* **25**(23):5657-5665, 2005.
- [74] Pospischil M., Rudolph M., Shulz D., Timofeev I. Destexhe A. Are we inhibited when we are awake ? A combined intracellular and computational analysis of membrane potential dynamics in cortical neurons of awake and naturally sleeping animals. *Soc. Neurosci. Abstracts* **31**:276.15, 2005.

- [75] Pospischil M., Piwkowska Z., Rudolph M., Bal T., Destexhe A. Calculating event-triggered average synaptic conductances from the membrane potential. *J. Neurophysiol.* **97**:2544-2552, 2007.
- [76] Press W. H., Flannery B. P., Teukolsky S. A., Vetterling W. T. Numerical Recipes. The Art of Scientific Computing. Cambridge, MA: *Cambridge University Press*, 1986.
- [77] Priebe N. J. & Ferster D. Direction selectivity of excitation and inhibition in simple cells of the cat primary visual cortex. *Neuron* **45**:133-145, 2005.
- [78] Prinz A. A., Abbott L. F., Marder E. The dynamic clamp comes of age. *Trends Neurosci.* **27**(4):218-224, 2004.
- [79] Richardson M. J. E. Effects of synaptic conductance on the voltage distribution and firing rate of spiking neurons. *Phys. Rev. E* **69**:051918, 2004.
- [80] Richardson M. J. E. and Badel L. The pre and post-spike dynamic I-V relations of layer-5 pyramidal cells. Talk given at the workshop “Quantitative Neuron Modeling: Predicting every spike?”, Lausanne, June 25th-26th, 2007.
- [81] Robinson H. P. & Kawai N. Injection of digitally synthesized synaptic conductance transients to measure the integrative properties of neurons. *J. Neurosci. Methods* **49**:157-165, 1993.
- [82] Roxin A., Brunel N., Hansel D. Role of delays in shaping spatiotemporal dynamics of neuronal activity in large networks. *Phys. Rev. Lett.* **94**:238103, 2005.
- [83] Rudolph M. & Destexhe A. Characterization of subthreshold voltage fluctuations in neuronal membranes. *Neural Computation* **15**:2577-2618, 2003a.
- [84] Rudolph M. & Destexhe A. The discharge variability of neocortical neurons during high-conductance states. *Neuroscience* **119**:855-873, 2003b.
- [85] Rudolph M. & Destexhe A. A fast-conducting, stochastic integrative mode for neocortical neurons in vivo. *J. Neurosci.* **23**:2466-2476, 2003c.
- [86] Rudolph M. & Destexhe A. An extended analytic expression for the membrane potential distribution of conductance-based synaptic noise. *Neural Computation* **17**:2301-2315, 2005.
- [87] Rudolph M. & Destexhe A. On the use of analytic expressions for the voltage distribution to analyze intracellular recordings. *Neural Computation* **18**:2917-2922, 2006a.

BIBLIOGRAPHY

- [88] Rudolph M. & Destexhe A. Multichannel shot noise approach to describe synaptic background activity in neurons. *Eur. Phys. J. B* **52**:125-132, 2006b.
- [89] Rudolph M., Piwkowska Z., Badoual M., Bal T., Destexhe A. A method to estimate synaptic conductances from membrane potential fluctuations. *J. Neurophysiol.* **91**:2884-2896, 2004.
- [90] Rudolph M., Piwkowska Z., Brette R., Destexhe A., Bal T. Precise dynamic-clamp injection of stochastic conductances using active electrode compensation. *Soc. Neurosci. Abstracts* 687.13, 2005a.
- [91] Rudolph M., Pelletier J.-G, Paré D., Destexhe A. Characterization of synaptic conductances and integrative properties during electrically-induced EEG-activated states in neocortical neurons in vivo. *J. Neurophysiol.* **94**:2805-2821, 2005b.
- [92] Rudolph M., Pospischil M., Timofeev I., Destexhe A.. Inhibition determines membrane potential dynamics and controls action potential generation in awake and sleeping cat cortex. *J. Neurosci.* **27**(20):5280-5290, 2007.
- [93] Sanchez-Vives M. V. & McCormick D. A. Cellular and network mechanisms of rhythmic recurrent activity in neocortex. *Nat. Neurosci.* **3**:1027-1034, 2000a.
- [94] Sanchez-Vives M. V., Nowak L. G., McCormick D. A. Cellular mechanisms of long-lasting adaptation in visual cortical neurons in vitro. *J. Neurosci.* **20**:4286-4299, 2000b.
- [95] Sharp A. A., O'Neil M. B., Abbott L. F., Marder E. The dynamic clamp: artificial conductances in biological neurons. *Trends Neurosci.* **16**(10):389-394, 1993a.
- [96] Sharp A. A., O'Neil M. B., Abbott L. F. Marder E. Dynamic clamp: computer-generated conductances in real neurons. *J. Neurophysiol.* **69**:992-995, 1993b.
- [97] Shelley M., McLaughlin D., Shapley R., Wielaard J. States of high conductance in a large-scale model of the visual cortex. *J. Comp. Neurosci.* **13**:93-109, 2002.
- [98] Shu Y., Hasenstaub A., Badoual M., Bal T., McCormick D. A. Barrages of synaptic activity control the gain and sensitivity of cortical neurons. *J. Neurosci.* **23**:10388-10401, 2003a.
- [99] Shu Y., Hasenstaub A., McCormick D. A. Turning on and off recurrent balanced cortical activity. *Nature* **423**:288-293, 2003b.

- [100] Steriade M. & McCarley R.W. Brainstem Control of Wakefulness and Sleep. *Plenum Press*, New York, 1990.
- [101] Steriade M., Nunez A., Amzica F. A novel slow (< 1 Hz) oscillation of neocortical neurons in vivo: depolarizing and hyperpolarizing components. *J. Neurosci.* **13**:3252-3265, 1993.
- [102] Steriade M., Timofeev I., Grenier F. Natural waking and sleep states: a view from inside neocortical neurons. *J. Neurophysiol.* **85**:1969-1985, 2001.
- [103] Stuart G., Spruston N., Sakmann B., Hausser M. Action potential initiation and backpropagation in neurons of the mammalian CNS. *Trends Neurosci.* **20**:125-131, 1997.
- [104] Timofeev I., Grenier F., Steriade M. Disfacilitation and active inhibition in the neocortex during the natural sleep-wake cycle: an intracellular study. *Proc. Natl. Acad. Sci. USA* **98**:1924-1929, 2001.
- [105] Traub R. D. & Miles R. Neuronal networks of the hippocampus. Cambridge, MA: Cambridge UP, 1991.
- [106] Uhlenbeck G. E. & Ornstein L. S. On the theory of the Brownian motion. *Phys. Rev.* **36**:823-841, 1930.
- [107] Vanier M. C., Bower J. M. A Comparative Survey of Automated Parameter-Search Methods for Compartmental Neural Models. *J. Comput. Neurosci.* **7**:149-171, 1999.
- [108] van Vreeswijk C. & Sompolinsky H. Chaos in neuronal networks with balanced excitatory and inhibitory activity. *Science* **274**:1724-1726, 1996.
- [109] Waters J. & Helmchen F. Background synaptic activity is sparse in neocortex. *J. Neurosci.* **26**:8267-8277, 2006.
- [110] Weaver C. M. & Wearne S. L. The role of action potential shape and parameter constraints in optimization of compartment models. *Neurocomputing* **69**:1053-1057, 2006.
- [111] Wehr M. & Zador A. M. Balanced inhibition underlies tuning and sharpens spike timing in auditory cortex. *Nature* **426**:442-446, 2003.
- [112] Wehr M. & Zador A. M. Synaptic mechanisms of forward suppression in rat auditory cortex. *Neuron* **47**:437-445, 2005.
- [113] Wilent W. & Contreras D. Dynamics of excitation and inhibition underlying stimulus selectivity in rat somatosensory cortex. *Nat. Neurosci.* **8**:1364-1370, 2005a.

BIBLIOGRAPHY

- [114] Wilent W. & Contreras D. Stimulus-dependent changes in spike threshold enhance feature selectivity in rat barrel cortex neurons. *J. Neurosci.* **25**(11):2983-2991, 2005b.
- [115] Wolfart J., Debay D., Le Masson G., Destexhe A., Bal T. Synaptic background activity controls spike transfer from thalamus to cortex. *Nat. Neurosci.* **8**:1760-1767, 2005.
- [116] Woody C. D. & Gruen E. Characterization of electrophysiological properties of intracellularly recorded neurons in the neocortex of awake cats: a comparison of the response to injected current in spike overshoot and undershoot neurons. *Brain Res.* **158**:343-357, 1978.
- [117] Xiang Z., Huguenard J. R., Prince D. A. Cholinergic switching within neocortical inhibitory networks. *Science* **281**:985-988, 1998.
- [118] Zou Q., Rudolph M., Roy N., Sanchez-Vives M., Contreras D., Destexhe A. Reconstructing synaptic background activity from conductance measurements in vivo. *Neurocomputing* **65**:673-678, 2005.